Department of Experimental Pharmacology and Toxicology

University Medical Centre Hamburg-Eppendorf

Director: Prof. Dr. med. Thomas Eschenhagen

Preclinical drug safety screening using induced pluripotent stem cell-derived cardiomyocytes in engineered heart tissue format

Dissertation

Submitted to the Department of Chemistry

Faculty of Mathematics, Informatics, and Natural Sciences

University of Hamburg

for the degree of

Doctor of Natural Sciences

(Dr. rer. nat.)

by

Umber Saleem

Hamburg, 2019

"It is not defeat that destroys you, it is being demoralized by defeat that destroys you."

(Imran Khan)

Dedicated to my mother.

TABLE OF CONTENT

LIST OF FIGURES

LIST OF TABLES

LIST OF ABBREVIATIONS

Abbreviation	Meaning
°C	Degree Celsius
µg	Microgram
µl	Microliter
µM	Micromolar
µm	Micrometre
2D	Two-dimensional
AAV6	Adeno-associated virus 6
AC	Adenylyl cyclase
ACE	Angiotensin converting enzyme
AKAP	A kinase anchoring protein
ANOVA	Analysis of variances
ANP	Atrial natriuretic peptide
AR	Adrenoceptor
AT_1	Angiotensin II receptor antagonists
ATP	Adenosine triphosphate
AU	Arbitrary unit
BDM	2,3-butanedione monoxime
bFGF	Basic fibroblast growth factor
BL	Baseline
BMI	Body mass index
BMP-4	Bone-morphogenetic protein 4
BNP	Brain natriuretic peptide
BPM	Beats per minute
BTS	N-Benzyl-p-Toluenesulfonamide
CAD	Coronary artery disease
CAS	Chemical Abstracts Service
Cas 9	CRISPR associated protein
CaT	Calcium transient
CICR	Calcium-induced calcium release
CM	Cardiomyocytes
cm^2	Square centimeter
CRISPR	Clustered regularly interspaced short palindromic repeats
CT	Cycle threshold
DB	Dobutamine
DMEM	Dulbecco's Modified Eagle Medium
DMSO	Dimethylsulfoxide
$DT_{80\%}$	Calcium decay time at 80% of peak height
EB	Embryoid body
ECC	Excitation contraction coupling
ECG	Electrocardiography
EDTA	Ethylenediaminetetraacetic acid
EHTs	Engineered heart tissues
EP	Epinephrine
Epi	Epinephrine
et al.	Et alii (and others)
FACS	Fluorescence-activated cell sorting
FCS	Fetal calf serum

FFR	Force frequency relationship
FGF-2	Fibroblast growth factor-2
FITC	Fluorescein isothiocyanate
FK	Forskolin
FP	Fluorescent protein
FRET	Förster resonance energy transfer
FTDA	bFGF, TGF-β1, dorsomorphin and activin A-based hiPSC culture medium
GECI	Genetically encoded calcium indicator
GFR	Growth Factor Reduced
GTP	Guanosine triphosphate
h	hour
HBSS	Hank's Balanced Salt Solution
HCl	Hydrochloric acid
HEPES	4-(2-hydroxyethyl)-1-piperazineethanesulfonic acid
hERG	human ether-a-go-go-related gene
Hertz	Hz
hESC	Human embryonic stem cell
hiPSC	Human induced pluripotent stem cell
HMG-CoA	Hydroxymethylglutaryl Co-enzyme A
IBMX	3-isobutyl-1-methylxanthine
IF	Immunofluorescence
IGF-1	Insulin-like growth factor-1
IHC	Immunohistochemistry
l	Litre
LA	Left atrium
LM	Levosimendan
LPA	Lysophosphatidic acid
LTCC	Voltage gated L-type Ca^{2+} channels
LV	Left ventricular
LVEDD	Left ventricular end diastolic diameter
LVEF	Left ventricular ejection fraction
M	Molar
mg	Milligram
min	minute
MLCK	Myosin light chain kinase
MN	Milrinone
MOI	Multiplicity of infection
MW	Molecular weight
NCX	Sodium calcium exchanger
NFH	Non-failing heart
NIE	Negative inotropic effect
nm	Nanometre
nM	Nanomolar
Norepi	Nor-epinephrine
ns	Not significant
OM	Omecamtiv mecarbil
PB	Pimobendan
PBS	Phosphate-buffered saline
PCR	Polymerase chain reaction
PDE	Phosphodiesterase

PDMS	Polydimethylsiloxane
PE	Phenylephrine
pH	-Log10 hydrogen ion activity
PIE	Positive inotropic effect
PKA	Protein kinase A
PLB	Phospholamban
PMT	Photomultiplier tube
ROS	Reactive oxygen species
rpm	Round per minute
$RT_{80\%}$	Relaxation time at 80% of peak height
RT-PCR	Reverse transcription-PCR
RyR	Ryanodine receptor
s	Seconds
S1P	Sphingosine-1-phosphate
SD	Standard deviation
SEM	Standard error of the mean
SNR	Signal to noise ratio
SR	Sarcoplasmic reticulum
SSR inhibitor	Selective serotonin reuptake inhibitor
T3	Triiodothyronine
TBS	Tris-buffered saline
TGF-β1	Transforming growth factor-β1
TMC	Time control
TnC	Troponin C
TN-I	Troponin I
Tris	2-Amino-2-(hydroxymethyl)propane-1,3-diol
$TTP_{-80\%}$	Time to peak for force and calcium transient read out at 80% of peak height
UGDP	University Group Diabetes Program
UKE	University Medical Centre Hamburg-Eppendorf
v/v	Volume/volume
VC	Vehicle control
VEGF	Vascular endothelial growth factor
Vs.	Versus
w/v	Weight/volume
WKY	Wistar-Kyoto rats
x g	Times gravity (Unit of relative centrifugal force (RCF)

1 <u>INTRODUCTION</u>

1.1. <u>Excitation-contraction coupling and calcium homeostasis</u>

The contraction of the heart is the product of a defined sequence of excitation, intracellular calcium release, and myofilament shortening. This process is referred to as cardiac excitation-contraction coupling (ECC). ECC starts with membrane depolarization that occurs via ion influx from the neighbouring cell through a connexin channel. It leads to the activation of voltage-gated Na^+ channels and rapid Na^+ influx. The depolarization inactivates Na^+ channels and leads to opening of voltage-gated L-type Ca^{2+} channels (LTCC). Calcium entry into the cells via LTCC triggers calcium-induced calcium release (CICR) from the sarcoplasmic reticulum (SR) via ryanodine receptors (RyR). This results in an increase in the cytoplasmic free calcium from 150 nM during relaxation to 600 nM during contraction phase respectively (Bers 2002). Calcium binds to troponin C (TnC), which undergoes a conformational change and displaces the tropomyosin from the actin filament cross-bridge binding site (Figure 1). Myosin cross bridges attach to actin and pull actin towards the centre of sarcomeres. This produces shortening of the myofilament and in consequence a contraction of the muscle cell. When the action potential is repolarised, calcium is removed from the cytoplasm into the SR via SR Ca^{2+} ATPase pump
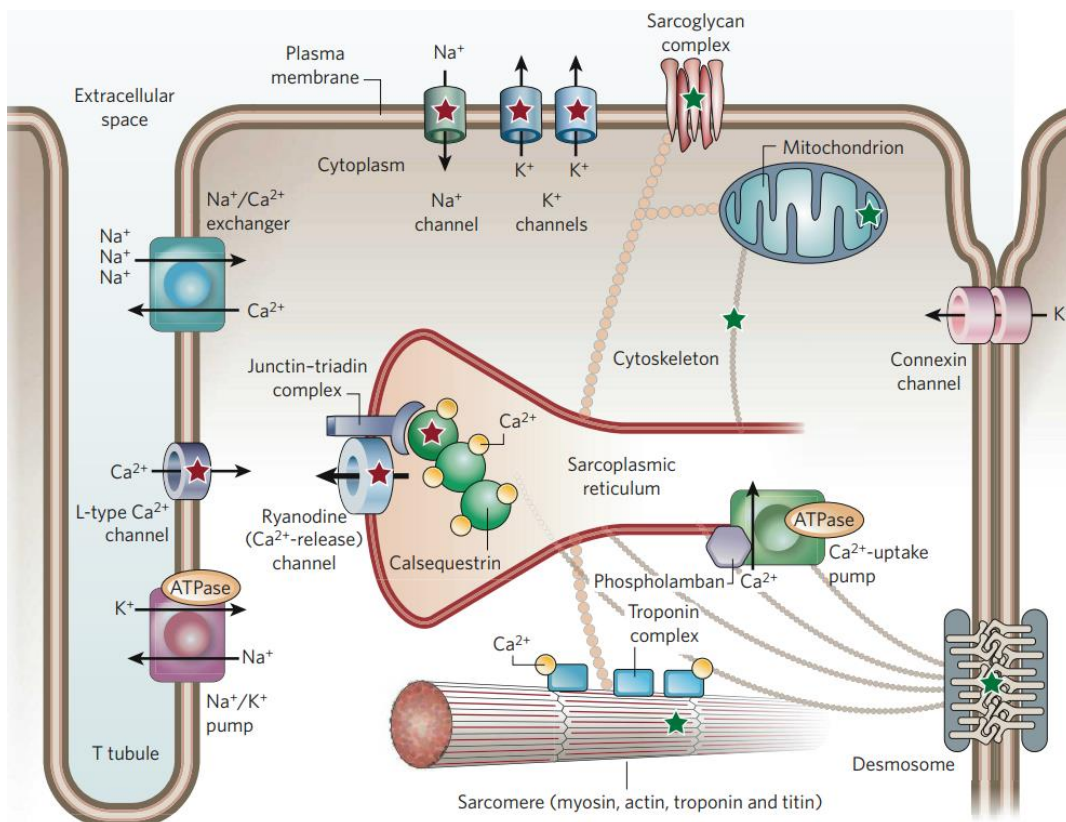
Figure 1: Excitation contraction coupling in cardiomyocyte and the important proteins involved in the process (Knollmann and Roden 2008).

or is transported out of the cell via Na$^+$/Ca^{2+} exchanger (NCX). In consequence, the concentration of free cytoplasmic calcium decreases leading to dissociation of calcium from TnC, the contractile machinery becomes inactive and the sarcomere relaxes (Bers 2002; Knollmann and Roden 2008; Marks 2013). Several mechanisms regulate the increase in cardiac contraction as a response to certain conditions.

The force-frequency relationship also known as Bowditch phenomenon describes the change in contractile force with increasing beat rate. Underlying mechanisms for force regulation by changing frequency of contraction have been widely studied since Bowditch (1871) described the phenomenon but are still not fully understood (Bowditch 1971; Endoh 1989; Maier et al. 2000; Taylor et al. 2004). Studies attempted to elucidate the underlying cellular mechanism have revealed an increase in calcium transient (CaT) amplitude with the increased frequency of stimulation (Bers et al. 2014). The increase in CaT is mediated by an increased calcium influx via the LTCC, increased calcium uptake into the SR and decreased calcium efflux via NCX (Klabunde 2012; Krishna et al. 2013; Bers et al. 2014). The Frank-Starling mechanism describes the increase in force as a result of increased preload. Increased preload (end-diastolic volume) stretches the cardiomyocytes (CM) and increases the sarcomere length, which increases generation of force and thereby stroke volume. Mechanistically, increased force is the result of an increase in TnC calcium sensitivity and thereby an increase in the rate of cross-bridge formation (Tavi et al. 1998; Endoh 2006; de Tombe et al. 2010). The complete mechanism underlying this phenomenon is not clear, yet. Proposed mechanisms involve i. inter-filament spacing i.e. sarcomere elongation presumably decreases the distance between actin and myosin and increases the probability of cross-bridge formation at a given calcium, ii. cooperative interaction between force generating cross-bridges increases with increase in sarcomeric length as number of cross-bridges increase with sarcomeric length, iii. role of cardiac TnI in sarcomeric length dependent activation i.e. replacement of cardiac TnI with skeletal TnI in transgenic mouse models lead to regain of the blunted length dependency, trivial for skeletal muscles (de Tombe et al. 2010; Muslin 2012).

The most important pharmacological mechanism to regulate cardiac contraction is the activation of β1- and β2-adrenoceptors (β-AR). These are 7-transmembrane receptors that activate the Gs protein. Activated Gs stimulates adenylylcyclase (AC) to form cyclic adenosine monophosphate (cAMP) from adenosine triphosphate (ATP). In turn, cAMP activates cAMP-dependent protein kinase A (PKA). PKA phosphorylates many proteins involved in ECC coupling. Phosphorylation of LTCC and phospholamban (PLN) leads to increased contraction force (+ve inotropy), and phosphorylation of PLN (dominant pathway) and troponin I (TnI) accelerates the relaxation (positive lusitropy) by increasing the calcium

uptake into the SR and decreasing the myofilament calcium sensitivity, respectively (Figure 2). Effects of PKA-mediated RyR phosphorylation to increase force are inconsistent and have shown increased, decreased or no effects (Bers 2002; Winslow et al. 2005). Phosphodiesterases (PDE) degrade cAMP and restrict the effects of β-adrenergic stimulation (Kiuchi et al. 1993; Brodde 1994; Guellich et al. 2014). Accordingly, PDE inhibitors can sensitize the cardiomyocytes to β-adrenergic stimulation.
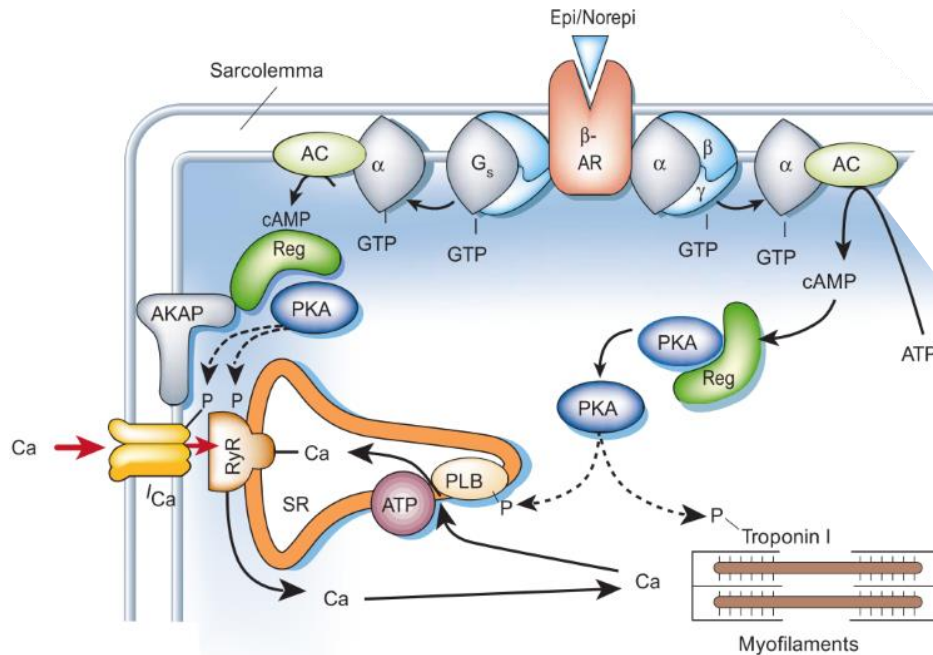
Figure 2: β-adrenoceptor-mediated regulation of excitation-contraction coupling by phosphorylation of target proteins. Epi: Epinephrine; Norepi: Norepinephrine; GTP: Guanosine triphosphate; AC: Adenylyl cyclase; ATP: Adenosine triphosphate; PKA: Protein kinase A; PLB: Phospholamban; RyR: Ryanodine receptor; SR: Sarcoplasmic reticulum; AKAP: A kinase anchoring protein; figure adapted from Bers 2002.

1.2. Cardiomyocytes in drug development

Cardiovascular diseases are the leading cause of death in the modern society and therefore cardiac drug development has been a mainstay for long. In addition, many drugs have been removed from the market due to cardiotoxic effects. By principle, the human cardiomyocyte is the best test substrate for drug screening application in both contexts. On the other hand, the availability of non-failing human primary cardiomyocytes at a large scale is not realistic and is limited by multiple factors. The availability of suitable donors is limited, variability among different donors and preparations is high, and lack of proliferation capability of cardiomyocytes leads to the inability to generate cardiomyocyte cell lines derived from primary cells. This led to the reliance of cardiac drug development applications on animal models, animal-derived heart tissue preparations and cardiomyocytes, and heterologous expression systems.

Nevertheless, human cardiomyocytes are far different from other animals with respect to gene expression and physiology, e.g. in mice, beating rate is high (500 beats per minute (BPM) vs. 60 BPM in humans), action potential duration is short, positive force-frequency relation is lacking and ion channels are expressed differently (Doevendans et al. 1998; Morano 1999; Nerbonne and Kass 2005; Davis et al. 2011). This results in low predictivity for the effects in humans. For example, predictive accuracy of toxicity in humans extrapolated from rodents and non-rodent's data is 43 and 63%, respectively (Olson et al. 2000). Mice have been shown to be 10-fold more tolerant to 37% of drugs than humans (May et al. 2009). Rats and dogs are also less sensitive and can tolerate 4.5- to 100-fold of the therapeutic concentration of many chemotherapeutic agents e.g. actinomycin-D, myleran, mithramycin, mitomycin C and fludarabine (Price et al. 2008).

Cardiac safety assessment recommendations for *in vitro* and *in vivo* analysis are stated in the ICH guideline S7A (ICH Expert Working Group 2000). Recommended *in vivo* analyses include measurement of heart rate and blood pressure, histopathology and electrocardiography (ECG). These tests evaluate many cardiac side effects but do not involve direct effects on cardiac contractility. The most accepted approach to evaluate cardiac contractility *in vivo* is the measurement of systolic left ventricular pressure (dp/dt) in instrumented animals. However, this parameter is also considered to be affected by heart rate, and pre- and after-load according to some authors (Markert et al. 2007; Hamlin and del Rio 2012) and does not give the direct assessment of cardiac contractility. *In vivo* analyses are further limited by species-dependent differences and low throughput. Diverse *in vitro* models have been established to evaluate the effects of drugs on cardiac contractility. Force measurement in isolated perfused heart preparations was established by Langendorff in 1897 (Langendorff 1895, 1903). This model has been used to study drug effects on contractility, heart rate and ECG in guinea-pig, rabbit and rat hearts. Unlike the *in vivo* experiments, the Langendorff perfused hearts enable for the assessment of the direct contractility. Furthermore, it allows for rate-controlled measurements. However, this model is devoid of afterload resistance (Belz et al. 1988; Vandecasteele et al. 1999; Schulz and Schmoldt 2003). Additional *in vitro* models like isometric contraction measurement by force transducers have been established to study drug effects on contractility of guinea pig, rabbit and rat ventricular tissues in isolated tissue bath assays under isometric conditions (Sossalla et al. 2010; Jackman et al. 2016; Shadrin et al. 2017). Other tissue preparations for contractility analysis include isolated atria, trabeculae and papillary muscle (Honerjäger et al. 1986; Scholz et al. 1987; Heller et al. 1989; Eschenhagen et al. 1991).

ICH guideline S7b recommends assays for *in vitro* analysis to identify compounds during preclinical drug development which trigger arrhythmia in humans (ICH Expert Working Group 2005). It is based on the analysis of drugs on the hERG channels that mediate delayed rectifier potassium current (I_{kr}).

Drugs with hERG channel inhibitory effects can lead to prolongation of the action potential and consequently arrhythmias. ICH guideline S7b recommends a primary screening in a heterologous expression system (hERG channel assay), telemetry study in instrumented dogs and confirmatory experiments in rabbit Purkinje fibres. Heterologous expression models are based on aneuploid cell lines i.e. human embryonic kidney (HEK) 293 cells, engineered to overexpress single ion channels. Despite the high throughput of this system, the model does not replicate the complexity of human cardiomyocytes and can lead to false positive results. As an example, verapamil is considered safe on account of dual blockage of potassium (I_{kr}) and calcium channels ($I_{Ca,L}$), but can be identified as a potentially harmful drug on the basis of single ion channel assays (Meyer et al. 2004).

1.3. hiPSC as a new tool

Given the limitations of animal assays described above, considerable effort has been invested to find additional tools for drug safety screening. Human induced pluripotent stem cell (hiPSC) technology offers exciting opportunities in the context of cardiac drug development. The hiPSC technology was established by the group of Shinya Yamanaka in 2007 (Takahashi et al. 2007). They identified factors that reprogram differentiated human cells into pluripotent stem cells and have the capability to differentiate in all cell types of the human organism. This has boosted the development of different protocols to differentiate hiPSC to functional human cardiomyocytes (Zhang et al. 2009; Burridge et al. 2011). Initially, these protocols were limited by an insufficient purity of cardiomyocytes and inefficient differentiation efficiency. Follow-up studies relied on key steps of mammalian *in vivo* embryonic heart development, with cocktails of growth factors and small molecules to induce first mesodermal progenitors and then cardiomyocytes (Yang et al. 2008). One decade after the discovery of hiPSC, this effort led to highly scalable and efficient cardiac differentiation protocols (Burridge et al. 2014; Zhang et al. 2015; Kempf et al. 2016; Breckwoldt et al. 2017) .

1.3.1. Differentiation of hiPSC into cardiomyocytes

From a biotechnological point of view, differentiation protocols can be categorized as two-dimensional (2D) monolayer protocols and three-dimensional (3D) embryoid body (EB)-based protocols. hiPSC have the property to self-assemble and form EBs which spontaneously differentiate into all three germ layers, provided the pluripotency factors are removed. This supported the idea of differentiation of pluripotent stem cells into specific lineages of the three germ layers (Desbaillets et al. 2000; Itskovitz-Eldor et al. 2000). EB generation can be supported by various ways including suspension culture, culture in round bottom 96-well plates, and rotating spinner flasks. Culture in rotating spinner flask gives rise to upscaling with high yield of cardiomyocytes (Kempf et al. 2015; Hartman et al. 2016; Breckwoldt et al. 2017). While 3D protocols are laborious during the first steps

and include an additional step for the EB generation, the cultures are very easy to handle and EBs are stable after formation and mesoderm induction. On the other hand, 2D protocols are less laborious during the first steps but have less potential for scale-up and greater chance of cell loss at the end of the differentiation when the monolayer of cardiomyocytes is beating (Eschenhagen et al. 2015; Kondrashov et al. 2018).

In both protocols, directed cardiac differentiation can be achieved by the addition of defined growth factor/small molecule cocktails in specific media to sequentially induce mesodermal and cardiac differentiation. Mesodermal induction is accomplished by the activation of NODAL signalling, Activin A, transforming growth factor-β (TGF-β) and/WNT signalling (Gsk3, CHIR99021). Cardiac lineage is then derived by the inhibition of canonical WNT signalling pathway (XAV939, IWR). Figure 3 depicts differentiation stages and factors involved in each stage (Willems et al. 2011; Burridge et al. 2012).
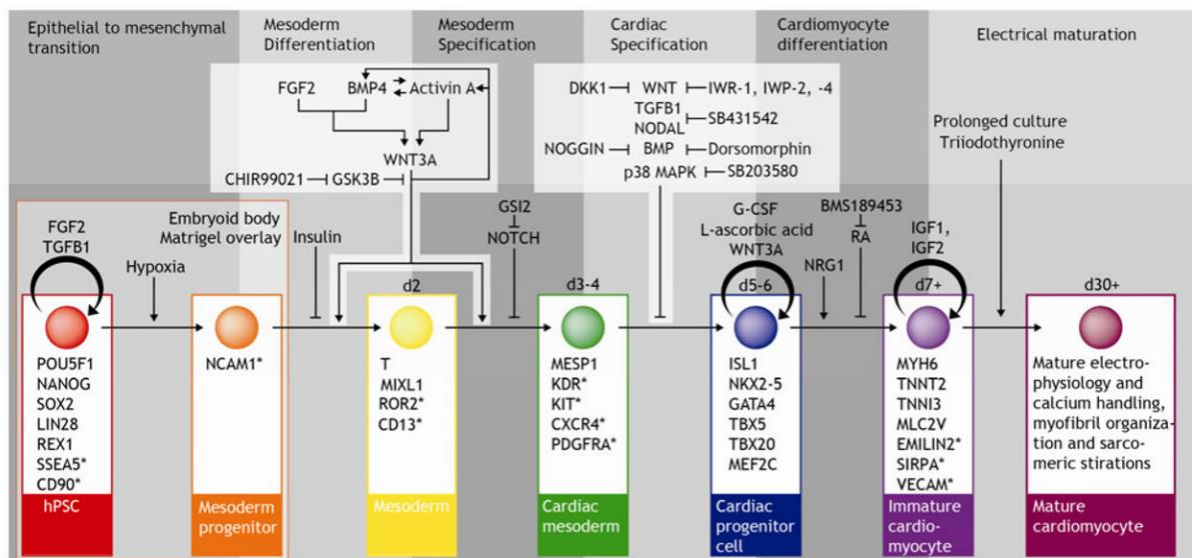
Figure 3: Schematic depiction of differentiation of hiPSC into cardiomyocytes with detailed knowledge of factors involved in different stages of differentiation (Burridge et al. 2012)

1.3.2. **Immaturity of hiPSC**

With the availability of hiPSC-CMs, the inherent limitation of species-dependent differences of all animal models was overcome. Nevertheless, hiPSC-CMs do have limitations as they primarily exhibit a very immature state resembling *in vivo* cardiomyocytes of fetal/neonatal but not adult state. hiPSC-CM immaturity is a multifaceted phenotype and comprises poorly organized short sarcomeres (hiPSC-CM 1.6 μm vs. adult CM 2.2 μm), chaotic myofilament alignment, immature mitochondria, poorly developed sarcoplasmic reticulum and lower cytoplasmic mitochondrial content. hiPSC-CM also lack

t-tubules, intercalated discs, binucleation and rod shape morphology. hiPSC-CM gene expression resembles the fetal heart (van den Berg et al. 2015) and shows abundant troponin I1 (fetal ssTnI), titin isoform N2BA and α-myosin heavy chain (MYH6) in contrast to troponin I3 [cTnI], titin isoform N2B and β-myosin heavy chain 7 (MYH7) in adult heart. Moreover, ryanodine receptor, SERCA, PLN and calsequestrin are expressed at lower levels in hiPSC-CM than in adult CM. On the functional front, these immature cells show higher levels of the pacemaker current I_f and spontaneous beating and lower levels of inward rectifying potassium current I_{kr} (reviewed by Denning et al. 2016). Furthermore, hiPSC-CM develop low baseline force, exhibit a narrow inotropic range, negative force-frequency relationship, weak post rest potentiation and small CaTs. In the metabolic context, hiPSC-CM mainly rely on glycolysis of glucose as compared to oxidation of lactate and fatty acids in adult CM (Blazeski et al. 2012; Rajamohan et al. 2013; Yang et al. 2014a; Denning et al. 2016).

1.3.3. Improvement in the maturation of hiPSC

Many attempts have been made to improve the maturation status of hiPSC-CM by supplementing media with growth factors, neurohormonal factors, bioactive lipids, electrical pacing, mechanical load, increased time of culture, 3D culture and dynamic 3D floating cultures (Denning et al. 2016; Jackman et al. 2016; Sharma et al. 2018).

Maturation: Humoral maturation of hiPSC-CM

Different biochemical factors have the potential to improve maturity. Human embryonic stem cells (hESC-CM) were subjected to the α-adrenoceptor agonist phenylephrine (PE, 10 µM) treatment for 48 h and showed increased cellular size and organized sarcomeres. The PE-mediated effect on cell size was completely blocked by inhibitors of p38–MAPK, mTOR or calcineurin/FKBP, indicating the involvement of known hypertrophic pathways (Földes et al. 2011). This aligns with earlier studies which demonstrated that norepinephrine (α- and β-AR agonist) increases protein synthesis in neonatal rat ventricular myocytes, and neonatal and fetal mouse myocytes (Müller et al. 2000).

Triiodothyronine (T3) plays a role in cardiac development (Krüger et al. 2008) and insulin-like growth factor-1 (IGF-1) is involved in the regulation of differentiation, proliferation and maturation (Ito et al. 1993; Montessuit et al. 2006). hiPSC-CMs in monolayer format were subjected to T3 treatment for one week and showed morphological evidence for improvement by enhancement in cellular anisotropy, size and sarcomeric length. Force (analysed in individual hiPSC-CMs using micropost-arrays) was 2-fold higher and contractile kinetics were improved (i.e. smaller time to contraction and relaxation) (Yang et al. 2014b). In another study, chemical differentiation of hiPSC into CM was supplemented with T3 and dexamethasone at day 16-30 followed by 5 days culture on

Introduction

Matrigel mattresses, and formation of an extensive T-tubule network was demonstrated. Functional improvement was identified by large calcium sparks and enhanced CICR, which was confirmed by simultaneous measurement of I_{Ca} and cytoplasmic calcium (Parikh et al. 2017).

Sphingosine-1-phosphate (S1P) and lysophosphatidic acid (LPA) improved cardiomyocyte production (2- to 3-fold more cardiac troponin T positive cells) when applied during early stages of the differentiation. SIP and LPA enhanced mesodermal induction, as evidenced by the nuclear accumulation of β-catenin (mediator of canonical WNT signalling) and synergism with CHIR99021 (glycogen synthase kinase 3 beta inhibitor). Furthermore, SIP and LPA application together with CHIR99021 enhanced the CHIR-mediated proliferation of hiPSC, demonstrated by increased cell number and phospho-histone H3 (proliferation marker) expression (Sharma et al. 2018). Altogether, these examples indicate that humoral factors can improve the maturation of hiPSC-CM, but no combination of humoral factors have been discovered to date which lead to an adult-like state.

Maturation: Tissue engineering and/or mechanical loading

Myocardium consists of myofibers that comprise of a three-dimensional, longitudinal arrangement of rod-shaped cardiomyocytes. Due to the rhythmic cardiac beating, cardiomyocytes are subjected to constant mechanical strain mediated by the resistance of circulating blood. The importance of mechanical loading was established by several studies. The effect of unidirectional stretch on cardiomyocyte biology was identified on neonatal rat cardiomyocytes. This led to the unidirectional cellular organization, increased bi-nucleation, rod-shaped morphology and hypertrophied cells (Vandenburgh et al. 1996). In line with this, Kira et al. reported increased cell size, cellular organization, protein synthesis and mitochondrial content by prolonged mechanical stimulation (Kira et al. 1994). An axial stretch model showed an increase in reactive oxygen species (ROS) production and mitochondrial membrane potential in mouse cardiomyocytes (Iribe et al. 2017). In addition to the importance of mechanical loading for cardiomyocyte biology the identification of cardiomyocyte ability to assemble to each other and form aggregates was an important prerequisite for cardiac tissue engineering technologies (Halbert et al. 1971; Lieberman et al. 1972; Purdy et al. 1972).

Several protocols have been established to generate engineered heart tissues (EHTs), i.e. by using a solid matrix (e.g. poly glycolic acid), preformed matrix (e.g. from pig hearts), a stack of matrix-free cell sheets and liquid hydrogels (e.g. fibrin, collagen I and Matrigel) with preformed casting molds. The first force generating, spontaneously beating EHTs were generated with collagen I as hydrogel and heart cells from embryonic chicken, cultured between Vecro-coated glass rods. These biconcaval constructs displayed highly organized myofilaments (Eschenhagen et al. 1997). The principle was taken forward to demonstrate the effects of chronic unidirectional stretch on collagen-based EHTs

made from chicken embryonic cardiomyocytes/neonatal rat cardiomyocytes. Increase in alpha-sarcomeric actin, cell length and width, and improved cellular alignment was reported (Fink et al. 2000). In the following years, Zimmermann et al. 2002 developed the protocol to cast collagen/Matrigel-based EHTs in circular molds and exposed them to phasic mechanical stretch. These native neonatal rat-derived EHTs regained adult characteristic features and histological analysis showed longitudinally oriented cardiac muscle bundles resembling native tissue. This technology was further improved to generate miniaturized 24-well format fibrin-based EHTs attached to polydimethylsiloxane (PDMS) posts and to develop an automated video-optical based system to analyse contraction parameters of EHTs. Flexible PDMS posts exert directed mechanical and auxotonic load. In this format, cardiomyocytes showed alignment along force lines (Hansen et al. 2010), it is based on a standardized protocol to generate EHTs and allows for sterile, manipulation-free and automated measurements of contractile force.

Tissue engineering enhances cell-to-cell interaction by using hydrogels and provides a 3D environment until cells form contact with each other and create their own extracellular matrix. hiPSC-CMs in three-dimensional EHT model have demonstrated morphological, structural, electrophysiological and metabolic maturity compared to 2D CM. hiPSC-CM EHTs have shown muscle bundles containing cross-striated near-adult shape CM with well-organized sarcomeres and high mitochondrial density (Mannhardt et al. 2016). Metabolically, hiPSC-CM in EHT format can use glucose, lactate and fatty acid as an energy substrate by oxidative metabolism and showed less anaerobic glycolysis (Ulmer et al. 2018). EHT format has also shown maturation on an electrophysiological level with a 1.8-fold increase in sodium current density (-18.5 ± 1.9 pA/pF) as compared to 2D-CM and a physiological upstroke velocity similar to adult human left ventricular tissues (219 ± 15 V/s; Lemoine et al. 2017). The increase in LTCC current ($I_{Ca,L}$) density upon β-adrenoceptor stimulation was larger in EHT than in 2D monolayer culture, but smaller than in adult atrial cardiomyocytes (Uzun et al. 2016).

In other attempts to improve hiPSC-CM maturation, tissues were generated by seeding hESC/hiPSC-CM embedded in collagen/Matrigel around a surgical suture thread and were subjected to electrical stimulation (up to 6 Hz) after 7 days of culture (Nunes et al. 2013). All analyses were compared to age-matched EBs. Such tissues showed an increase in size of CM, ultra-structural organization and number of mitochondria, and exhibited more elongated cells. Genetic expression analysis showed decreased levels of atrial natriuretic peptide (ANP), brain natriuretic peptide (BNP) and α-MHC (MHC 6) and upregulation of potassium inwardly-rectifying channel KCNJ2 (Kir2.1). Electrophysiologically, these electrically stimulated tissues displayed a smaller excitation threshold, larger capture rate and conduction velocity. The functional analysis provided further evidence of maturation by displaying calcium handling properties indicative of the functional sarcoplasmic

reticulum and higher CaT response to caffeine. A further contribution to the cardiac tissue engineering field was made by generating 7x7/18x18 mm 3D fibrinogen-based cardiac patches. Small cardiac patches showed >5 mN and large patches >20 mN force, approaching adult human myocardium (Shadrin et al. 2017). To improve the maturity of hiPSC-CM, metabolic selection of cardiomyocytes was done at the end of differentiation by removal of glucose and supplementation of lactate. Additionally, periodic serum-free cell culture was executed. These patches showed uniform cell density and robust electrical coupling throughout the patch despite their large size. Cardiomyocytes in these patches showed ubiquitous t-tubules, H-zones and I-bands. Implantation of the cardiac patch in the dorsal skinfold window in nude mice resulted in vascularization of the cardiac patch with the host blood vessels. These cardiac patches, when grafted onto rat hearts, maintained their pre-implantation electrical properties and did not induce arrhythmias. Despite substantial improvement in maturity, functional coupling of host vs. graft was lacking (Shadrin et al. 2017). Recently, Leonard et al. cultured cardiomyocytes in an enhanced afterload model by casting EHT with one flexible and one solid PDMS post to increase load during culture by using braces of varying resistance. They were able to demonstrate enhanced auxotonic twitch forces with an increase in afterload. The morphological improvement was evident by hypertrophy, an increase in sarcomeric length and elongated cardiomyocytes (Leonard et al. 2018).

Cultured cardiomyocytes have a high metabolic turnover, this can lead to depletion of nutrients and oxygen. This can be particularly critical for EHTs where cells are packed in the hydrogel and are not in direct contact with the liquid phase. Dynamic, free-floating culture of fibrin-based engineered cardio bundles of hiPSC- and neonatal rat-CMs have been used to enhance the nutrient availability and led to increase in CM size, sarcomeric proteins and contractile force (Jackman et al. 2016). Taken together, these findings indicate substantial improvement in the degree of maturity of hiPSC by mechanical loading.

Maturation: Cellular composition

The human heart is not composed of cardiomyocytes alone, but represents a composition of non-myocytes and cardiomyocytes. This interaction likely affects maturation directly or indirectly. The co-culture with non-myocytes led to increased electrophysiological maturation and ion channel development (HCN4) in hESC-CM (Kim et al. 2010). When cultured with cardiac fibroblasts in a 2:1 ratio (cardiomyocytes: cardiac fibroblasts), 3D cardiac minitissues showed improvement in the cell-cell and cell-matrix interactions, evident by abundant integrin-β1 and connexin-43. These tissues phenotypically resembled native-heart and exhibited elongated fibres with frequent sarcomeric TnI and α-actinin positive cells (Saini et al. 2015). In addition to fibroblasts, addition of endothelial cells to

collagen-based EHTs generated from hESC-CM in a uniaxial mechanical stretch model enhanced cardiomyocyte proliferation and DNA synthesis. Co-culture with endothelial and/or human marrow stromal cells also led to the formation of vascular network in cardiac constructs (Tulloch et al. 2011). In another study, cardiac microtissues were developed in round bottom 96-well plates in combination with cardiac fibroblast and endothelial cells (Ravenscroft et al. 2016). These microtissues provided evidence for mature contractile phenotype by displaying enhanced CaT amplitudes, larger spontaneous contraction rate and contraction force in response to positive and negative inotropic compounds than microtissues containing CM only. In addition, these microtissues showed higher expression of genes (S100A1, telethonin/TCAP) encoding for proteins critically important for calcium handling and sarcomeric assembly, respectively. Recently, morphological and functional improvements were reported by modulating the cellular composition of engineered cardiac tissues and by the use of defined feeding media (Tiburcy et al. 2017). These engineered cardiac tissues showed increase force when casted by combining CMs with human foreskin fibroblasts in a ratio of 70%/30%. Positive force-frequency relationship was demonstrated with modified serum free feeding media which was absent in the standard culture media with serum. This modified serum-free media included 4% B27 (without insulin), TGF-β1, fibroblast growth factor-2 (FGF-2), IGF-1 and vascular endothelial growth factor (VEGF).

Maturation: Culture duration

Maturity of cardiomyocytes can be improved by culturing cells for longer duration. Prolonged (80-120 days) low-density-seeded culture of hiPSC- and ESC-CM showed maturation of structural, contractile and morphological features (Lundy et al. 2013). These CMs demonstrated a high degree of anisotropy, increased cell size, longitudinal cell shape, greater sarcomere alignment and increased fraction of multinucleated CMs. On the functional front, older cultures showed a 2-fold increase in contraction, and decrease in contraction kinetics. Despite these improvements, β-adrenergic stimulation mediated positive inotropic effect (PIE) was absent which is a fundamental functional characteristic of the native human heart. In the following years, culture time was extended further up to 1 year and these cells showed increased cell size, better organized long sarcomeres and increased transcript level of cardiac markers (Kuppusamy et al. 2015). However, such longer preanalytical culture periods are not feasible for many applications. In addition, only very few cells developed a well-structured mature phenotype.

Maturation: Electrical stimulation

In vivo cardiomyocytes are constantly exposed to electrical signals for synchronous contractions and relaxations. Continuous electrical stimulation of hiPSC-CM EHT displayed elongated cardiomyocytes

with the high cytoplasm-to-nucleus ratio. These structural changes were accompanied by functional maturation indicated by 1.5-fold more force than non-stimulated control group (Hirt et al. 2014). In line with this, in another study, hESC/hiPSC-CM tissues ("biowires") were generated and subjected to electrical stimulation (up to 6 Hz) after 7 days of culture. All analyses were compared to age-matched EBs. These tissues demonstrated many signs of morphological and electrophysiological maturity as compared to their counterpart controls (discussed in detail in paragraph for "Tissue engineering and/or mechanical loading" (Nunes et al. 2013). In another attempt to improve maturation, Ruan et al. studied the effect of electrical stimulation (2 Hz) and static stretch on hiPSC-CM embedded in a collagen matrix and demonstrated increased contractility reaching 1.34 ± 0.19 mN/mm^2, and increased RyR and SERCA expression as compared to static stress application or electrical stimulation alone. Although this study provided evidence for the importance of synergistic approaches to improve maturation, it demonstrated a negative force-frequency relationship (Ruan et al. 2016). In a recent study, two maturation approaches (co-culture with non-myocytes and electrical stimulation) have been implemented together to increase maturation. Cardiac tissues generated with 75% CM, 25% fibroblasts and subjected to ramped electrical stimulation demonstrated remarkable ultrastructure organization, t-tubules, longer sarcomeres (2.2 µm), increased mitochondrial density, oxidative metabolism and positive force-frequency relationship (Ronaldson-Bouchard et al. 2018).

1.3.4. <u>Regulation of β-adrenergic signalling</u>

Contractile force is regulated by β-adrenoceptors as mentioned in section 1.1. PDE restrict β-adrenergic signalling in the heart by hydrolyzing cAMP. Molecular and functional analysis have revealed PDE3 and 4 as the most relevant isoforms in rodent cardiomyocytes (Johnson et al. 2012), whereas in the human heart PDE3 has been identified as the major contributor (Richter et al. 2011). Consequently, selective PDE3 inhibition in human atrial trabeculae increased force and $I_{Ca,L}$ while inhibition of PDE4 did not show any effects (Berk et al. 2016). In human ventricular trabeculae, PDE3 and 4 inhibition had no effects alone, but β1- and β2-adrenoceptors-mediated PIE and positive lusitropic effects were potentiated (Molenaar et al. 2013). Altogether, these findings indicate that PDE3 is the dominant isoform in the adult human heart (Eschenhagen 2013). A previous study by our group revealed a strong PIE of PDE4 inhibition by rolipram and a small effect of PDE3 inhibition by milrinone in the hiPSC-CM EHTs, suggesting differential PDE regulation in hiPSC-CM than in the human heart (Mannhardt et al. 2017a).

1.4. *In vitro* contractility assays

Many methods have been described to measure contraction of hESC-/hiPSC-CM. Atomic force microscopy measures the relative repulsion of a cantilever during contraction (Liu et al. 2012); mechanical force transducers connected to engineered constructs measure force under isometric conditions (Zhang et al. 2013; Ruan et al. 2016). Video-based edge detection systems (e.g. those developed by IonOptix) measure the movement of a selected point of the hiPS-CM monolayer (Pointon et al. 2015). Traction force microscopy, another image-based system, estimates the contraction force of single cardiomyocytes by measuring the deflection of fluorescent beads embedded in a polyacrylamide gel (Jacot et al. 2010; Ribeiro et al. 2015). Video based contractility analysis calculates force based on tissue shortening (Ronaldson-Bouchard et al. 2018) or movement of fluorescent, flexible, PDMS micro-posts (Yang et al. 2014b; Hinson et al. 2015). Impedance assays measure deviations in electrical impedance in relation to voltage applied to electrodes underneath the cellular monolayer (Abassi et al. 2012; Navarrete et al. 2013; Nunes et al. 2013; Guo et al. 2013; Scott et al. 2014).

In our laboratory, a video-based optical system was established to analyse the contractility of EHTs (Hansen et al. 2010). This contractility system includes a customized software that controls the movement of the camera via X, Y and Z axis and films EHT for a defined period of time (Figure 4). The software algorithm detects the top and bottom ends of the EHT marked with blue squares and analyses contraction by monitoring the deflection of the two PDMS posts (Hansen et al. 2010; Mannhardt et al. 2017b).
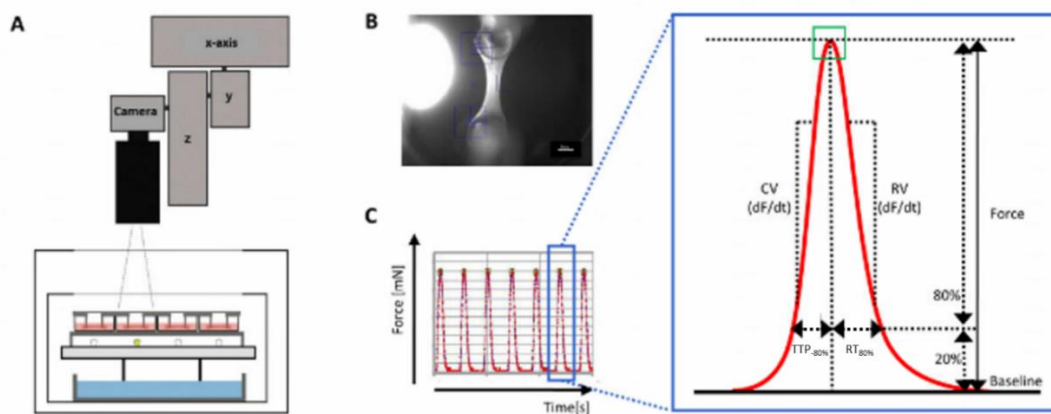
Figure 4: Schematic depiction of contraction analysis set-up for engineered heart tissue (EHT). (A) Analysis set-up with gas and temperature regulated incubation chamber with 24-well cell culture plate containing EHTs attached to PDMS rack. Computer controlled camera above the incubation chamber positions the defined well and makes videos of the beating EHT. (B) Live image of EHT during recording. (C) Exemplary contraction peaks showing the force of EHT over 10-second duration. The magnified region shows the parameters of contraction analysed by custom-made software including force, time to peak force (TTP$_{-80\%}$), relaxation time (RT$_{80\%}$), contraction velocity (CV) and relaxation velocity (RV). Figure adapted from Mannhardt et al. 2017b.

1.5. *In vitro* calcium transient assays

The video-optical based system analyses contractions of EHT from neonatal rat heart cells and hiPSC-CM (Hansen et al. 2010; Mannhardt et al. 2017b) with great sensitivity. Nevertheless, force is a complex read-out and is affected by changes of the action potential, CaT and myofilaments. Additional CaT measurements of cytoplasmic calcium during contraction and relaxation phase of ECC can improve the scope of the assay.

CaT is conventionally analysed by loading cells with calcium-sensitive dyes. The loading with dyes can be done immediately before an experiment, but it is more difficult to standardize and shows higher variability particularly in preparations that are more complex. Dyes are either non-ratiometric (fluo 4, fluo 4FF, fluo 2MA) or ratiometric (fura 2, fura 4F). Ratiometric dyes show better signal to noise ratios and are less affected by baseline shifts. On the other hand, the excitation with two different wavelengths for ratiometric measurements requires a more sophisticated experimental set-up (Orchard and Lakatta 1985; Congwu et al. 2001; de Lange et al. 2013). Although some dyes offer faster on- and off-kinetics, calcium imaging is complicated due to the low penetration of dyes into the tissues, chemical toxicity and extrusion of dye out of the cell during long measurements (Palmer and Tsien 2006; Rehberg et al. 2008; Kaestner et al. 2014).

CaTs have been analysed in hESC/hiPSC-CM by using fluorescent dyes such as fura 2 (Pointon et al. 2015), fluo 4 (Sanchez-Freire et al. 2014) and FLIPR® (Grimm 2018) in single cells; fura 2-AM (Mummery 2003) in monolayer culture; and fluo-4 (Ronaldson-Bouchard et al. 2018), fluor 4-AM (Ruan et al. 2016) and fura 2 (Stoehr et al. 2014) in EHTs. Most of the CaT data has been derived by fluorescent imaging or confocal imaging-based set-ups, measurement systems and data analysis softwares used to analyse CaT vary between the different laboratories. Our group has previously established the analysis of CaT with fura-2 AM. While this set-up allowed us to analyse CaTs at baseline, variability in loading, bleaching and run down hindered the characterization of drug effects.

1.5.1. Genetically encoded calcium indicators

Genetically encoded calcium indicators (GECIs) represent a relatively new group of calcium sensors and are becoming popular due to compelling advantages over organic dyes (Broussard et al. 2014; Kim and Jayaraman 2014; Gong et al. 2015). GECIs are expressed in CMs with the help of viral vehicles thereby the problematic issue with variable intracellular loading was resolved. Viral transduction, however, requires at least a few days for the GECIs to be expressed resulting in a higher chance of off-target toxicity. GECIs have also other nominal advantages, i.e. cell-specific calcium imaging and

stable expression (over weeks to months) that allows repetitive measurements and can be very useful particularly for disease modelling (Song et al. 2015; Mao et al. 2018). However, slow on- and off-kinetics are an inherent limitations of GECIs and are being addressed by the development of a new generation of fast-acting GECIs e.g. GCaMP6, YC3.6 and TN-XL (Kaestner et al. 2014).

The first protein-based indicator used to analyse calcium changes was aequorin that was extracted from the jellyfish. This technology flourished with the development of new fluorescent proteins (FP) based GECIs. They are comprised of sensing/binding domain and a reporter consisting of one or two FP. In the case of single FP-based sensors such as GCaMP, calcium binding to the binding moiety of the sensor changes the chromophore environment of the FP, leading to decrease or increase in the fluorescence intensity (Figure 5; Nakai et al. 2001; Akerboom et al. 2012). In the two FP-based sensors, changes in the sensing or binding domain lead to FRET (Förster resonance energy transfer) with overlapping spectra for absorption and emission. Single FP-based sensors have a high signal to noise ratio (SNR) compare to their counterpart FRET-based sensors which have gained them a lot of interest (Badura et al. 2014). In addition, FRET-based sensors have the advantage of lack of motion artefacts due to ratiometric imaging, which is a major challenge when using single FP-based sensors. These motion artefacts can be overcome with the use of reference fluorophores. Moreover, pharmacological methods are also available to overcome motion artefacts such as myosin inhibitors 2,3-butanedione monoxime (BDM) and blebbistatin that reduce movement of the cells. However, pharmacological inhibition of myosin may have profound effects on the investigation of arrhythmia mechanisms (Herron et al. 2012).
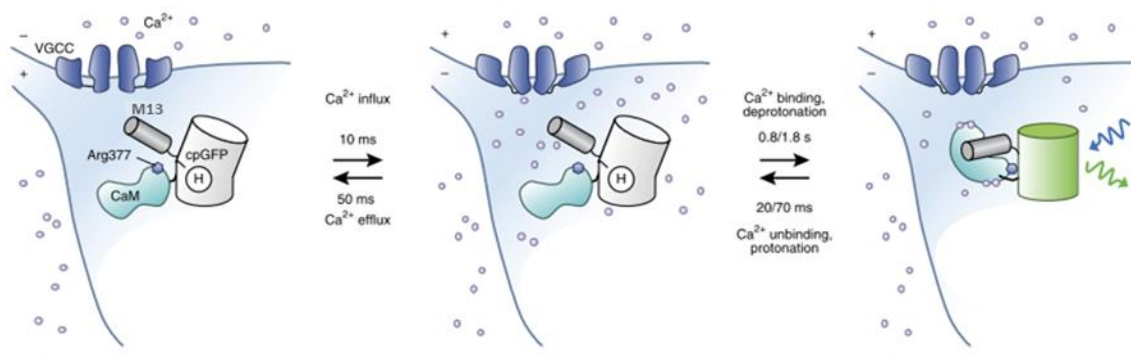
Figure 5: Schematic illustration of GCaMP response to calcium with increased fluorescence. Calcium (small closed circles) enters the cell through the open voltage-gated calcium channels (VGCC) at 1st-time point. Calcium-induced binding of calmodulin to M13, a peptide from myosin light chain kinase (MLCK), changes the position of M13 resulting in deprotonation of the chromophore at the 3rd time point. This is followed by a shift in the absorption spectra and emission of green light (~510 nm) upon excitation with blue light (~488 nm) (Adapted from Lin and Schnitzer 2016).

GECIs was used recently for CaT measurement in cardiomyocytes. GCaMP6f has been used to image calcium sparks in dyads of adult rat cardiomyocytes (Shang et al. 2014). HESCs have been transduced to stably express GCaMP3 to map CaT from the myocardial grafts (Shiba et al. 2012). Recently R-GECO1 was expressed in hiPSC-CM by using a lentiviral vector to analyse CaT. However, this analysis was limited to determining the number of CaT per minute and did not provide a quantitative description of the time of calcium rise and decay (Song et al. 2015).

1.6. Disease modelling and possibility to combine with CRISPR Cas9

The hiPSC technology has become a powerful tool to study different inherited cardiac diseases in human-derived cardiomyocytes, without the biases of interspecies differences. Many such attempts have been made to model different diseases in hiPSC i.e. ion channel mutation related arrhythmias have reported similarities between clinical data and corresponding hiPSC disease models (Moretti et al. 2010; Itzhaki et al. 2011; Sinnecker et al. 2013).

The EHT technology offers an exciting opportunity to combine it with the CRISPR Cas9 system and establish isogenic controls of disease models differing only in the mutation but having the same genetic background (Mosqueira et al. 2018). This advancement has gained interest from the pharmaceutical companies to replace suboptimal drug safety assessment with the physiologically relevant human cardiac cells of the respective disease lines.

2 <u>AIM OF THE THESIS</u>

Many drugs have been withdrawn from the market or excluded during the drug development process due to cardiotoxic effects. Current preclinical safety assessment relies on artificial ion channel modulation assays in cell lines and animal models and are considered suboptimal, in terms of both sensitivity and specificity, the latter leading to unnecessary failure during drug development. Reasons include limited complexity of the cell culture systems, limited functional readout and, in case of animal experiments, species differences. Unlimited and efficient supply of hiPSC-CM and cardiac tissue engineering techniques that improve the maturity of hiPSC-CM provide an opportunity for the development of hiPSC-CM based-pre-clinical drug screening assays and may overcome at least some of the limitations of currently used assays. The video-optical analysis of EHTs detects effects of drugs on contractile function without providing information about the potential mechanisms. Parallel analysis of CaT would increase the value of the assay. Therefore, the aim of this thesis was 1) to establish an automated, high throughput, new generation of the EHT drug screening system to sequentially analyse contraction and CaT by using GECIs, 2) to validate the system by testing a set of indicator compounds, 3) to reaffirm the system by blinded screening of 27 compounds in two hiPSC cell lines and 4) to investigate the maturity of EHTs with respect to phosphodiesterases.

3 MATERIALS AND METHODS

More details on reagents, materials and devices used is included in the supplement section.

3.1. Media compositions

Table 1: Culture media compositions and storage details.

Medium	Composition
EB-based differentiation	
FTDA (bFGF, TGF-β1, dorsomorphin and Activin A-based hiPSC culture medium for EB-based differentiation)	DMEM/F12 without glutamine Transferrin 5 mg/l L-glutamine 2 mM Human serum albumin 0.1% (v/v) Sodium selenite 5 µg/l Human recombinant insulin 5 mg/l Lipid mix 1/1000 (v/v) Activin A 2.5 ng/ml Dorsomorphin 50 nM bFGF 30 ng/ml Transforming growth factor-β 1 (TGF-ß1) 0.5 ng/ml Penicillin/streptomycin (optional) 0.5% (v/v) The sterile filtered medium was stored at 4 °C for maximum one week and was supplemented with bFGF immediately before use.
EB formation medium	FTDA Polyvinyl alcohol 4 mg/ml in 1x PBS Y-27632 10 µM The freshly prepared medium was always used.
Mesoderm induction medium	RPMI 1640 HEPES (pH 7.4) 10 mM Polyvinyl alcohol 4 mg/ml Human serum albumin 0.05% (v/v) Phosphoascorbate 250 µM Lipid mix 1/1000 (v/v) Transferrin 5 mg/l Sodium selenite 5 µg/l Y-27632 10 µM BMP-4 10 ng/ml Activin A 3 ng/ml bFGF 5 ng/ml Sterile filtered medium (0.2 µm filter) was stored up to 1 week at 4°C without growth factors and was used after supplementation with growth factors (BMP-4, Activin A, bFGF)
Mesoderm induction washing medium	RPMI 1640 HEPES 10 mM Polyvinyl alcohol 4 mg/ml Penicillin/streptomycin (optional) 0.5-1% (v/v)
Cardiac specification washing medium	RPMI 1640 HEPES (pH 7.4) 10 mM Penicillin/streptomycin (optional) 0.5% (v/v)
Cardiac specification medium I	RPMI 1640 HEPES 10 mM Phosphoascorbate 250 µM Lipid mix 1/1000 (v/v) Transferrin 5 mg/l Sodium selenite 5 µg/l

	Y-27632 1 µM XAV939 1 µM or DS-I-7 100 nM Human serum albumin 0.05% (v/v) Penicillin/streptomycin 0.5% (v/v) Sterile filtered medium (0.2 µm filter) was stored up to 1 week at 4°C without XAV939/DS-I-7, which were added freshly.
Cardiac specification medium II	RPMI 1640 1-Thioglycerol 500 µM HEPES (pH 7.4) 10 mM Penicillin/streptomycin 0.5% (v/v) Y-27632 1 µM B27 with insulin 2% (v/v) XAV939 1 µM or DS-I-7 100 nM Sterile filtered medium (0.2 µm filter) was stored up to 1 week at 4°C without XAV939/DS-I-7 and B-27, which were added freshly.
Cardiac specification medium III	RPMI 1640 1-Thioglycerol 500 µM HEPES 10 mM Penicillin/streptomycin 0.5% (v/v) Y-27632 1 µM B27 with insulin 2% (v/v) The medium was filter sterilized (0.2 µm filter) and stored at 4°C for up to 1 week without B27, which was added freshly.
2D differentiation	
Day 1 medium (2D differentiation)	StemPro media StemPro supplement 26 µl/ml Matrigel 1:100 Glutamine 1:100 BMP-4 1ng/ml
Day 2 medium (2D differentiation)	StemPro media StemPro supplement 26 µl/ml Glutamine 1:100 BMP-4 10 ng/ml Activin A 8 ng/ml
Day 4 medium (2D differentiation)	RPMI 1640 1xB27 (-insulin) 2% (v/v) KY02111 10 µM XAV939 10 µM
Day 6 medium (2D differentiation)	RPMI 1640 1xB27 (+insulin) 2% (v/v) KY02111 10 µM XAV939 10 µM
Day 8 medium (2D differentiation)	RPMI 1640 1xB27 (+insulin)
EHT casting medium	DMEM Fetal calf serum (FCS), heat inactivated 10% (v/v) Penicillin/streptomycin 1% (v/v) 2 mM L-glutamine The medium was prepared freshly before use.
EHT culture medium	DMEM Horse serum 10% (v/v) Penicillin/streptomycin 1% (v/v) Human recombinant insulin 10 µg/ml Aprotinin 33 µg/ml The medium was prepared freshly before use.

Tyrode´s solution	NaCl, 120 mM
	NaHCO$_3$, 22.6 mM
	KCl, 5.4 mM
	glucose, 5 mM
	MgCl$_2$, 1 mM
	mM CaCl$_2$, 0.1-5
	NaH2PO$_4$, 0.4 mM
	Na$_2$EDTA, 0.05 mM
	HEPES 25 mM

3.2. Cardiac differentiation

3.2.1. 3D embryoid body-based differentiation protocol

Two hiPSC lines (ERC18 and C25) were differentiated in an embryoid body (EB) format by three-stage growth factor-based protocol recently published by our group (Breckwoldt et al. 2017). hiPSCs were expanded for 1 week before the start of differentiation which started with the homogenous EB formation using stirred spinner flasks with glass bulb impellers on magnetic rotors. Mesodermal induction was achieved by using a growth factor mix of Activin A, bFGF and BMP-4. This was followed by cardiac differentiation, induced by supplementing medium with insulin and by inhibiting the WNT signalling pathway (XAV939 or DS-I-7). Beating cardiomyocytes were observed by day 8-10. Differentiation protocol is described in detail in three steps. Figure 6 demonstrates the different steps involved in the EB-based differentiation protocol.

Step 1: Embryoid body formation

Spinner flasks were washed with distilled water and autoclaved before the start of differentiation procedure. HiPSCs were expanded for one week in T-80 flasks by passaging two times a week. 6.5×10^5 cells per cm^2 were seeded which gave rise to a density of 1.9×10^5 to 2.5×10^5 cells per cm^2. Cells were dissociated with EDTA after pre-treatment with 10 μM Y-27632 at 37 °C for 1 h and washed with 1xPBS. EB formation media was added and trituration was done to get a single cell suspension. The cell suspension was transferred to 50-ml Falcon tube, spun down at 250 x g for 5 min and was resuspended with EB formation medium. Cells were counted by using trypan blue dye and Neubauer chamber and resuspended in EB formation medium at a concentration of 30×10^6/100 ml EB formation medium. The cell suspension was added to spinner flasks and placed on the rotors with a speed of 40 rpm and incubated at 37 °C, 5% CO$_2$ and 5% O$_2$.
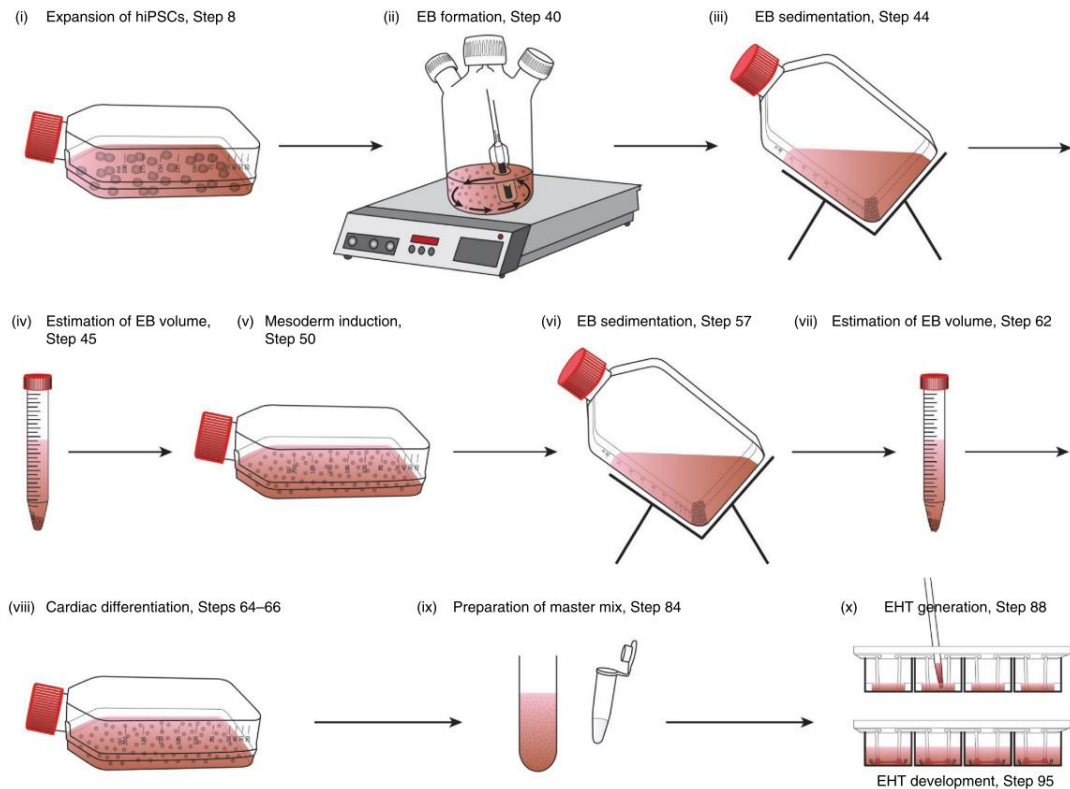
Figure 6: Schematic depiction of cardiac differentiation by embryoid body-based protocol. (i) Expansion of hiPSCs in Geltrex coated T80 flasks. (ii) Formation of EBs in spinner flasks. (iii) Sedimentation of EBs on V-shaped racks. (iv) Estimation of EB volume in graduated 15-ml Falcon tubes. (v) Transfer of EBs to Pluronic-F-127-coated T175 suspension flasks and supplementation with mesoderm progenitor induction growth factors (BMP4, bFGF and Activin A). (vi) EBs sedimentation. (vii) EB volume estimation (viii) Transfer to Pluronic-F-127-coated T175 suspension flasks and cardiac differentiation with small molecule WNT inhibition. (ix) Cardiomyocytes dissociation and preparation of fibrin-based master-mix for EHT generation. (x) Casting and development of EHTs.

Step 2: Mesoderm induction

Suspension culture flasks were prepared by coating with 1 ml/10 cm^2 1% (v/v) Pluronic® F-127 solution and incubated at 37 °C for one night. Before usage, flasks were washed two times with 1x PBS (~2 ml/10 cm^2) and mesoderm induction medium (40 ml/T175-ml flask) was added. EB suspension was transferred to T175-ml flasks (not more than 200 ml/flask), which were placed on pre-warmed V-shaped racks to allow the sedimentation of EBs. 50 ml of the cell suspension was transferred and sedimented in 50-ml Falcon for 5-10 min to estimate the EB volume. After sedimentation, 40 ml supernatant was removed and remaining 10 ml medium with EBs was transferred to 15-ml graduated Falcon tubes. EB volume was determined after sedimentation and total EB volume was calculated. After sedimentation, 90% supernatant was removed from the T175-ml flasks and remaining media with EBs were pooled into 1 flask in case of handling of more flasks. EBs were washed by using pre-warmed mesoderm induction washing media and allowed to sediment again with washing medium for about 10-15 min. Following the removal of about 95% media, EBs were resuspended in

mesoderm induction media and added to Pluronic® F-127 solution coated T175-ml flasks (180-250 µl EBs/flask). Flasks were incubated at 37 °C, 5% O_2, 5% CO_2, and 90% humidity for 3 days. 50% medium was replaced daily with fresh mesodermal induction media. Media change was done by placing flasks on V-shaped racks to sediment EBs. After sedimentation, 50% supernatant was replaced with fresh media.

Step 3: Cardiac specification

About 90% of the mesoderm induction media was removed from the flasks by placing the flasks on V-shaped racks to let EBs sediment. EBs were washed with 20-30 ml pre-warmed cardiac specification washing media. In case of handling of more than one flask, flasks content was pooled before further processing. After addition of washing media, 15 ml of the EBs suspension was added into a 15-ml graduated Falcon tube to estimate EB volume. Then, EBs were resuspended in pre-warmed cardiac specification media I (185-250 µl EBs/T175 flasks in 46 ml medium). Media was changed daily (50%) with cardiac specification media-I for 3 days. On the 3rd day, the complete media exchange was done with cardiac specification media-II. 50% media exchange was performed daily for the next 4 days with the same media. On the 7th day, the complete media exchange was done with cardiac specification media-II followed by 50% media exchange daily until EBs were dissociated.

3.2.2. <u>2D cardiac differentiation protocol</u>

Cardiac differentiation of R-PAT cell line was performed by using a 2D protocol as described by Kondrashov et al. 2018. Undifferentiated hiPSCs were expanded in Matrigel-coated 6-well plates by using Essential 8 (E8) culture medium. Cells were seeded at a density of 4×10^4 cells/cm^2 and expanded for 48 h to reach 75-85% confluency to start the differentiation process. Differentiation was performed by following the below-mentioned steps:

Day 0: Cells were incubated with StemPro34 media containing StemPro34 supplement, Matrigel, BMP-4 and glutamine for 12-16 h.

Day 1: Cheese-like holes were observed in the culture on day 1 and cells were incubated with StemPro34 medium supplemented with StemPro34 supplement, BMP-4, Activin A, and glutamine.

Day 2: Shedding of many dead cells was observed at this stage and the medium was exchanged using RPMI containing B27-minus insulin and WNT-inhibitors KY02111 and XAV939.

Day 4: Cells were incubated with a similar medium as used on day 2 except that B27-plus insulin was used.

Day 6: Cells were maintained in RPMI containing B27-plus insulin until the dissociation at day ~11-15. The medium was exchanged every other day.

3.2.3. Dissociation of hiPSC-cardiomyocytes

When differentiating by EB-based differentiation protocol, cell culture flasks were placed on V-shaped racks to let EBs sediment. The supernatant was removed as much as possible and EBs were washed twice with warm calcium-free HBSS, 20-25 ml/flask. HBSS was replaced with collagenase II-based dissociation buffer (20-25 ml/flask) and incubated at 37° C, 5% CO_2, 90% humidity, 20% O_2 for 2.5-3.5 h.

In case of 2D differentiation, the supernatant was removed, and cells were washed twice with calcium free HBSS, 3 ml/well. For dissociation, cells were incubated with collagenase II-based dissociation buffer for 1.5-2.5 h, 2-3 ml/well, depending upon the density of the cells.

After 2 h of incubation, the progress of dissociation was checked microscopically after each additional half an hour, since dissociation time varies and depends upon many factors, e.g. collagenase batch, EBs size and quantity in case of EB-based differentiation, cell density in the case of 2D differentiation. Flasks/plates were also carefully tapped to check the dispersion of EBs/monolayer into small clusters. After observing the signs of dissociation of the EBs/monolayer (cellular disintegration), 10-ml serological pipette was used to gently triturate the cells (maximally 3 times). The cell suspension was added into 50-ml Falcons (1:1 v/v) containing pre-warmed DMEM supplemented with 6 µl/ml DNase to stop the dissociation process. The cell suspension was centrifuged at 100 x g for 10 min and the cell pellet was resuspended in a suitable amount of DMEM for cell counting by trypan blue dye and Neubauer counting chamber (5 ml for small pellet and 10-20 ml for larger pellets). The cell suspension was filtered by 100 µm cell strainer, when required, to remove DNA clumps caused by dead cells. The cell suspension was distributed to cast EHTs and freeze down for flow cytometry and for later use, and was centrifuged in separate Falcon tubes. Two tubes were prepared with 200,000 cells per tube for flow cytometry analysis.

3.2.4. Freezing and thawing of hiPSC-CM

For freezing, hiPSC-CMs (pellet form) were resuspended in cold freezing medium ($1-30x10^6$ cells/ml) and distributed into cryovials. 1 ml freezing medium was used per vial with maximally $30x10^6$ cells/vial. After transfer to cryovials, cells were frozen at -80 °C for initial 24 h, followed by -150 °C where it can be stored for several years.

For thawing, cryovial content was transferred to 50-ml Falcon, the vial was rinsed with 1 ml pre-warmed DMEM, and rinse was added to Falcon tube with cell suspension dropwise over 90 s with the continuous gentle swirling of the tube. 8 ml DMEM was slowly added to the tube, 1st ml dropwise over 30 s and remaining 8 ml over 30 s. The cell suspension was mixed by gently inverting the tube

two to three times and cells were counted by the trypan blue dye and Neubauer chamber. The cell suspension was centrifuged at 100 g for 5 min to form a pellet.

3.2.5. Flow cytometry analysis of hiPSC-cardiomyocytes

Two cryovials were thawed as described in section 3.2.4, transferred to two FACS tubes, washed twice with 3 ml 1xPBS, centrifuged at 200 g for 5 min and the supernatant was discarded. Cells were suspended in 500 µl of ice-cold methanol and kept on ice for 20 min. Cells were washed twice with 500 µl FACS buffer and further permeabilized by resuspending in 500 µl FACS buffer and incubated at 4°C for minimum 45 min or overnight. For staining of intracellular antigens, cells from one FACS tube were resuspended into 100 µl FACS buffer containing respective primary isotype control (e.g. REA control (I)-FITC). Cells from the second tube were resuspended in 100 µl FACS buffer containing primary or directly labelled antibody (anti-cardiac Troponin T-FITC). After an incubation period of 30 min at 4°C, cells were washed twice with FACS buffer. Staining process was repeated if a secondary antibody was required. Finally, stained cells were resuspended into 150 µl of PBS and analysed with the FACSCanto II (BD) and the FACSDiva software (BD).

3.3. EHT generation and analysis

EHTs were generated according to the protocol described in the recent publication of our group (Mannhardt et al. 2017b). Figure 7 illustrates the EHT generation and development process. This procedure started with the preparation of casting molds in the 24-well cell culture plate by adding 1.5 ml of agarose per well and placing a Teflon spacer in the wells with liquid agarose. Agarose was solidified at room temperature after 10-15 min. During the solidification time, a master-mix was prepared according to Table 2 in round bottom 15-ml tubes by adding all components, except thrombin, depending upon the number of EHTs required. Master-mix was triturated gently 10-15 times for the homogenous distribution of all the components. Master-mix and all the components used to prepare master-mix except thrombin were kept ice cold to prevent the changes in the consistency of master-mix due to Matrigel. $1x10^6$ cells were used to cast 1 EHT. Upon solidification of agarose (colour becomes opaque), the spacers were removed, and the PDMS racks were positioned on the 24-well plates so that pairs of PDMS posts reach into the casting molds. 100 µl master-mix was mixed with 3 µl thrombin and pipetted into strip format agarose casting molds. After casting of EHTs, the cell culture plate was incubated at 37 °C, 40% O_2, 7% CO_2 and 90% humidity for 1.5 h. DMEM (400-500 µl) was added to each well and the plate was gently shaken and incubated again for 15-20 min. PDMS racks containing fibrin gels attached to PDMS posts were gently transferred to the new plate containing 1.5 ml EHT culture medium/well. The plate was incubated at 37 °C, 40% O_2, 7%

CO_2 and 90% humidity. The medium was changed 3 times per week on Mondays, Wednesdays and Fridays. Single cell contractions were observed in EHTs at about day 3-5 and post-deflection at day 6-10.
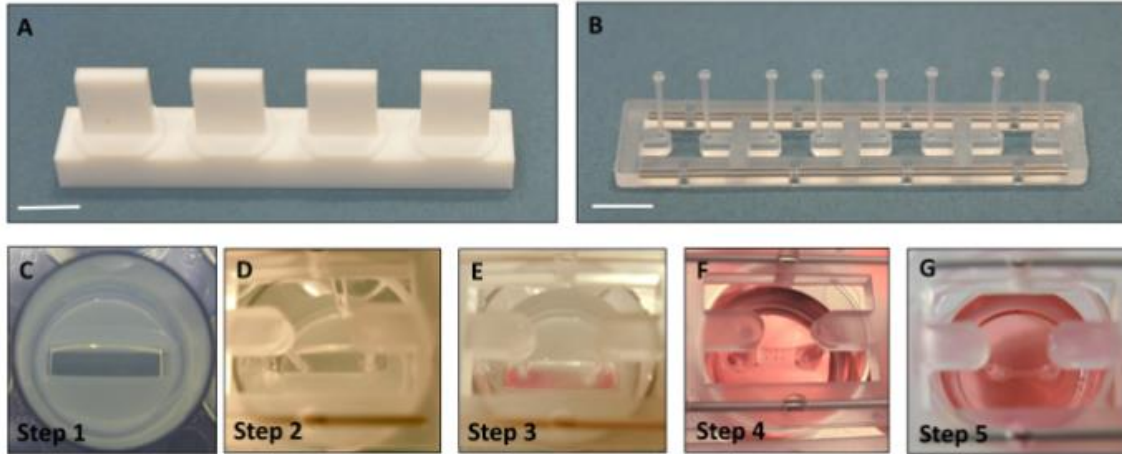
Figure 7: EHT generation and development: (A) Teflon spacer, (B) PDMS rack; scale bar for A and B: 1 cm. (C) Agarose casting mold in 24-well plate after removal of Teflon spacer (top view). (D) Agarose casting mold with PDMS racks positioned on top with a pair of posts inside the casting mold. (E) Fibrin gel embedding cardiomyocytes formed around the flexible PDMS posts. (F) Freshly casted EHT in EHT medium at day 0. (G) Fully remodelled EHT at day 15 (Mannhardt et al. 2017b).

Table 2: Calculation of master-mix for 1 EHT

hiPSC-CMs	1.10×10^6
2x DMEM	6.13 µl
10% (v/v) Matrigel	11.00 µl
Fibrinogen	2.78 µl
0.1% (v/v) Y-27632	0.11 µl
Thrombin	3.34 µl
EHT casting medium	86.64 µl
Total volume	110 µl

For CaT measurements, EHTs were transduced with lentivirus/adeno-associated virus 6 (AAV6) carrying GCaMP6f construct. Master-mix was mixed with virus preparation before casting EHTs. Multiplicity of infection (MOI) of the virus used was in the range of 0.25-0.3 for lentivirus and 10^5-10^6 for AAV6. For methods section on virus preparation please see chapter 0.

3.3.1. Contractility measurements

EHT contractility measurements were performed with video optical analysis as described by Mannhardt et al. 2017b. 24-well plate with EHTs was placed in a temperature- and gas-controlled incubator chamber. A camera was positioned above the glass roof of this chamber. A custom-made software controls the movement of the camera via X, Y and Z axis and film EHT for the defined period.

The software algorithm detects the top and bottom positions marked with blue squares and analyses the contraction by monitoring the deflection of PDMS posts and calculates force, frequency, time to peak force (TTP$_{-80\%}$) and relaxation time (RT$_{80\%}$) based on the predefined formula (see Figure 4 above).

3.3.2. Calcium transient analysis

A custom made setup described by Stoehr et al. was modified for the sequential analysis of force and CaT based on GCaMP fluorescence intensity (Stoehr et al. 2014). This system contained 3 components, 1) IonOptix with a photomultiplier and a shutter, 2) an inverted Axiovert 200M (Carl Zeiss) fluorescence microscope equipped with a motorized table, two objectives 10X for the CaT and 1.25X for the contraction analysis and with a mercury light source to excite EHT, and 3) a computer with a customized software (Figure 8). Fluorescence recording was restricted to a defined area (0.1x0.4 mm^2) in the centre of the EHT, which moves minimally during contraction and was identified prior to CaT recording by using a video camera. Another video camera attached to the front port of fluorescence microscope films the EHT for contractility analysis.
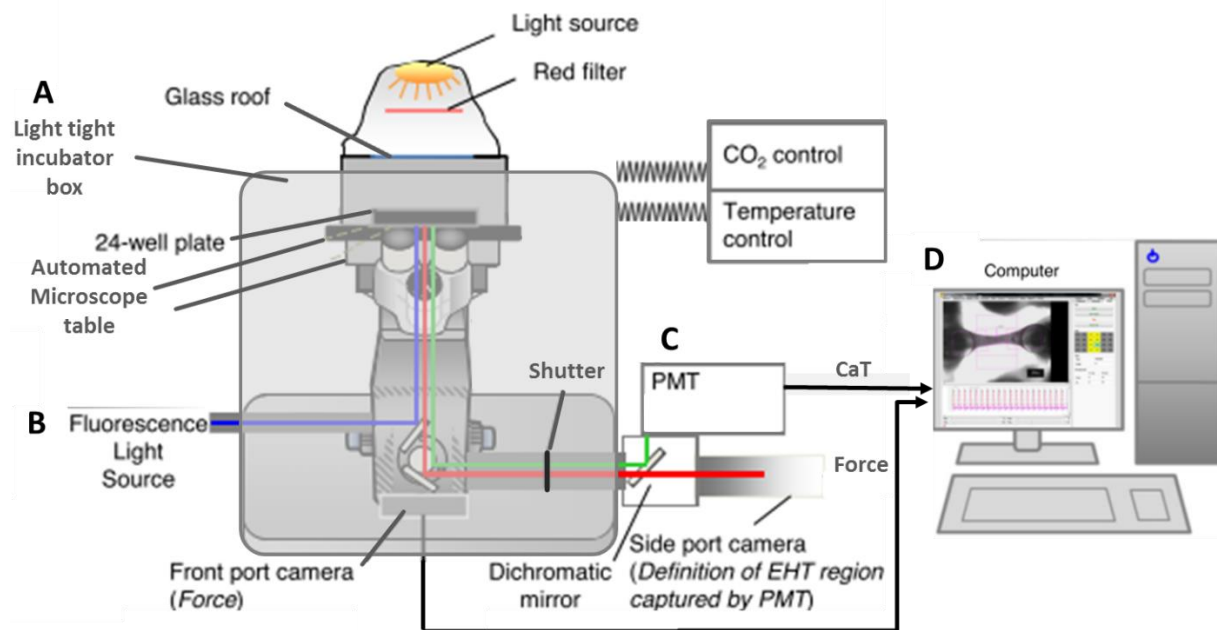
Figure 8: A schematic portrayal of the microscope-based set-up for sequential contractile force (video optical) and calcium transients (CaT, light intensity) analysis. (A) Light tight, temperature- and gas-controlled incubation chamber with 24-well plate holder on an automated motorized microscope table. (B) Fluorescence light source containing a mercury lamp; front port camera to record videos for contractile analysis; side port camera to define the EHT region being captured by a photomultiplier tube (PMT). (C) PMT converts the light signal into electrical signals. (D) Computer with customized software to analyse contraction and CaT (modified from Stoehr et al. 2014).

For sequential force and CaT analysis, the EHT plate was placed in the temperature- and gas-controlled incubation chamber of the test system. Upon illumination of EHTs by the blue light (~488 nm), the

confirmation of the calcium indicator GCaMP5G/GCaMP6f changes on binding with calcium and intensity of fluorescent green light increases (~510 nm). A photomultiplier converts this light signal into an electrical signal and a customized software records fluorescence light intensity as a surrogate for CaT. For these original recordings, CaT amplitude, $TTP_{-80\%}$ CaT and calcium decay time ($DT_{80\%}$) are automatically calculated. Contractility measurements were analysed similarly as mentioned in 3.3.1 except that the motorized table is used in this setup as compared to motorized X, Y and Z-axis in the EHT contractility analysis instrument (Figure 4) which move the camera to defined positions on the 24-well plate.

EHTs were electrically stimulated with the graphite pacing system as previously described (Hirt et al. 2012). The pacing frequency varied and was 1.5- to 2.5-fold higher than the spontaneous beating frequency of the EHTs. Voltage was used in the range of 2.5-3.5 V. Carbon electrodes were washed after each measurement with distilled water for 3 days with the daily water change, followed by sterilization in the autoclave prior to the next experiment.

3.3.3. Protocol for drug screening (contractility and calcium transient)

24-well cell culture plates were filled with Tyrode´s solution/DMEM high glucose (DMEM-H), 2.0/1.5 ml per well and incubated at 37 °C, 7% CO_2, 40% O_2, one day before the experiment to adequately equilibrate to the experimental conditions. Tyrode´s solution was prepared, sterile filtered and stored at 4 °C for a maximum one month. Calcium concentration of Tyrode´s solution/DMEM-H was adjusted to 1.8 mM or 0.5-1.0 mM (previously determined EC_{50}) to investigate the effects of positive inotropes.

Drugs were weighed, dissolved in their suitable vehicles (water/4 mM HCl/DMSO), sterile filtered, aliquoted and frozen at -20 °C or -80 °C (when required). 3 or 5 different sub-stock solutions were prepared as 1000x of the working concentrations. Sub-stock solutions were prepared freshly on the day of the experiment.

Working concentrations of the drugs were prepared in the cell culture plate by adding 2.0/1.5 µl of the respective sub-stock per 2.0/1.5 ml of Tyrode/DMEM-H in each well. Plates were gently shaken for thorough mixing and transferred back to the incubator until needed. The contraction force and CaT of EHTs were measured by following the below-mentioned steps.

1. Measurement of EHTs in EHT culture medium under spontaneous beating.
2. Transfer of EHTs into cell culture plate pre-filled with Tyrode´s solution/DMEM-H after placing carbon electrodes into wells.
3. Spontaneous and electrically stimulated measurement in 1.8 mM Ca^{2+} Tyrode/DMEM-H after 30 min incubation. Pacing frequency was generally 1.5- to 2.0-fold of spontaneous frequency.

4. Washing of EHTs in Tyrode´s solution/DMEM-H with 0.2-0.4 mM Ca^{2+} to reduce the force to 30-40% of their original force value.
5. Spontaneous and electrically stimulated measurement in Tyrode´s solution/DMEM-H with 0.6-1.0 mM Ca^{2+} (previously determined EC_{50}) after 20 min incubation.
6. Electrically stimulated measurement after 20-30 min incubation with the 1st concentration of the drug. This step was repeated to measure all the concentrations of the drug.
7. Spontaneous measurement in the absence of electrical pacing at the highest concentration.
8. Two times washing of EHTs in 1.8 mM Ca^{2+} Tyrode´s solution/DMEM-H, each for minimum 15 min to wash off the drug.
9. Removal of electrodes and transfer of EHTs back to the EHT culture medium.

Treated EHTs were not used in any experiment for the next 48 h. The customized Whitebox report converter was used to extract data from the PDF reports generated by the EHT analysis instrument. GraphPad Prism 6.0 software was used to prepare graphs.

3.3.4. Protocol for isoprenaline concentration response-curve in EHTs pre-incubated with PDE inhibitors

1. The contraction force of EHTs was recorded by following the above-mentioned procedure for drug screening from step 1-step 5.
2. Phosphodiesterase inhibitors were incubated for 30 min followed by spontaneous and electrically stimulated contraction measurement in the EHT analysis instrument.
3. EHTs were incubated with 0.1 nM isoprenaline for 20 min and recording was performed under electrical stimulation.
4. Step 3 was repeated to analyse the contraction force of EHTs at 0.3, 1, 3, 10, 30 and 100 nM. At the highest concentration, an additional recording was performed under spontaneous beating of EHTs to observe the effect of PDE inhibitors on the spontaneous beating frequency of EHTs.
5. EC_{50} values were calculated by using GraphPad Prism 5.0 by nonlinear regression fit with the equation "dose-response-stimulation log (agonist) vs. normalized response".

3.4. Immunohistochemical analysis of EHTs

Immunohistochemical analysis was performed according to the protocol described by Knaust 2017. EHTs were fixed with Histofix® while being attached to the posts of PDMS racks for 24 h on day 40-50 of casting and stored in TBS/azide at 4 °C. For cross sections, EHT were gently detached from the PDMS post and embedded in 2% (w/v) agarose and agarose was allowed to solidify. Agarose block holding the EHT was transferred to ethanol in a 2-ml Eppendorf tube. For longitudinal sections, EHTs were transferred into TBS/azide without agarose embedding. The subsequent process was kindly executed by Kristin Hartmann from the Mouse Pathology Core Facility (UKE, Hamburg, Germany). Sections of 4 µm thickness were cut after paraffin embedding. Samples were stained for alpha-actin (1:200) and GFP (1:1000). The subsequent staining procedures were performed by using the tissue stainer Ventana, BenchMark XT (Roche) with the 'Ultra View Universal DAB Detections Kit'.

3.5. Qualitative and quantitative PCR

RNA isolation was performed as described by (Knaust 2017). In brief, RNA was isolated from EHTs aged ≥20 days with 'RNeasy Plus Mini Kit' (Qiagen)' according to the manufacturer's instructions. EHTs were homogenized in RLT-Plus buffer by using TissueLyser (Qiagen) at 30 Hz for 2 min. RNA concentration was determined by measuring the absorbance at a wavelength of 260 nm with a spectrophotometer (NanoDrop® ND-1000, PeqLab). RNA was stored at -80 °C for further processing.

RNA was reverse transcribed into cDNA using the High Capacity cDNA Reverse Transcription Kit (Applied Biosystems) according to manufacturers' instructions. The samples were stored at -20 °C for further use.

Controls without reverse transcription (-RT) served as negative controls. PCR primers are listed in Table S4. Myocardial tissue was obtained from patients undergoing cardiac surgery at the University Heart Center Hamburg. The study followed the declaration of Helsinki. All patients gave written informed consent. Patient characteristics are given in Table S5.

Quantitative PCR was done on the AbiPrism 7900HT Fast Real-Time PCR System (Applied Biosystems) with SYBR Green (Fermentas) according to manufacturer's instructions in three technical triplicates. Values represent the mean of biological and technical triplicates. Glucoronidase beta was used as the housekeeping gene (GUSB_for: 5'-AAACGATTGCAGGGTTTCAC-3'; GUSB_rev: 5'-CTCTCGTCGGTGACTGTTCA-3').

Qualitative and quantitative PCR was performed with the assistance of Thomas Schulze.

3.6. Lentivirus and AAV6 vector for GCaMP6f expression

3.6.1. Construction and production of a lentiviral vector

To express the Ca^{2+} sensor Fast-GCaMP6f-RS09 under control of the EF1α promoter together with a puromycin resistance, the previously described lentiviral vector LeGO-EF1a i-Pur2 was digested with BamHI and NotI (Weber et al. 2008). A PCR was performed using Phusion polymerase and Addgene plasmid #67160 as a template encoding GCaMP6f with an N-terminal 6 x His Tag, a T7 Tag and an Xpress Tag with the following primer pair: 5´-GTCGTGAGGAATTCGGATCCaccATGGGTTCTCATCATCATCATCATC and 5´-ATTTACGTAGCGGCCGCTTACTTCGCTGTCATCATTTGTAC introducing a BamHI and a NotI restriction site, respectively. PCR product and digested plasmid LeGO-EF1a i-Pur2 were incubated with 5X In-Fusion HD Enzyme Premix (Clontech, In-Fusion HD Cloning Kit) according to the recommendations of the manufacturer. Resulting clones were checked by restriction digest, PCR and were finally verified by sequencing.

A stock of VSV-G pseudotyped viral particles was produced at the Vector Facility of the University Medical Center Eppendorf (Dr. Ingke Braren) using lentiviral packaging plasmids psPAX2 (Addgene plasmid #12260) and pMD2.G (Addgene plasmid #12259). After concentration by ultracentrifugation for 2 h at 4°C (25,000 rpm, SW32Ti rotor) on a 20% sucrose cushion, the pellet was resuspended in NKM medium. The functional titer was determined by transduction of HEK293T cells and quantified by flow cytometry (FACS CantoII, BD Biosciences; FITC Channel), and further used for transduction of cardiomyocytes. The efficiency of transduction was evaluated by live cell fluorescence microscopy.

3.6.2. Construction and production of an AAV6 vector

AAV transfer plasmids were derived from pFBGR (kindly provided by Robert Kotin, National Heart, Lung and Blood Institute, National Institutes of Health, Bethesda, MD, USA). For packaging of AAV serotype 6 particles, pSR646 (Addgene plasmid 65215) was employed. To improve transduction control, GFP was introduced under control of baculoviral late basic promoter pB was inserted into pFBGR and mCherry was introduced into pSR646 generating pFBGR-Ultra and pSR646-Ultra (Philipps et al. 2005). InFusion HD Cloning Kit (Clontech) was used according to the recommendations of the manufacturer for two-fragment reactions. pB was amplified from Baculovirus Genomic DNA using 5´-GCAATTGTTGTTGTTAAATTCCGTTTTGCGACGATGC and GTTTAAATTGTGTAATTTATGTAGCTG), GFP was amplified from pscAAV-GFP and mCherry was amplified from pSicoR-Ef1a-mCh-Puro-GFPi (Addgene plasmid 31848) using 5´- TTACACAATTTAAACGctagcATGGTGAGCAAGGGCGAGG and 5´-tgcaataaacaagttaacTTACTTGTACAGCTCGTCCATGC).

For insertion of GCaMP6f (Fast-GCaMP6f-RS09, Addgene plasmid 67160) in pFBGR-Ultra under the control of a CMV promoter, two fragments were generated by PCR using PrimeStar GLX Polymerase (Clontech) using two primers each to amplify CMV promoter (5´-GagcggccgcacgcgtGTGATGCGGTTTTGGCAGTACATC and 5´-AATTCAGTTCCAAAGGTTGGAATCTAAAAGAGAGAAACAATTAG) from pscAAV-GFP (Cellbiolabs) and GCaMP6f (5´-CTTTGGAACTGAATTCATGGGTTCTCATCATCATCATCATCATG and 5´-tatagggcgaattgggtaccTTACTTCGCTGTCATCATTTGTACAAACT) from Addgene plasmid 67160. pFBGR-Ultra was cut with MluI and KpnI and both fragments were inserted simultaneously using the InFusion HD Cloning Kit (Clontech) according to the recommendations of the manufacturer to generate an AAV transfer plasmid pFBGR-Ultra scCMV-GCaMP6f. Final AAV transfer plasmids were confirmed by restriction digestion, PCR using specific primers mentioned above and by sequencing.

Baculovirus genomic DNA carrying AAV genomic components on the one hand and packaging elements, on the other hand, were produced by using the Bac-to-Bac System (Life Technologies) after

transformation of *E.coli* DH10Bac according to the recommendations of the manufacturer. Colonies were grown on Kanamycin/Tetracyclin/Gentamycin plates supplemented with IPTG/Bluo-Gal and large white colonies were propagated in 5 ml 2YT medium overnight. Baculoviral DNA was extracted by Miniprep alkaline lysis, precipitated with 2-propanol and resuspended in 50 µl ddH$_2$O. Sf9 cells were seeded in 12 well plates and baculovirus DNA derived from pFBGR-Ultra GCaMP6f and pSR646-Ultra was transfected using TransIT-Insect (MoBITec) according to the recommendations of the manufacturer. After 3 days, cells were collected and expanded to approximately 1E+07 fluorescing Sf9 cells.

For the production of AAV6, 5E+08 Sf9 cells (Merck) were cultivated in InsectXpress Medium (Lonza) and 1% of baculovirus-transduced Sf9 cells were added in a ratio of 1:1 corresponding to the AAV genomic DNA and the AAV packaging elements, monitored by green and red fluorescence, respectively. After 4 days, cells were harvested and spun down for 20 min at 2,000 x g. The cell pellet was resuspended in (50 mM Tris base, 150 M NaCl, 5 mM MgCl$_2$, pH 8,5) viral particles were released from the nucleus by three freeze-thaw cycles. Virus-containing supernatants were incubated overnight with PEG-8000/NaCl to a final concentration of 20% and 1 M, respectively, at 4°C and then centrifuged for 30 min at 4°C and 3,000 x g. The resulting pellet was combined with cell lysates. Benzonase (Merk KGaA, Darmstadt, Germany; final concentration of 250 U/ml) was added and incubated for 1 h at 37°C. Cell debris was pelleted for 20 min at 12,000 x g.

AAV6 was purified using AVB Sepharose (GE Healthcare) and eluted with 25 mM citric acid, 100 mM NaCl, pH 2.6) and neutralized with 1 M Tris-HCl, pH 8. Viral particles were precipitated at 4°C overnight after addition of 2,5 x PEG-8000/NaCl to a final concentration of 20% and 1 M, respectively. After centrifugation for 30 min at 4°C and 3,000 x g, pellets were resuspended in NKM. The genomic titers of DNAse resistant recombinant AAV6 particles were determined by quantitative PCR using the SYBR Green qPCR Master MIX 2 (ThermoScientific) and an ABI 7900 HT cycler (ABI). Viral vectors were quantified using T7/SV40 specific primers (5´- cctatagtgagtcgtattacgcgc and 5´- gctgcaataaacaagttgggccat). Real-time PCR was done in 10 µl with 0.3 µM for each primer. Fluorescence was measured at the end of each annealing phase. The AAV transfer plasmid was employed as a copy number standard. A standard curve for quantification was generated by serial dilutions of the respective vector plasmid DNA. The cycling conditions were as follows: 50 °C for 2 min, 95°C for 10 min, followed by 35 cycles of 95°C for 15 s and 60°C for 60 s. Calculations were done using SDS 2.4 software (ABI). Additionally, functional titers were determined by transduction of HEK293T cells with serial dilutions of AAV6-GCaMP6f and quantification by FACS measurement (FITC Channel, 488 nm) using FACS CantoII (BD Biosciences). Viral vectors were kindly prepared by Dr. Ingke Braren from the HEXT Vector Core Facility (UKE, Hamburg, Germany).

4 <u>RESULTS</u>

4.1. <u>Large scale production of cardio myocytes</u>

Cardiomyocytes (C25 and ERC18) were efficiently produced at large scale by EB-based differentiation in spinner flasks (Figure 9). For example, in a series of 9 differentiation runs, 985×10^6 cardiomyocytes were differentiated with an efficiency of 87±7%.
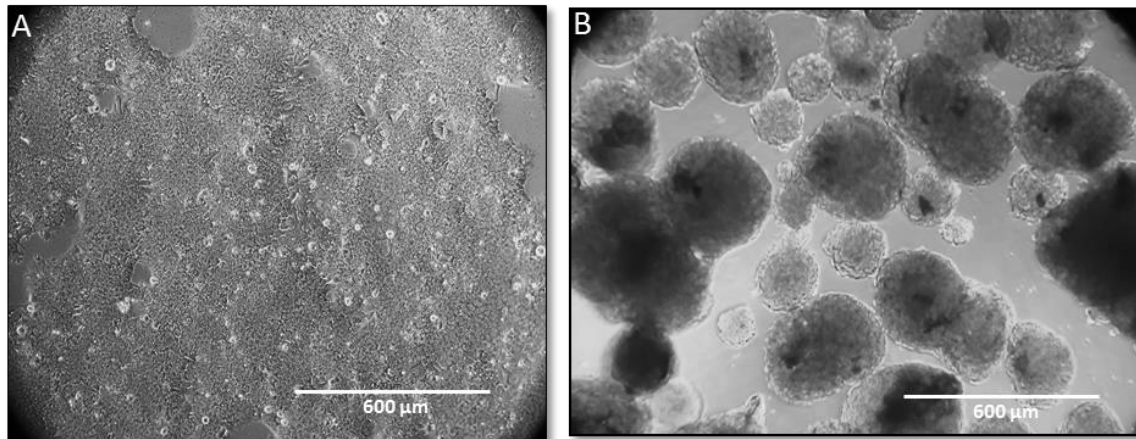
Figure 9: Cardiac differentiation of C25 and ERC18 by EB-based protocol. (A) hiPSC at the start of differentiation. (B) Differentiated cardiomyocytes in the form of spontaneously beating EBs at day 15.

The R-PAT cell line was successfully differentiated by a 2D differentiation protocol with a high throughput for blinded screening, yielding 490×10^6 cardiomyocytes in 3 runs with differentiation efficiency of 90±4%. Figure 10 depicts hiPSC cells at day 2 of differentiation with cheese-like holes and differentiated cardiomyocytes before dissociation, spontaneously beating as a monolayer.
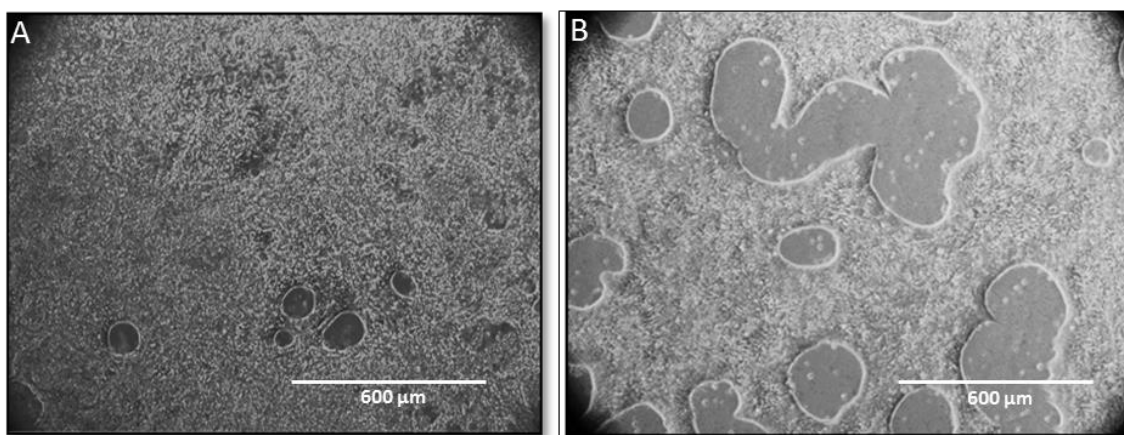
Figure 10: Cardiac differentiation of R-PAT by 2D protocol. (A) hiPSC in 2D layer at day 2 of differentiation with cheese like holes. (B) Spontaneously beating cardiomyocytes in 2D layer at day 12.

4.2. Establishment of a system for combined contraction/calcium transient measurements

4.2.1. Baseline characterization

HiPSC-CM in 2D monolayer were lentivirally transduced with the calcium indicators GCaMP5G and GCaMP6f (Fast-GCaMP6f-RS09) with a MOI of 0.3 (Figure 11). HiPSC-CM in EHT format were transduced before casting by using AAV6/lentivirus with an MOI of $10^6/0.3$. Transduction of hiPSC-CM EHTs after casting a few days before the analysis was not successful and resulted in low fluorescence levels.
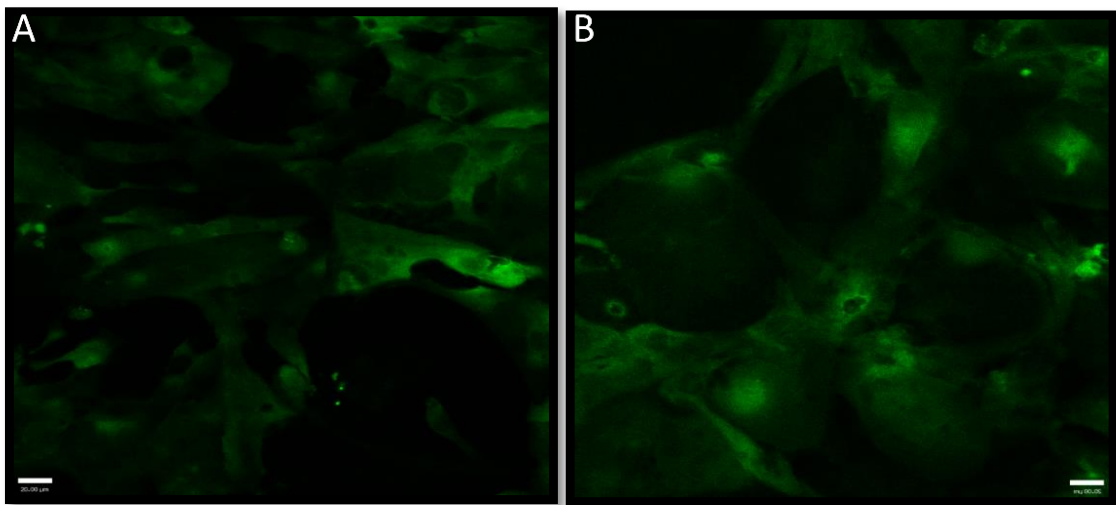
Figure 11: Representative images of hiPSC-CMs after lentiviral transduction with GCaMP5 (A), and GCaMP6f (B). Videos were recorded from beating cardiomyocytes with a confocal microscope. The images display cardiomyocytes during contraction when GCaMP fluorescence intensity is high (scale bar: 20 µm).

Use of GCaMP5G resulted in CaT (fluorescence intensity) signals with $TTP_{-80\%}$ values of 0.181±0.009 s (SD, n=5), 28% longer than $TTP_{-80\%}$ of force (0.141±0.003 s; n=3). Calcium decay values (0.33±0.007 s; SD, n=5) were 100% longer than $RT_{80\%}$ (0.165±0.007 s; n=5; Figure 12A). This slow kinetic of GCaMP5G resulted in clockwise force calcium loops, which are not physiological. GCaMP6f provided CaT with faster calcium $TTP_{-80\%}$ (0.154±0.004 s; SD, n=5; 23% smaller than $TTP_{-80\%}$ force) and calcium $DT_{80\%}$ (0.226±0.016 s; SD, n=3; 35% longer than $RT_{80\%}$) values and this resulted in counter-clockwise force calcium loops (Figure 12B).
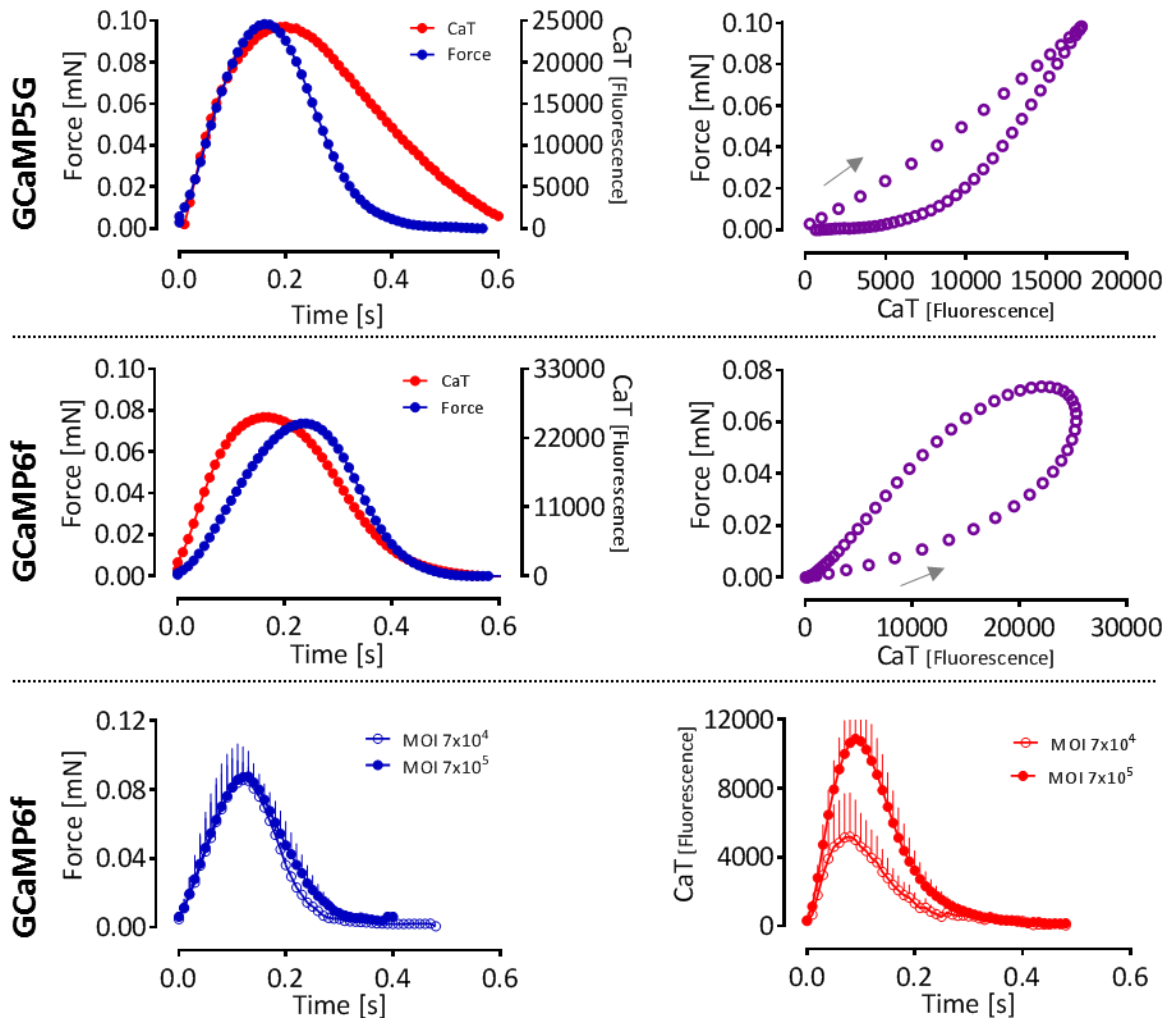
Figure 12: Optimization of GCaMP-based measurements of calcium transients (CaT). (A; left) Average force and CaT peaks of hiPSC-CM EHTs after lentiviral transduction with GCaMP5G; (A; right) Depiction of the same data as force/calcium loop, arrow indicates the start of contraction, n=5. (B; left) Average force and CaT peaks of hiPSC-CM EHTs after lentiviral transduction with GCaMP6f; (B; right) Depiction of the same data as force/calcium loop, n=5. (C) Average force (left) and CaT (right) peaks of hiPSC-CM EHTs transduced with AAV6-GCamP6f (MOI of $7x10^4$ and $7x10^5$, n=3). Measurements were done in modified Tyrode's solution at 1.8 mM Ca^{2+} under electrical stimulation with 1.5 Hz for Figure 12A, 12B, and 2 Hz for Figure 12C. Data are depicted as mean in Figure A, B and as mean±SEM in Figure C.

4.2.2. <u>Specificity of the fluorescence signal and motion artefacts</u>

Calcium transient measurements by fluorescence signals can be disturbed by motion artefacts, e.g. capture of fluorescence from larger areas of the substrate due to compaction during contraction. To evaluate the specificity of the fluorescence signal of GCaMP6f-transduced EHTs, the intensity of the fluorescence signal was evaluated from EHTs transduced with AAV6-GCaMP6f with an MOI of $7x10^4$ and $7x10^5$. The analysis of force and CaT (Figure 12C) indicated that force is similar for both MOIs while CaT amplitude was 2-fold higher for an MOI of $7x10^5$ vs. $7x10^4$ (10885 vs. 5192 AU, respectively). A second line of evidence for the specificity of the fluorescence signal is provided by faster CaT kinetics

of EHTs transduced with GCaMP6f vs. GCaMP5 (Figure 12A, B), which is in line with faster kinetics for GCaMP6f demonstrated in other models (Badura et al. 2014).

Immunohistochemical analysis by GFP-staining revealed efficient transduction of hiPSC-CM in EHT format by GCaMP6f (Figure 13B). Cardiac alpha-actin staining revealed that transduction with GCaMP6f did not interfere with myofilament organization or cellular alignment along the long axis of the EHT (Figure 13 A).
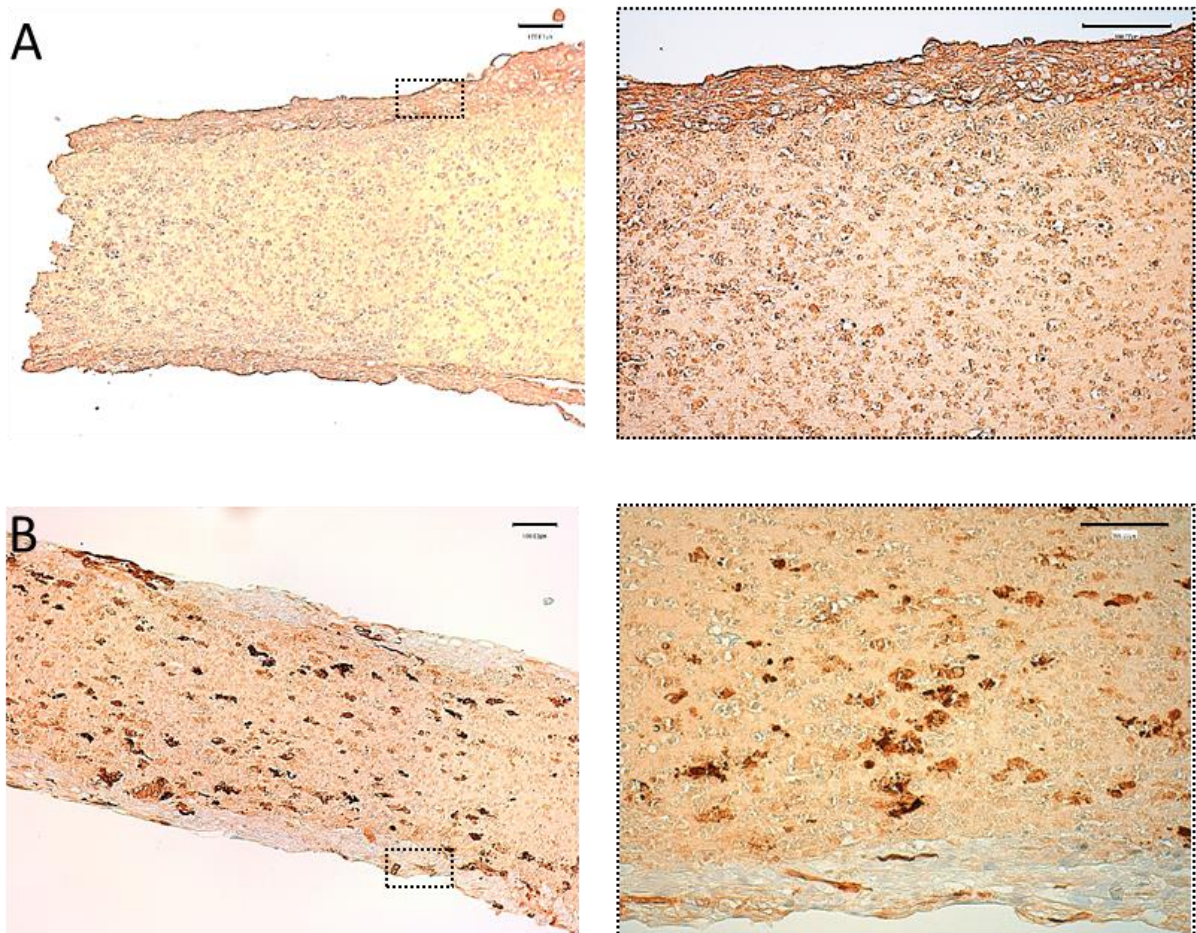
Figure 13: Immunohistochemical staining of GCaMP6f transduced EHTs for alpha-actin (A) and GFP (B). Left panel: 10x; right panel: 20x. Scale bar: 100 µm.

Motion artefacts are a limitation of CaT recordings in contracting muscle tissues (Fralix et al. 1990; Brandes et al. 1992; Kaestner et al. 2014). To reduce the impact of motion artefacts in this model, CaT recordings were performed in a small area of approximately $0.1 \times 0.4 \text{ mm}^2$ in the centre of the EHT, where motion during contraction is the least (Figure 14D). To understand the contribution of motion artefacts to the CaT signals, fluorescence was recorded in EHTs which were not transduced (Figure 14A). Fluorescence intensity amplitude (motion artefact) was 20-fold less than the average fluorescence intensity values with GCaMP6f Figure 14B: 24000 AU vs. Figure 14A: 1200 AU) and its

kinetics were superimposed with kinetics for force, particularly in the contraction phase. To further elucidate the motion artefact, EHTs were virally transduced with GFP-only (Figure 14B). Fluorescence intensity of these EHTs was similar to non-transduced EHTs (Figure 14A) and resulted in superimposed kinetics of fluorescence and force and showed higher variability (Figure 14B). Force-calcium relation did not present as a loop, but as a line with superimposition of contraction and relaxation phase.
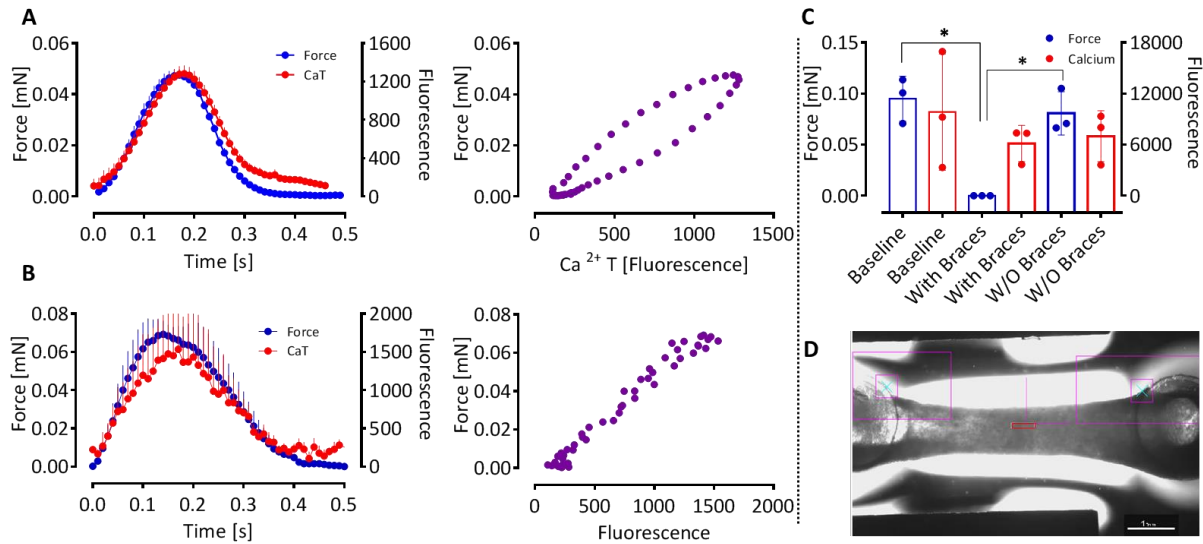
Figure 14: Motion artefact analysis. (A; left) Average contraction- and fluorescence intensity-peaks of untransduced hiPSC-CM EHTs; (A; right) Force/calcium loops of data depicted in Figure 14A, n=5. (B; left) Average contraction- and fluorescence intensity-peaks of hiPSC-CM EHTs transduced with GFP; (B; right) Force/calcium loops of data depicted in Figure 14B, n=4. (C) Scatter plot depiction of the contraction force and fluorescence intensity in neonatal rat EHTs transduced with GCaMP6f at baseline and in the presence and absence (after removal) of metal braces, n=3. One-way ANOVA with Sidak post-test, force baseline vs. force with braces; force with braces vs. force without braces (W/O), p<*0.05. Data in Figure 14A, B and C are depicted as mean±SEM or mean only for loops. Measurements were done in modified Tyrode's solution at 1.8 mM Ca^{2+} under electrical stimulation of 2.0, 1.5 and 4.5 Hz for Figure 14A, B and C, respectively. (D) Live image of an EHT during analysis, with a red rectangle in the centre of the EHT representing the area chosen to collect fluorescence light intensity, scale bar 1 mm. Purple squares are indicating positions for contractility analysis.

As a second line of evidence to define the contribution of motion artefacts to the CaT signals, neonatal rat EHTs were generated on hollow PDMS posts according to a previously established protocol (Hirt et al. 2012). Contractile GCaMP6f-transduced neonatal rat EHTs were subjected to afterload enhancement by introducing metal braces into the hollow PDMS posts. The presence of metal braces impeded muscle shortening during the contraction. Recording of force and CaT revealed a significant reduction of shortening (expressed as force), but not of fluorescence light intensity (CaT) upon introduction of metal braces. The reduction of shortening was reversed after removal of the metal braces (Figure 14C). In summary, these data provide evidence against a substantial contribution of motion artefacts to the GCaMP6f-signals.

4.2.3. **Compound-specific effects**

A set of indicator compounds with known effects on cardiac contractility was chosen to validate this system. The results are demonstrated in Figure 15. The β-adrenergic agonist isoprenaline (10 nM) led
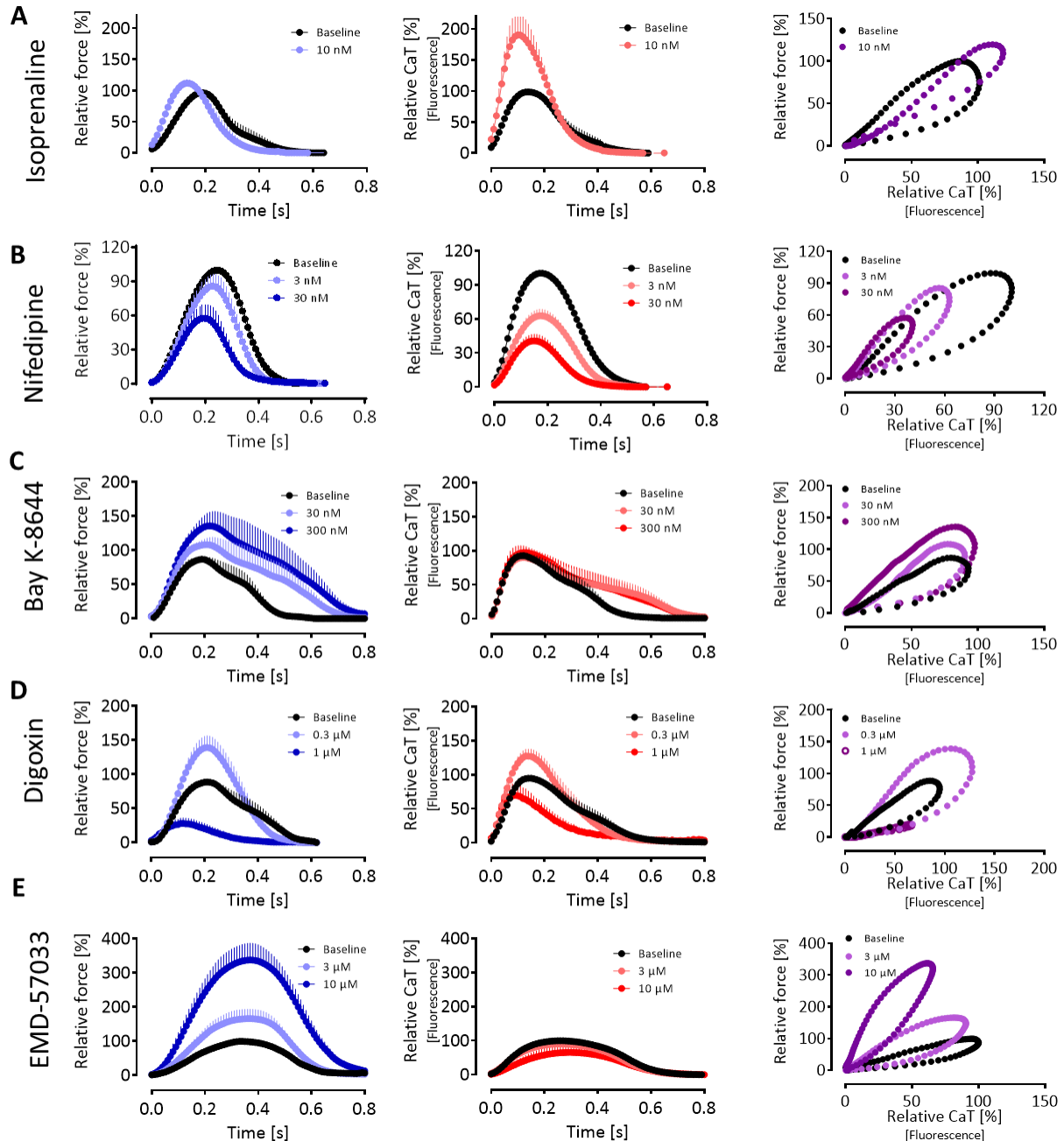
Figure 15: Force and calcium transient (CaT) analysis of indicator compounds. Average peaks of force (blue, left), CaT (red, middle), and force calcium loops (purple, right) of hiPSC EHTs at baseline (black) and after compound incubation (blue/red/purple). Depicted are the relative effects in percentage of maximum baseline in modified Tyrode's solution. Positive inotropic drugs (A, C, D and E) were analysed at submaximal calcium (0.6-1 mM Ca^{2+}) and negative inotropic drug (B) at 1.8 mM Ca^{2+}. All measurements were performed under electrical pacing: (A) Isoprenaline n=8/2, 1.5 and 2.0 Hz; (B) Nifedipine n=5/1, 1.5 Hz; (C) BayK-8644 n=7/2, 1.0 and 1.5 Hz; (D) Digoxin n=10/2, 1.0 Hz; (E) EMD-57033 n=5/1, 1.0 Hz. Replicates are indicated as number of EHTs/number of different batches of cardiomyocytes. Data are depicted as mean±SEM or mean only for loops.

to an increase in force (+15%) and a reduction in TTP$_{-80\%}$ (-15%). Surprisingly and quite unusual, we could not detect a significant positive lusitropic effect (=reduction in RT$_{80\%}$). The effects on contractile function were accompanied by an increase in calcium peak (+39%) and reduction in calcium TTP$_{-80\%}$ (-22%). Force calcium loop depiction demonstrated for a given calcium more force during contraction and less force during relaxation in addition to the higher force and calcium maximum. The LTCC inhibitor nifedipine (30 nM) led to a concentration-dependent decrease in force (-45%) and in calcium peak (-60%). Secondary to this, TTP$_{-80\%}$ and RT$_{80\%}$ were also significantly reduced. Force calcium loop depiction demonstrated more force for a given calcium during contraction and relaxation, and smaller force and calcium amplitude values.

The LTCC opener BAY K-8644 (300 nM) led to an increase in force (+25%) and RT$_{80\%}$. This was accompanied by an increase in time to CaT decay (+42%), but not CaT amplitude. Force calcium loop depiction demonstrated minor changes during contraction, more force for a given calcium during relaxation and higher force amplitude. The sodium potassium pump inhibitor digoxin (300 nM) led to an increase in force (+23%) and calcium amplitude (+19%). At higher concentration (1 µM) digoxin toxicity led to lower force and calcium amplitude. Force calcium loop depiction demonstrated a harmonic increase in force and calcium amplitude. The myofilament calcium sensitizer EMD-57033 led to an increase in force (+65%) and no change in CaT. Force calcium loops demonstrated an increase in force per calcium for contraction and relaxation and higher force amplitude.

4.2.4. <u>Force frequency relationship</u>

The positive correlation between force and beating frequency (Bowditch effect) is well described for human myocardium (Mulieri et al. 1992). However, in recent studies, we were not able to demonstrate this effect in spontaneously beating hiPSC-CM EHTs (Mannhardt et al. 2016). We hypothesized that a positive force-frequency relationship is masked by high spontaneous beating frequencies of hiPSC-CM EHT with frequencies of 1.0-1.5 Hz. Spontaneous beating of hiPSC-CM is dependent on I$_f$ current, hence we evaluated force-frequency relationship in hiPSC-CM EHTs in the presence of ivabradine (300 nM), which reduces spontaneous beating frequencies to 25% (Mannhardt et al. 2016). In the presence of ivabradine hiPSC-CM EHTs could be paced between 0.5-2.5 Hz (Figure 16A). An increase in frequency between 0.5 and 1.5 Hz was accompanied by an increase in force by 58%. Force declined at higher frequencies. TTP$_{-80\%}$ and RT$_{80\%}$ declined over the entire pacing range with a maximum of 45% and 40%, respectively. CaT amplitudes showed a similar pattern, increased from 44% to 100% between 0.5 and 1.75 Hz, and declined at higher frequencies. Time to calcium peak and time to calcium decay decreased gradually by 40% and 43% between 0.5 and 2.5 Hz (Figure 16B).

Corresponding average contraction- and CaT-peaks and force calcium loops at 0.5, 1.75 and 2.5 Hz are depicted in Figure 16C, D, E.
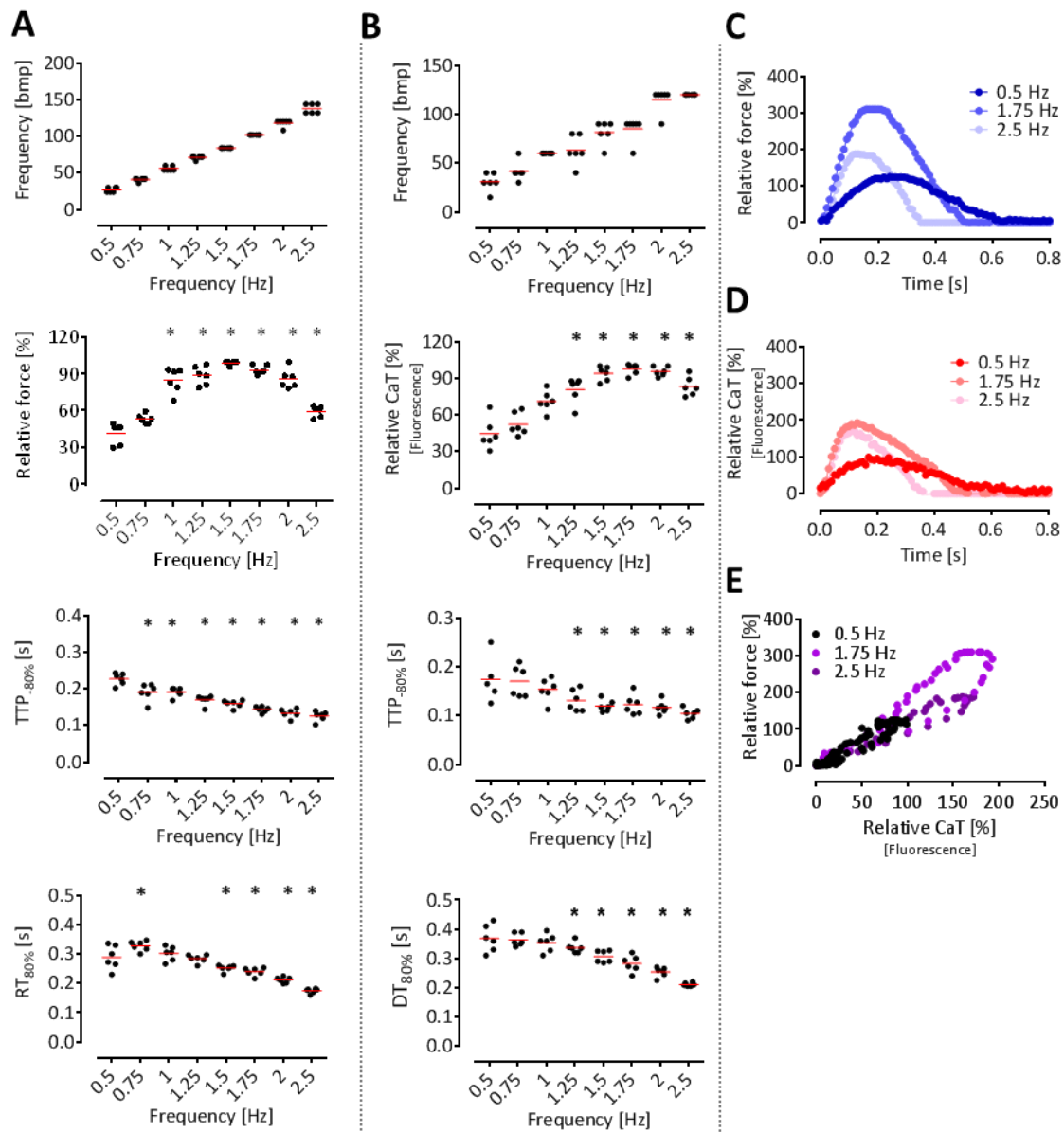
Figure 16: Force- and calcium transient (CaT)-frequency relationship in the presence of ivabradine (300 nM). (A) Frequency, relative force (normalized to own maximum), time to peak force (TTP$_{-80\%}$), relaxation time (RT$_{80\%}$). (B) Frequency, relative CaT (normalized to own maximum), time to peak CaT (TTP$_{-80\%}$) and calcium decay time (DT$_{80\%}$). Depicted are scatter plots with mean values (indicated by red line). One-way ANOVA with Dunnett's post-test vs. 0.5 Hz, *$p<0.05$. (C and D) Depiction of selected data from A and B as average force and CaT peaks. Indicated are the mean values relative to the baseline. (E) Depiction of selected data from A and B as force/calcium loops. Measurements were done in modified Tyrode's solution at submaximal calcium (0.6 mM Ca^{2+}).

4.2.5. **Omecamtiv mecarbil**

Omecamtiv mecarbil (OM) binds to the catalytic domain of myosin and acts as a myosin activator. OM was demonstrated to increase force and TTP$_{-80\%}$ while CaT remained unchanged in rat
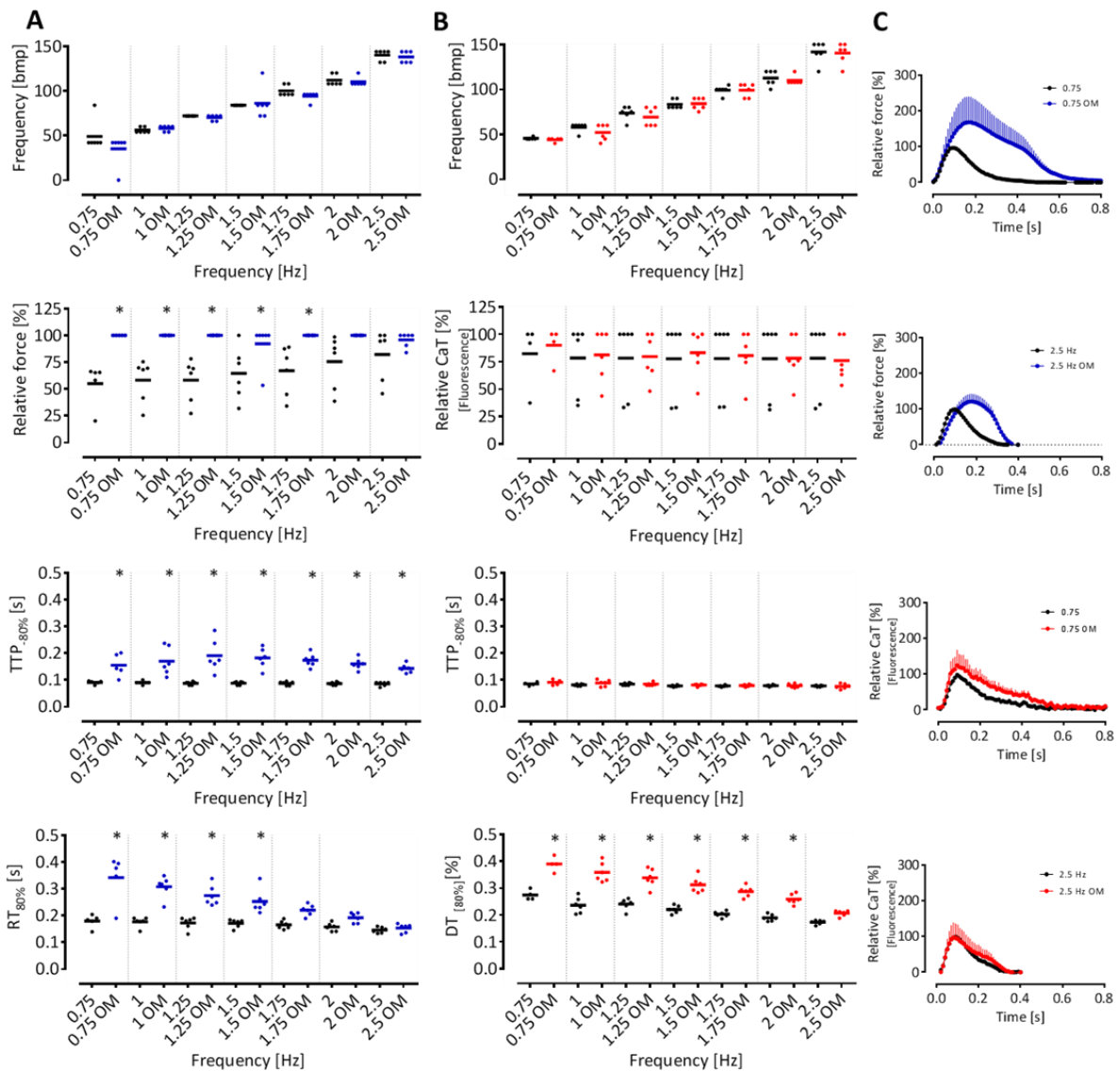
Figure 17: Effects of omecamtiv mecarbil (OM) at 1 µM on contraction force and calcium transients (CaT). (A) Frequency, relative force (normalized to own maximum), time to peak force (TTP$_{-80\%}$), relaxation time (RT$_{80\%}$). (B) Frequency, relative CaT (normalized to own maximum), time to peak CaT (TTP$_{-80\%}$) and calcium decay time (DT$_{80\%}$). Depicted are scatter plots with mean values (indicated by blue or red lines for force and CaT, respectively). One-way ANOVA with Dunnett's post-test vs. OM, *p<0.05. (C) Average contraction and CaT peaks at 0.75 and 2.5 Hz in the presence and absence of OM. Depicted are the mean values with SEM relative to the baseline. Measurements were done in modified Tyrode's solution at submaximal calcium (0.6 mM Ca^{2+}).

cardiomyocytes (Malik et al. 2011). Two previous studies demonstrated that the inotropic effect of OM shows a reverse frequency dependency in canine myocytes (Butler et al. 2015; Horváth et al. 2017). In pilot experiments with hiPSC-CM EHTs at pacing frequencies between 1.5 and 2.0 Hz (above the spontaneous beating frequency), a pronounced increase in TTP$_{-80\%}$ for force but very minor PIE was seen (data not shown). In analogy to the demonstration of positive FFR (Figure 16), the effect of OM (1 µM) was analysed in the presence of ivabradine (300 nM) at frequencies between 0.75 and 2.5 Hz (Figure 17). hiPSC-CM EHTs followed the pacing signals at all frequencies in the presence and

absence of OM (Figure 17A, B, left panel). The PIE effect was +80% at 0.75 Hz and gradually decreased to +17% at 2.5 Hz. This was accompanied by a change in $TTP_{-80\%}$ and $RT_{80\%}$ of +72% and +90% at 0.75 Hz with a gradual change to +68% and +5% at 2.5 Hz (Figure 17A). CaT amplitude and time to calcium peak did not show any change. The calcium $DT_{80\%}$ was increased by +42% at 0.75 Hz and gradually declined to an increase by 37% at 2 Hz Figure 17B. Average contraction and CaT peaks in the presence and absence of OM at 0.75 and 2.5 Hz depicted the similar findings.

4.3. Blinded analysis

In the next step, blinded compound analysis was performed as part of the Crack-IT initiative. In this initiative four academic partners (Chris Denning, Nottingham, UK; Godfrey Smith, Glasgow, UK; Christine Mummery, Leiden, Holland; Thomas Eschenhagen/Arne Hansen, Hamburg, Germany) formed a consortium with GlaxoSmithKline (GSK®) UK, represented by Peter Clements. The consortium was initiated by the National Centre for the Replacement, Refinement and Reduction of Animal Research and aimed to "generate a physiologically-relevant contractility platform with cells that are phenotypically 'mature', possess a robust contractile apparatus, move calcium between intracellular and extracellular spaces and metabolically generate substantive amounts of energy" (https://crackit.org.uk/challenge-13-inpulse). During the first two years, the academic partners developed and fine-tuned their test systems with a set of indicator compounds under non-blinded conditions. In the final phase, a blinded screen was conducted and the different steps of this are demonstrated in a flow chart (Figure 18). During meetings in 2015-2016 a list of potentially useful indicator compounds was assembled. Based on this, GSK® defined the final list of indicator compounds and a testing order. The list is shown in Table 3. The first 10 compounds were defined as first priority by the pharmaceutical partner. GSK® ordered the compounds from commercial suppliers and aliquoted the powder for blinded analysis. In September 2017 the compounds were sent to the academic partners with detailed instruction on reconstitution and dilution of working concentrations from stock concentration. From September 2017 until May 2018 the academic partners screened the compounds on their respective test systems. The group of Christine Mummery used a 2D single cell hiPSC-CM platform (Ribeiro et al. 2015), the group of Chris Denning used a 2D monolayer assay with hiPSC-CM, and the group of Godfrey Smith used 2D monolayer assay with rabbit cardiomyocytes. Our contribution was my analysis on 3D EHTs with CaT and contractility as readouts. The effects of 27 compounds were analysed on contractility for two independent hiPSC lines (ERC18 and R-PAT). CaT were analysed for one hiPSC line, ERC18. Furthermore, only the first 10 compounds in the rank order of the blinded compound list and in addition, all compounds which showed a PIE or a NIE in the contractility analysis were subjected to CaT analysis.
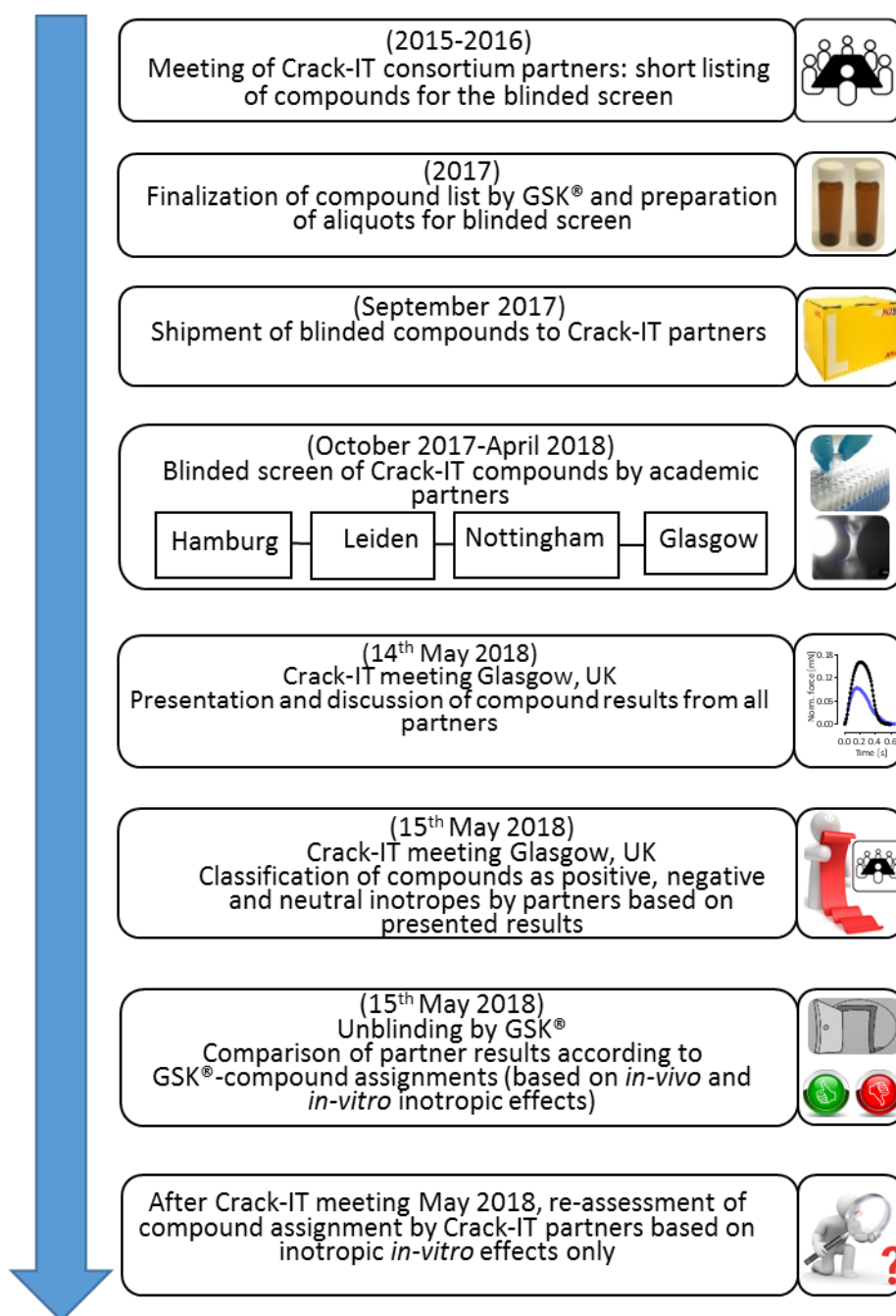
Figure 18: Blinded screening layout. Flow chart depicts the steps involved in multipartner-blinded screening of 27 compounds, as part of the Crack-IT consortium.

Prior to the meeting in Glasgow on May 14/15 2018 all partners submitted their screening results to Chris Denning who served as the coordinator of this initiative. During the meeting, all partners presented their results. These often included results for more than only one cell line and for electrophysiology and/or CaT in addition to contractility. The result was not necessarily conclusive, hence each partner did an integrated assessment of their results for each compound and categorized the compound as positive, neutral or negative inotrope. This was followed by compound unblinding during this meeting by Peter Clements (GSK®). The compound categorization of the partners was

compared with inotropic assignment by GSK®Table 3. It turned out that this assignment was mainly based on *in vitro* contractility data, but also included *in vivo* contractility data for some compounds e.g. atenolol, clonidine, glibenclamide (GSK®-assignments). Based on a common agreement by the partners, the assignment was revised for some compounds to better reflect the expectation for an *in vitro* contractility analysis (Crack-IT assignments). Both assignments are listed in Table 3.

Table 3: Table enlists compounds assigned as positive (PI), negative (NI) and neutral (=) inotropes by GSK® (GSK®-assignments, based on mainly *in vitro* but also *in vivo* data), and Crack-IT-consortium partners (Crack-IT-assignments, based on *in vitro* data only.

	Rank number	Compound	Mechanism	GSK®-assignments	Crack-IT-assignments
Positive inotropes	1	Epinephrine	Non-selective α1-, β1- and β2-adrenoceptor agonist	PI	PI
	2	Forskolin	Adenylyl cyclase stimulator	PI	PI
	11	Dobutamine	α1-, β1- and β2-adrenoceptor agonist	PI	PI
	21	Terbutaline	β2-adrenoceptor agonist	PI	PI
	3	Levosimendan	Calcium sensitizer, PDE3 inhibitor, K_{ATP} channel agonist	PI	PI
	4	Pimobendan	Calcium sensitizer, PDE3 inhibitor	PI	PI
	14	Omecamtiv	Cardiac specific myosin activator	PI	PI
	13	Milrinone	PDE3 inhibitor	PI	PI
Negative inotropes	7	Verapamil	L-type calcium channel blocker, hERG blocker	NI	NI
	22	Flecainide	Sodium channel blocker, hERG blocker	NI	NI
	19	Sorafenib	Multi-targeted kinase inhibitor	NI	NI
	9	Sunitinib	Multi-targeted TK inhibitor	NI	NI
	16	Citalopram	SSR inhibitor, hERG & L-type Ca^{2+} channel inhibitor	NI	NI
	18	Itraconazole	Triazole antifungal, mechanism unclear	NI	NI
	28	Zimelidine	SSR inhibitor	=	NI
	20	Ivabradine	I_f inhibitor	=	NI
Neutral inotropes	5	Acetylsalicylic acid	Cyclooxygenase inhibitor	=	=
	23	Paracetamol	Prostaglandin synthesis inhibitor	=	=
	10	Captopril	ACE inhibitor	=	=
	15	Enalapril	ACE inhibitor	=	=
	17	Clonidine	α2-adrenoceptor agonist	NI	=
	24	Phentolamine	Non-selective α-adrenoceptor antagonist	=	=
	6	Atenolol	β1-AR>β2-adrenoceptor antagonist	NI	=
	27	Sildenafil	PDE5 Inhibitor	=	=
	12	Glibenclamide	K_{ATP} channel antagonist	PI	=
	25	Tolbutamide	K_{ATP} channel antagonist, Adenylyl cyclase stimulator	=	=
	26	Pravastatin	HMG CoA reductase inhibitor	=	=

The inotropic effects of several compounds of this list are self-explanatory and will not be introduced in further detail. Their mechanisms of action are also indicated in table 3. These include the PIEs of terbutaline, omecamtiv mecarbil, milrinone, pimobendan, levosimendan, forskolin and epinephrine; the NIEs of verapamil, sunitinib, sorafenib, flecainide and itraconazole and the lack of inotropic effects (=neutral) for sildenafil, pravastatin, phentolamine, paracetamol, enalapril, captopril and acetylsalicylic acid. For other compounds this is less obvious and for some of these it is also discrepant between the GSK® and Crack-IT assignments. These include glibenclamide, clonidine, ivabradine, zimelidine, citalopram, dobutamine, tolbutamide and atenolol.

Ivabradine is an I_f antagonist and previous studies showed concentration-dependent inhibition of I_f in cardiomyocytes without effects on contractility parameters and action potential duration until 3 µM (Bois et al. 1996; Difrancesco 2010; Suenari et al. 2012). At concentrations greater than 3 µM, I_f selectivity is decreased and LTCC current decreases (-18% in atrial cells of Albino rabbits; -39% in rabbit pulmonary vein cardiomyocytes (Bois et al. 1996; Suenari et al. 2012). In the similar context, ivabradine decreased contraction force in isolated human atrial preparations (in 7/10 patients at 100 µM) and in guinea-pig left atria (at ≥10 µM) and papillary muscles (at 100 µM) (Pérez et al. 1995; Boldt et al. 2010). Therefore, its assignment as a neutral inotrope was revised and it was re-categorized as a negative inotrope.

Zimelidine is a selective serotonin reuptake inhibitor and used as an antidepressant. Initially it was assigned as a neutral inotrope. Based on a report describing *in vitro* NIEs in dogs (sarcomeric shortening), rats and hiPSC-CM (impedance assay) at 100 µM (Scott et al. 2014), it was re-assigned as a negative inotrope. Citalopram is another antidepressant also belonging to the group of selective serotonin reuptake inhibitors. Citalopram was shown to have NIEs by a A1 adenosine receptor agonistic effect (Pousti et al. 2004). It was also shown to inhibit hERG (at 10 µM in heterologous hERG expressing cells) and LTCCs (at 30 µM in guinea pig and rat ventricular cardiomyocytes) (Pacher et al. 2000; Witchel et al. 2002; Zahradník et al. 2008). Therefore, it was assigned as a negative inotrope.

Clonidine is an α2-adrenoceptor agonist and acts as a negative inotrope only in *in vivo* settings in the presence of an intact nervous system (McRitchie and Chalmers 1981). In this setting, clonidine acts as an agonist at presynaptic α2-adrenoceptor and leads to a sympatholytic effect by suppressing the release of norepinephrine. Its assignment as a negative inotrope is not justified for an *in vitro* contractility assay without functional neurons. The assignment was therefore changed from negative to neutral inotrope.

Atenolol is a selective competitive β-1 adrenoceptor blocker. The NIE is well established *in vivo* because atenolol reduced the effect of sympathetic innervation by β-adrenergic agonists in isolated

human atria and ventricles pre-stimulated with epinephrine and norepinephrine (Leenen et al. 1988; Lemoine et al. 1988). Minimal or no inotropic effects have been reported on isolated heart muscles from kitten and guinea pigs (Kaumann and Blinks 1980) and hiPSC-CM, neonatal rat and canine myocytes (Harmer et al. 2012; Scott et al. 2014), because in all these *in vitro* models no β-adrenergic activation was present. In conclusion, atenolol can only be classified as negative inotropic agent in *in vivo* model but not in models without sympathetic stimulation. Based on these findings, its assignment was changed from negative to neutral inotrope.

Glibenclamide is an anti-diabetic agent (sulfonylurea group) and inhibits ATP sensitive potassium channels (K_{ATP}) to increase insulin secretion in pancreatic β-cells. K_{ATP} channels are also expressed in cardiomyocytes and are inactive under normoxia in the presence of high ATP concentrations. During ischemia intracellular ATP concentration drops and K_{ATP} channels are activated, which leads to shortening of the action potential with a shortening of the plateau phase and smaller LTCC currents and lower force. Under these conditions, a K_{ATP} channel inhibitor like glibenclamide prolong the action potential duration, leading to larger LTCC and a PIE (Decking et al. 1995). This PIE is not expected under normoxic conditions. The assignment for glibenclamide was therefore changed from positive to neutral inotrope.

Tolbutamide is also an anti-diabetic from the sulfonylurea group like glibenclamide. For tolbutamide early data showed potent stimulatory effects on adenylyl cyclase (Levey et al. 1971), which would be compatible with a PIE under normoxic conditions. However studies on contractility in different animal models revealed that tolbutamide had only very small PIEs at very high concentration (1.0, 3.0 mM) in rabbit and cat trabeculae which were absent in dog trabeculae (Cornish and Miller 1975; Curtis et al. 1975). Since the highest concentration in the Crack-IT screen was only 100 µM, tolbutamide remained classified as neutral inotrope.

Dobutamine is clinically used as a selective β1-adrenoceptor agonist because it increases cardiac contractility. Pharmacologically it has binding activity at β1-adrenoceptors and with 3-5 fold lower potency at β2-adrenoceptor. In addition, dobutamine is also an agonist at α1-adrenoceptors (Williams and Bishop 1981; Ruffolo 1987; Warne et al. 2011). The clinical relevance for the balance between vasoconstrictoric α1-adrenoceptor and vasodilatory β2-adrenoceptor effects was demonstrated in a dog model, in which dobutamine infusion led to a decrease in peripheral resistance. Co-administration of dobutamine with propranolol led to a vasoconstrictory effect while vasodilatation was observed by a co-administration with practolol (β1-adrenoceptor antagonist) and phentolamine (α-adrenoceptor antagonist; Vatner et al. 1974). Dobutamine was classified as a positive inotrope, both by GSK® and by Crack-IT assignment.

Contractility and CaT measurements were done at submaximal calcium (0.5-1 mM Ca^{2+}) in modified Tyrode´s solution (R-PAT) or DMEM high glucose (ERC18) under electrical stimulation. In consequence of the lower spontaneous beating frequency of R-PAT EHTs, electrical stimulation was performed with 0.7-1 Hz vs. 1.5-2.5 Hz for ERC18. An experimental run down of time controls (~50% decline in force amplitude, data not shown) for ERC18 EHTs in Tyrode´s solution under baseline conditions required us to use serum-free DMEM high glucose media with adjustable calcium concentration. Despite this improvement, ERC18 EHTs showed <10% decrease in force and an increase in $TTP_{-80\%}$ and $RT_{80\%}$ over the time course of 5-6 h. R-PAT EHTs were still analysed in Tyrode´s solution and showed <10% changes in $TTP_{-80\%}$ and $RT_{80\%}$, but -15% decline in force (Figure S3). Compounds were tested in cumulative concentration-response curves over two log-units. For this screen, EHTs were lentivirally transduced with GCaMP6f to perform CaT measurements. Results are presented as normalized to pool of time control and relative to mean baseline for force and CaT data except for the average peak demonstration that shows absolute values normalized to time control. A statistically significant relative effect size of ≥15% was agreed to be considered as a relevant effect (threshold criteria).

4.3.1. <u>Quality control</u>

EHTs of ERC18 and R-PAT cell lines were characterized at ≥20 days of development under baseline conditions. EHTs of ERC18 cell line (n=134 EHTs/1 Batch) had an average force of 0.22±0.02 mN (SD), $TTP_{-80\%}$ 0.165±0.008 s (SD) and $RT_{80\%}$ 0.147±0.011 s (SD) with electrical pacing of 1.5 Hz (Figure 19A). R-PAT EHTs (145 EHTs/2 Batches) showed an average force of 0.14±0.027 mN (SD), $TTP_{-80\%}$ 0.183±0.042 s (SD) and $RT_{80\%}$ 0.294±0.041 s (SD) under electrical stimulation of 1 Hz (Figure 19B). Figure 19C shows the average contraction peaks for both cell lines.

As a first quality control step, EHTs with forces less than 0.1 mN at 1.8 mM external Ca^{2+} were excluded from the drug screening experiment according to previous studies of our group (Mannhardt et al. 2017a). By second line of quality control, EHTs were further characterized for their effects to representative positive and negative inotropic drugs, isoprenaline and nifedipine. Both hiPSC cell lines, ERC18 and R-PAT showed an isoprenaline-mediated (30 nM) PIE of +12% (from 0.17±0.027 to 0.19±0.022 mN; SD, n=8) and +180% (from 0.05±0.014 to 0.14±0.014 mN; SD, n=7), respectively. ERC18 EHTs showed a positive clinotropic effect ($TTP_{-80\%}$: -29%, from 0.164±0.008 to 0.127±0.004 s; SD, n=8) and R-PAT did not show a clinotropic but a positive lusitropic effect ($RT_{80\%}$: -14%, from 0.263±0.042 to 0.231±0.043 s; SD, n=8 (Figure 20A). The NIE of nifedipine (30 nM) was observed in both cell lines and amounted to -63% in ERC18 (from 0.13±0.016 to 0.08±0.017 mN; SD, n=6) and -57% in R-PAT (from 0.11±0.015 to 0.07±0.013 mN; SD, n=8; Figure 20B).
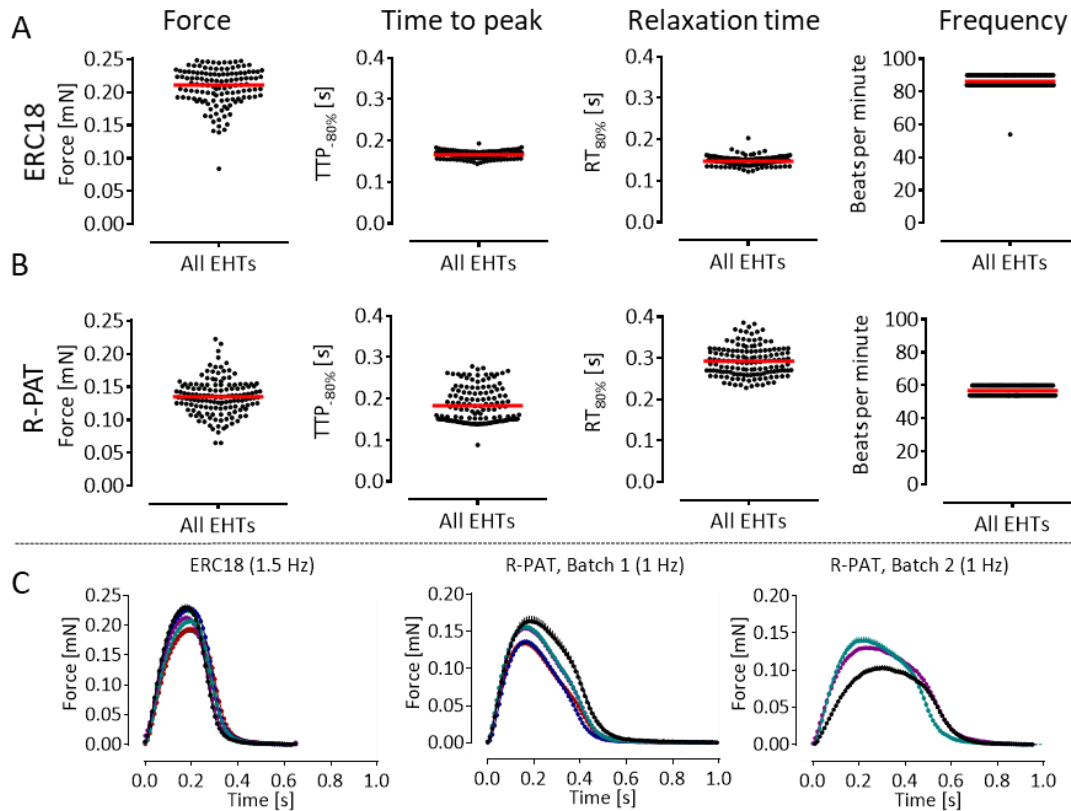
Figure 19: Characterization of EHTs (ERC18 and R-PAT) used for blinded drug screening. (A and B) Scatter plots with mean (indicated by red line) for force, time to peak force (TTP$_{-80\%}$), relaxation time (RT$_{-80\%}$) and frequency, ERC18: n=134/1 batch; R-PAT: 144/2 batches. (C) Average contraction peaks for ERC18 and R-PAT (mean±SEM). Different colours represent individual experiments. Measurements were done at 1.8 mM Ca^{2+} in modified Tyrode's solution and DMEM-H for ERC18 and R-PAT, respectively, under electrical stimulation of 1.5 and 1 Hz for ERC18 and R-PAT, respectively.

The concentration-response curves and average force and CaT peaks for all compounds for two hiPSC lines are presented in the supplement (Figure S1 and Figure S2), sub-grouped according to positive, negative or neutral inotropic effects based on Crack-IT assignments. Table 4 enlists all compounds categorized according to positive, negative and neutral inotropic assignment with maximum effect sizes for force, TTP$_{-80\%}$ for force, RT$_{80\%}$, CaT amplitude, TTP$_{-80\%}$ for CaT, calcium DT$_{80\%}$. Data in the result section refers to ERC18 hiPSC cell line unless otherwise specified. Results for R-PAT hiPSC line are presented in Figure S1 and Figure S2.

4.3.1. Positive inotropes matching inotropic assignment

Eight compounds were assigned as positive inotropes (Table 3), namely epinephrine, forskolin, dobutamine, terbutaline, levosimendan, pimobendan, OM, milrinone. 5/8 compounds were correctly identified as positive inotropes in both cell lines. The cAMP-dependent compounds forskolin, dobutamine and terbutaline showed an increase in the contraction force by +17% (not significant), +18% and +29%, respectively. Effects on TTP$_{-80\%}$/RT$_{80\%}$ were more pronounced than the PIE in most cases (forskolin: -22%/-35%, dobutamine: -22%/39%, terbutaline: -30%/-33%). This data was supp-
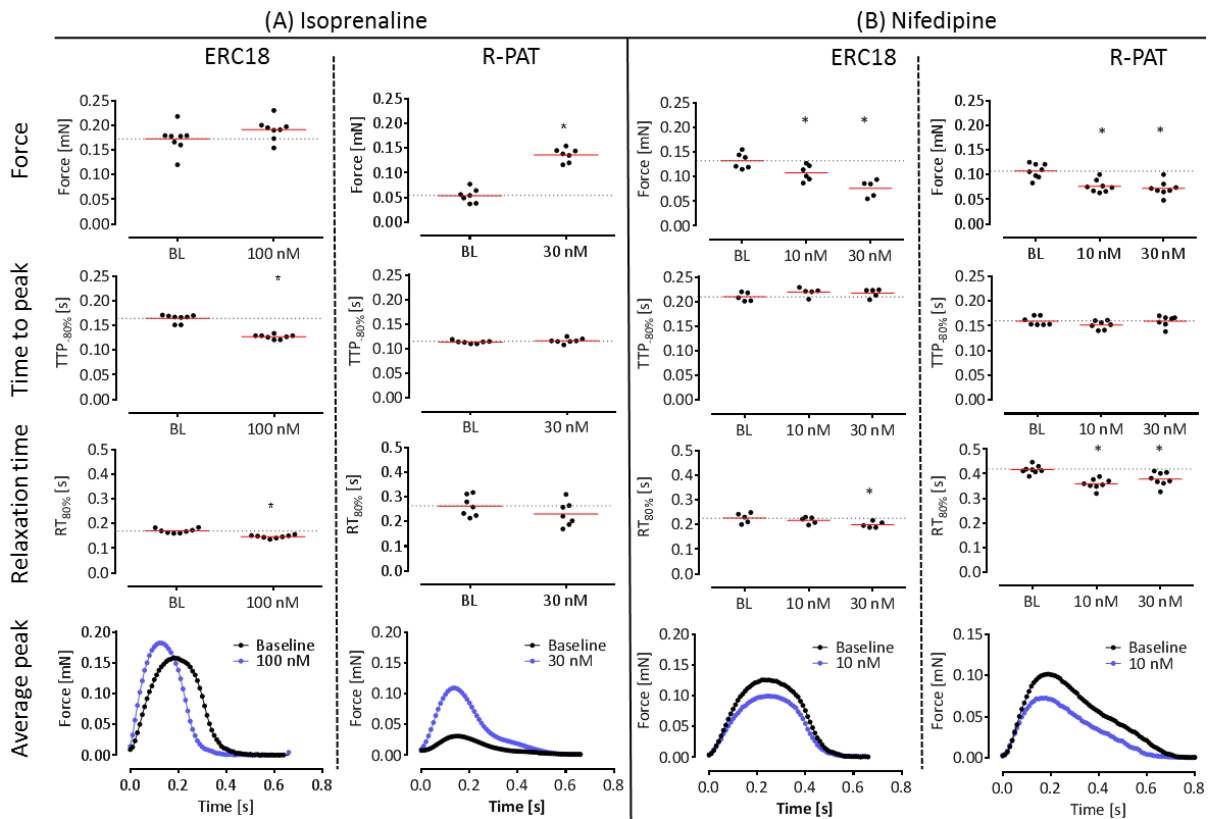
Figure 20: Quality control of ERC18 and R-PAT EHTs by determining response to indicator drugs, isoprenaline and nifedipine. Data are presented as scatter plots (mean indicated by red line), and average contraction peaks with mean values, before (black, BL: baseline) and after drug (blue), BL=Baseline. (A) Effect of isoprenaline (100 nM for ERC18; 30 nM for R-PAT) at 0.6 mM Ca^{2+}, t-test vs. BL, *$p<0.05$. Notably, 30 nM isoprenaline was used for R-PAT because at 100 nM beating frequency exceeded the pacing frequency. (B) Effect of nifedipine (10 and 30 nM) at 0.6 mM and 1 mM Ca^{2+} for R-PAT and ERC18, respectively, One-way ANOVA with Dunnett's post-test vs. BL, *$p<0.05$. EHTs were electrically stimulated at 1.5 Hz and 1 Hz for ERC18 and R-PAT, respectively.

orted by CaT measurements with an increase of CaT amplitude by +156%, +180, +150% for forskolin, dobutamine and terbutaline, respectively (Table 4). Milrinone showed a tendency of PIE of +7% at highest concentrations for ERC18 and +18 for R-PAT. In addition, a concentration-dependent decrease in $TTP_{-80\%}$ of -18% for ERC18 and -11% for R-PAT was detected (Table 4). The pattern of effects was suggestive of a cAMP/PKA-mediated mode of action despite of lack of consistent and significant effects on force. OM showed an increase in contraction force by +22%, $TTP_{-80\%}$ force +38%, peak CaT +45% and $TTP_{-80\%}$ CaT +16%.

Two compounds were identified as positive inotropes in one cell line, but as neutral inotrope in the second. Epinephrine showed PIE (Force: +20%), positive clinotropic ($TTP_{-80\%}$: -16%) and lusitropic effects ($RT_{80\%}$: -22%) in R-PAT and was categorized as a positive inotrope, but misclassified as a neutral inotrope in ERC18 (force: +16% (not significant), $TTP_{-80\%}$ -9% (not significant) and $RT_{80\%}$: -13% (not significant), CaT amplitude: +138%). Pimobendan was categorized as positive inotrope in ERC18 (force: +13% (not significant), $TTP_{-80\%}$: -11% (not significant), $RT_{80\%}$: +14%, CaT amplitude: +25% (not-

Table 4: Effects of compounds on force and calcium transient (CaT) of hiPSC-CM EHTs tested in two cell lines, R-PAT and ERC18. Listed are relative mean values (percentage vs. mean baseline) for force, CaT, time to force and CaT peaks (TTP$_{-80\%}$), relaxation time (RT$_{80\%}$), calcium decay time (DT$_{80\%}$) and stimulation frequency (S. freq.) depicted as beats per minute (BPM) at relative concentrations (Conc.). Data represents maximal effects corrected for time control. In case the maximum effect for a certain parameter was detected at a concentration lower/higher than for the other parameters, this is indicated by superscripted concentration. Colour coding highlights statistically significant and presumably relevant (≥15% effect size) increased (green) and decreased (yellow) effects. Orange colour marks statistically non-significant but ≥ 20% effect size. Notably, there is a discrepancy between concentration response curves and average peaks in some cases due to different sets of time controls for normalization. SSR inhibitor: Selective serotonin reuptake inhibitor; ACE: Angiotensin converting enzyme; PDE: Phosphodiesterase.

	Compound	Mode of action	Cell line	Mode	Force/CaT [%]	TTP$_{-80\%}$ [%]	RT$_{80\%}$/DT$_{80\%}$ [%]	S. freq. (BPM)	Conc. [µM]
Positive inotropes	Epinephrine	Non-selective α1-, β1- and β2-adrenoceptor agonist	R-PAT	Force	+20	-16$^{1\,µM}$	-22	60	0.3
			ERC18	Force	+16	-13	-9	136	1
			ERC18	CaT	+138	-28$^{0.1\,µM}$	-10	135	1
	Forskolin	Adenylyl cyclase stimulator	R-PAT	Force	+10$^{1\,µM}$	-4	-22$^{3\,µM}$	72	10
			ERC18	Force	+17	-35	-23	84	10
			ERC18	CaT	+156	-26$^{1\,µM}$	-8	130	10
	Dobutamine	α1-, β1- and β2-adrenoceptor agonist	R-PAT	Force	+43$^{3\,µM}$	-25	-22	60	10
			ERC18	Force	+18	-39	0	118	10
			ERC18	CaT	+111	-13	-15	128	1
	Terbutaline	β2-adrenoceptor agonist	R-PAT	Force	+17	-24	-33	60	3
			ERC18	Force	+29	-30	-16	90	10
			ERC18	CaT	+105	-16	-22	120	10
	Levosimendan	Calcium sensitizer PDE3 inhibitor K$_{ATP}$ channel agonist	R-PAT	Force	+2	-6	-14$^{1\,µM}$	42	1
			ERC18	Force	+13	-7	0	90	1
			ERC18	CaT	+21	-15	-6	105	1
	Pimobendan	Calcium sensitizer PDE3 inhibitor	R-PAT	Force	+11	-2	+12	42	100
			ERC18	Force	+13	-11	+14	90	100
			ERC18	CaT	+25	-13	0	112.5	100
	Omecamtiv mecarbil	Cardiac specific myosin activator	R-PAT	Force	+53	+37	-26	60	0.3
			ERC18	Force	+22	+38	0	90	1
			ERC18	CaT	+45	+16	0	120	1
	Milrinone	PDE3 inhibitor	R-PAT	Force	+18	-11	-9	54	30
			ERC18	Force	+7	-18	0	90	100
Negative inotropes	Verapamil	L-type calcium channel blocker, hERG blocker	R-PAT	Force	-100$^{0.1\,µM}$	-7	-6	60	0.03
			ERC18	Force	-89	-25	-16	90	0.1
			ERC18	CaT	-44	-5	-17	112	0.03
	Flecainide	Sodium channel blocker, hERG blocker	R-PAT	Force	-100$^{3\,µM}$	-16$^{0.3\,µM}$	-26	60	1
			ERC18	Force	-74$^{10\,µM}$	-21	+42	90	3
			ERC18	CaT	-33	-14	+34	112	10
	Sorafenib	Multi-targeted kinase inhibitor	R-PAT	Force	-50	+14	+2	42	10
			ERC18	Force	-50	+5	-24	120	10
			ERC18	CaT	-41	-14$^{1\,µM}$	+6$^{1\,µM}$	120	10
	Sunitinib	Multi-targeted TK inhibitor	R-PAT	Force	+8	+1	0	55	3
			ERC18	Force	-3	+5	-5	90	10
			ERC18	CaT	-64	+8	-3	120	10
	Citalopram	SSR inhibitor, hERG & L-type calcium channel inhibitor	R-PAT	Force	-100$^{10\,µM}$	-4	0	40	3
			ERC18	Force	-100$^{10\,µM}$	+2	0	107	3
			ERC18	CaT	-57$^{10\,µM}$	-6	+4	112	3
	Itraconazole	Triazole antifungal, mechanism unclear	R-PAT	Force	-51	+12	-33	38	3
			ERC18	Force	-100$^{10\,µM}$	+8	-29	84	3
			ERC18	CaT	-33	-6	-8	120	3
	Zimelidine	SSR inhibitor	R-PAT	Force	-100$^{10\,µM}$	-16	-20	40	3
			ERC18	Force	-95	-25	+43$^{10\,µM}$	90	30
			ERC18	CaT	-53	-17	+28	120	10
	Ivabradine	I$_f$ inhibitor	R-PAT	Force	-16	-27	-2	42	10
			ERC18	Force	-56	-27	-2	42	10

Table 4: (continued)

Compound	Mode of action	Cell line	Model	Force/CaT [%]	TTP [%]	RT$_{80\%}$/DT$_{80\%}$ [%]	S. freq. (BPM)	Conc. [µM]
Acetylsalicylic acid	Cyclooxygenase inhibitor	R-PAT	Force	-13	+1	+15	40	1000
		ERC18	Force	+5	-6	-15	90	1000
			CaT	+10	0	+2	90	1000
Paracetamol	Prostaglandin synthesis inhibitor	R-PAT	Force	-19	-20	-6	58	1000
		ERC18	Force	+3	-12	+10	90	1000
Captopril	ACE inhibitor	R-PAT	Force	-15	-10	+6	40	100
		ERC18	Force	-1	-9	-4	144	100
			CaT	+17	-13	-5	90	10
Enalapril	ACE inhibitor	R-PAT	Force	+33	-1	-14	60	100
		ERC18	Force	0	-3	-4	90	100
Clonidine	α2-adrenoceptor agonist	R-PAT	Force	+10	-2	-12	40	0.3
		ERC18	Force	+4	-2	-1	90	1
Phentolamine	Non-selective α-adrenoceptor antagonist	R-PAT	Force	-100$^{10\,µM}$	-18	-28	40	3
		ERC18	Force	-100$^{30\,µM}$	-16	+40	90	3
			CaT	-80$^{30\,µM}$	-10	+35	112	10
Atenolol	β1-AR>β2-adrenoceptor antagonist	R-PAT	Force	-25	0	+14	40	10
		ERC18	Force	+3	-13	-13	90	10
			CaT	-4	+4	-7	120	10
Sildenafil	PDE5 Inhibitor	R-PAT	Force	+7	-4	6	90	10
		ERC18	Force	+7	-6	-6	86	10
Glibenclamide	K$_{ATP}$ channel antagonist	R-PAT	Force	+6	+10	0	90	10
		ERC18	Force	+6	+10	-2	90	10
Tolbutamide	K$_{ATP}$ channel antagonist, Adenylyl cyclase stimulator	R-PAT	Force	-11	-8	+4	40	100
		ERC18	Force	+23	-3	-9	90	100
			CaT	+21	-5	-11	120	100
Pravastatin	HMG CoA reductase inhibitor	R-PAT	Force	-5	-10	14	40	100
		ERC18	Force	+15	-15	-19	84	100
			CaT	+27	-2	-11	112	10

(Left vertical label: Neutral inotropes)

significant), but misclassified as a neutral inotrope in R-PAT (force: +11% (not significant), TTP$_{-80\%}$: -2% (not significant), RT$_{80\%}$: +12%).
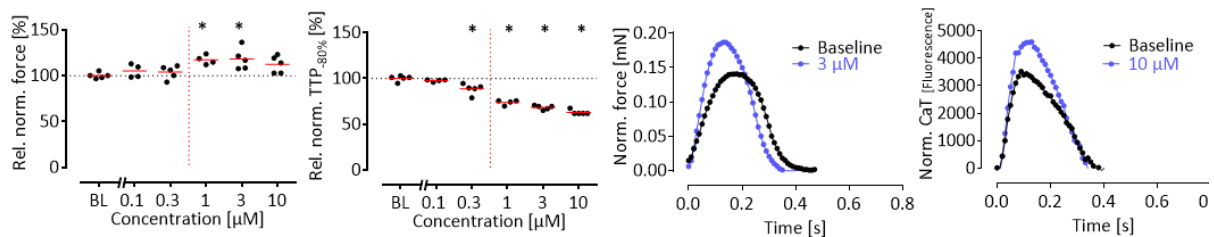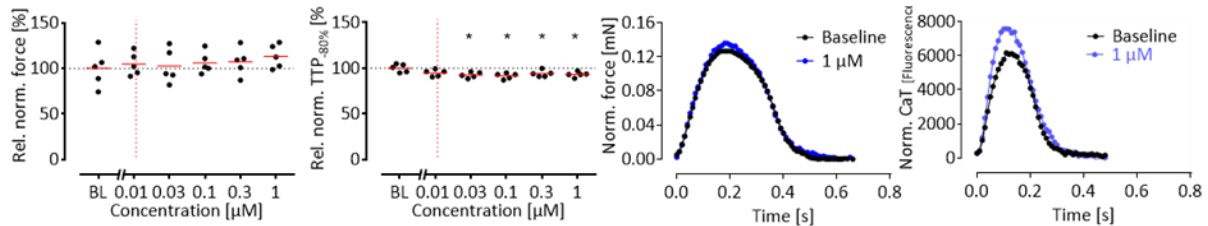

Figure 21: Effects of dobutamine on force and calcium transient (CaT). Left to right: force, time to peak force (TTP$_{-80\%}$), average contraction and CaT peaks (black: baseline; blue: dobutamine 3 µM for contraction and 10 µM for CaT). Data are indicated as relative to baseline (BL) and normalized to time control, and depicted as scatter plots with mean values indicated by red lines (in the left two graphs) and as average peaks with mean values (in the right two graphs). Force: n=4; CaT: n=4. Statistical analysis was performed by one-way ANOVA with Dunnett's post-test vs. BL, *p<0.05.

As an example for positive inotropes, the concentration-response curve of dobutamine demonstrated a PIE (+18%) and positive clinotropic effect (TTP$_{-80\%}$, -39%, Figure 21). In analogy, CaT measurement showed an increase in amplitude of 111% (Figure S1). The average CaT peak (Figure 21) shows a smaller increase in CaT amplitude because different sets of time control data were used to normalize

concentration response curves and average peaks as stated in (5.2.2). The concordance between the two cell lines is shown in Figure S1 and Figure S2.

4.3.2. <u>Positive inotropes NOT matching inotropic assignment</u>

Levosimendan did not show a significant increase in force amplitude in either cell line (+2%/+13%). This was accompanied by a not significant increase in CaT amplitude (+21%, Figure 22). $TTP_{-80\%}$ showed a small, not significant reduction (-7%). Thus, we misclassified this compound as neutral inotrope.

Figure 22: Effects of levosimendan on force and calcium transient (CaT). Left to right: force, time to peak force ($TTP_{-80\%}$), average contraction and CaT peaks (black: baseline; blue: levosimendan 1 µM). Data are indicated as relative to baseline (BL) and normalized to time control, and depicted as scatter plots with mean values indicated by red lines (in the left two graphs) and as average peaks with mean values (in the right two graphs). Force: n=5; CaT: n=4. Statistical analysis was performed by one-way ANOVA with Dunnett's post-test vs. BL, *p<0.05.

4.3.3. <u>Negative inotropes matching inotropic assignment</u>

Eight compounds were assigned as negative inotropes, namely verapamil, flecainide, sorafenib, sunitinib, citalopram, itraconazole, zimelidine and ivabradine. 7/8 compounds were correctly classified as negative inotropes. All these 7 compounds showed a decrease in contraction force of more than -50% at the highest tested concentration (verapamil: -89%; flecainide: -74% (at 10 µM); sorafenib: -50%; citalopram: -65%; itraconazole: -51%; zimelidine: -100% and ivabradine: -56%).

Flecainide is a sodium channel blocker and blocks fast sodium channel responsible for rapid depolarization during phase 0 of cardiac action potential. As a class effect of all sodium channel blocker, flecainide also reduces the contractile force by poorly understood mechanisms (Schulze and Knops 1982; Josephson et al. 1984). Contraction force analysis in EHTs showed a concentration-dependent decrease in contraction force (-74%) and $TTP_{-80\%}$ (-21%), accompanied by an increase in $RT_{80\%}$ (+42%, Figure 23). Data at 10 µM were not included in the analysis, as EHTs did not follow the electrical pacing at this concentration. Like force values, CaT amplitude decreased by -33% and calcium $DT_{80\%}$ increased by +34% (Figure S1 and Figure S2).
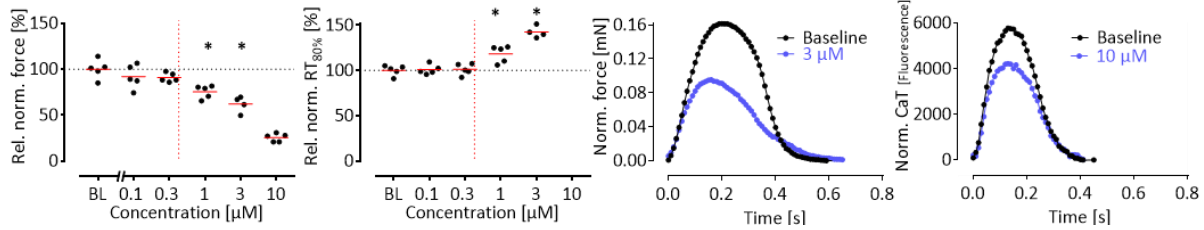
Figure 23: Effects of flecainide on force and calcium transient (CaT). Left to right: force, time to peak force (TTP$_{-80\%}$), average contraction and CaT peaks (black: baseline; blue: flecainide 3 µM for contraction peak and 10 µM for CaT). Data are indicated as relative to baseline (BL) and normalized to time control, and depicted as scatter plots with mean values indicated by red lines (in the left two graphs) and as average peaks with mean values (in the right two graphs). Force: n=5; CaT: n=4. Statistical analysis was performed by one-way ANOVA with Dunnett's post-test vs. baseline conditions (BL), *p<0.05.

4.3.4. Negative inotropes NOT matching inotropic assignment

Sunitinib was not identified as negative inotrope as it did not show any decrease in force (-3%). TTP$_{-80\%}$ and RT$_{80\%}$ were also unaffected, +5% and -5%, respectively (Figure 24, Figure S1 and Figure S2. Notably, in contrast to force, CaT measurements showed a decrease by -64% (Figure S1 and Figure S2). It was classified as a false negative result.
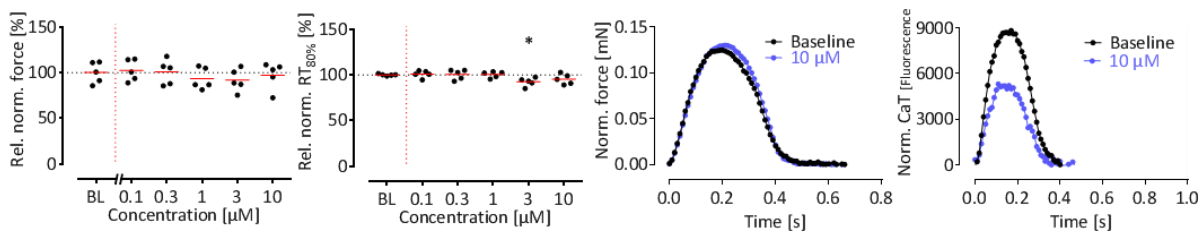

Figure 24: Effects of sunitinib on force and calcium transient (CaT). Left to right: force, time to peak force (TTP$_{-80}$), average contraction and CaT peaks (black: baseline; blue: sunitinib 10 µM. Data are indicated as relative to baseline (BL) and normalized to time control, and depicted as scatter plots with mean values indicated by red lines (in the left two graphs) and as average peaks with mean values (in the right two graphs). Force: n=5; CaT: n=4. Statistical analysis was performed by one-way ANOVA with Dunnett's post-test vs. baseline conditions (BL), *p<0.05.

4.3.5. Neutral inotropes matching inotropic assignment

Eleven compounds were assigned as neutral inotropes (acetylsalicylic acid, paracetamol, captopril, enalapril, clonidine, phentolamine, atenolol, sildenafil, glibenclamide, tolbutamide and pravastatin). 7/11 compound were correctly classified as neutral inotropes in both cell lines (acetylsalicylic acid, paracetamol, captopril, clonidine, atenolol, sildenafil and glibenclamide). Classification as "neutral" was based on relevant (>15%) and consistent changes in force/CaT. Notably, paracetamol and atenolol showed a -19% and -25%, respectively, decrease in contraction force in R-PAT at the highest tested concentration (1000 µM and 10 µM, respectively), but this was interpreted as not concentration-dependent and was not accompanied by any effects on contraction kinetics (Table 4).

Enalapril was correctly classified in ERC18 and misclassified as positive inotrope in R-PAT (force: +33%). Tolbutamide and pravastatin were correctly classified in R-PAT but misclassified as positive inotrope in ERC18 (Tolbutamide: force: +23%, CaT: +21% (not significant); pravastatin: force: +15% (not significant), CaT: + 27%) (Figure S1 and Figure S2).

As an example, the angiotensin converting enzyme inhibitor captopril showed no effects on force and calcium in concentration response curve in both cell lines (Figure 25, Table 4)
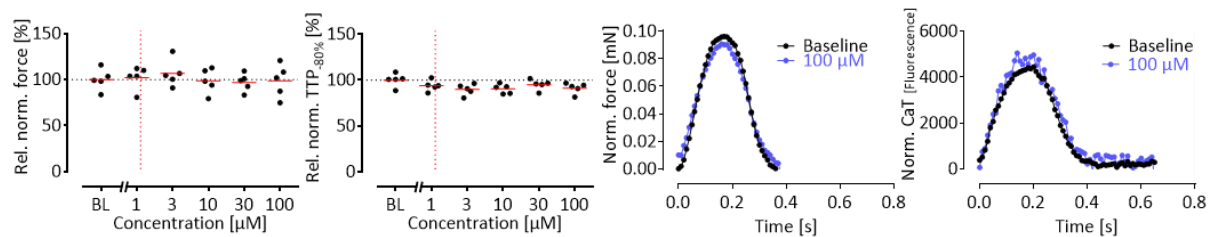

Figure 25: Effects of captopril on force and calcium transient (CaT). Left to right: force, time to peak force (TTP$_{-80\%}$), average contraction and CaT peak (black: baseline; blue: captopril 100 µM). Data are indicated as relative to baseline (BL) and normalized to time control, and depicted as scatter plots with mean values indicated by red lines (in the left two graphs) and as average peaks with mean values (in the right two graphs). Force: n=5; CaT: n=6. Statistical analysis was performed by one-way ANOVA with Dunnett's post-test vs. BL, *$p<0.05$.

4.3.1. Neutral inotropes NOT matching inotropic assignment

Phentolamine is a non-selective α1- and α2-adrenoceptor antagonist and showed strong NIEs of -100% at 10 and 30 µM in R-PAT and ERC18, respectively and a decrease in CaT in ERC18 (Figure S1, Table 4). This was accompanied by decreased TTP$_{-80\%}$ (-18%) and RT$_{80\%}$ in R-PAT (-28%) and decreased TTP$_{-80\%}$ (-16%), increased RT$_{80\%}$ (+40%) and calcium DT$_{80\%}$ (35%) in ERC18 (Figure 26).
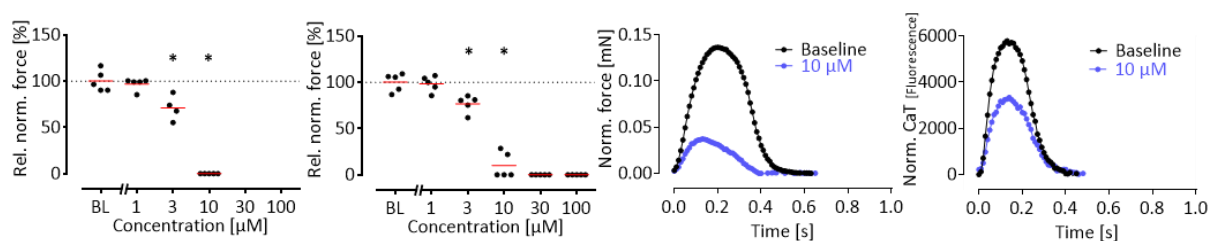

Figure 26: Effects of phentolamine on force and calcium transient (CaT) in R-PAT and ERC18 cell line. Left to right: force R-PAT, force ERC18, average contraction peak and average calcium transient peak ERC18 (black: baseline; blue: phentolamine 10 µM). Data are indicated as relative to baseline (BL) and normalized to time control, and depicted as scatter plots with mean values indicated by red lines (in the left two graphs) and as average peaks with mean values (in the right two graphs). Force: n=5; CaT: n=4. Statistical analysis was performed by one-way ANOVA with Dunnett's post-test vs. baseline BL, *$p<0.05$.

Table 5: Table summarizes the predictive accuracy (%) of blinded screening in two cell lines R-PAT and ERC18, individually and combined.

	Positive inotropes	Neutral inotropes	Negative inotropes	Total
R-PAT	6/8 (75%)	9/11 (82%)	7/8 (88%)	22/27 (82%)
ERC18	6/8 (75%)	8/11 (73%)	7/8 (88%)	21/27 (78%)
R-PAT+ERC18	12/16 (75%)	17/22 (77%)	14/16 (88%)	43/54 (80%)

4.4. Effects of a single high concentration of positive inotropes at a low frequency

The small effect size of positive inotropes compared to negative inotropes has been a limitation of drug screening in our hiPSC-CM EHT model (Mannhardt et al. 2017a) and many other studies (Liu et al. 2012; Jackman et al. 2016; Tiburcy et al. 2017) compared to ex-vivo human heart tissues (Mügge et al. 1985; Böhm et al. 1991; Schotten et al. 2001). The present blinded screening results in ERC18 and R-PAT confirmed this problem and revealed an average effect size of +19±13% (SD, n=77) for positive inotropes as compared to -74±29% (SD, n=59) for negative inotropes (calculated from Table 4). Based on the reverse frequency-dependence of omecamtiv mecarbil effects (Butler et al. 2015; Horváth et al. 2018; Paragraph 4.2.5), we hypothesized that larger effect sizes of positive inotropes can be demonstrated at lower beating frequencies. Moreover, it is well known that bolus applications of a single high concentration often exerts stronger inotropic effects than cumulative concentration-response curves (Guimarães 1972; Garcia-Sevilla et al. 1974; Sørensen 1990).

A new series of experiments was therefore designed in which the spontaneous beating rate of EHTs was reduced by addition of ivabradine (300 nM, 3 h incubation) and highest concentrations of drugs were applied as a bolus. Ivabradine reduced the spontaneous frequency of EHTs from ~1.5 to 0.5 Hz and EHTs were paced at three different stimulation frequencies (0.5 Hz, 1.5 Hz and 2.5 Hz) after drug application. Levosimendan 1 µM (highest concentration tested in the blinded screen), which failed to depict PIEs in the blinded screen, now exerted a PIE effect at 0.5 Hz and a reverse frequency correlation (Figure 27, peak force at 0.5 Hz: +22±17% SD; 1.5 Hz: +19%±15% SD; 2.5 Hz: +8%±9% SD). The reduction of $TTP_{-80\%}$ was also significant only at 0.5 Hz and showed a reverse frequency dependency (0.5 Hz: -18±4% SD; 1.5 Hz: -6%±5% SD; 2.5 Hz: -7%±3% SD). The results for $RT_{80\%}$ were less consistent and did not show a reverse frequency dependency (Figure 27A. This analysis shows an increase in force effect size by lowering beating frequency and single high concentration compound administration. Among these two changes in the measurement protocols, ivabradine-mediated reduction in beating frequency might be more relevant because administration of single high

concentration of levosimendan in the absence of ivabradine did not lead to a higher inotropic effect size (Figure 27A).

Table 6 : Effects of positive inotropes on hiPSC-CM EHTS of ERC18 as a single concentration administration at 0.5 Hz, and in cumulative concentration-response curve (CCRC) at 1.5-2.3 Hz. Listed are relative changes in percentage compared to mean baseline for force, time to peak force (TTP$_{-80\%}$), relaxation time (RT$_{80\%}$) at stimulation frequency (beats per minute, BPM) for 6 inotropes analysed in two groups 1) under stimulation frequency of 0.5 Hz (bolus) and 2) 1.5-2.3 Hz (CCRC).

	0.5 Hz (ivabradine)/single				1.5-2.3 Hz/CCRC			
	Force [%]	TTP$_{-80\%}$ [%]	RT$_{80\%}$ [%]	Frequency (BPM)	Force [%]	TTP$_{-80\%}$ [%]	RT$_{80\%}$ [%]	Frequency (BPM)
Epinephrine	+22	-17	+14	30	+16	-13	-9	136
Forskolin	+57	-34	-2	30	+17	-35	-23	84
Dobutamine	+42	-41	-8	30	+18	-39	0	118
Levosimendan	+22	-18	+8	30	+13	-7	0	90
Pimobendan	+27	-15	+37	30	+13	-11	+14	90
Milrinone	+18	-28	-1	30	+7	-18	0	90
Average	**+31**	**-26**	**+8**	**30**	**+14**	**-21**	**-3**	**101**
SD	±15	±11	±13	0	±4	±13	±11	±21

Under the same conditions (ivabradine 300 nM, 0.5 Hz pacing, bolus), epinephrine, forskolin, dobutamine, pimobendan and milrinone exerted significant PIEs (epinephrine: +22±24%; forskolin: +57±17%; dobutamine: +42±23%; pimobendan: +27±12%; milrinone: +18±10%; SD, n=5, Figure 27C, D). The average PIE of these 5 compounds was 2.2-fold greater under these conditions (+31±15%) than during the blinded screen (cumulative, 1.5-2.3 Hz; +14±4%, SD, n=39; Table 6). The clinotropic effect size was 1.2-fold higher (-26±11% at 0.5 Hz vs.-21±13% at 1.5-2.3 Hz). Notably, no similar correlation was observed for the lusitropic effect (Figure 27C, D). In fact, RT$_{80\%}$ did not decrease in the presence of epinephrine, forskolin, dobutamine and milrinone, even though positive lusitropic effects would have been expected. Pimobendan, PDE3 inhibitor and a calcium sensitizer, showed a pronounced prolongation in the RT$_{80\%}$, compatible with the calcium sensitizing mechanism.

Taken together, this series of experiments showed that positive inotropic and clinotropic effects in EHTs could be better evaluated at lower pacing rate and with a bolus application than at higher rate and cumulative concentration-response curves.
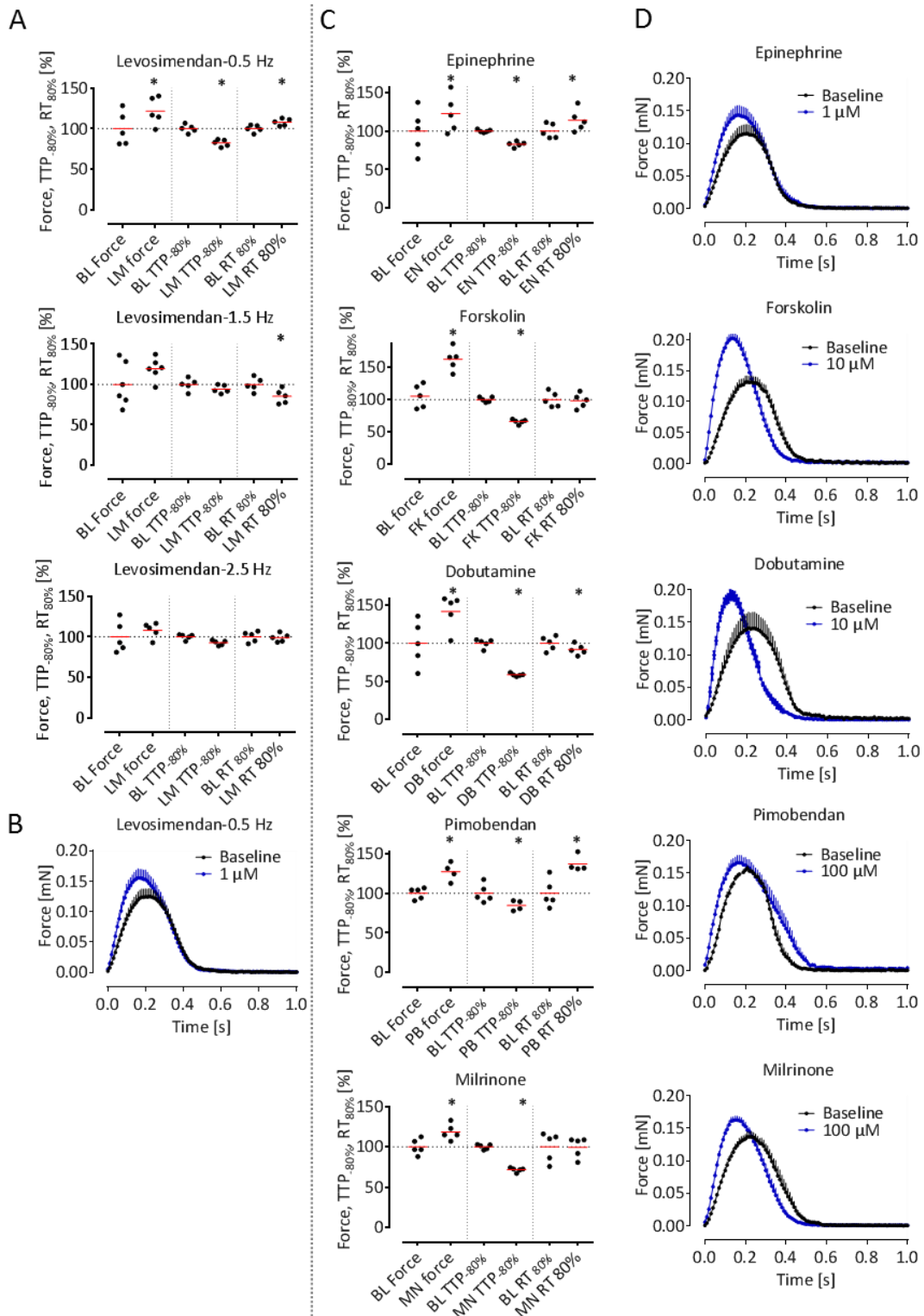
Figure 27: Effects of a single high concentration of positive inotropes at low frequency in the presence of ivabradine (300 nM). Data are depicted as relative effects to mean baseline in scatter plot format (mean±SEM) for force, time to peak force (TTP$_{-80\%}$), and relaxation time (RT$_{80\%}$). Average peaks indicate mean±SEM in the absence (black) and presence of drug (blue). (A) Effects of levosimendan (1 µM, n=5) at a frequency of 0.5, 1.5 and 2.5 Hz. BL: Baseline, LM: levosimendan. (B) Average peak depiction at 0.5 Hz. (C) Effects of epinephrine (EP, 1 µM, n=5), forskolin (FK, 10 µM, n=5), dobutamine (DB, 10 µM, n=5), pimobendan (PB, 100 µM, n=5) and milrinone (MN, 100 µM, n=5) at 0.5 Hz. (D) Average peak depiction of the data in Figure 27C. One-way ANOVA with Dunnett's post-test vs. baseline (BL), *p<0.05.

4.5. Regulation of phosphodiesterases in hiPSC EHTs

4.5.1. Expression of PDE in hiPSC-CM EHTs and non-failing heart (NFH)

The previous section revealed that high beating frequency correlate with small PIE sizes. In addition, immaturity of important intracellular regulators of force development might contribute. A previous study (Mannhardt et al. 2017a) revealed a strong effect of PDE4 inhibitor rolipram and a small effect of PDE3 inhibitor milrinone, suggesting unusual PDE regulation in hiPSC-CM. This section therefore focused on the regulation of PDEs in hiPSC-CM.

PCR primers were designed to determine the transcript levels of the following PDE isoforms and family members: PDE1A/B/C, PDE2A, PDE3A/B, PDE4A/B/C/D, PDE5A and PDE7A. In a first step, qualitative RT-PCR was performed on total RNA of hiPSC-CM EHTs and human non-failing heart (NFH). PDE isoforms 1B, 1C, 2A, 3A, 4A, 4B, 4C, 4D and 7A gave robust signals in both samples. In contrast, only a faint band was detected for PDE5A, whereas PDE1A and 3B could not be amplified in either sample (Figure 28A). The direct comparison between hiPSC-CM and NFH revealed a stronger band in NFH for PDE1B, 2A, 3A, 4A and 4C (Figure 28A). This was confirmed in a second step where a quantitative PCR was performed for PDE3 and PDE4 isoforms in hiPSC-CM EHTs and NFH and showed a significantly lower expression (0.5-fold) of PDE3A and 4A transcripts in hiPSC-CM vs. NFH (Figure 28B). Estimation of absolute expression level by raw cycle threshold (CT) values suggested that in NFH PDE3A (mean CT: 24.8), PDE4A (mean CT: 25.8) and PDE4D (mean CT: 25.6) were expressed at high level and PDE3A (mean CT: 27.7), PDE4B (mean CT: 27.8) and PDE4D (mean CT: 27.6) were expressed at high level in hiPSC-CM EHT (Figure S4).

4.5.2. Effects of PDE inhibitors on force

The lower expression of PDE3A and 4A in hiPSC EHTs vs. NFH led to the question how selective inhibitors of PDE isoforms regulate contractile force. To address this question, force measurements were performed in hiPSC-CM EHTs equilibrated in Tyrode´s solution with 0.6 mM Ca^{2+} (~EC_{50}) and electrically stimulated at 1.5-2.0 Hz. The concentration response curve of isoprenaline was performed after incubation with/without PDE inhibitors. Figure 28C demonstrates the effect of PDE inhibitors and isoprenaline on force. Time control recordings and vehicle control (0.1% DMSO) showed no effect on force (Figure 28C). Isoprenaline alone increased force by +51%. The PDE3 inhibitors cilostamide (300 nM) or milrinone (10 µM), the PDE5 inhibitor tadalafil (10 nM) or the non-selective PDE inhibitor IBMX (10 µM) did not increase force when applied alone (Figure 28C). In contrast, the PDE4 inhibitor rolipram (10 µM) led to a PIE of +42%. Isoprenaline in the presence of PDE inhibitors increased force by +40±13% (SD, n=5, Figure 28C) with a smaller effect in the presence of rolipram.
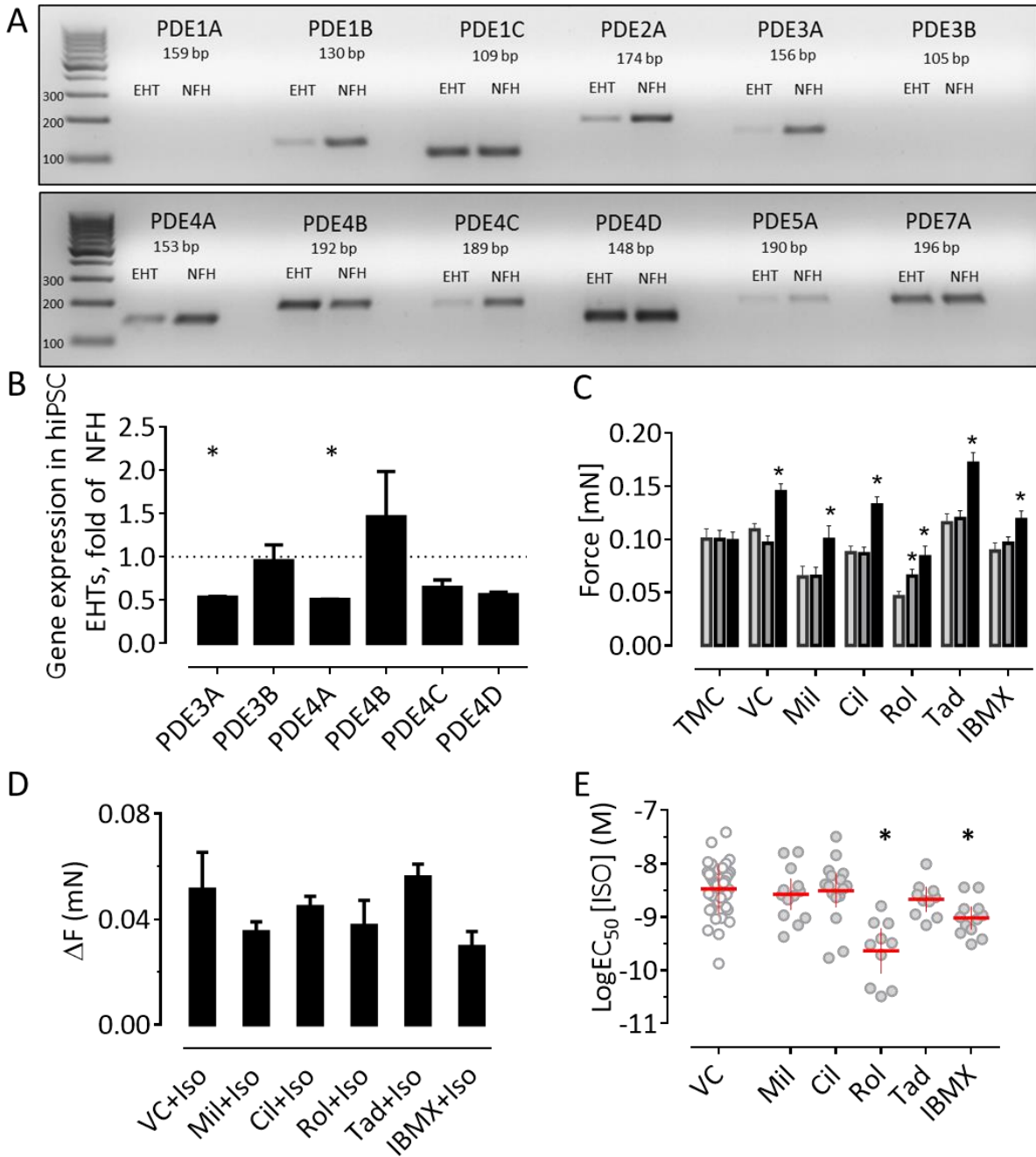
Figure 28: Regulation of phosphodiesterases in hiPSC EHTs. (A) Qualitative RT-PCR of different PDE-isoforms (35 cycles). NFH: non-failing heart. (B) Quantitative RT-PCR. Relative gene expression of PDE3 and 4 isoforms in hiPSC-CM EHT, normalized to NFH, mean±SEM, n=5 (ΔΔCT). Unpaired t-test vs. NFH,*p<0.05. (C) Effect of PDE inhibitors on force and on isoprenaline response (100 nM) in electrically stimulated (1.5-2.0 Hz) hiPSC-EHTS. Bars show mean±SEM. One-way ANOVA with Bonferroni's post-test vs. their respective baseline conditions (BL), *p<0.05. Light grey: baseline; grey: PDE inhibitor; black: isoprenaline in the presence of PDE inhibitor. TMC: time control (n=20/5); VC: Vehicle control, DMSO 0.1% (n=24/5); Mil: milrinone (10 μM, n=19/4), Cil: cilostamide (300 nM, n=19/3); Rol: rolipram (10 μM, n=10/2); Tad: tadalafil (10 nM, n=12/2); IBMX (10 μM, n=15/3), n/n=number of EHTs/number of differentiation batches (the number of EHTs were used for statistics). (D) Depiction of the same data as Δforce (PDE+Iso vs. baseline) as in C. Mean±SEM, One-way ANOVA vs. respective baseline. (E) Effect of PDE inhibitors on the inotropic potency of isoprenaline in electrically stimulated (1.5-2.0 Hz) hiPSC-CM EHTs, expressed as Log EC$_{50}$ for isoprenaline. Scatter plot and mean±SEM. One-way ANOVA followed by Dunnett's post-test vs. vehicle control; *p<0.05. VC: n=40/6; Mil: 10 μM, n=13/3; Cil: 300 nM, n=16/3; Rol: 10 μM, n=11/2; Tad: 10 nM, n=12/2; IBMX: 10 μM, n=13/3.

Figure 28D demonstrates the Δforce values for isoprenaline effects. No statistical difference in Δforce values was detected (One-way ANOVA).

4.5.1. <u>Effects of PDE inhibitors on isoprenaline potency</u>

Concentration-response curves for isoprenaline were performed in hiPSC-CM EHTs in the presence and absence of PDE inhibitors. Figure 28E displays the EC_{50} values for this experiment in a scatter plot graph. The EC_{50} of isoprenaline for the force response was 2.6 nM when applied alone (Figure 28E). In the presence of the PDE3 inhibitors cilostamide (300 nM) or milrinone (10 µM), the potency of isoprenaline remained unchanged (2.5 nM, 3.0 nM, respectively). Pre-incubation with the PDE4 inhibitor rolipram (10 µM) led to a decrease in isoprenaline EC_{50} value (0.2 nM). The PDE5 inhibitor tadalafil did not change the isoprenaline potency (EC_{50}: 2.6 nM). The non-selective PDE inhibitor IBMX increased the isoprenaline potency to 0.9 nM.

5 <u>DISCUSSION</u>

This study describes an advanced test system to sequentially analyse contraction and CaT in hiPSC-CM EHTs. The main findings are as follows: 1) A test system was established to sequentially analyse contractility and CaT in EHTs virally transduced with GCaMP6f. 2) Indicator drugs exhibited compound-specific effects on force and CaT, precisely replicating known mechanisms of action. 3) hiPSC-CM EHTs showed a positive force-frequency- and CaT-frequency-relationship between 0.5 and 1.5 Hz. 4) OM's PIE showed a reverse frequency relationship in hiPS-CM EHTs. 5) Two hiPSC cell lines were efficiently differentiated on a larger scale for blinded drug screening of 27 compounds. 6) 6/8 positive inotropes, 7/8 negative inotropes and 8/11 or 9/11 neutral inotropes were correctly identified. 7) The small effect size of positive inotropes in this screen could be improved by applying a single high concentration (bolus) at low frequency (reverse frequency relationship) compared to a cumulative analysis at higher frequency. 8) PDE activity in hiPSC-EHTs is predominated by PDE4 in contrast to the adult human heart in which PDE3 is dominant.

5.1. <u>Establishment of the system</u>

A test system was established to sequentially analyse force and CaT in hiPSC-CM EHTs virally transduced by GECIs. Two GECIs (GCaMP5G and GCaMP6f) and two viral vectors (lentivirus and AAV6) were tested. Both AAV6 and lentiviral vectors were sufficient to transduce hiPSC-CM when the viral particles were combined with the EHT master-mix at the time point of EHT generation. Both viruses enable efficient and stable transduction. Lentivirus is easy to produce and yields high titers. On the other hand, it can mediate cytotoxicity at higher MOI, integrates into the genome, and leads to insertional mutagenesis. The latter is particularly relevant for *in vivo* applications but not for *in vitro* transduction of non-proliferating cardiomyocytes (Picanço-Castro et al. 2008). In contrast, AAV is not integrating and has low toxicity, and is therefore preferred for *in vivo* application (Kotterman et al. 2015). By delivering viral particles during EHT generation, expression of the sensor is also present during the process of EHT development that can lead to potential toxicity and lower force development (data not shown). This toxicity is related to the calcium buffering effect of calcium sensors expressed in the cytoplasm of the cardiomyocytes. When calcium is released from the SR during electromechanical coupling, the calcium ions do not reach the myofilaments because they are snatched away by GCaMP sensors in the cytoplasm (Helmchen et al. 1996; Tian et al. 2009). Hence, contraction and cellular shortening are impeded by GCaMP sensors. Nevertheless, this approach turned out to be very robust and led to long-term stable expression of the GECI with high signal-to-noise ratios for weeks in contracting EHTs. Alternatively, we tried to optimize transduction of hiPSC-CM EHTs only a few days before analysis. This approach turned out not to be successful and

did not result in robust detection of CaT. Reasons for failure might be the poor accessibility of cardiomyocytes in the fibrin matrix.

GCaMP5G transduction led to fluorescence signals with $TTP_{-80\%}$ for CaT similar to $TTP_{-80\%}$ for force, and calcium $DT_{80\%}$ longer than $RT_{80\%}$ (Figure 12A). These slow on and off kinetics were overcome with GCaMP6f (Figure 12B), which is the faster acting member of the GCaMP family and was shown to have a 3-, to 4-fold faster decay response over other GCaMP members (Badura et al. 2014). Despite these improvements, time to CaT amplitude peak is still reached slower than with calcium-sensitive dyes. In consequence, force calcium loops from dye-based recording show an initial phase of calcium rise and a second phase of force increase after calcium amplitude is reached (Stoehr et al. 2014), while these two phases are merged in loops from GCaMP6f recordings (Figure 12A, B).

Motion artefacts have been reported to fraught the CaT measurements (Cleemann and Morad 1991; Brandes et al. 1992; Broussard et al. 2014). This is particularly important for models with auxotonic contractions (as this one) where the development of force is accompanied by substantial muscle shortening. To reduce the impact of motion artefacts in this model, we always recorded fluorescence intensity from a small, 0.1x0.4 mm^2 surface area in the centre of the EHT where motion during contraction is small (Figure 14D). Under these conditions, fluorescence measurements of untransduced and GFP-only-transduced EHTs showed (much smaller than with GCaMP sensors) fluorescence light and kinetics superimposed with force (Figure 14A, B). For untransduced and GFP-transduced EHTs, fluorescence signal did not reach baseline level after the CaT, as indicated in the average peak (Figure 14A, B). This is likely an artefact due to the very low fluorescence signal intensity and poor signal to noise ratio in this case. The similarity of force and fluorescence signal kinetics and lack of sequential order of CaT amplitude preceding force amplitude argue in favour of a motion artefact. On the other hand, this finding supports the specificity of the GCaMP-derived fluorescence signals (CaT) demonstrated in Figure 12. Afterload-enhancement with high resistance metal braces revealed strongly reduced force amplitude, but did not affect CaT amplitude. Unaltered CaT amplitude under conditions where motion is reduced indicates that motion artefacts do not have a high relevance for the fluorescent signal intensity in the present settings (Figure 14C).

Characterization of indicator compounds revealed an increase in information and thereby possibly predictive value by combining readout for force and CaT (Figure 15). Specifically, the PIEs of isoprenaline (10 nM), Bay K-8644 (300 nM), digoxin (0.3 µM) and EMD-57033 (10 µM) were accompanied by characteristic changes of CaT. Isoprenaline and digoxin increased the CaT amplitude. While for digoxin the kinetics of CaT remained unchanged, isoprenaline led to a reduction in time to calcium peak. BAY K-8644 (300 nM) led to a pronounced increase in time to calcium decay and no

increase in amplitude as recently described for this concentration range (Sen et al. 1990; Cerignoli et al. 2012). The inotropic effect of EMD-57033 was not associated with any change in CaT as described previously and expected for an almost pure calcium sensitizer (Ishitani et al. 2001, Maack et al. 2018). The true value of the combined analysis will probably be even larger during drug development and high throughput screening, when analysing compounds with unknown mode of action or patient-specific disease cell lines.

The lack of a positive force-frequency relationship in hiPSC-CM EHTs in past reports (Mannhardt et al. 2016; Ruan et al. 2016) was interpreted as an indicator for cardiomyocyte immaturity. The discovery of a positive force frequency-relationship in this model masked by high spontaneous frequency is therefore an important finding (Figure 16). It confirms that a positive force frequency is replicated in this model, however, experimental conditions that reduce the spontaneous beating rate (ivabradine) were required to demonstrate it. To substantiate this finding, a positive correlation between CaT and frequency was also demonstrated, which is in line with past reports on FFR in different mammalian species (Gwathmey et al. 1990; Monasky and Janssen 2009). Notably, the positive FFR in the human myocardium was demonstrated between 0.3-1.0 Hz (Gwathmey et al. 1990) 0.5-2 Hz (Hasenfuss et al. 1996) and 0.2-2.9 Hz, respectively (Mulieri et al. 1992). In contrast, rabbit and rat trabeculae showed a positive FFR at 1 to 4 Hz and 4 to 8 Hz, respectively (Monasky and Janssen 2009), demonstrating that a positive FFR prevail in the range of physiological heart rate for the different species (Endoh 2004). Mechanistically, cardiomyocytes increase calcium load with increasing frequency. The LTCCs are important for calcium entry into the cardiomyocytes. Sarcoplasmatic calcium reuptake and NCX are important to reduce cytoplasmic calcium during relaxation. The slower kinetic of calcium efflux via NCX leads to intracellular accumulation with increasing frequency since the relative contribution of NCX to calcium removal decreases with higher frequencies (Endoh 2004). The demonstration of a positive FFR accompanied by a positive correlation with CaT in hiPSC-EHT between 0.5-1.5 Hz indicates that this complex interplay between different calcium handling mechanisms is functional in the hiPSC-EHT model. Notably, while the force amplitude values declined at rates >1.75 Hz, the CaT amplitude started to decline at higher frequencies (2.5 Hz). This dissociation between force and CaT amplitudes at high frequencies has also been previously described for mammalian heart preparations (Endoh 2004) pointing to the relevance of this finding. Nevertheless, an open question is why the FFR turned into a negative correlation above 1.5 Hz while the human heart beats at up to 3 Hz *in vivo*. On the one hand, this could be related to the lack of full maturation of calcium handling machinery in hiPSC-EHTs, on the other hand this could also be an observation specifically related to this cell line. In favour of the latter argues the observation that in a large screen of different cell lines in the context of the "ERC IndivuHeart" project in our laboratory (not presented

in this thesis), FFR showed substantial diversity with a positive correlation for some cell lines of up to 5 Hz.

The principle of lowering the baseline frequency in hiPSC-CM EHTs with ivabradine to demonstrate a positive FFR (Figure 16) was taken forward to analyse the effect of OM. The data confirmed the reverse frequency-dependency of the inotropic effect previously reported in two canine models (Butler et al. 2015; Horváth et al. 2017). In addition to the PIE, this experiment also revealed an increase in $TTP_{-80\%}$ as previously described (Figure 17). OM did not show any effect on CaT amplitude, which is in line with the reported mechanism of action and recent reports (Butler et al. 2015; Horváth et al. 2017). Lack of change of the CaT amplitude (in contrast to force amplitude) also argues against a motion artefact. Mechanistically, the smaller PIE of OM at higher frequency is likely related to the phenomenon of myofilament calcium desensitization at higher frequencies (Morii et al. 1996; Endoh 2004; Varian and Janssen 2007) in part mediated by increased phosphorylation of myosin light chain 2 and troponin I at a higher frequency of 4 Hz (Varian and Janssen 2007).

5.2. Blinded screening.

The contractility/CaT assay was further validated by the blinded screening of 27 compounds. Cardiomyocytes were differentiated and 450 EHTs were generated successfully to analyse force and CaT.

5.2.1. Quality control

EHT from the two cell lines, ERC18 and R-PAT, differed in terms of baseline force, $RT_{80\%}$ (Figure 19) and spontaneous beating frequency (not shown). The latter may account for some of the differences in force and kinetics such as $RT_{80\%}$ because R-PAT had to be paced at a higher rate and contraction kinetics are strongly rate-dependent (Figure 19). Also, the differences in differentiation protocol might be relevant for the differences in baseline parameters. Both cell lines met the quality control criteria by exhibiting the expected positive inotropic response to isoprenaline-mediated β-adrenoceptor stimulation and negative inotropic response to LTCC block by nifedipine (Figure 19. Notably, ERC14 showed a 14-fold smaller isoprenaline-induced increase (+11%) in force amplitude than R-PAT (+154%). This difference is likely related, at least in part, to the high baseline force values of ERC18, leaving small room for further force enhancement. This small increase in force amplitude by isoprenaline is consistent with the small effect size of positive inotropes in the blinded screen. Despite the small PIE, a strong positive clinotropic effect (23%) was seen, which again aligns well with the +29% positive clinotropic effect of other cAMP-dependent compounds (epinephrine, forskolin, terbutaline and dobutamine) in ERC18 in the blinded screen. In R-PAT, the clinotropic effect was absent and the

lusitropic effect was very small. Notably, baseline $RT_{80\%}$ for R-PAT was very long (0.29 s, Figure 20B). This on the one hand may raise the expectation for strong positive lusitropic effects, on the other hand it might be an indicator of relaxation disturbance and poor reaction to positive lusitropic mechanisms. Pronounced nifedipine-mediated NIEs in both cell lines (42% in ERC18 and 32% in R-PAT) adheres very well to the large effect sizes of negative inotropes in the blinded screen.

5.2.2. Time-matched vehicle controls

Cell line-specific experimental run down in Tyrode´s solution was observed and was markedly reduced for ERC18 by replacing it with DMEM-H. Previous studies have also reported changes in contractility of guinea pig hearts and electrophysiological properties of dog right ventricular papillary muscle in Tyrode´s solution (Fulop et al. 2003). Even in DMEM-H, ERC18 showed a decrease in force and an increase in $TTP_{-80\%}$ and $RT_{80\%}$ during the course of the experiment, but the effect size was <10%. This compares to a 15% decrease in force for R-PAT in Tyrode´s solution (Figure S). Time-dependent run down in force for R-PAT could also have been improved by using DMEM-H, but this was not tested.

The experimental rundown for contractility parameter was an important issue in this blinded screen. To compensate for this limitation, data were normalized to time-matched vehicle controls. 2-4 EHTs were used as time-matched controls and 4-6 EHTs were used for each compound and four compounds were analysed in parallel. Due to lower replicate number of time-matched controls for individual experiments, data for time matched controls were pooled and drug effects were normalized to this pooled time control data. This normalization step helped us to achieve 75% accuracy (Table 5) in predicting drug effects of positive inotropes. On the other hand, this normalization procedure is not perfect since experimental rundown was variable between different experiments. In fact, false classification of 3 neutral compounds as positive inotropes (enalapril, tolbutamide and pravastatin) in the present study could be related to the use of pooled time controls (Table 4). Further improvement in predictivity is expected in future screen by normalization to a proper number of time-matched controls of the same experiment. This will require higher numbers of time controls for each experiment and thereby reduces the throughput of the assay.

5.2.3. Compound assignment

Careful selection of indicator compounds with defined effects/modes of action under *in vitro* conditions is required for a validation experiment of this kind and differences between *in vivo* and *in vitro* effects need to be considered. This is particularly true for competitive receptor antagonists (e.g. β-adrenoceptor antagonist atenolol) which require the presence of the respective agonist (e.g. epinephrine) to exert their effect. Notably, some β-blockers (e.g. propranolol; Labow et al. 1991) do

exert negative inotropy by "membrane-stabilizing" effects, likely sodium channel block (Matthews and Baker 1982) in the absence of receptor agonists. Other compounds, such as clonidine, require an intact sympathetic nervous system that does not exist in engineered hiPSC-CM preparations.

5.2.4. Positive versus negative inotropes

In general, hiPSC-CM models show weaker PIEs compared to experiments in *ex vivo* heart tissue (Jackman et al. 2016; Mannhardt et al. 2016; Tiburcy et al. 2017). In part, this is related to the smaller increase in LTCC current (Uzun et al. 2016). Furthermore, all other previously described markers of hiPSC-CM immaturity are likely to contribute to this (Denning et al. 2016). Many positive inotrope compounds exert their effect via β-adrenergic effects which are known to show desensitisation, in particular under *in vitro* conditions (Limas and Limas 1984). This might have contributed to the transient PIE sometimes observed at intermediate concentrations that fainted away at high concentrations (e.g. epinephrine). To increase the accuracy, a separate experiment with a single high concentration of the compound needs to be included in future studies of this kind.

Figure 27 suggests that the accuracy to detect positive inotropes can be further increased if this is done under low beating frequency by ivabradine pre-incubation. An open question at this point is if ivabradine could not be included as a baseline condition in a screen of this kind. At 300 nM ivabradine is a specific I_f current inhibitor (Bois et al. 1996). This intervention would likely also facilitate to perform all experiments with the exact same beating frequency that was not possible in this screen. On the other hand, the lack of positive lusitropic effect for several cAMP/PKA-mediated compounds (Table 6) is a note of caution for the general use of ivabradine as baseline condition and requires further assessment.

The screening data further suggest that NIEs can be detected easier in hiPSC-CM models which is in line with earlier reports with hiPSC-CM models (Pointon et al. 2015). Reasons for this might include the following: 1. many NIE compounds do not show desensitisation; 2. The prerequisites for PIEs are higher and require baseline conditions with submaximal force and a higher degree of maturation of calcium handling and myofilament organisation; 3. Suboptimal testing conditions (temperature, pH, energy substrate depletion, off-target effects of the compound under investigation) are overall much more likely to reduce than increase force, hence the direction of effect is the same as for NIEs; 4. Many test assays show decreases in force in the course of the experiment (rundown), hence PIE can often only be demonstrated when the experiment is sufficiently powered with time controls.

5.2.5. <u>Acute versus delayed effects, transient versus steady state effects</u>

Many negative inotropic compounds show acute effects, which can be detected in concentration-response curves with standard incubation times of 20-40 min. On the other hand, NIE mediated by structural toxicity do not necessarily follow the same kinetic and can also occur after prolonged incubation times. In this context the NIE of sunitinib was likely missed in this screen, since it also showed only a delayed (>24 h) NIE in rat EHT recently (Jacob et al. 2016) and recent own unpublished experiments confirmed this in hiPSC-EHT. For future screens of this kind it might therefore be helpful to extend incubation time for the highest concentration for 24 h if no effect is detected after 20-40 min.

5.2.6. <u>Work load</u>

In this screening experiment concentration-response curves for 4 compounds (n=4-6) were analysed in parallel with 3-5 EHTs for time control. The average time for such an experiment was 8 h (2 h per compound). Manual data processing, normalization to time-matched control and analysis took on average another 4 h per compound. This can likely be reduced substantially to 1 h per compound with automated softwares, which are currently under development in cooperation with the UKE core facility for bioinformatics. Integrating the conclusions from previous paragraphs (higher number of time controls per experiment, extending analysis of highest concentration for 24 h in case no effect is detected, additional experiment with a single high concentration in the presence of ivabradine) would require another 4 h per compound and would result in approximately 7 h for the experimental part per compound in future experiments. Notably, this calculation does not include preanalytical aspects like hiPSC-CM differentiation, EHT generation and maintenance.

5.2.7. <u>Positive inotropes matching the inotropic assignment</u>

In the present blinded screen, the inotropic effect of positive inotropes was +19% on average across both cell lines. The accuracy of detection of PIEs was 75% (Table 4). This represents a substantial improvement compared to a previous blinded screen (Mannhardt et al. 2017a). One reason for the better outcome is likely the combination of force and CaT vs. force alone in the previous study (Mannhardt et al. 2017a). In fact, CaT analysis in parallel with contraction facilitated the prediction of the inotropic effect of compounds where small inotropic effect size complicated the correct interpretation. Forskolin, levosimendan, pimobendan and milrinone did not show significant inotropic effects (≥15%) but CaT analysis of forskolin, levosimendan and pimobendan revealed +156%, +21%, +25% increase in CaT analysis, respectively. This was instrumental for the correct categorization of forskolin and pimobendan. Some positive inotropes showed inconsistent results between both cell

lines (e.g. epinephrine, pimobendan). The chances are high that these compounds will be picked up consistently by analysis under low frequencies and as bolus application.

5.2.8. <u>Positive inotropes NOT matching the inotropic assignment</u>

Levosimendan's mechanism of action is to increase the myofilament calcium sensitivity by binding to cardiac troponin C. It also acts by inhibiting PDE 3 (Ørstavik et al. 2014) and opening ATP dependent potassium K_{ATP} channels (Yokoshiki et al. 1997). It increased peak shortening in canine myocytes (Harmer et al. 2012) and showed CaT increments in rabbit ventricular cardiomyocytes (Sato et al. 1998). It was incorrectly classified as a neutral inotrope in the current study due to lack of effect on contraction force in R-PAT and ERC18 (Figure 22). In line with our findings, it has also been classified as a neutral inotrope in hiPSC-CM and neonatal rat cardiomyocytes (Scott et al. 2014) pointing to the difficulty to demonstrate the PIE of levosimendan *in vitro*. On the other hand, levosimendan did show a +21 % (not significant) increase in the amplitude of CaT and decrease in time to CaT peak (-15%), but this finding was not taken into account when classifying this compound as neutral since the effect did not reach significance. In addition, as for pimobendan, future screens integrating the analysis at low pacing rate (in the presence of ivabradine) increases the likelihood to pick it up (details in section 4.4).

5.2.9. <u>Negative inotropes matching the inotropic assignment</u>

Seven out eight inotropes matched the inotropic assignment. Flecainide, a sodium channel blocker, belongs to class IC of antiarrhythmic drugs. It blocks fast sodium channels responsible for rapid depolarization during phase 0 of the cardiac action potential and exhibits NIEs by an unknown mechanism (Lynch et al. 2013). The results obtained with EHTs of both cell lines replicate its established NIE. This was accompanied by a reduction in CaT amplitude. Furthermore, flecainide has also been shown to prolong action potential in atrial and ventricular papillary muscles in guinea pigs (Borchard and Boisten 1982) and hiPSC-CM (Gibson et al. 2014) by blocking I_{Kr} (Reviewed by Darbar 2014). We observed similar findings indirectly in ERC18 EHTs showing an increase of $RT_{80\%}$. On the other hand, no increase in $RT_{80\%}$ was observed for R-PAT EHTs. This might be related to the much longer $RT_{80\%}$ for R-PAT EHTs at baseline (Figure 19B, C).

5.2.10. <u>Negative inotropes NOT matching the inotropic assignment</u>

Among negative inotropes in the screening list, only sunitinib did not match the inotropic assignment. Sunitinib is a tyrosine kinase inhibitor and reduces the contractile force *in vitro* (Rainer et al. 2012) and is associated with left ventricular dysfunction *in vivo* (Lorenzo et al. 2009). The present study revealed no effect on contraction force and kinetics at up to 10 µM in any of both cell lines after 30-min incubation (Figure 24). This is consistent with previous studies showing no effects after 2 h and NIEs

after 48 h at 10 µM in rat EHTs (Jacob et al. 2016) and prolonged field potential duration at 1 µM after 4 h in human embryonic stem cell-derived cardiomyocytes (Clements et al. 2015). Recent own unpublished experiments confirmed the delayed onset of NIEs in hiPSC-EHT. On the other hand, two recent studies have reported NIEs in human right atrial appendages at 2.5 µM after 5 min (Rainer et al. 2012), and hiPSC-CM and neonatal rat CM at 30 µM after 20 min (Scott et al. 2014). While the differences in sensitivity cannot be unravelled easily, the *in vivo* NIE is not acute and early onset. Notably, although no effect on contraction was observed, CaT analysis revealed a -64% decrease in amplitude (10 µM, n=3). While this observation could suggest that CaT might be a more sensitive parameter to demonstrate the NIE of sunitinib this would also imply a calcium sensitising effect and requires further experiments to role out a matter of chance or artefact.

5.2.11. Neutral inotropes matching the inotropic assignment

8/11 compounds were correctly classified as neutral inotropes in ERC18 with no pronounced effects on contraction and CaT. Captopril was among these and past reports did not demonstrate any effects in different cardiac models (Wang et al. 1996; Harmer et al. 2012; Scott et al. 2014). For the correct classification of neutral compounds the definition of thresholds for relevant changes is critically important. In fact, the small variability particularly for EHT contraction kinetics lead to small changes (e.g. less than 10%) which become significant in statistical analysis. In the current screen this was arbitrarily set to 15%, but might need further refinement in the future.

5.2.12. Neutral inotropes NOT matching the inotropic assignment

Three neutral inotropic compounds (enalapril, tolbutamide and pravastatin) were not correctly classified as neutral, but as positive inotropes in one of the cell lines. This false positive classification is very likely based on the normalization strategy with pooled time controls. In fact, retrospective normalization of the data to the time controls of this specific experiment revealed no effect (-1%) on contraction. This strongly argues for data normalization to specific time match controls.

Tolbutamide is an anti-diabetic agent of the sulfonylurea group that stimulates β-cells to secrete insulin by blocking K_{ATP} channels of β-cells. Literature findings on tolbutamide effect on force are inconsistent. Some studies have reported a low sensitivity of K_{ATP} channels towards tolbutamide on human right atrial myocytes (Zünkler et al. 1997) and no effect on the frequency, beating rhythm and intracellular calcium concentrations in cultured mice cardiomyocytes (Saito et al. 1986). Similarly, tolbutamide failed to exert significant inotropic effects on hiPSC-CM, neonatal rat or canine myocytes (Harmer et al. 2012; Scott et al. 2014). However, tolbutamide increased contractility of rabbit atria (Palmer et al. 1971), the spontaneous firing rate of dog Purkinje's fibres, adenylyl cyclase activity in

rabbit and human ventricular muscle (Lasseter et al. 1972) and rate of left ventricular pressure rise (dp/dt) of human myocardium *in vivo* during diagnostic cardiac catheterization (Hildner et al. 1975). In the present study, we classified tolbutamide as positive inotrope for ERC18 and neutral for R-PAT. The PIE was further confirmed by another posthoc experiment in a different differentiation batch, showing a 17% increase at 10 μM (n=5, data not shown). Taken together, it remains somewhat unclear how to classify tolbutamide and therefore whether the classification for ERC18 or R-PAT is correct.

Pravastatin is a competitive inhibitor of HMG CoA reductase (hydroxymethylglutaryl CoA). In previous studies, pravastatin did not show effects on the contractile activity of hiPSC-CM, neonatal rat CM or canine myocytes (Harmer et al. 2012; Scott et al. 2014). In the present blinded screening, pravastatin was misclassified as a positive inotrope because of a transient, non-significant increase in force at 3-10 μM for ERC18 accompanied by a decrease in $TTP_{-80\%}$ and $RT_{80\%}$ (Table 4). This pattern was misinterpreted as an effect of a cAMP-dependent positive inotrope, desensitizing with time. As for enalapril, posthoc analysis with experiment-specific time controls revealed no effects on $TTP_{-80\%}$ and $RT_{80\%}$ (+5% and -7%, respectively), indicating that this misclassification could have been again avoided by normalization to controls of this specific experiment.

Phentolamine is a competitive non-selective α1- and α2-adrenoceptor antagonist. Some studies have reported no effects on rabbit and rat papillary muscle (reviewed by Wallis et al. 2015). Others have reported a negative inotropic effect (NIE) on neonatal rat CM and hiPSC-CM in impedance-based assays (Scott et al. 2014) and canine myocytes (Harmer et al. 2012). An indirect but similar observation was reported in another study showing a concentration-dependent decrease in maximum rate of rise of action potential (13.3-53.0 μM) in papillary muscle of guinea pigs (Sada 1978), suggesting an antagonistic effect of phentolamine on I_{Na} and LTCC. In line with this interpretation, phentolamine in the present study completely ceased the EHT contraction (-100%) at 10 and 30 μM in R-PAT and ERC18, respectively and decreased the CaT by 80% in ERC18 (Table 4). Nevertheless, the strong and consistent effect is not in line with past reports and not conclusive and requires further experimental studies.

5.3. Regulation of phosphodiesterases in hiPSC EHTs

The non-selective PDE inhibitor (IBMX) or combined PDE3/4 inhibitors (milrinone, pimobendan, enoximone) increased contractile force in unstimulated human heart preparations (Böhm et al. 1991; Bethke et al. 1992a; Schmitz et al. 1992; Focaccio et al. 1996). The selective PDE3 inhibitor (cilostamide) increased $I_{Ca,L}$ and force, whereas the selective PDE4 inhibitor rolipram produced no increase in force and only a small increase in $I_{Ca,L}$ in unstimulated human atrial myocytes (Molina et al. 2012). In unstimulated human LV myocytes, cilostamide or rolipram alone had no effect on force, but cilostamide shifted the concentration-response curve for epinephrine and norepinephrine to the left

(Molenaar et al. 2013). Rolipram was without effect. Altogether, these data indicate PDE3 dominance over PDE4 in adult human cardiomyocytes to regulate β-adrenergic signalling (Eschenhagen 2013).

In our present data, we showed that hiPSC-CM EHTs differ in their regulation by PDE. Rolipram-mediated selective PDE4 inhibition showed a +42% increase in force in unstimulated EHTs (Figure 28C). In addition, the inotropic effect of isoprenaline was potentiated by rolipram and IBMX. In contrast, cilostamide or milrinone did not show any significant effects (Figure 28E). These results indicate that hiPSC-CM EHTs have a strong PDE contribution in the regulation of basal and stimulated cAMP and PDE4 plays a dominant role.

This raises a question whether PDE4 predominance over PDE3 is a hiPSC-CM peculiarity or it points towards their relative immaturity. The latter seems to be the case as many studies have reported a PDE4 to PDE3 switch during postnatal heart development in mammals. $I_{Ca,L}$ was found to be predominantly regulated by PDE4 in new-born rabbits, but by PDE3 in adult rabbits (Akita et al. 1994). Similar changes were reported in pig atria regarding cAMP regulation and force development (Galindo-Tovar et al. 2009).

In the rat heart, a PDE4 dominant pharmacological model, rolipram increased the force in atrial tissue, but not in ventricular (Christ et al. 2009). Similarly, PDE4 inhibition showed the highest effect in spontaneous beating right atria (+60%), small effect in left atria (+40%) and no effect in LV (Christ et al. 2009). These findings raises the question whether force regulation in hiPSC-CM EHT by PDE4 resembles an atrial phenotype. While high PDE sensitivity is suggestive of a sinoatrial phenotype, the low repolarization fraction, the absence of $I_{K,ACh}$, (Horváth et al. 2018) and the abundance of MLC2v positive cells (Mannhardt et al. 2016) all indicate that standard hiPSC EHT exhibit a ventricular phenotype.

In line with the effects of PDE inhibitors on basal, unstimulated force, the catecholamine response was regulated only by the PDE4 isoform (Figure 28E). The finding that potentiation by the non-selective PDE inhibitor IBMX was not larger than selective PDE4 inhibition alone argues against the relevant contribution of other PDE isoforms in hiPSC-CM. In line with this assumption, lack of potentiation was determined for tadalafil, a selective PDE5 inhibitor. In human and rat LV preparations, potentiation by selective PDE inhibition (cilostamide or rolipram) resulted in a half-log unit shift of catecholamine concentration-response curve (Christ et al. 2009; Molenaar et al. 2013). As demonstrated in Figure 28E, in hiPSC-EHT, the potentiation of catecholamine by rolipram resulted in a one-log unit shift. This finding again demonstrates the strong contribution of PDE to the regulation of cAMP in this model. The larger effect of rolipram on force and potentiation of isoprenaline effects (Figure 28C, E) are very

likely related to the fact that rolipram at 10 µM is 9-fold of the IC_{50} (1.1 µM) and IBMX at 10 µM is 0.6-fold the IC_{50} (16.2 µM) as determined in guinea-pig ventricular tissue (Bethke et al. 1992a, b).

Altogether, these experiments provide evidence for the restriction of β-adrenergic signalling by PDE4 in hiPSC-CM.

6 <u>OUTLOOK</u>

The set-up established in the present study enables the sequential measurement of force and CaT in the hiPSC-CM EHTs. The following aspects need to be addressed for further refinement:

- Test system development for simultaneous (in contrast to sequential) force and CaT analysis to increase the level of automation and user-friendliness
- Evaluation of the inclusion of ivabradine (300 nM) as baseline condition
- Refinement of threshold criteria to identify relevant effect sizes
- Verifying the added value of proposed additional experiments (single high concentration, 24 h long term recording)
- The longer term perspective is also to include a readout for voltage (voltage sensitive dye, field potential) which would allow to analyse the three important parameter of ECM in a single experiment.

7 <u>SUMMARY</u>

Cardiovascular side effects are an important major cause for attrition during the process of drug development. Preclinical cardiac assessment relies on *in vitro* and *in vivo* animal experimentation. The predictive value of these experiments is low. The principally unlimited availability of human induced pluripotent stem cell-derived cardiomyocytes (hiPSC-CM) was the basis for the development of assays for pre-clinical cardiac assessment based on this cell source. As one example, culturing hiPSC-CM in three-dimensional fibrin based engineered heart tissues (EHT) and semi-automated video optical analysis of contractility was developed at the Department of Experimental Pharmacology and Toxicology, University Medical Centre Hamburg-Eppendorf. This provides an innovative test-bed for cardiac assessment. The present thesis aimed to combine the established contractility test system with the analysis of calcium transients (CaT) by using genetically encoded calcium indicators (GECIs). The suitability of the test system was evaluated in the context of an international, multi-site blinded screening project.

Viral transduction of EHTs to express GECIs (GCaMP5G and GCaMP6f) was established with lentivirus and adeno-associated virus 6 (AAV6). The video-optical EHT contractility test system was expanded to sequentially analyse GCaMP6f fluorescence intensity as a surrogate for CaT. Both GECIs showed specific signals with high signal to noise ratios. EHTs transduced with GCaMP5G showed slower on- and off-kinetics. The test system was validated with a set of indicator compounds (e.g. isoprenaline, nifedipine, BayK-8644 and digoxin), which revealed compound specific effects on force and CaT, well compatible with the respective mechanisms of action. The advanced test system was used to study force- and CaT-frequency relationship in the presence of ivabradine (300 nM) which reduces baseline frequency. Under these conditions, a positive force- and CaT-frequency relationship was demonstrated in a range of 0.5-1.5 Hz but not at higher frequencies. Omecamtiv mecarbil was also analysed in the presence of ivabradine and showed a pronounced positive inotropic effect at low frequencies and a small positive inotropic effect at higher frequencies (+240% at 1.0 Hz, +63% at 2.5 Hz, reverse frequency dependency).

The test system was subjected to a blinded screening of 27 compounds with half-log concentration-response curves. Most of the compounds showed the expected effects on inotropy with a predictive accuracy of 75% for positive, 88% for negative inotropes, and 77% for neutral inotropes. Small effect size of positive inotropic effects, delayed cardiotoxic negative inotropic effects, and misclassification of neutral inotropes because of normalization to pooled time controls were identified as relevant weaknesses of this screening approach.

In a separate part of this thesis, the regulation of force by different isoforms of phosphodiesterases (PDE) in hiPSC-CM EHTs was investigated that revealed a predominance of PDE4 over PDE3 unlike adult human heart where PDE3 is the most important isoform. PDE4 dominance is likely an indicator of the immaturity of hiPSC-CM.

Overall, this study described the combination of CaT analysis with the video-optical contractility analysis in hiPSC-CM EHTs as a meaningful extension and the results emphasis the potential use of this model for preclinical cardiac drug assessment applications.[i]

---

[i]This Ph.D. thesis contains data and paragraphs that are part of the two publications of Umber Saleem, which are in the review and the writing process.

8 ZUSAMMENFASSUNG

Unerwünschte kardiovaskuläre Wirkungen sind ein wichtiger Grund für die geringe Effizienz bei der Entwicklung neuer Wirkstoffe. Die präklinische Analyse von kardialen Effekten in der Wirkstoffentwicklung basiert auf der *in vitro-* und *in vivo*-Analyse von Versuchstieren. Die Vorhersagekraft für die Effekte am Menschen ist jedoch gering. Die prinzipiell unbegrenzte Verfügbarkeit von Kardiomyozyten aus humanen induzierten pluripotenten Stammzellen (hiPSC-CM) war die Grundlage für die Entwicklung von Technologien zur präklinischen Analyse solcher kardialen Effekte *in vitro*. Als ein Beispiel wurde die Kultur von hiPSC-CM im dreidimensionalen streifen-förmigen *engineered heart tissue* (EHT) Format als ein innovatives Modell im Institut für Experimentelle Pharmakologie und Toxikologie am Universitätsklinikum Hamburg-Eppendorf entwickelt. Diese Promotionsarbeit hatte das Ziel das etablierte EHT-Model zu erweitern und zusätzlich Calciumtransienten (CaT) mit Hilfe von genetisch kodierten Calcium-Sensoren (genetically encoded calcium sensor, GECI) parallel zu analysieren. Die Eignung des erweiterten Testsystems wurde im Rahmen eines internationalen multizentrischen Ringversuchs mit verblindeten Substanzen getestet.

Die virale Transduktion von EHTs mit GECIs (GCaMP5G, GCaMP6f) wurde mit Lentiviren oder Adeno-assoziierten Viren (AAV6) etabliert. Das video-optische EHT-Kontraktionssystem wurde um die sequentielle Analyse von GCaMP6f-Fluoreszenzintensität als Surrogat für den CaT erweitert. Für beide Sensoren ließen sich spezifische Signale mit hohem Signal-Rausch-Verhältnis darstellen. Hierbei zeigten GCaMP5G-EHTs langsame *on-* und *off*-Kinetiken. Das erweiterte Testsystem wurde durch Indikatorsubstanzen (z.B. Isoprenalin, Nifedipin, BayK-8644, Digoxin) getestet und zeigte Substanz-spezifische Effekte auf CaT und Kraft. Mit dem erweiterten Testsystem wurde die CaT- bzw. Kraft-Frequenz-Beziehung in Gegenwart von Ivabradine (300 nM) getestet, was zu einer Verminderung der basalen spontanen Frequenz führt. Unter diesen Bedingungen konnte eine positive Korrelation zwischen CaT bzw. Kraft und der Stimulationsfrequenz in einem Bereich von 0,5-1,5 Hz, aber nicht bei höheren Frequenzen, dargestellt werden. Zusätzlich wurde der Effekt von Omecamtive mecarbil auf CaT und Kraft in Gegenwart von Ivabradine getestet und es zeigte sich ein kleiner positiv inotroper Effekt bei hohen Frequenzen und ein großer Effekt bei geringen Frequenzen (+240% at 1.0 Hz, +63% at 2.5 Hz, inverse Kraft-Frequenz Beziehung).

Im nächsten Schritt wurde das erweiterte Testsystems verwendet um 27 Substanzen innerhalb eines internationalen multizentrischen Ringversuchs (CRACK IT Konsortium) unter verblindeten Bedingungen mit halb-logarithmischen Konzentrations-Wirkungskurven zu analysieren. Die zu erwarteten inotropen Effekt konnten mit einer Genauigkeit von 75% (positiv inotrope Effekte), 88%

(negativ inotrope Effekte) und 77% (neutrale inotrope Effekte) vorhergesagt werden. Die kleine Effektgröße der positiv inotropen Substanzen, der verzögerte Effekt von toxisch-negativ inotropen Substanzen und die inkorrekte Klassifizierung von neutralen Substanzen aufgrund einer Normalisierung zu gepoolten und nicht Experiment-spezifischen Zeitkontrollen wurden als wesentliche Limitationen von diesem Ansatz identifiziert.

In einem weiteren Teilprojekt wurde die Kraftregulation durch Isoformen der Phosphodiesterase (PDE) in hiPSC-CM EHTs analysiert. Es zeigte sich eine Prädominanz der Isoform PDE4 im Gegensatz zu adultem menschlichem Herzgewebe in dem PDE3 die wichtigste Rollen einnimmt. Die Prädominanz von PDE4 ist wahrscheinlich ein Hinweis auf den unvollständigen Reifegrad der hiPSC-CMs.

Zusammenfassend beschreibt diese Promotionsarbeit die Kombination von CaT-Analyse mit video-optischer Kraftanalyse von hiPSC-CM EHTs als eine sinnvolle Ergänzung und die Ergebnisse betonen die mögliche Verwendung dieses Systems zur präklinischen Analyse kardialer Effekte.[ii]

[ii] Summary was translated from English to German by Prof. Dr. Arne Hansen.

9 <u>BIBLIOGRAPHY</u>

Abassi YA, Xi B, Li N, et al (2012) Dynamic monitoring of beating periodicity of stem cell-derived cardiomyocytes as a predictive tool for preclinical safety assessment. Br J Pharmacol 165:1424–41. doi: 10.1111/j.1476-5381.2011.01623.x

Akerboom J, Chen T-W, Wardill TJ, et al (2012) Optimization of a GCaMP Calcium Indicator for Neural Activity Imaging. J Neurosci 32:13819–13840. doi: 10.1523/JNEUROSCI.2601-12.2012

Akita T, Joyner RW, Lu C, et al (1994) Developmental changes in modulation of calcium currents of rabbit ventricular cells by phosphodiesterase inhibitors. Circulation 90:469–78

Badura A, Sun XR, Giovannucci A, et al (2014) Fast calcium sensor proteins for monitoring neural activity. Neurophotonics 1:025008. doi: 10.1117/1.NPh.1.2.025008

Belz GG, Meinicke T, Schäfer-Korting M (1988) The relationship between pharmacokinetics and pharmacodynamics of enoximone in healthy man. Eur J Clin Pharmacol 35:631–5. doi: 10.1007/BF00637599

Berk E, Christ T, Schwarz S, et al (2016) In permanent atrial fibrillation, PDE3 reduces force responses to 5-HT, but PDE3 and PDE4 do not cause the blunting of atrial arrhythmias. Br J Pharmacol 173:2478–2489. doi: 10.1111/bph.13525

Bers DM (2002) Cardiac excitation-contraction coupling. Nature 415:198–205. doi: 10.1038/415198a

Bers DM, Morotti S, Greenstein JL, et al (2014) Ca 2+ current facilitation is CaMKII-dependent and has arrhythmogenic consequences. Front Pharmacol 5:144. doi: 10.3389/fphar.2014.00144

Bethke T, Eschenhagen T, Klimkiewicz A, et al (1992a) Phosphodiesterase inhibition by enoximone in preparations from nonfailing and failing human hearts. Arzneimittelforschung 42:437–45

Bethke T, Meyer W, Schmitz W, et al (1992b) Phosphodiesterase inhibition in ventricular cardiomyocytes from guinea-pig hearts. 107:127–133

Blazeski A, Zhu R, Hunter DW, et al (2012) Cardiomyocytes derived from human induced pluripotent stem cells as models for normal and diseased cardiac electrophysiology and contractility. Prog Biophys Mol Biol 110:166–77. doi: 10.1016/j.pbiomolbio.2012.07.013

Böhm M, Morano I, Pieske B, et al (1991) Contribution of cAMP-phosphodiesterase inhibition and sensitization of the contractile proteins for calcium to the inotropic effect of pimobendan in the

Bibliography

failing human myocardium. Circ Res 68:689–701. doi: 10.1161/01.RES.68.3.689

Bois P, Bescond J, Renaudon B, Lenfant J (1996) Mode of action of bradycardic agent, S 16257, on ionic currents of rabbit sinoatrial node cells. Stockton Press

Boldt A, Gergs U, Pönicke K, et al (2010) Inotropic effects of ivabradine in the mammalian heart. Pharmacology 86:249–258. doi: 10.1159/000320454

Borchard U, Boisten M (1982) Effect of flecainide on action potentials and alternating current-induced arrhythmias in mammalian myocardium. J Cardiovasc Pharmacol 4:205–12

Bowditch H (1971) Uber die Eigenthumlichkeiten der Reizbarkeit, welche die Muskelfasern des Herzens zeigen. Arb Physiol Anstalt Leipzig 6:139–176

Brandes R, Figueredo VM, Camacho SA, et al (1992) Suppression of motion artifacts in fluorescence spectroscopy of perfused hearts. Am J Physiol 263:H972-80

Breckwoldt K, Letuffe-Brenière D, Mannhardt I, et al (2017) Differentiation of cardiomyocytes and generation of human engineered heart tissue. Nat Protoc 12:1177–1197. doi: 10.1038/nprot.2017.033

Brodde O (1994) Beta-adrenoceptors in cardiac disease. Pharmacol Ther 60:405–430

Broussard GJ, Liang R, Tian L (2014) Monitoring activity in neural circuits with genetically encoded indicators. Front Mol Neurosci 7:1–17. doi: 10.3389/fnmol.2014.00097

Burridge PW, Keller G, Gold JD, Wu JC (2012) Production of de novo cardiomyocytes: Human pluripotent stem cell differentiation and direct reprogramming. Cell Stem Cell 10:16–28. doi: 10.1016/j.stem.2011.12.013

Burridge PW, Matsa E, Shukla P, et al (2014) Chemically defined generation of human cardiomyocytes. Nat Methods 11:855–60. doi: 10.1038/nmeth.2999

Burridge PW, Thompson S, Millrod M a., et al (2011) A universal system for highly efficient cardiac differentiation of human induced pluripotent stem cells that eliminates interline variability. PLoS One 6:e18293. doi: 10.1371/journal.pone.0018293

Butler L, Cros C, Oldman KL, et al (2015) Enhanced characterization of contractility in cardiomyocytes during early drug safety assessment. Toxicol Sci 145:396–406. doi: 10.1093/toxsci/kfv062

Cerignoli F, Charlot D, Whittaker R, et al (2012) High throughput measurement of Ca^{2+} dynamics for drug risk assessment in human stem cell-derived cardiomyocytes by kinetic image cytometry. J

Pharmacol Toxicol Methods 66:246–56. doi: 10.1016/j.vascn.2012.08.167

Christ T, Galindo-Tovar A, Thoms M, et al (2009) Inotropy and L-type Ca 2+ current, activated by β 1- and β 2-adrenoceptors, are differently controlled by phosphodiesterases 3 and 4 in rat heart. Br J Pharmacol 156:62–83. doi: 10.1111/j.1476-5381.2008.00015.x

Cleemann L, Morad M (1991) Role of Ca2+ channel in cardiac excitation-contraction coupling in the rat: evidence from Ca2+ transients and contraction. J Physiol 432:283–312

Clements M, Millar V, Williams AS, Kalinka S (2015) Bridging Functional and Structural Cardiotoxicity Assays Using Human Embryonic Stem Cell-Derived Cardiomyocytes for a More Comprehensive Risk Assessment. Toxicol Sci 148:241–260. doi: 10.1093/toxsci/kfv180

Congwu D, MacGowan GA, Farkas DL, Koretsky AP (2001) Calcium measurements in perfused mouse heart: Quantitating fluorescence and absorbance of Rhod-2 by application of photon migration theory. Biophys J 80:549–561. doi: 10.1016/S0006-3495(01)76037-7

Cornish EJ, Miller RC (1975) Effects of changes in external calcium concentration and frequency of stimulation on inotropic responses to isoprenaline and tolbutamide in rabbit atria. Clin Exp Pharmacol Physiol 2:335–43

Curtis GP, Setchfield J, Lucchesi BR (1975) The cardiac pharmacology of tolbutamide. J Pharmacol Exp Ther 194:264–273

Darbar D (2014) Standard Antiarrhythmic Drugs. In: Cardiac Electrophysiology: From Cell to Bedside, Sixth Edit. Elsevier Inc., pp 1095–1110

Davis RP, van den Berg CW, Casini S, et al (2011) Pluripotent stem cell models of cardiac disease and their implication for drug discovery and development. Trends Mol Med 17:475–84. doi: 10.1016/j.molmed.2011.05.001

de Lange WJ, Grimes AC, Hegge LF, Ralphe JC (2013) Ablation of cardiac myosin–binding protein-C accelerates contractile kinetics in engineered cardiac tissue. J Gen Physiol 141:73–84. doi: 10.1085/jgp.201210837

de Tombe PP, Mateja RD, Tachampa K, et al (2010) Myofilament length dependent activation. J Mol Cell Cardiol 48:851–8. doi: 10.1016/j.yjmcc.2009.12.017

Decking UKM, Reffelmann T, Schrader J, Kammermeier H (1995) Hypoxia-induced activation of KATP channels limits energy depletion in the guinea pig heart. Am J Physiol Circ Physiol 269:H734–H742. doi: 10.1152/ajpheart.1995.269.2.H734

Bibliography

Denning C, Borgdorff V, Crutchley J, et al (2016) Cardiomyocytes from human pluripotent stem cells: From laboratory curiosity to industrial biomedical platform. Biochim Biophys Acta - Mol Cell Res 1863:1728–1748. doi: 10.1016/j.bbamcr.2015.10.014

Desbaillets I, Ziegler U, Groscurth P, Gassmann M (2000) Embryoid bodies: an in vitro model of mouse embryogenesis. Exp Physiol 85:645–51. doi: 10.1263/jbb.103.389

Difrancesco D (2010) The role of the funny current in pacemaker activity. Circ Res 106:434–446. doi: 10.1161/CIRCRESAHA.109.208041

Doevendans PA, Daemen MJ, De Muinck ED, Smits JF (1998) Cardiovascular phenotyping in mice. Cardiovasc Res 39:34–49. doi: 10.1016/S0008-6363(98)00073-X

Endoh M (1989) Frequency-dependent inhibition of the intracellular calcium transients by calmodulin antagonists in the aequorin-injected rabbit papillary muscle. Adv Exp Med Biol 255:461–70

Endoh M (2004) Force–frequency relationship in intact mammalian ventricular myocardium: physiological and pathophysiological relevance. Eur J Pharmacol 500:73–86. doi: 10.1016/J.EJPHAR.2004.07.013

Eschenhagen T (2013) PDE4 in the human heart - Major player or little helper? Br J Pharmacol 169:524–527. doi: 10.1111/bph.12168

Eschenhagen T, Fink C, Remmers U, et al (1997) Three-dimensional reconstitution of embryonic cardiomyocytes in a collagen matrix: a new heart muscle model system. FASEB J 11:683–694

Eschenhagen T, Mende U, Schmitz W, et al (1991) Beta-adrenoceptor stimulation-induced increase in cardiac Gi-protein expression and in carbachol sensitivity. Eur Heart J 12 Suppl F:127–31

Eschenhagen T, Mummery C, Knollmann BC (2015) Modelling sarcomeric cardiomyopathies in the dish: From human heart samples to iPSC cardiomyocytes. Cardiovasc Res 105 (4):424–438. doi: 10.1093/cvr/cvv017

Fink C, Ergün S, Kralisch D, et al (2000) Chronic stretch of engineered heart tissue induces hypertrophy and functional improvement. FASEB J 14:669–679. doi: 10.1007/0-387-21547-6_18

Focaccio A, Peeters G, Movsesian M, et al (1996) Mechanism of action of OPC-8490 in human ventricular myocardium. Circulation 93:817–25

Földes G, Mioulane M, Wright JS, et al (2011) Modulation of human embryonic stem cell-derived

cardiomyocyte growth: A testbed for studying human cardiac hypertrophy? J Mol Cell Cardiol 50:367–376. doi: 10.1016/j.yjmcc.2010.10.029

Fralix TA, Heineman FW, Balaban RS (1990) Effects of tissue absorbance on NAD(P)H and Indo-1 fluorescence from perfused rabbit hearts. FEBS Lett 262:287–292. doi: 10.1016/0014-5793(90)80212-2

Fulop L, Szigeti G, Magyar J, et al (2003) Differences in electrophysiological and contractile properties of mammalian cardiac tissues bathed in bicarbonate - and HEPES-buffered solutions. Acta Physiol Scand 178:11–18. doi: 10.1046/j.1365-201X.2003.01114.x

Galindo-Tovar A, Vargas ML, Escudero E, Kaumann AJ (2009) Ontogenic changes of the control by phosphodiesterase-3 and -4 of 5-HT responses in porcine heart and relevance to human atrial 5-HT 4 receptors. Br J Pharmacol 156:237–249. doi: 10.1111/j.1476-5381.2008.00023.x

Garcia-Sevilla JA, Erill S, Garcia-Sevilla JA, Erill S (1974) Comparative study of cumulative and non-cumulative dose-response curves for noradrenaline and adrenaline in the isolated rat vas deferens. Eur J Pharmacol 27:360–362

Gibson JK, Yue Y, Bronson J, et al (2014) Human stem cell-derived cardiomyocytes detect drug-mediated changes in action potentials and ion currents. J Pharmacol Toxicol Methods 70:255–267. doi: 10.1016/j.vascn.2014.09.005

Gong Y, Huang C, Li JZ, et al (2015) High-speed recording of neural spikes in awake mice and flies with a fluorescent voltage sensor. Sciencexpress 350:1–11. doi: 10.1126/science.aab0810

Grimm F (2018) A human population-based organotypic in vitro model for cardiotoxicity screening. ALTEX 77843:1–14. doi: 10.14573/1805301

Guellich A, Mehel H, Fischmeister R (2014) Cyclic AMP synthesis and hydrolysis in the normal and failing heart. Pflugers Arch Eur J Physiol 466:1163–1175. doi: 10.1007/s00424-014-1515-1

Guimarães S (1972) The slopes of cumulative and non-cumulative dose-response curves for nonadrenaline and isoprenaline. Eur J Pharmacol 17:44–49

Guo L, Coyle L, Abrams RMC, et al (2013) Refining the Human iPSC-Cardiomyocyte Arrhythmic Risk Assessment Model. Toxicol Sci 136:581–594. doi: 10.1093/toxsci/kft205

Gwathmey JK, Slawsky MT, Hajjar RJ, et al (1990) Role of intracellular calcium handling in force-interval relationships of human ventricular myocardium. J Clin Invest 85:1599–1613. doi: 10.1172/JCI114611

Bibliography

Halbert SP, Bruderer R, Lin TM (1971) In vitro organization of dissociated rat cardiac cells into beating three-dimensional structures. J Exp Med 133:677–95

Hamlin RL, del Rio C (2012) dP/dt(max)--a measure of "baroinometry". J Pharmacol Toxicol Methods 66:63–5. doi: 10.1016/j.vascn.2012.01.001

Hansen A, Eder A, Bönstrup M, et al (2010) Development of a drug screening platform based on engineered heart tissue. Circ Res 107:35–44. doi: 10.1161/CIRCRESAHA.109.211458

Harmer AR, Abi-Gerges N, Morton MJ, et al (2012) Validation of an in vitro contractility assay using canine ventricular myocytes. Toxicol Appl Pharmacol 260:162–172. doi: 10.1016/J.TAAP.2012.02.007

Hartman ME, Dai DF, Laflamme M a. (2016) Human pluripotent stem cells: Prospects and challenges as a source of cardiomyocytes for in vitro modeling and cell-based cardiac repair. Adv Drug Deliv Rev 96:3–17. doi: 10.1016/j.addr.2015.05.004

Hasenfuss G, Reinecke H, Studer R, et al (1996) Calcium cycling proteins and force-frequency relationship in heart failure. Basic Res Cardiol 91 Suppl 2:17–22

Heller T, Kscher M, Neumann J, et al (1989) Effects of adenosine analogues on force and cAMP in the heart. Influence of adenosine deaminase. Eur J Pharmacol 164:179–187

Helmchen F, Imoto K, Sakmann B (1996) Ca2+ Buffering and Action Potential-Evoked Ca2+ Signaling in Dendrites of Pyramidal Neurons. Biophys J 70:1069–1081

Herron TJ, Lee P, Jalife J (2012) Optical imaging of voltage and calcium in cardiac cells & tissues. Circ Res 110:609–623. doi: 10.1161/CIRCRESAHA.111.247494

Hildner FJ, Yeh BK, Javier RP, et al (1975) Inotropic action of tolbutamide on human myocardium. Cathet Cardiovasc Diagn 1:47–57

Hinson JT, Chopra A, Nafissi N, et al (2015) Titin mutations in iPS cells define sarcomere insufficiency as a cause of dilated cardiomyopathy. Science 349:982–6. doi: 10.1126/science.aaa5458

Hirt MN, Boeddinghaus J, Mitchell A, et al (2014) Functional improvement and maturation of rat and human engineered heart tissue by chronic electrical stimulation. J Mol Cell Cardiol 74:151–161. doi: 10.1016/j.yjmcc.2014.05.009

Hirt MN, Sörensen N a., Bartholdt LM, et al (2012) Increased afterload induces pathological cardiac hypertrophy: a new in vitro model. Basic Res Cardiol 107:1–16. doi: 10.1007/s00395-012-0307-z

Bibliography

Honerjäger P, Loibl E, Steidl I, et al (1986) Negative inotropic effects of tetrodotoxin and seven class 1 antiarrhythmic drugs in relation to sodium channel blockade. Naunyn-Schmiedeberg's Arch Pharmacol 332:184–195

Horváth A, Lemoine MD, Löser A, et al (2018) Low Resting Membrane Potential and Low Inward Rectifier Potassium Currents Are Not Inherent Features of hiPSC-Derived Cardiomyocytes. Stem Cell Reports 10:822–833. doi: 10.1016/j.stemcr.2018.01.012

Horváth B, Szentandrássy N, Veress R, et al (2017) Frequency-dependent effects of omecamtiv mecarbil on cell shortening of isolated canine ventricular cardiomyocytes. Naunyn Schmiedebergs Arch Pharmacol 390:1239–1246. doi: 10.1007/s00210-017-1422-z

ICH Expert Working Group (2000) Safety Pharmacology Studies For Human Pharmaceuticals S7A. Int Conf Harmon Tech Requir Regist Pharm Hum Use 1–13. doi: 10.1001/jama.288.14.1749

ICH Expert Working Group (2005) S7B Nonclinical Evaluation of the Potential for Delayed Ventricular Repolarization (QT Interval Prolongation) by Human Pharmaceuticals. Int Conf Harmon Tech Requir Regist Pharm Hum Use 70:61133–61134

Iribe G, Kaihara K, Yamaguchi Y, et al (2017) Mechano-sensitivity of mitochondrial function in mouse cardiac myocytes. Prog Biophys Mol Biol 130(Pt B):315–322. doi: 10.1016/j.pbiomolbio.2017.05.015

Ishitani T, Hattori Y, Sakuraya F, et al (2001) Effects of Ca2+ sensitizers on contraction, [Ca2+]i transient and myofilament Ca2+ sensitivity in diabetic rat myocardium: potential usefulness as inotropic agents. J Pharmacol Exp Ther 298:613–22

Ito H, Hiroe M, Hirata Y, et al (1993) Insulin-like growth factor-I induces hypertrophy with enhanced expression of muscle specific genes in cultured rat cardiomyocytes. Circulation 87:1715–1721. doi: 10.1161/01.CIR.87.5.1715

Itskovitz-Eldor J, Schuldiner M, Karsenti D, et al (2000) Differentiation of human embryonic stem cells into embryoid bodies compromising the three embryonic germ layers. Mol Med 6:88–95. doi: 10859025

Itzhaki I, Maizels L, Huber I, et al (2011) Modelling the long QT syndrome with induced pluripotent stem cells. Nature 471:225–9. doi: 10.1038/nature09747

Jackman CP, Carlson AL, Bursac N (2016) Dynamic culture yields engineered myocardium with near-adult functional output. Biomaterials 111:66–79. doi: 10.1016/j.biomaterials.2016.09.024

Bibliography

Jacob F, Yonis AY, Cuello F, et al (2016) Analysis of Tyrosine Kinase Inhibitor-Mediated Decline in Contractile Force in Rat Engineered Heart Tissue. PLoS One 11:e0145937. doi: 10.1371/journal.pone.0145937

Jacot JG, Kita-Matsuo H, Wei KA, et al (2010) Cardiac myocyte force development during differentiation and maturation. Ann N Y Acad Sci 1188:121–127. doi: 10.1111/j.1749-6632.2009.05091.x

Johnson WB, Katugampola S, Able S, et al (2012) Profiling of cAMP and cGMP phosphodiesterases in isolated ventricular cardiomyocytes from human hearts: Comparison with rat and guinea pig. Life Sci 90:328–336. doi: 10.1016/j.lfs.2011.11.016

Josephson MA, Ikeda N, Singh BN (1984) Effects of flecainide on ventricular function: clinical and experimental correlations. Am J Cardiol 53:95B–100B

Kaestner L, Scholz A, Tian Q, et al (2014) Genetically encoded Ca2+ indicators in cardiac myocytes. Circ Res 114:1623–1639. doi: 10.1161/CIRCRESAHA.114.303475

Kaumann AJ, Blinks JR (1980) Stimulant and depressant effects of beta-adrenoceptor blocking agents on isolated heart muscle. A positive inotropic effect not mediated through andrenoceptors. Naunyn Schmiedebergs Arch Pharmacol 311:205–18

Kempf H, Kropp C, Olmer R, et al (2015) Cardiac differentiation of human pluripotent stem cells in scalable suspension culture. Nat Protoc 10:1345–61. doi: 10.1038/nprot.2015.089

Kempf H, Olmer R, Haase A, et al (2016) Bulk cell density and Wnt/TGFbeta signalling regulate mesendodermal patterning of human pluripotent stem cells. Nat Commun 7:13602. doi: 10.1038/ncomms13602

Kim C, Majdi M, Xia P, et al (2010) Non-Cardiomyocytes Influence the Electrophysiological Maturation of Human Embryonic Stem Cell-Derived Cardiomyocytes During Differentiation. Stem Cells Dev 19:783–795. doi: 10.1089/scd.2009.0349

Kim DS, Jayaraman V (2014) Engineering Fluorescent Calcium Sensor Proteins for Imaging Neural Activity. Janelia Research Campus, Howard Hughes Medical Institute

Kira Y, Nakaoka T, Hashimoto E, et al (1994) Effect of long-term cyclic mechanical load on protein synthesis and morphological changes in cultured myocardial cells from neonatal rat. Cardiovasc drugs Ther 8:251–62

Kiuchi K, Shannon RP, Komamura K, et al (1993) Myocardial beta-adrenergic receptor function during

the development of pacing-induced heart failure. J Clin Invest 91:907–14. doi: 10.1172/JCI116312

Klabunde RE (2012) Cardiovascular Physiology Concepts, 2nd Edit. Lippincott Williams & Wilkins

Knaust AE (2017) Disease modelling of a phospholamban p . Arg14del mutation in hiPSC-derived cardiomyocytes. University Medical Centre Hamburg-Eppendorf

Knollmann BC, Roden DM (2008) A genetic framework for improving arrhythmia therapy. Nature 451:929–936. doi: 10.1038/nature06799

Kondrashov A, Duc Hoang M, Smith J, et al (2018) Simplified footprint-free Cas9/CRISPR editing of cardiac-associated genes in human pluripotent stem cells. Stem Cells Dev 27:391–404. doi: 10.1089/scd.2017.0268

Kotterman MA, Chalberg TW, Schaffer D V. (2015) Viral Vectors for Gene Therapy: Translational and Clinical Outlook. Annu Rev Biomed Eng 17:63–89. doi: 10.1146/annurev-bioeng-071813-104938

Krishna A, Valderrábano M, Palade PT, Clark JW (2013) Rate-dependent Ca 2+ signalling underlying the force-frequency response in rat ventricular myocytes: a coupled electromechanical modeling study. Theor Biol Med Model 10:54. doi: 10.1186/1742-4682-10-54

Krüger M, Sachse C, Zimmermann WH, et al (2008) Thyroid hormone regulates developmental titin isoform transitions via the phosphatidylinositol-3-kinase/Akt pathway. Circ Res 102:439–447. doi: 10.1161/CIRCRESAHA.107.162719

Kuppusamy KT, Jones DC, Sperber H, et al (2015) Let-7 family of microRNA is required for maturation and adult-like metabolism in stem cell-derived cardiomyocytes. Proc Natl Acad Sci 112:E2785-94. doi: 10.1073/pnas.1424042112

Labow RS, Desjardins S, Keon WJ (1991) Validation of a human atrial trabecular preparation for evaluation of inotropic substances. J Pharmacol Methods 26:257–68

Langendorff O (1895) Untersuchungen am überlebenden Säugethierherzen. Arch für die Gesammte Physiol des Menschen und der Tiere 61:291–332. doi: 10.1007/BF01812150

Langendorff O (1903) Geschichtliche Betrachtungen zur Methode des überlebenden Warmblüterherzens. Muench Med Wochenschr 50:508–509

Lasseter KC, Levey GS, Palmer RF, McCarthy JS (1972) The effect of sulfonylurea drugs on rabbit myocardial contractility, canine purkinje fiber automaticity, and adenyl cyclase activity from

rabbit and human hearts. J Clin Invest 51:2429–34. doi: 10.1172/JCI107056

Lemoine H, Schönell H, Kaumann AJ (1988) Contribution of beta 1- and beta 2-adrenoceptors of human atrium and ventricle to the effects of noradrenaline and adrenaline as assessed with (-)-atenolol. Br J Pharmacol 95:55–66

Lemoine MD, Mannhardt I, Breckwoldt K, et al (2017) Human iPSC-derived cardiomyocytes cultured in 3D engineered heart tissue show physiological upstroke velocity and sodium current density. Sci Rep 7:1–11. doi: 10.1038/s41598-017-05600-w

Leonard A, Bertero A, Powers JD, et al (2018) Afterload promotes maturation of human induced pluripotent stem cell derived cardiomyocytes in engineered heart tissues. J Mol Cell Cardiol 118:147–158. doi: 10.1016/j.yjmcc.2018.03.016

Levey GS, Palmer RF, Lasseter KC, McCarthy J (1971) Effect of tolbutamide on adenyl cyclase in rabbit and human heart and contractility of isolated rabbit atria. J Clin Endocrinol Metab 33:371–374. doi: 10.1210/jcem-33-2-371

Lieberman M, Roggeveen AE, Purdy JE, Johnson EA (1972) Synthetic strands of cardiac muscle: growth and physiological implication. Science 175:909–11

Limas CJ, Limas C (1984) Rapid recovery of cardiac beta-adrenergic receptors after isoproterenol-induced "down"-regulation. Circ Res 55:524–31

Lin MZ, Schnitzer MJ (2016) Genetically encoded indicators of neuronal activity. Nat Neurosci 19:1142–53. doi: 10.1038/nn.4359

Liu J, Sun N, Bruce MA, et al (2012) Atomic Force Mechanobiology of Pluripotent Stem Cell-Derived Cardiomyocytes. PLoS One 7:e37559. doi: 10.1371/journal.pone.0037559

Lorenzo G Di, Autorino R, Bruni G, et al (2009) Cardiovascular toxicity following sunitinib therapy in metastatic renal cell carcinoma: a multicenter analysis. Ann Oncol 20:1535–1542. doi: 10.1093/annonc/mdp025

Lundy SD, Zhu W-Z, Regnier M, Laflamme MA (2013) Structural and Functional Maturation of Cardiomyocytes Derived from Human Pluripotent Stem Cells. Stem Cells Dev 22:1991–2002. doi: 10.1089/scd.2012.0490

Lynch JJ, Regan CP, Beatch GN, et al (2013) Comparison of the intrinsic vasorelaxant and inotropic effects of the antiarrhythmic agents vernakalant and flecainide in human isolated vascular and cardiac tissues. J Cardiovasc Pharmacol 61:226–232. doi: 10.1097/FJC.0b013e31827afd29

Bibliography

Maier LS, Bers DM, Pieske B (2000) Differences in Ca(2+)-handling and sarcoplasmic reticulum Ca(2+)-content in isolated rat and rabbit myocardium. J Mol Cell Cardiol 32:2249–58. doi: 10.1006/jmcc.2000.1252

Malik FI, Hartman JJ, Elias KA, et al (2011) Cardiac myosin activation: A potential therapeutic approach for systolic heart failure. Science (80-) 331:1439–1443. doi: 10.1126/science.1200113

Mannhardt I, Breckwoldt K, Letuffe-Brenière D, et al (2016) Human Engineered Heart Tissue: Analysis of Contractile Force. Stem Cell Reports 7:29–42. doi: 10.1016/j.stemcr.2016.04.011

Mannhardt I, Eder A, Dumotier B, et al (2017a) Blinded contractility analysis in hipsc-cardiomyocytes in engineered heart tissue format: Comparison with human atrial trabeculae. Toxicol Sci 158:164–175. doi: 10.1093/toxsci/kfx081

Mannhardt I, Saleem U, Benzin A, et al (2017b) Automated Contraction Analysis of Human Engineered Heart Tissue for Cardiac Drug Safety Screening. J Vis Exp e55461. doi: 10.3791/55461

Mao T, O'Connor D, Scheuss V, et al (2018) Characterization and Subcellular Targeting of GCaMP-Type Genetically-Encoded calcium indicators. PLoS One 3:e1796

Markert M, Klumpp A, Trautmann T, et al (2007) The value added by measuring myocardial contractility "in vivo" in safety pharmacological profiling of drug candidates. J Pharmacol Toxicol Methods 56:203–11. doi: 10.1016/j.vascn.2007.03.004

Marks AR (2013) Calcium cycling proteins and heart failure: Mechanisms and therapeutics. J Clin Invest 123:46–52. doi: 10.1172/JCI62834

Matthews JC, Baker JK (1982) Effects of propranolol and a number of its analogues on sodium channels. Biochem Pharmacol 31:1681–5

May JE, Xu J, Morse HR, et al (2009) Toxicity testing: The search for an in vitro alternative to animal testing. Br J Biomed Sci 66:160–165. doi: 10.1080/09674845.2009.11730265

McRitchie RJ, Chalmers JP (1981) Paradoxical inotropic effects of clonidine and labetalol in the conscious rabbit. J Cardiovasc Pharmacol 3:818–27

Meyer T, Leisgen C, Gonser B, Günther E (2004) QT-Screen: High-Throughput Cardiac Safety Pharmacology by Extracellular Electrophysiology on Primary Cardiac Myocytes. Assay Drug Dev Technol 2:507–14. doi: 10.1089/adt.2004.2.507

Bibliography

Molenaar P, Christ T, Hussain RI, et al (2013) PDE3, but not PDE4, reduces ß1- and ß2- adrenoceptor-mediated inotropic and lusitropic effects in failing ventricle from metoprolol-treated patients. Br J Pharmacol 169:528–538. doi: 10.1111/bph.12167

Molina CE, Leroy J, Richter W, et al (2012) Cyclic adenosine monophosphate phosphodiesterase type 4 protects against atrial arrhythmias. J Am Coll Cardiol 59:2182–2190. doi: 10.1016/j.jacc.2012.01.060

Monasky MM, Janssen PML (2009) The positive force-frequency relationship is maintained in absence of sarcoplasmic reticulum function in rabbit, but not in rat myocardium. J Comp Physiol B Biochem Syst Environ Physiol 179:469–479. doi: 10.1007/s00360-008-0331-3

Montessuit C, Palma T, Viglino C, et al (2006) Effects of insulin-like growth factor-I on the maturation of metabolism in neonatal rat cardiomyocytes. Pflugers Arch Eur J Physiol 452:380–386. doi: 10.1007/s00424-006-0059-4

Morano I (1999) Tuning the human heart molecular motors by myosin light chains. J Mol Med (Berl) 77:544–54

Moretti A, Bellin M, Welling A, et al (2010) Patient-Specific Induced Pluripotent Stem-Cell Models for Long-QT Syndrome. N Engl J Med 363:1397–409. doi: 10.1056/NEJMoa0908679

Morii I, Kihara Y, Konishi T, et al (1996) Mechanism of the Negative Force-Frequency Relationship in Physiologically Intact Rat Ventricular Myocardium. Jpn Circ J 60:593–603. doi: 10.1253/jcj.60.593

Mosqueira D, Mannhardt I, Bhagwan JR, et al (2018) CRISPR/Cas9 editing in human pluripotent stem cell-cardiomyocytes highlights arrhythmias, hypocontractility, and energy depletion as potential therapeutic targets for hypertrophic cardiomyopathy. Eur Heart J 39:3879–3892. doi: 10.1093/eurheartj/ehy249

Mügge A, Posselt D, Reimer U, et al (1985) Effects of the beta2-adrenoceptor agonists fenoterol and salbutamol on force of contraction in isolated human ventricular myocardium. Klin Wochenschr 63:26–31. doi: 10.1007/BF01537483

Mulieri LA, Hasenfuss G, Leavitt B, et al (1992) Altered myocardial force-frequency relation in human heart failure. Circulation 85:1743–50

Müller M, Fleischmann B, Selbert S, et al (2000) Selection of ventricular-like cardiomyocytes from ES cells in vitro. FASEB J 14:2540–2548. doi: 10.1096/fj.00-0002com

Bibliography

Mummery C (2003) Differentiation of Human Embryonic Stem Cells to Cardiomyocytes: Role of Coculture With Visceral Endoderm-Like Cells. Circulation 107:2733–40. doi: 10.1161/01.CIR.0000068356.38592.68

Muslin AJ (2012) The Pathophysiology of Heart Failure. Muscle 523–535. doi: 10.1016/B978-0-12-381510-1.00037-5

Nakai J, Ohkura M, Imoto K (2001) A high signal-to-noise Ca(2+) probe composed of a single green fluorescent protein. Nat Biotechnol 19:137–41. doi: 10.1038/84397

Navarrete EG, Liang P, Lan F, et al (2013) Screening drug-induced arrhythmia events using human induced pluripotent stem cell-derived cardiomyocytes and low-impedance microelectrode arrays. Circulation 128:S3-13. doi: 10.1161/CIRCULATIONAHA.112.000570

Nerbonne JM, Kass RS (2005) Molecular physiology of cardiac repolarization. Sci STKE 85:1205–1253. doi: 10.1152/physrev.00002.2005.

Nunes SS, Miklas JW, Liu J, et al (2013) Biowire: a platform for maturation of human pluripotent stem cell-derived cardiomyocytes. Nat Methods 10:781–7. doi: 10.1038/nmeth.2524

Olson H, Betton G, Robinson D, et al (2000) Concordance of the Toxicity of Pharmaceuticals in Humans and in Animals. Regul Toxicol Pharmacol 32:56–67. doi: 10.1006/rtph.2000.1399

Orchard CH, Lakatta EG (1985) Intracellular calcium transients and developed tension in rat heart muscle. A mechanism for the negative interval-strength relationship. J Gen Physiol 86:637–51. doi: 10.1085/jgp.86.5.637

Ørstavik Ø, Ata SH, Riise J, et al (2014) Inhibition of phosphodiesterase-3 by levosimendan is sufficient to account for its inotropic effect in failing human heart. Br J Pharmacol 171:5169–5181. doi: 10.1111/bph.12647

Pacher P, Bagi Z, Lakó-Futó Z, et al (2000) Cardiac electrophysiological effects of citalopram in guinea pig papillary muscle Comparison with clomipramine. Gen Pharmacol Vasc Syst 34:17–23. doi: 10.1016/S0306-3623(99)00048-8

Palmer AE, Tsien RY (2006) Measuring calcium signaling using genetically targetable fluorescent indicators. Nat Protoc 1:1057–1065. doi: 10.1038/nprot.2006.172

Palmer RF, Lasseter KC, Mccarthy J (1971) Tolbutamide: an inotropic effect on rabbit atria. Lancet (London, England) 1:604

Parikh SS, Blackwell DJ, Gomez-Hurtado N, et al (2017) Thyroid and Glucocorticoid Hormones

Bibliography

Promote Functional T-Tubule Development in Human-Induced Pluripotent Stem Cell-Derived Cardiomyocytes. Circ Res 121:1323–1330. doi: 10.1161/CIRCRESAHA.117.311920

Pérez O, Gay P, Franqueza L, et al (1995) Effects of the two enantiomers, S-16257-2 and S-16260-2, of a new bradycardic agent on guinea-pig isolated cardiac preparations. Br J Pharmacol 115:787–794. doi: 10.1111/j.1476-5381.1995.tb15002.x

Picanço-Castro V, Fontes AM, Russo-Carbolante EM de S, Covas DT (2008) Lentiviral-mediated gene transfer – a patent review. Expert Opin Ther Pat 18:525–539. doi: 10.1517/13543776.18.5.525

Pointon A, Harmer AR, Dale IL, et al (2015) Assessment of Cardiomyocyte Contraction in Human-Induced Pluripotent Stem Cell-Derived Cardiomyocytes. Toxicol Sci 144:227–237. doi: 10.1093/toxsci/kfu312

Pousti A, Deemyad T, Malihi G (2004) Mechanism of inhibitory effect of citalopram on isolated guinea-pig atria in relation to adenosine receptor. Hum Psychopharmacol Clin Exp 19:347–350. doi: 10.1002/hup.593

Price PS, Keenan RE, Swartout JC (2008) Characterizing interspecies uncertainty using data from studies of anti-neoplastic agents in animals and humans. Toxicol Appl Pharmacol 233:64–70. doi: 10.1016/J.TAAP.2008.03.026

Purdy JE, Liebeman M, Roggeveen AE, Kirk RG (1972) Synthetic strands of cardiac muscle. Formation and ultrastructure. J Cell Biol 55:563–78

Rainer PP, Doleschal B, Kirk JA, et al (2012) Sunitinib causes dose-dependent negative functional effects on myocardium and cardiomyocytes. BJU Int 110:1455–1462. doi: 10.1111/j.1464-410X.2012.11134.x

Rajamohan D, Matsa E, Kalra S, et al (2013) Current status of drug screening and disease modelling in human pluripotent stem cells. Bioessays 35:281–98. doi: 10.1002/bies.201200053

Ravenscroft SM, Pointon A, Williams AW, et al (2016) Cardiac Non-myocyte Cells Show Enhanced Pharmacological Function Suggestive of Contractile Maturity in Stem Cell Derived Cardiomyocyte Microtissues. Toxicol Sci 152:99–112. doi: 10.1093/toxsci/kfw069

Rehberg M, Lepier A, Solchenberger B, et al (2008) A new non-disruptive strategy to target calcium indicator dyes to the endoplasmic reticulum. Cell Calcium 44:386–399. doi: 10.1016/j.ceca.2008.02.002

Ribeiro MC, Tertoolen LG, Guadix JA, et al (2015) Functional maturation of human pluripotent stem

Bibliography

cell derived cardiomyocytes in vitro – Correlation between contraction force and electrophysiology. Biomaterials 51:138–150. doi: 10.1016/J.BIOMATERIALS.2015.01.067

Richter W, Xie M, Scheitrum C, et al (2011) Conserved expression and functions of PDE4 in rodent and human heart. Basic Res Cardiol 106:249–262. doi: 10.1007/s00395-010-0138-8

Ronaldson-Bouchard K, Ma SP, Yeager K, et al (2018) Advanced maturation of human cardiac tissue grown from pluripotent stem cells. Nature 556:239–243. doi: 10.1038/s41586-018-0016-3

Ruan J-L, Tulloch NL, Razumova M V, et al (2016) Mechanical Stress Conditioning and Electrical Stimulation Promote Contractility and Force Maturation of Induced Pluripotent Stem Cell-Derived Human Cardiac Tissue. Circulation 134:1557–1567. doi: 10.1161/CIRCULATIONAHA.114.014998

Ruffolo RR (1987) The pharmacology of dobutamine. Am J Med Sci 294:244–8

Sada H (1978) Effect of phentolamine, alprenolol and prenylamine on maximum rate of rise of action potential in guinea-pig papillary muscles. Naunyn Schmiedebergs Arch Pharmacol 304:191–201

Saini H, Navaei A, Van Putten A, et al (2015) 3D Cardiac Microtissues Encapsulated with the Co-Culture of Cardiomyocytes and Cardiac Fibroblasts. Adv Heal care Mater 4:1961–71. doi: 10.1002/adhm.201500331

Saito K, Fukunaga H, Matuoka T, et al (1986) Effects of tolbutamide on cultured heart cells of mice. J Mol Cell Cardiol 18:449–54

Sanchez-Freire V, Lee AS, Hu S, et al (2014) Effect of human donor cell source on differentiation and function of cardiac induced pluripotent stem cells. J Am Coll Cardiol 64:436–48. doi: 10.1016/j.jacc.2014.04.056

Sato S, Talukder MAH, Sugawara H, et al (1998) Effects of levosimendan on myocardial contractility and Ca2+ transients in aequorin-loaded right-ventricular papillary muscles and indo-1-loaded single ventricular cardiomyocytes of the rabbit. J Mol Cell Cardiol 30:1115–1128. doi: 10.1006/jmcc.1998.0677

Schmitz W, Eschenhagen T, Mende U, et al (1992) Phosphodiesterase inhibition and positive inotropy in failing human myocardium. Basic Res Cardiol 87 Suppl 1:65–71

Scholz H, Böhm M, Brückner R, et al (1987) Mechanism of the "Antiadrenergic" Effects of Adenosine on Myocardial Force of Contraction. In: Topics and Perspectives in Adenosine Research. Springer Berlin Heidelberg, pp 369–382

Bibliography

Schotten U, Ausma J, Stellbrink C, et al (2001) Cellular mechanisms of depressed atrial contractility in patients with chronic atrial fibrillation. Circulation 103:691–698. doi: 10.1161/01.CIR.103.5.691

Schulz M, Schmoldt A (2003) Therapeutic and toxic blood concentrations of more than 800 drugs and other xenobiotics. Pharmazie 58:447–74. doi: 10.1186/cc11441

Schulze JJ, Knops J (1982) Effects of flecainide on contractile force and electrophysiological parameters in cardiac muscle. Arzneimittelforschung 32:1025–9

Scott CW, Zhang X, Abi-Gerges N, et al (2014) An Impedance-Based Cellular Assay Using Human iPSC-Derived Cardiomyocytes to Quantify Modulators of Cardiac Contractility. Toxicol Sci 142:331–338. doi: 10.1093/toxsci/kfu186

Sen LY, O'Neill M, Marsh JD, Smith TW (1990) Inotropic and calcium kinetic effects of calcium channel agonist and antagonist in isolated cardiac myocytes from cardiomyopathic hamsters. Circ Res 67:599–608. doi: 10.1161/01.RES.67.3.599

Shadrin IY, Allen BW, Qian Y, et al (2017) Cardiopatch platform enables maturation and scale-up of human pluripotent stem cell-derived engineered heart tissues. Nat Commun 8:1825. doi: 10.1038/s41467-017-01946-x

Shang W, Lu F, Sun T, et al (2014) Imaging Ca2+ nanosparks in heart with a new targeted biosensor. Circ Res 114:412–420. doi: 10.1161/CIRCRESAHA.114.302938

Sharma A, Zhang Y, Buikema JW, et al (2018) Stage-specific Effects of Bioactive Lipids on Human iPSC Cardiac Differentiation and Cardiomyocyte Proliferation. Sci Rep 8:6618. doi: 10.1038/s41598-018-24954-3

Shiba Y, Fernandes S, Zhu W-Z, et al (2012) Human ES-cell-derived cardiomyocytes electrically couple and suppress arrhythmias in injured hearts. Nature 489:322–5. doi: 10.1038/nature11317

Sinnecker D, Goedel A, Dorn T, et al (2013) Modeling long-QT syndromes with iPS cells. J Cardiovasc Transl Res 6:31–6. doi: 10.1007/s12265-012-9416-1

Song L, Awari DW, Han EY, et al (2015) Dual optical recordings for action potentials and calcium handling in induced pluripotent stem cell models of cardiac arrhythmias using genetically encoded fluorescent indicators. Stem Cells Transl Med 4:468–75. doi: 10.5966/sctm.2014-0245

Sørensen EV (1990) Effects of positive inotropic drugs on the frequency of contraction of the isolated atria: influence of dose regimen and age. Pharmacol Toxicol 67:69–72

Sossalla S, Fluschnik N, Schotola H, et al (2010) Inhibition of elevated Ca2+/calmodulin-dependent

protein kinase II improves contractility in human failing myocardium. Circ Res 107:1150–1161. doi: 10.1161/CIRCRESAHA.110.220418

Stoehr A, Neuber C, Baldauf C, et al (2014) Automated analysis of contractile force and Ca2+ transients in engineered heart tissue. Am J Physiol Heart Circ Physiol 306:H1353-63. doi: 10.1152/ajpheart.00705.2013

Suenari K, Cheng CC, Chen YC, et al (2012) Effects of ivabradine on the pulmonary vein electrical activity and modulation of pacemaker currents and calcium homeostasis. J Cardiovasc Electrophysiol 23:200–206. doi: 10.1111/j.1540-8167.2011.02173.x

Takahashi K, Tanabe K, Ohnuki M, et al (2007) Induction of Pluripotent Stem Cells from Adult Human Fibroblasts by Defined Factors. Cell 131:861–872. doi: 10.1016/j.cell.2007.11.019

Tavi P, Han C, Weckström M (1998) Mechanisms of stretch-induced changes in [Ca2+](i) in rat atrial myocytes: Role of increased troponin C affinity and stretch-activated ion channels. Circ Res 83:1165–77. doi: 10.1161/01.RES.83.11.1165

Taylor DG, Parilak LD, Lewinter MM, Knot HJ (2004) Quantification of the rat left ventricle force and Ca2+- frequency relationships: Similarities to dog and human. Cardiovasc Res 61:77–86. doi: 10.1016/j.cardiores.2003.09.022

Tian L, Hires SA, Mao T, et al (2009) Imaging neural activity in worms, flies and mice with improved GCaMP calcium indicators. Nat Methods 6:875–881. doi: 10.1038/nmeth.1398

Tiburcy M, Hudson JE, Balfanz P, et al (2017) Defined Engineered Human Myocardium with Advanced Maturation for Applications in Heart Failure Modelling and Repair. Circulation 135:1832–1847. doi: 10.1161/CIRCULATIONAHA.116.024145

Tulloch NL, Muskheli V, Razumova M V, et al (2011) Growth of engineered human myocardium with mechanical loading and vascular coculture. Circ Res 109:47–59. doi: 10.1161/CIRCRESAHA.110.237206

Ulmer BM, Stoehr A, Schulze ML, et al (2018) Contractile Work Contributes to Maturation of Energy Metabolism in hiPSC-Derived Cardiomyocytes. Stem cell reports 10:834–847. doi: 10.1016/j.stemcr.2018.01.039

Uzun AU, Mannhardt I, Breckwoldt K, et al (2016) Ca(2+)-Currents in Human Induced Pluripotent Stem Cell-Derived Cardiomyocytes Effects of Two Different Culture Conditions. Front Pharmacol 7:300. doi: 10.3389/fphar.2016.00300

Bibliography

van den Berg CW, Okawa S, Chuva de Sousa Lopes SM, et al (2015) Transcriptome of human foetal heart compared with cardiomyocytes from pluripotent stem cells. Development 142:3231–8. doi: 10.1242/dev.123810

Vandecasteele G, Eschenhagen T, Scholz H, et al (1999) Muscarinic and β-adrenergic regulation of heart rate, force of contraction and calcium current is preserved in mice lacking endothelial nitric oxide synthase. Nat Med 5:331–334. doi: 10.1038/6553

Vandenburgh HH, Solerssi R, Shansky J, et al (1996) Mechanical stimulation of organogenic cardiomyocyte growth in vitro. Am J Physiol 270:C1284-92. doi: 10.1152/ajpcell.1996.270.5.C1284

Varian KD, Janssen PML (2007) Frequency-dependent acceleration of relaxation involves decreased myofilament calcium sensitivity. Am J Physiol - Hear Circ Physiol 292:H2212–H2219. doi: 10.1152/ajpheart.00778.2006

Vatner SF, McRitchie RJ, Braunwald E (1974) Effects of Dobutamine on Left Ventricular Performance, Coronary Dynamics, and Distribution of Cardiac Output in Conscious Dogs. J Clin Invest 53:1265–1273. doi: 10.1172/JCI107673

Wallis R, Gharanei M, Maddock H (2015) Predictivity of in vitro non-clinical cardiac contractility assays for inotropic effects in humans - A literature search. J Pharmacol Toxicol Methods 75:62–69. doi: 10.1016/J.VASCN.2015.05.009

Wang J, Zhang L, Qi JH, et al (1996) Effects of captopril and enalaprilat on intracellular Ca2+ content in isolated cardiomyocytes from rats. Zhongguo Yao Li Xue Bao 17:233–5

Warne T, Moukhametzianov R, Baker JG, et al (2011) The structural basis for agonist and partial agonist action on a β(1)-adrenergic receptor. Nature 469:241–4. doi: 10.1038/nature09746

Weber K, Bartsch U, Stocking C, Fehse B (2008) A Multicolor Panel of Novel Lentiviral "Gene Ontology" (LeGO) Vectors for Functional Gene Analysis. Mol vol 16:698–706. doi: 10.1038/mt.2008.6

Willems E, Spiering S, Davidovics H, et al (2011) Small-molecule inhibitors of the Wnt pathway potently promote cardiomyocytes from human embryonic stem cell-derived mesoderm. Circ Res 109:360–4. doi: 10.1161/CIRCRESAHA.111.249540

Williams RS, Bishop T (1981) Selectivity of dobutamine for adrenergic receptor subtypes: in vitro analysis by radioligand binding. J Clin Invest 67:1703–11. doi: 10.1172/JCI110208

Bibliography

Winslow RL, Hinch R, Greenstein JL (2005) Mechanisms and Models of Cardiac Excitation-Contraction Coupling. In: Tutorials in Mathematical Biosciences II. Springer-Verlag Berlin/Heidelberg 2005, pp 97–131

Witchel HJ, Pabbathi VK, Hofmann G, et al (2002) Inhibitory actions of the selective serotonin re-uptake inhibitor citalopram on HERG and ventricular L-type calcium currents. FEBS Lett 512:59–66

Yang L, Soonpaa MH, Adler ED, et al (2008) Human cardiovascular progenitor cells develop from a KDR+ embryonic-stem-cell-derived population. Nature 453:524–8. doi: 10.1038/nature06894

Yang X, Pabon L, Murry CE, et al (2014a) Engineering Adolescence: Maturation of Human Pluripotent Stem Cell-derived Cardiomyocytes. Circ Res 114:511–523. doi: 10.11610.1161/CIRCRESAHA.114.300558

Yang X, Rodriguez M, Pabon L, et al (2014b) Tri-iodo-l-thyronine promotes the maturation of human cardiomyocytes-derived from induced pluripotent stem cells. J Mol Cell Cardiol 72:296–304. doi: 10.1016/j.yjmcc.2014.04.005

Yokoshiki H, Katsube Y, Sunagawa M, Sperelakis N (1997) Levosimendan, a novel Ca2+ sensitizer, activates the glibenclamide-sensitive K+ channel in rat arterial myocytes. Eur J Pharmacol 333:249–259. doi: 10.1016/S0014-2999(97)01108-4

Zahradník I, Minarovic I, Zahradníková A (2008) Inhibition of the cardiac L-type calcium channel current by antidepressant drugs. J Pharmacol Exp Ther 324:977–84. doi: 10.1124/jpet.107.132456

Zhang D, Shadrin IY, Lam J, et al (2013) Tissue-engineered cardiac patch for advanced functional maturation of human ESC-derived cardiomyocytes. Biomaterials 34:5813–5820. doi: 10.1016/j.biomaterials.2013.04.026

Zhang J, Wilson GF, Soerens AG, et al (2009) Functional cardiomyocytes derived from human induced pluripotent stem cells. Circ Res 104:e30-41. doi: 10.1161/CIRCRESAHA.108.192237

Zhang M, Schulte JS, Heinick A, et al (2015) Universal cardiac induction of human pluripotent stem cells in two and three-dimensional formats: implications for in vitro maturation. Stem Cells 33:1456–69. doi: 10.1002/stem.1964

Zimmermann WH, Schneiderbanger K, Schubert P, et al (2002) Tissue engineering of a differentiated cardiac muscle construct. Circ Res 90:223–230. doi: 10.1161/hh0202.103644

Bibliography

Zünkler BJ, Henning B, Ott T, et al (1997) Effects of Tolbutamide on ATP-Sensitive K+ Channels from Human Right Atrial Cardiac Myocytes. Pharmacol Toxicol 80:69–75. doi: 10.1111/j.1600-0773.1997.tb00286.x

10 SUPPLEMENT

10.1. Blinded screening

Figure S1: Concentration response curves in two hiPSC cell lines, R-PAT and ERC18, using two modalities; contraction and calcium transient (CaT). CaT measurements were performed in R-PAT only. Data are presented as relative to baseline and normalized to time-matched vehicle controls in scatter plot format with mean indicated by red line. Statistical analysis was performed by one-way ANOVA with Dunnett's post-test vs. baseline conditions (BL), *p < 0.05. Dotted red line indicates effective therapeutic concentration values from literature. n=4-6 EHTs. Q=Quiescent.

10.1.1. Scatter plots of positive inotropes

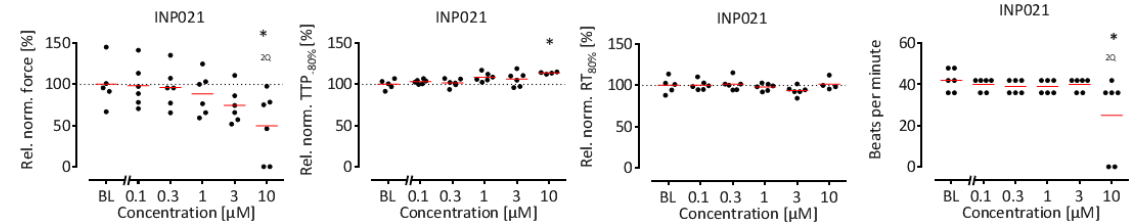Epinephrine (INP029), Cell line: R-PAT, Modality: Contractility
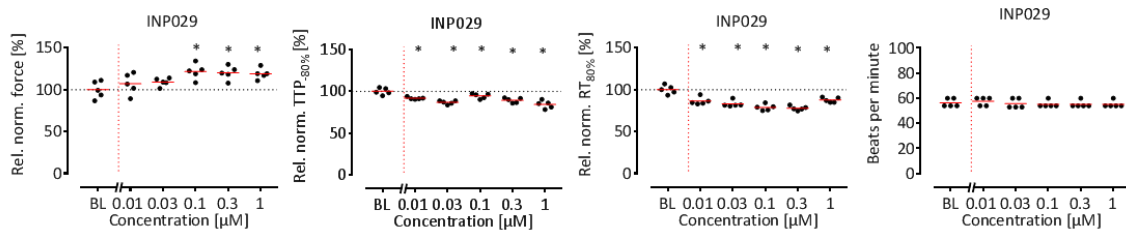
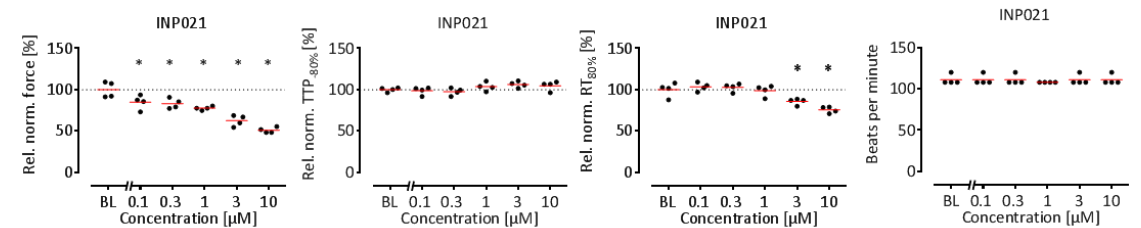Epinephrine (INP029), Cell line: ERC18, Modality: Contractility
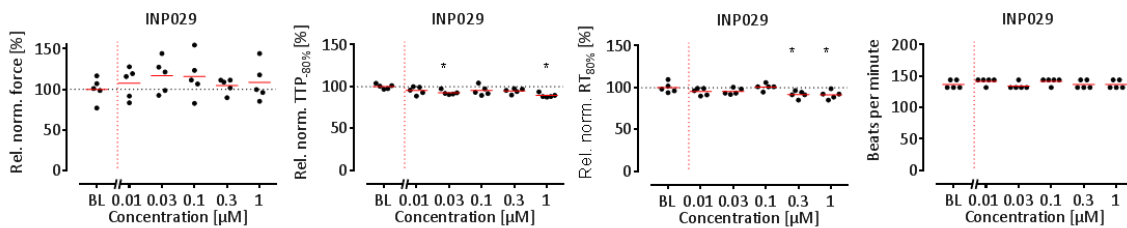
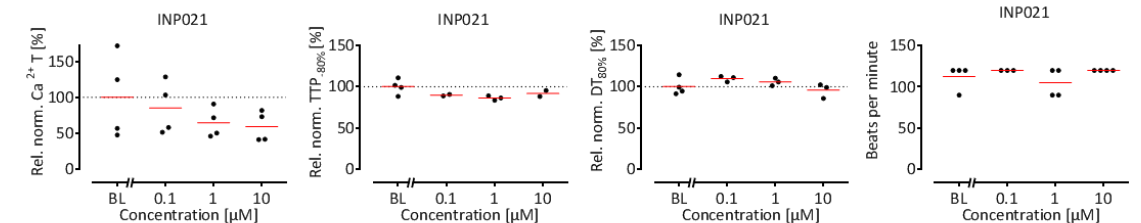Epinephrine (INP029), Cell line: ERC18, Modality: Calcium
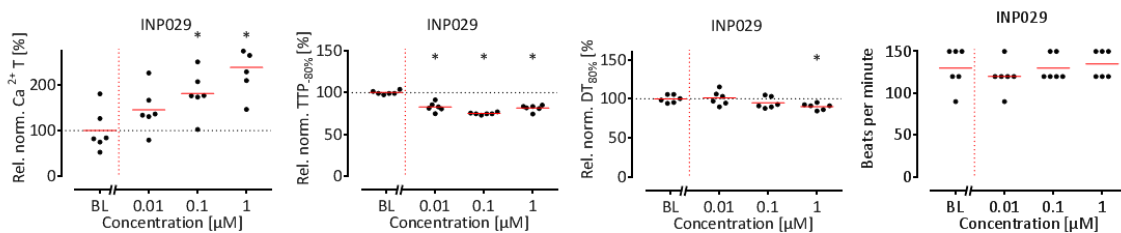
Forskolin (INP028), Cell line: R-PAT, Modality: Contractility
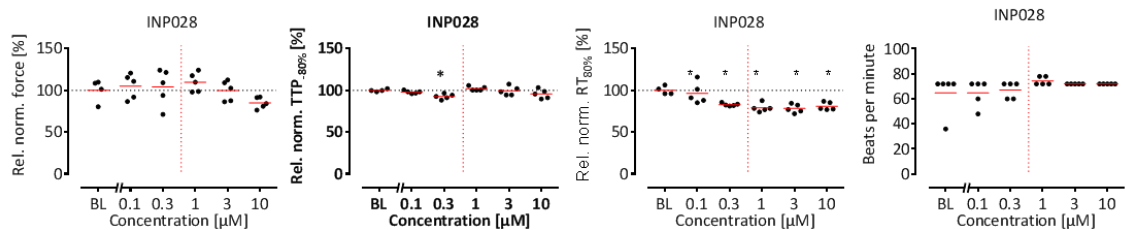
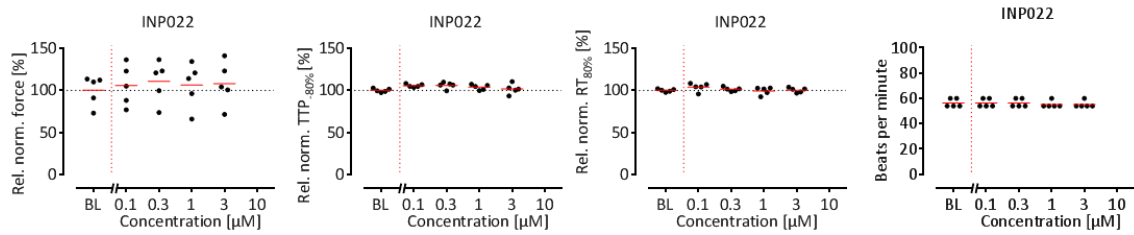Forskolin (INP028), Cell line: ERC18, Modality: Contractility
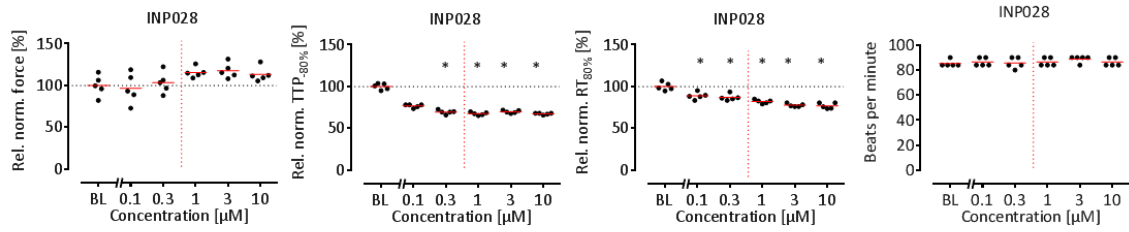
Forskolin (INP028), Cell line: ERC18, Modality: Calcium
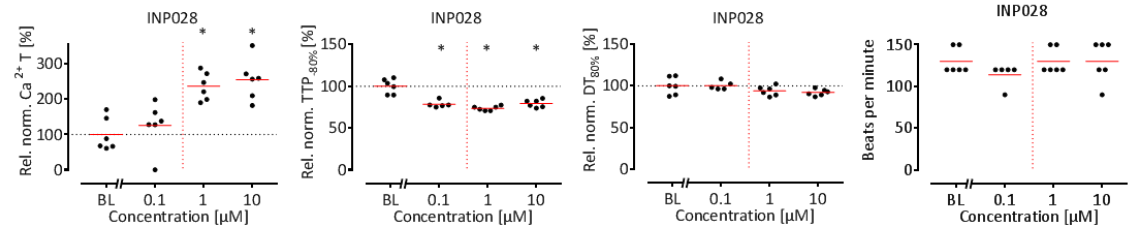
Dobutamine (INP001), Cell line: R-PAT, Modality: Contractility
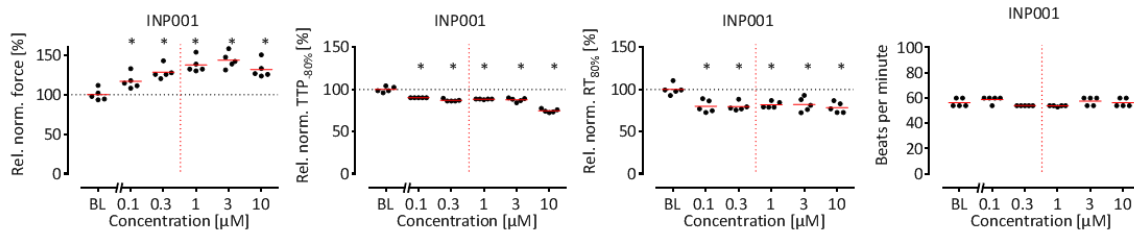
Dobutamine (INP001), Cell line: ERC18, Modality: Contractility
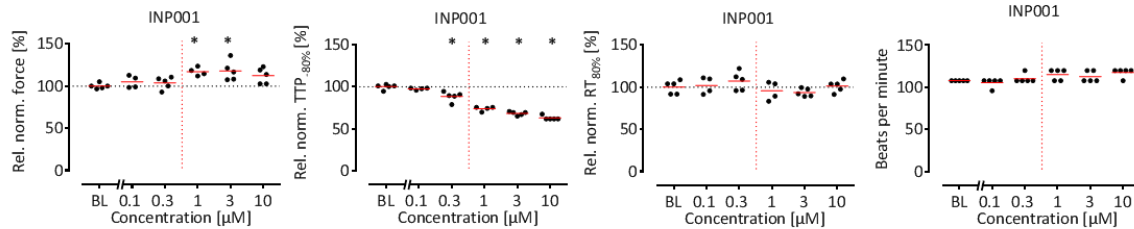
Dobutamine (INP001), Cell line: ERC18, Modality: Calcium
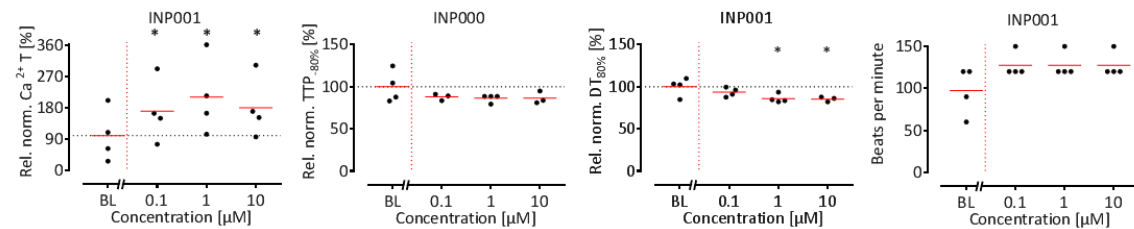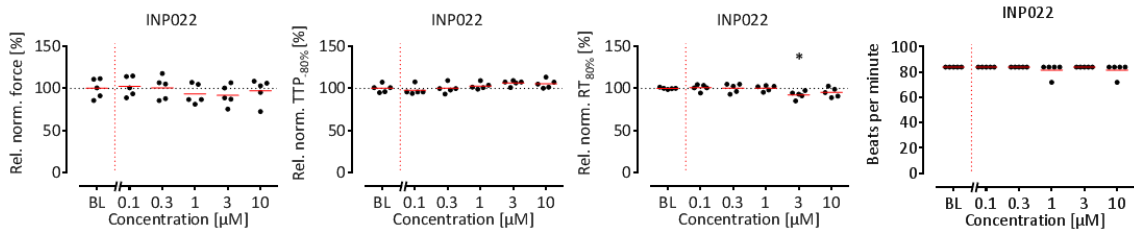
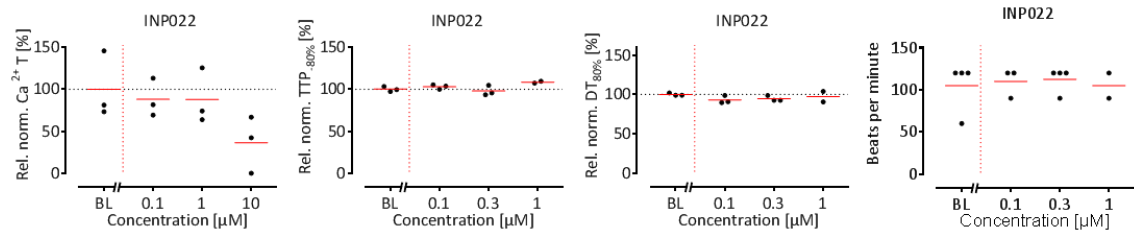## Terbutaline (INP009), Cell line: R-PAT, Modality: Contractility
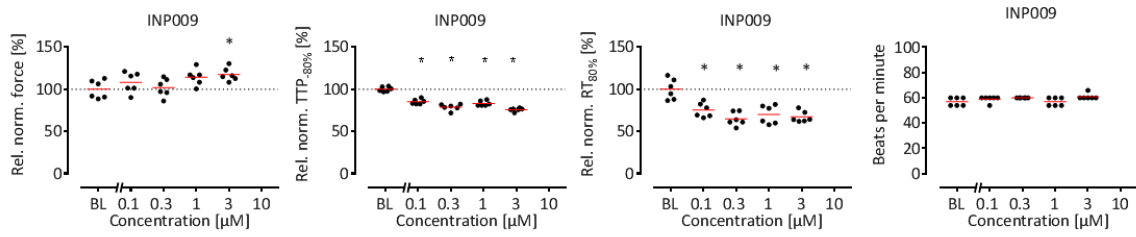
Terbutaline (INP009), Cell line: ERC18, Modality: Contractility
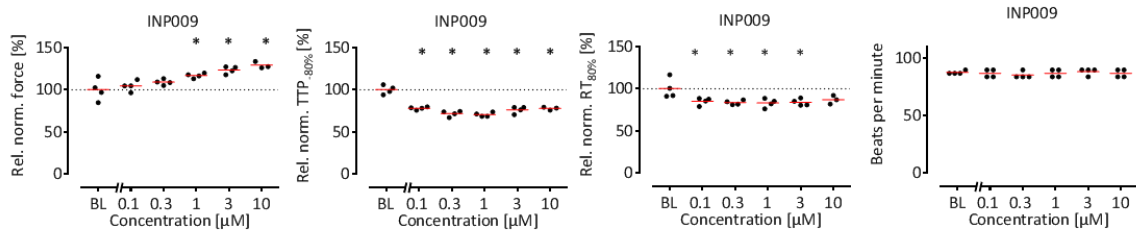
Terbutaline (INP009), Cell line: ERC18, Modality: Calcium
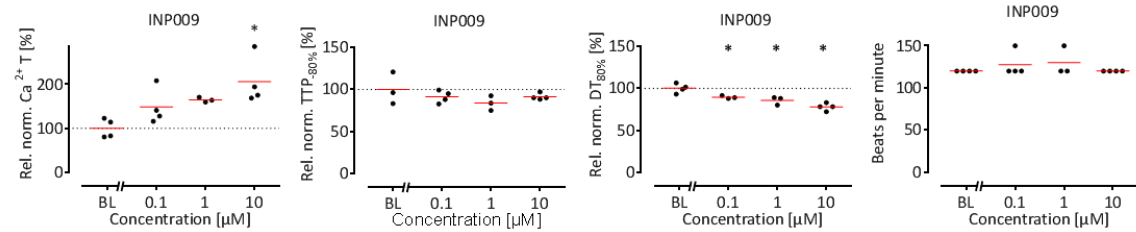
Pimobendan (INP026), Cell line: R-PAT, Modality: Contractility
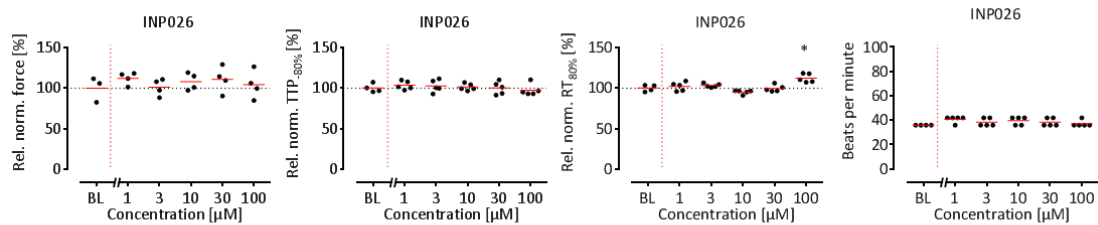
Pimobendan (INP026), Cell line: ERC18, Modality: Contractility
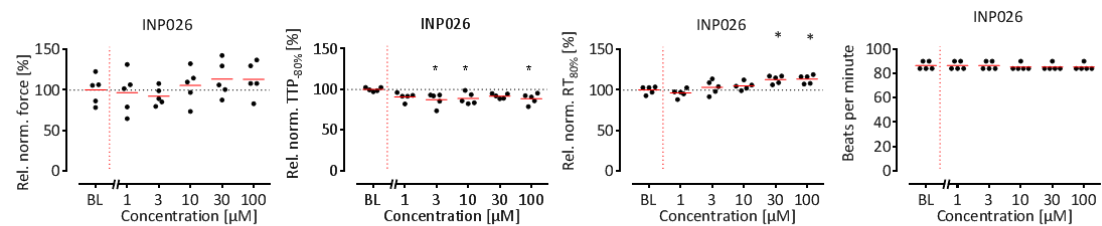
Pimobendan (INP026), Cell line: ERC18, Modality: Calcium
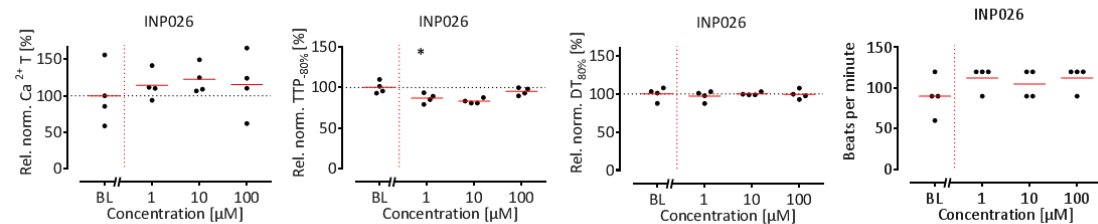
Levosimendan (INP005), Cell line: R-PAT, Modality: Contractility
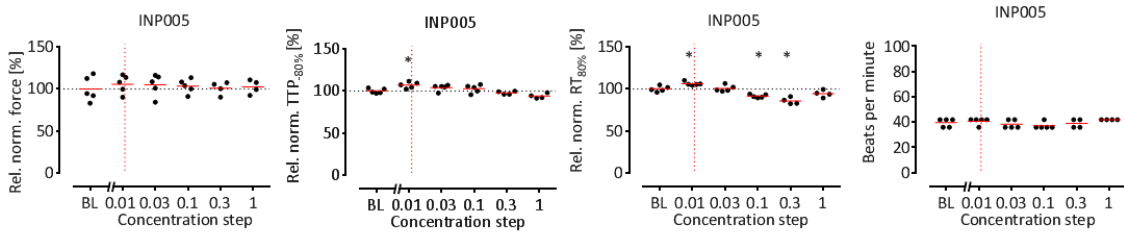
Levosimendan (INP005), Cell line: ERC18, Modality: Contractility
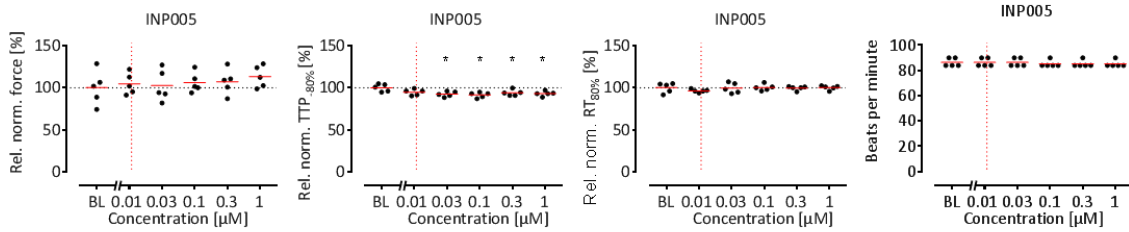
Levosimendan (INP005), Cell line: ERC18, Modality: Calcium
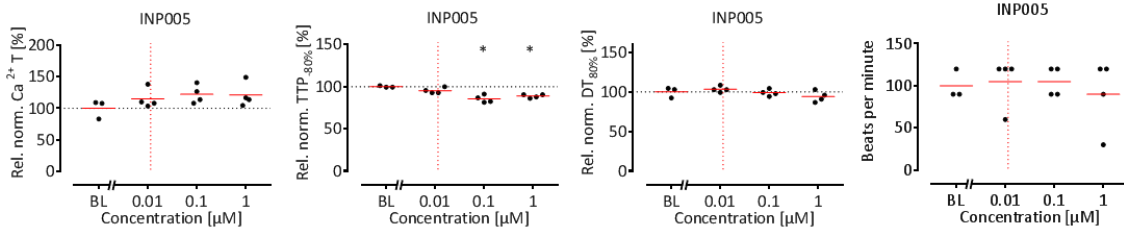
Omecamtiv (INP007), Cell line: R-PAT, Modality: Contractility
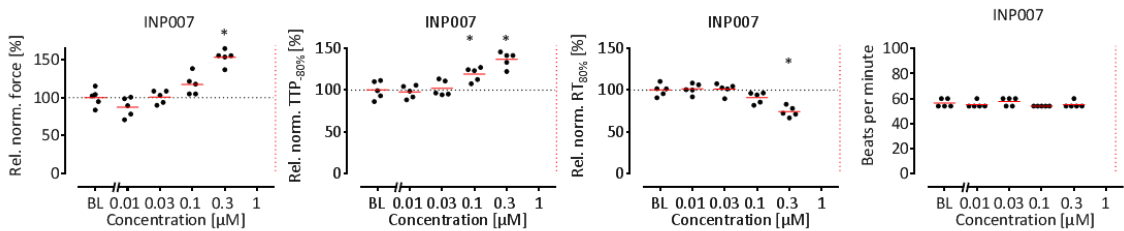
Omecamtiv (INP007), Cell line: ERC18, Modality: Contractility
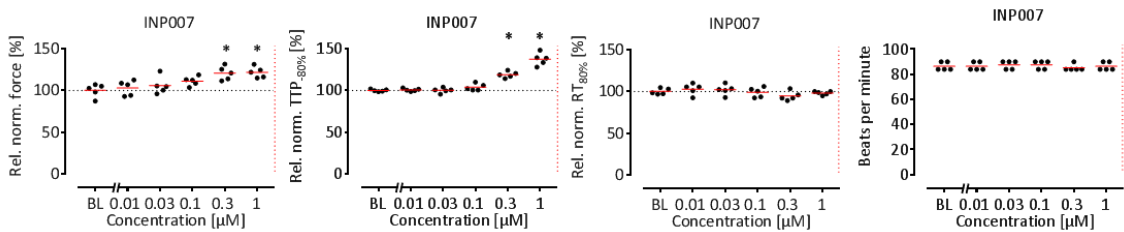
Omecamtiv (INP007), Cell line: ERC18, Modality: Calcium
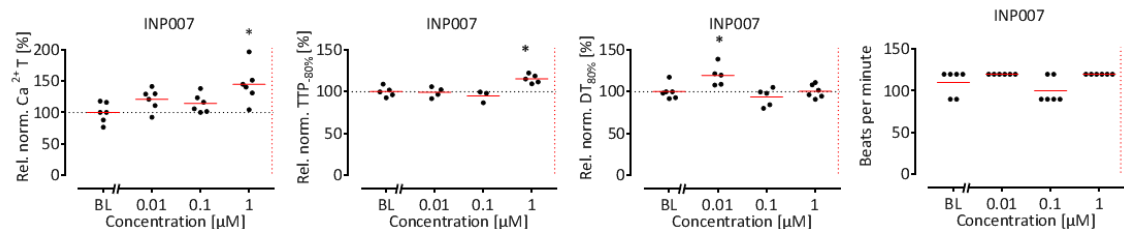
Milrinone (INP027), Cell line: R-PAT, Modality: Contractility
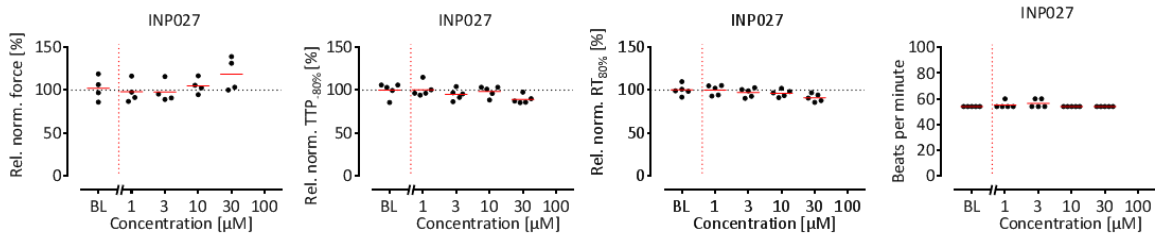
Milrinone (INP027), Cell line: ERC18, Modality: Contractility
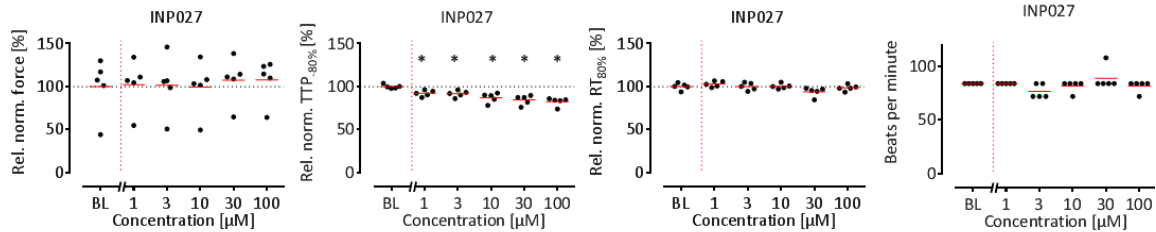
10.1.2. <u>Scatter plots of negative inotropes</u>

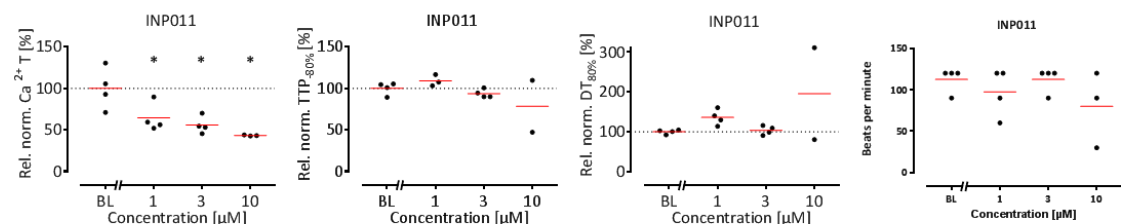Verapamil (INP017), Cell line: R-PAT, Modality: Contractility
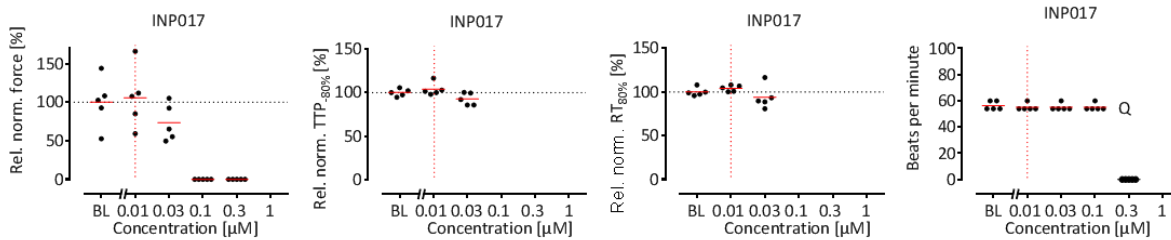
Verapamil (INP017), Cell line: ERC18, Modality: Contractility
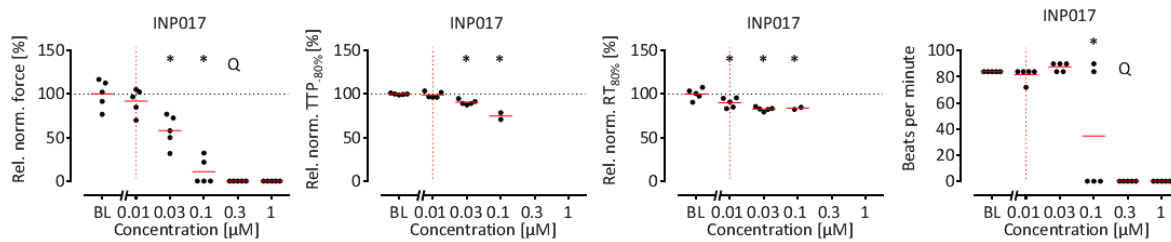
Verapamil (INP017), Cell line: ERC18, Modality: Calcium
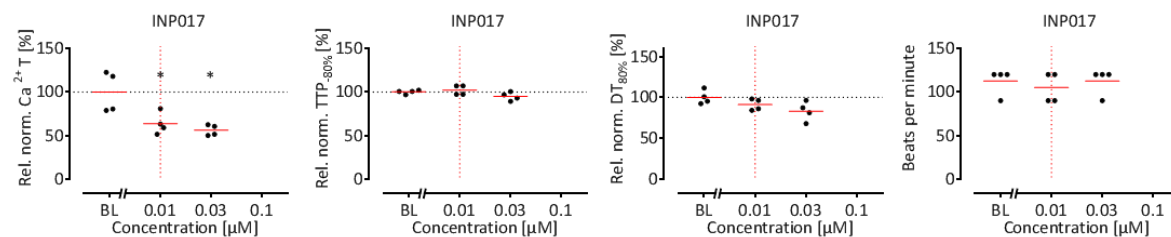
Flecainide (INP023), Cell line: R-PAT, Modality: Contractility
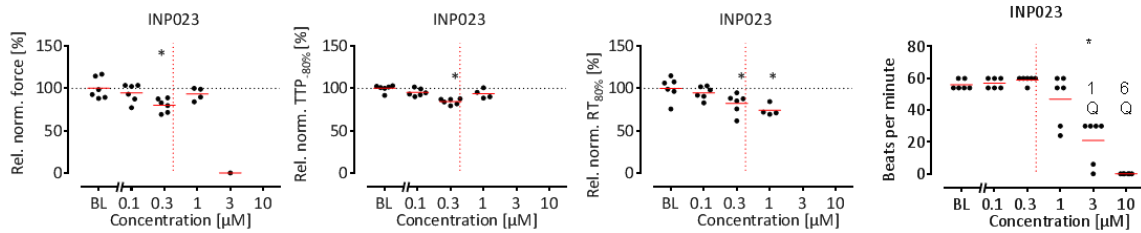
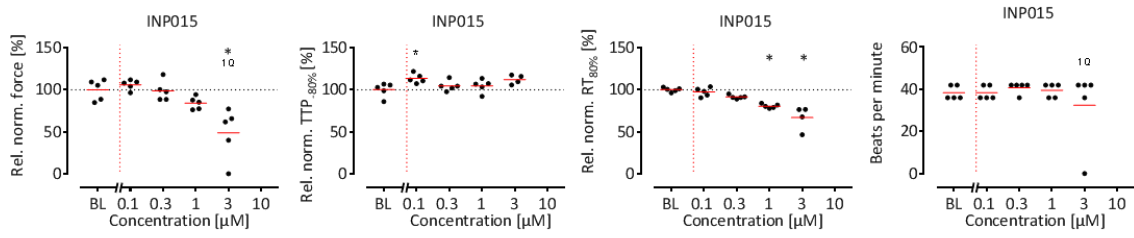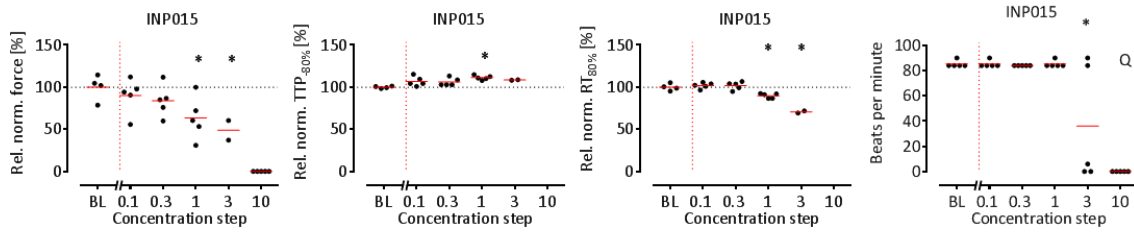Flecainide (INP023), Cell line: ERC18, Modality: Contractility
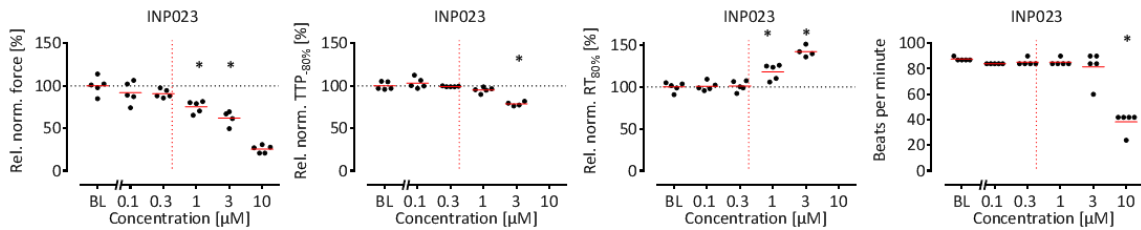
Flecainide (INP023), Cell line: ERC18, Modality: Calcium
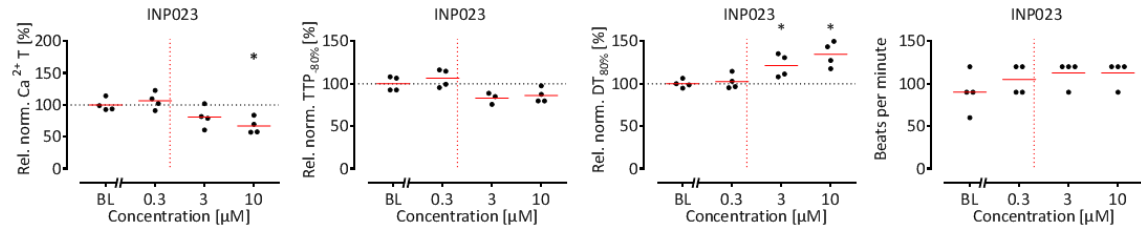
Sorafenib (INP021), Cell line: R-PAT, Modality: Contractility

Sorafenib (INP021), Cell line: ERC18, Modality: Contractility

Sorafenib (INP021), Cell line: ERC18, Modality: Calcium

Sunitinib (INP022), Cell line: R-PAT, Modality: Contractility

Sunitinib (INP022), Cell line: ERC18, Modality: Contractility

Sunitinib (INP022), Cell line: ERC18, Modality: Calcium

Citalopram (INP011), Cell line: R-PAT, Modality: Contractility
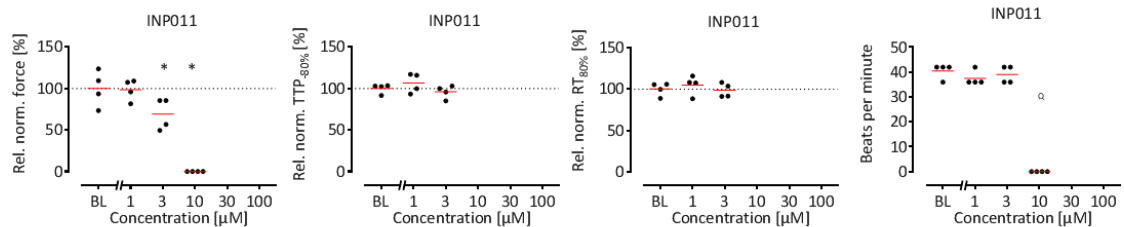
Citalopram (INP011), Cell line: ERC18, Modality: Contractility
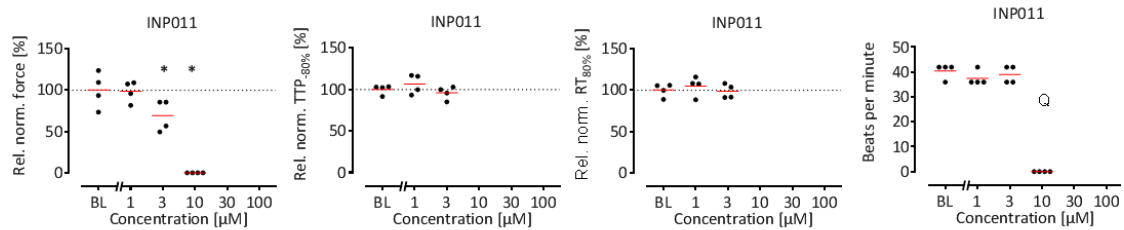
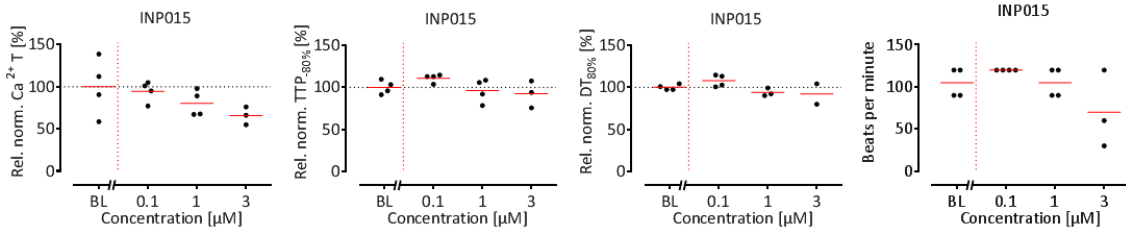Citalopram (INP011), Cell line: ERC18, Modality: Calcium

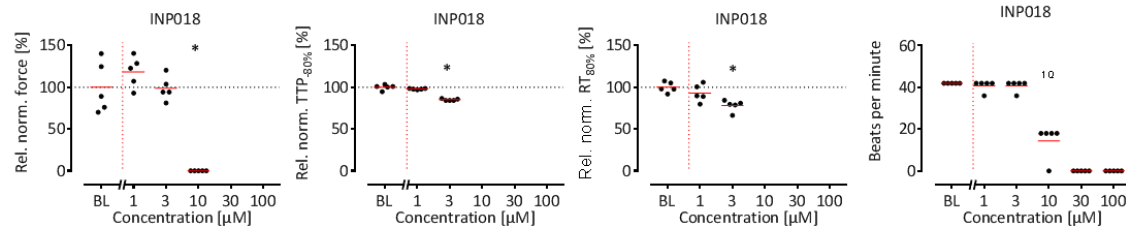Itraconazole (INP015), Cell line: R-PAT, Modality: Contractility

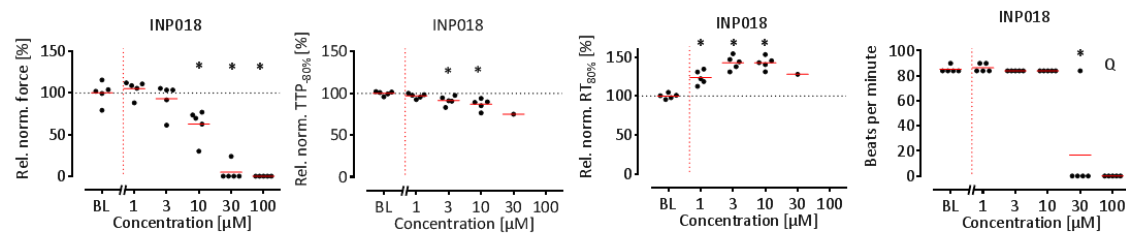Itraconazole (INP015), Cell line: ERC18, Modality: Contractility

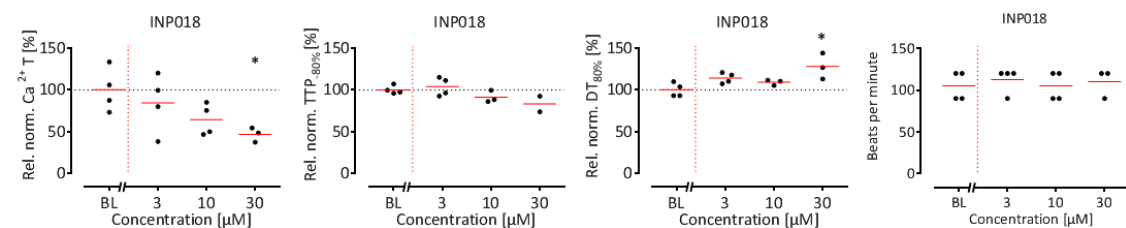Itraconazole (INP015), Cell line: ERC18, Modality: Calcium

Zimelidine (INP018), Cell line: R-PAT, Modality: Contractility

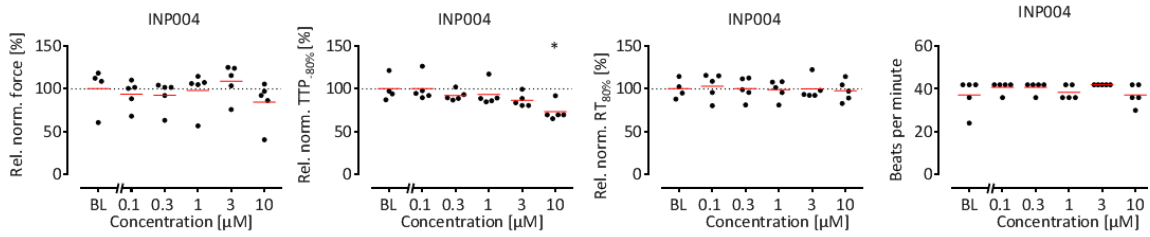Zimelidine (INP018), Cell line: ERC18, Modality: Contractility

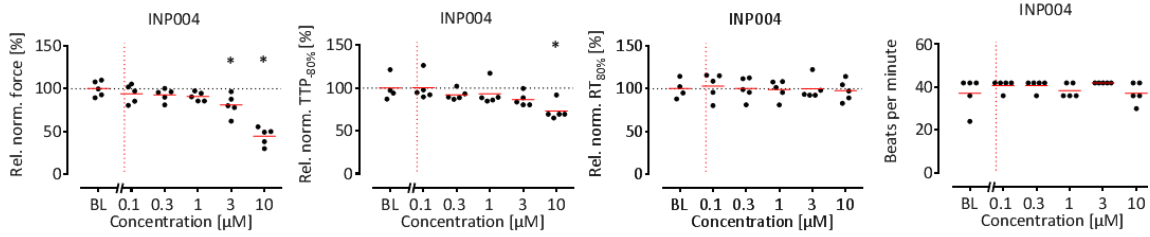Zimelidine (INP018), Cell line: ERC18, Modality: Calcium

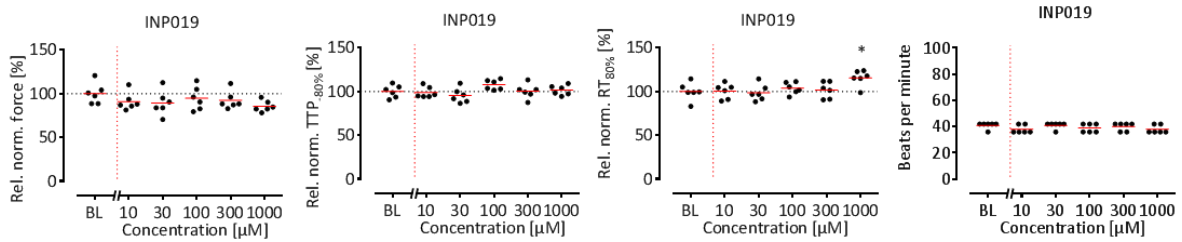Ivabardine (INP004), Cell line: R-PAT, Modality: Contractility

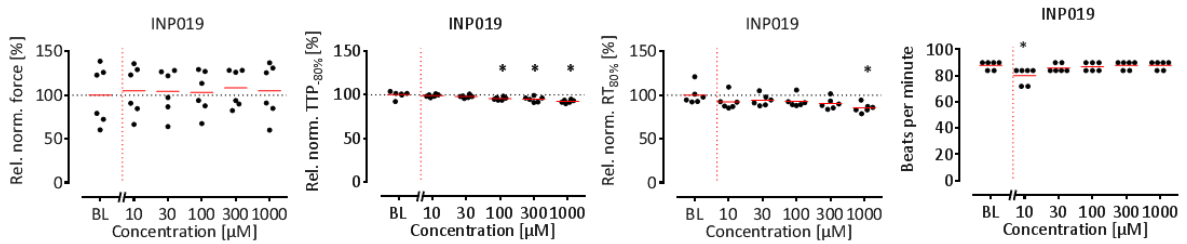Ivabardine (INP004), Cell line: ERC18, Modality: Contractility

10.1.3. Scatter plots of neutral inotropes

Acetylsalicylic acid (INP019), Cell line: R-PAT, Modality: Contractility

Acetylsalicylic acid (INP019), Cell line: ERC18, Modality: Contractility

Acetylsalicylic acid (INP019), Cell line: ERC18, Modality: Calcium
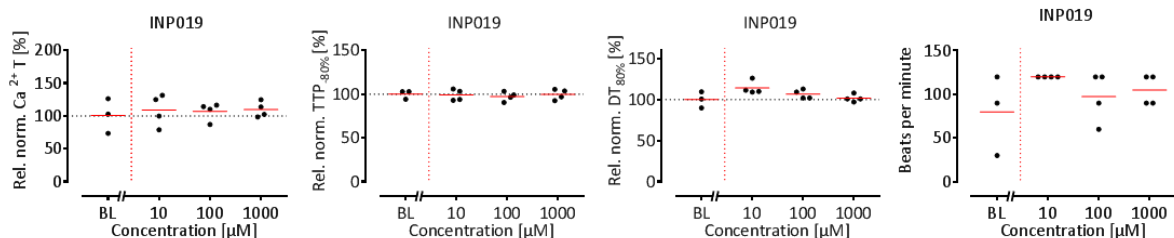
Paracetamol (INP006), Cell line: R-PAT, Modality: Contractility
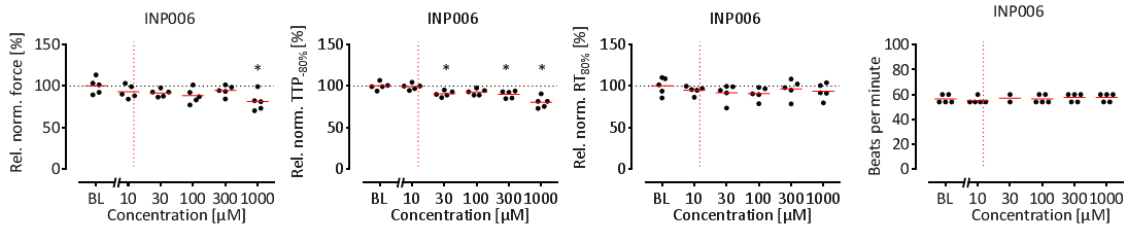
Paracetamol (INP006), Cell line: ERC18, Modality: Contractility

Captopril (INP020), Cell line: R-PAT, Modality: Contractility
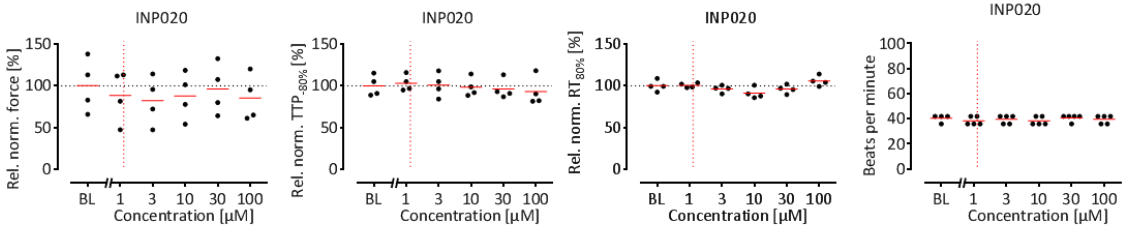
Captopril (INP020), Cell line: ERC18, Modality: Contractility
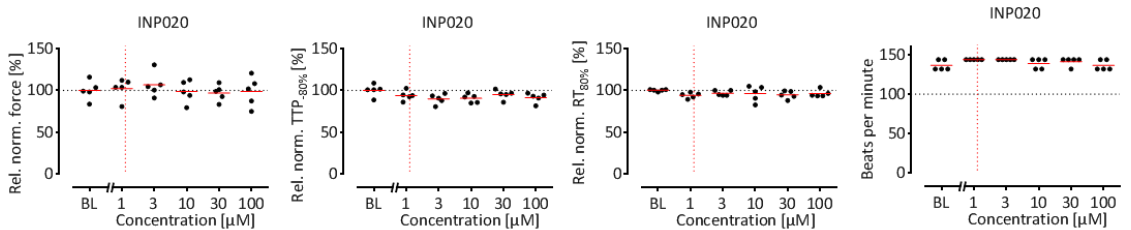
Captopril (INP020), Cell line: ERC18, Modality: Calcium
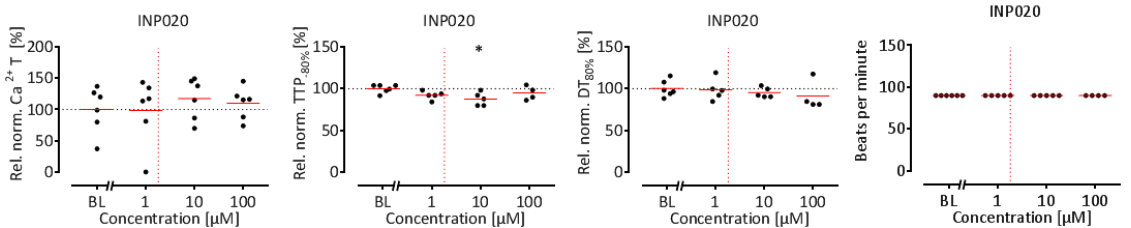
Atenolol (INP025), Cell line: R-PAT, Modality: Contractility
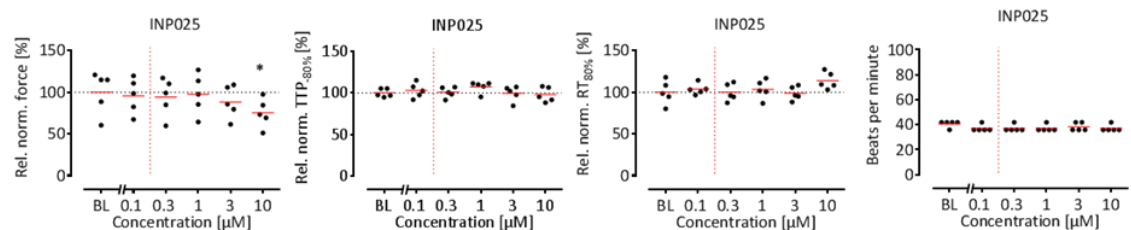
Atenolol (INP025), Cell line: ERC18, Modality: Contractility
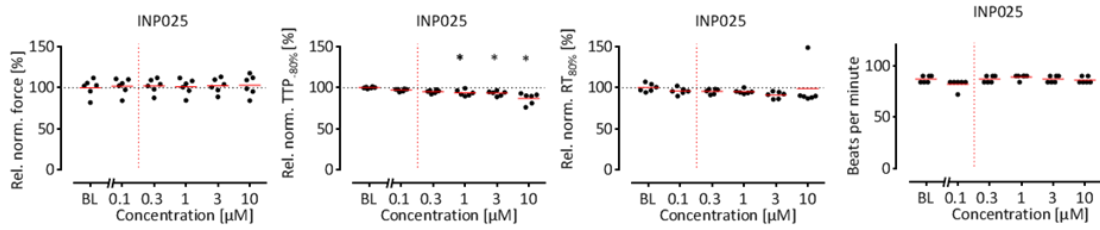
Atenolol (INP025), Cell line: ERC18, Modality: Calcium
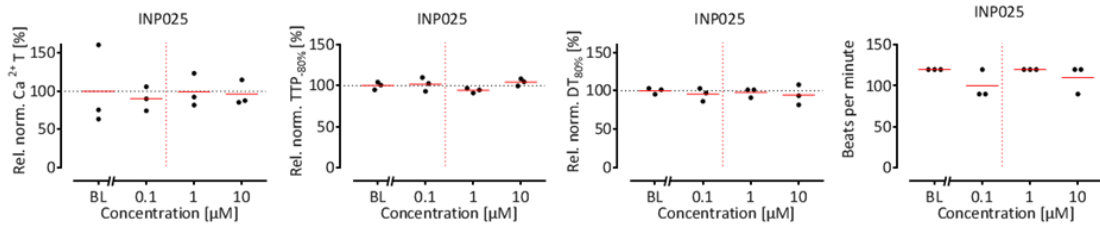
Tolbutamide (INP016), Cell line: R-PAT, Modality: Contractility
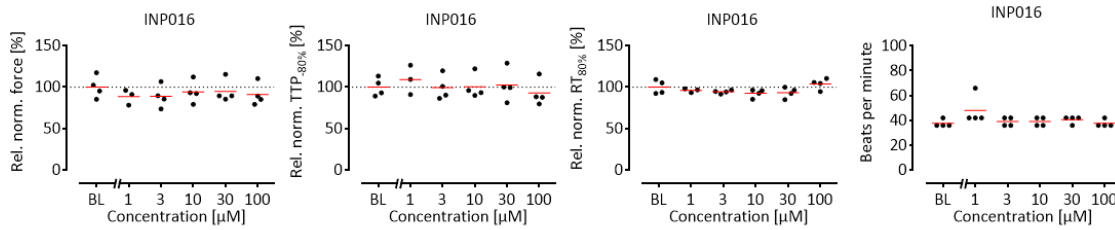
Tolbutamide (INP016), Cell line: ERC18, Modality: Contractility
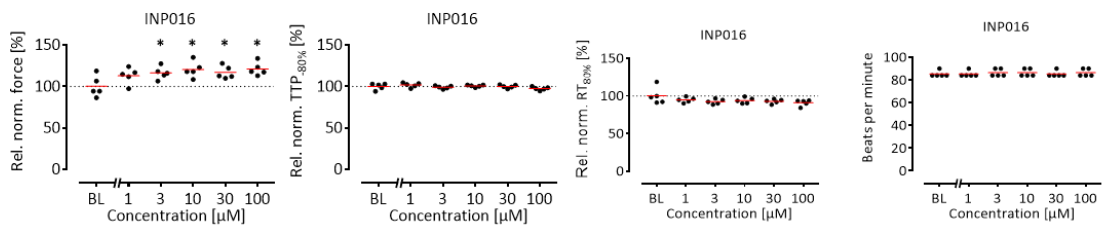
Tolbutamide (INP016), Cell line: ERC18, Modality: Calcium
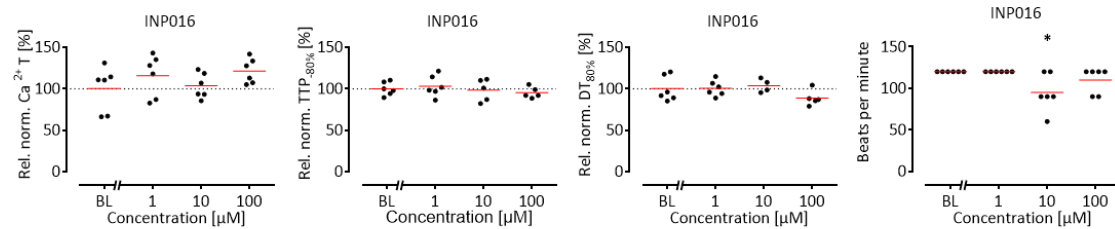
Pravastatin (INP010), Cell line: R-PAT, Modality: Contractility
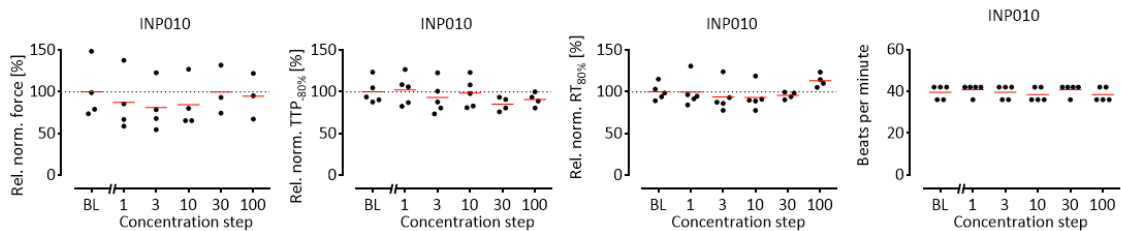
Pravastatin (INP010), Cell line: ERC18, Modality: Contractility
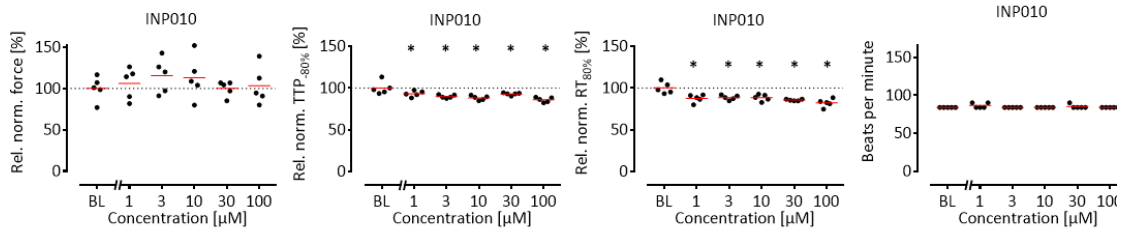
Pravastatin (INP010), Cell line: ERC18, Modality: Calcium
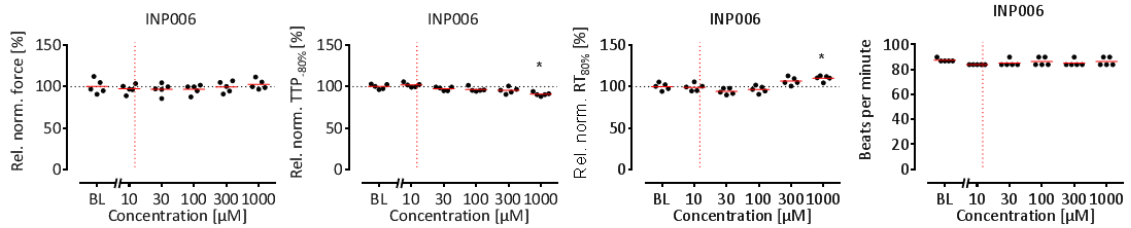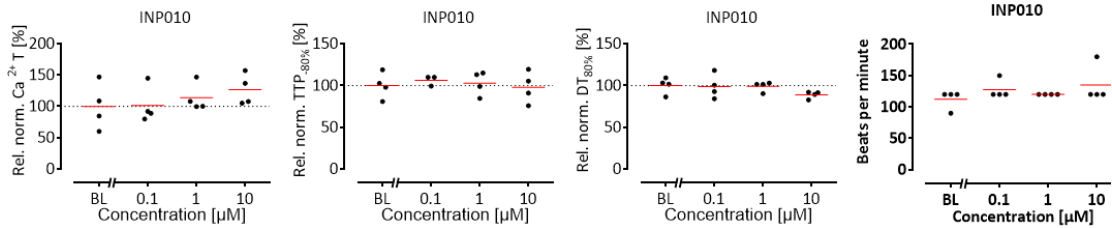

Enalapril (INP002), Cell line: R-PAT, Modality: Contractility
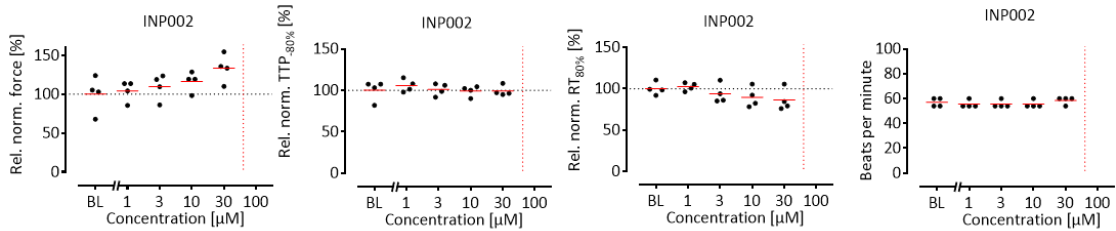
Enalapril (INP002), Cell line: ERC18, Modality: Contractility
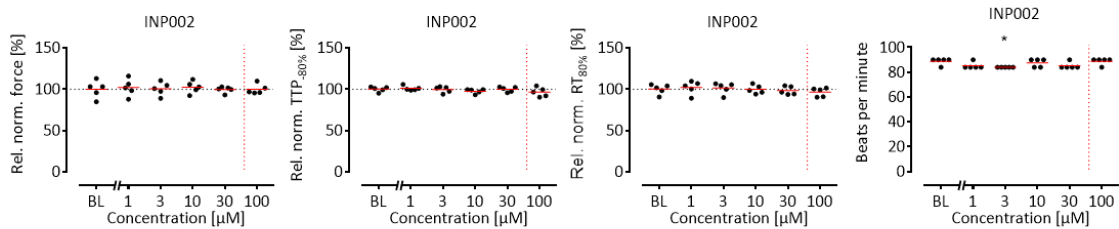
Clonidine (INP024), Cell line: R-PAT, Modality: Contractility
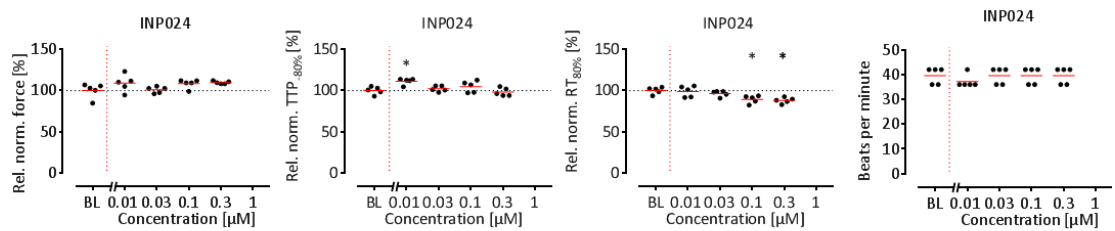
Clonidine (INP024), Cell line: ERC18, Modality: Contractility
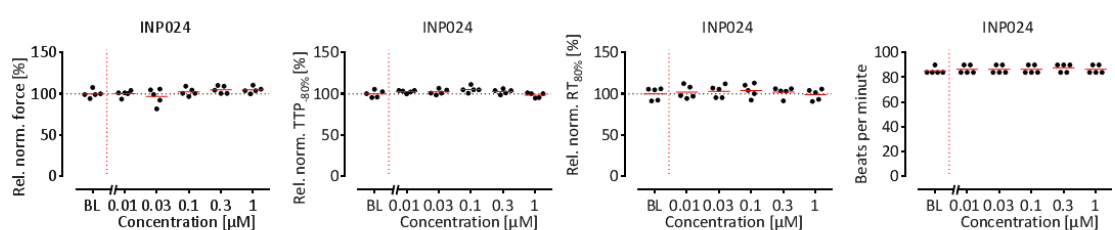
Sildenafil (INP014), Cell line: R-PAT, Modality: Contractility
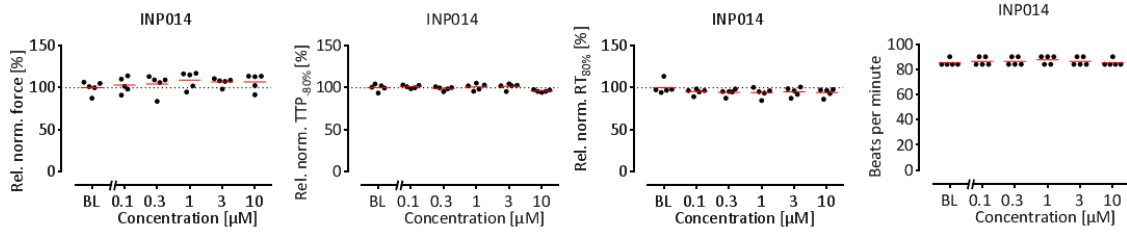
Sildenafil (INP014), Cell line: ERC18, Modality: Contractility
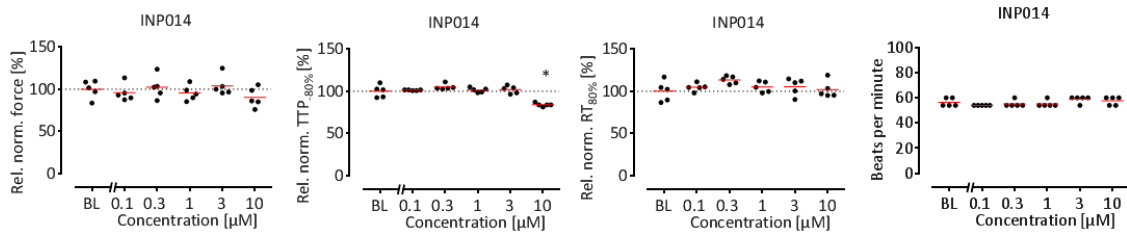
Phentolamine (INP008), Cell line: R-PAT, Modality: Contractility
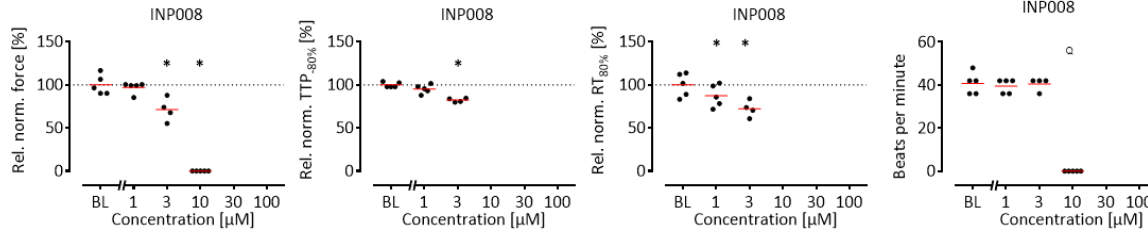
Phentolamine (INP008), Cell line: ERC18, Modality: Contractility
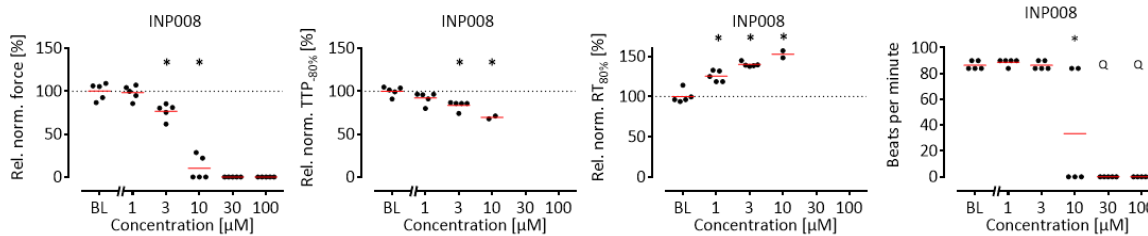
Phentolamine (INP008), Cell line: ERC18, Modality: Calcium
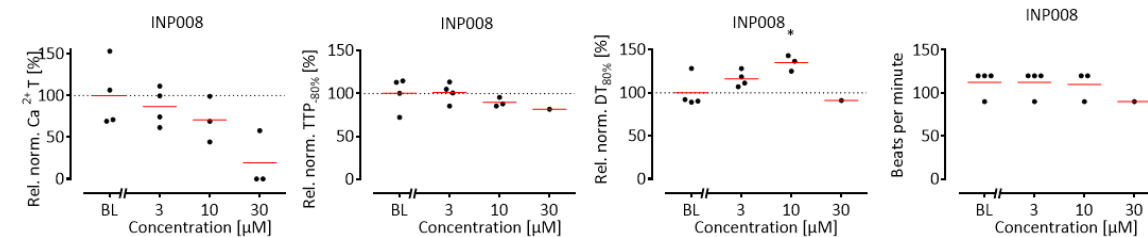
Glibenclamide (INP003), Cell line: R-PAT, Modality: Contractility
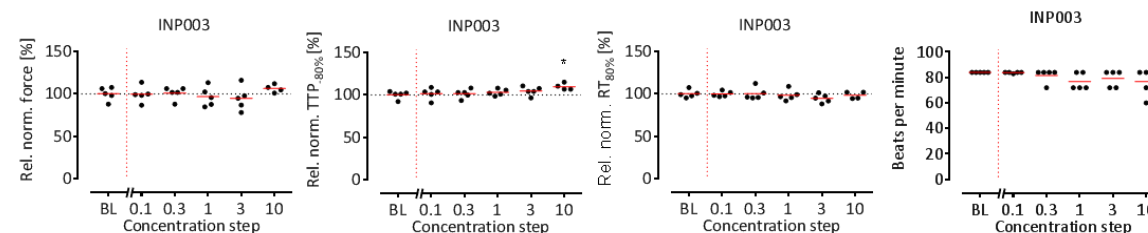
Glibenclamide (INP003), Cell line: ERC18, Modality: Contractility
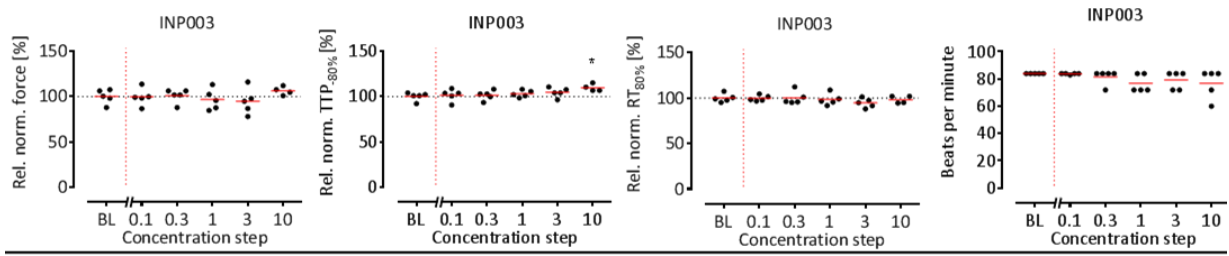
10.1.4. Average peaks of positive inotropes

Figure S2: Average contraction peaks of the data presented in Figure S1.
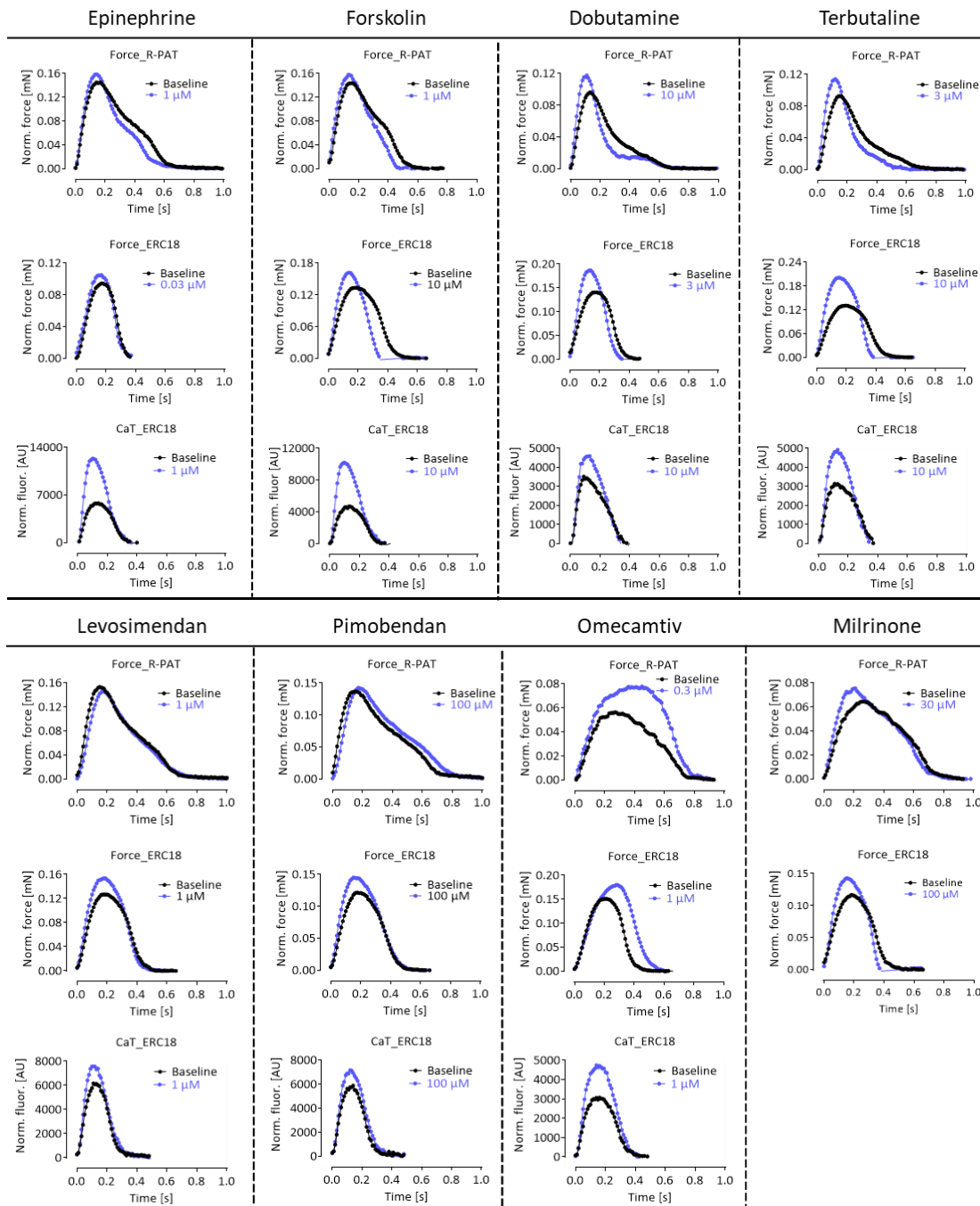
Average peaks of negative inotropes
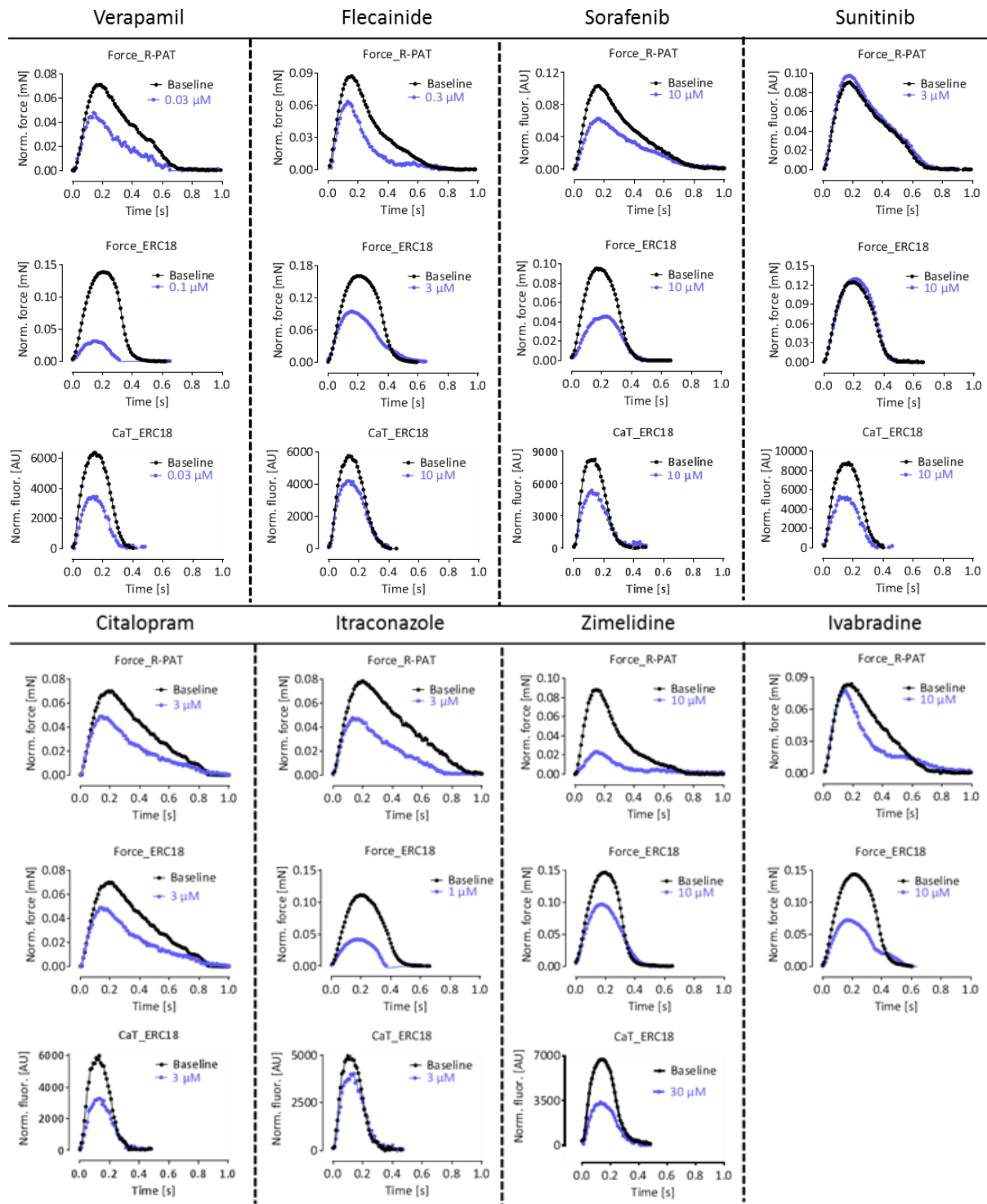
Average peaks of neutral inotropes
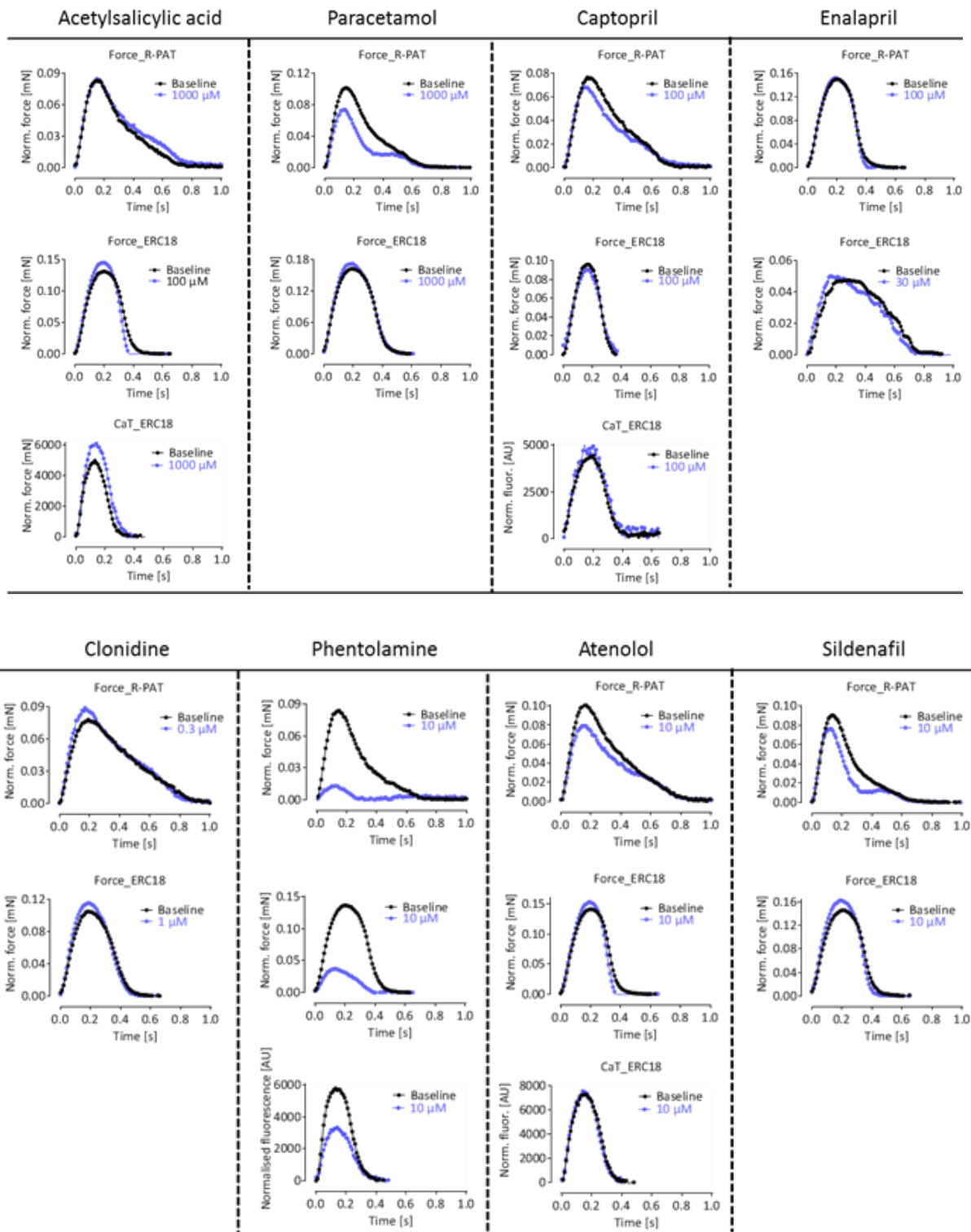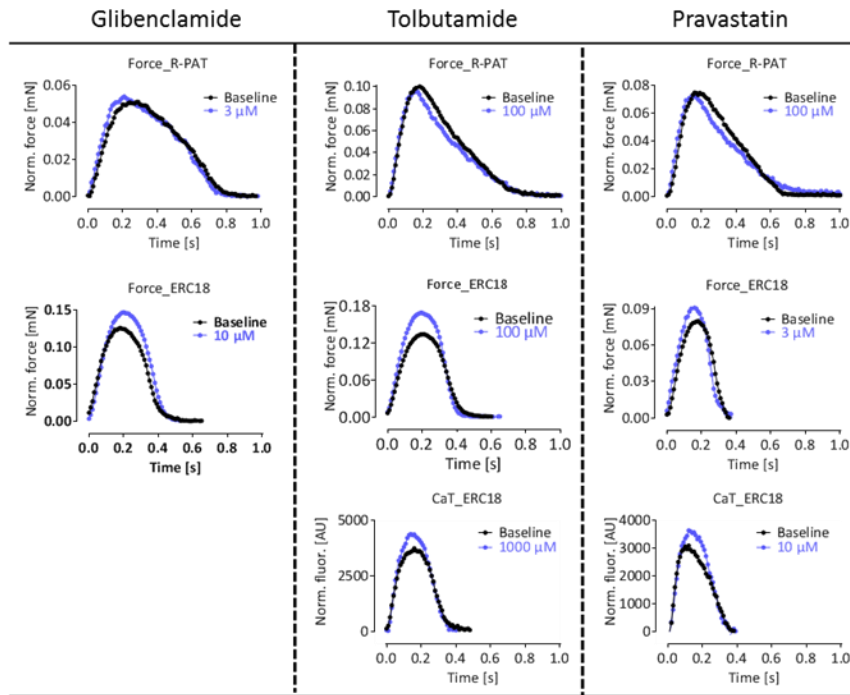
10.1.5. Time match controls for blinded screening
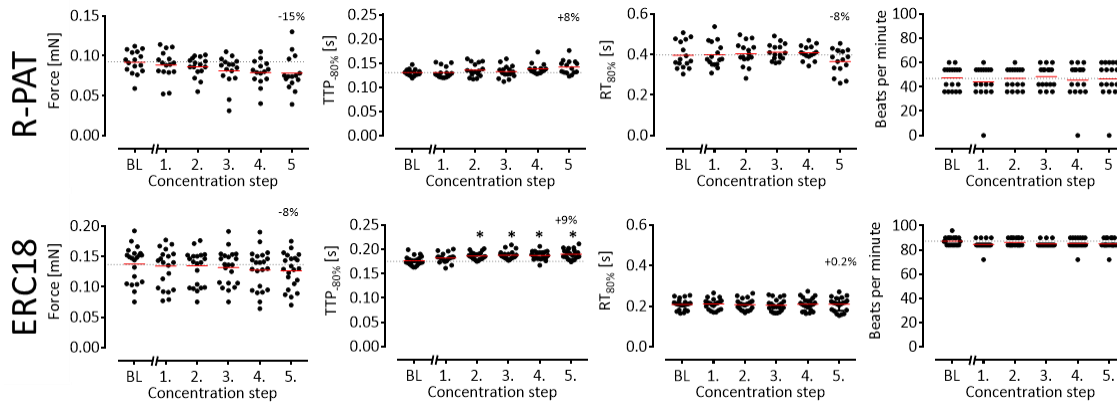
Figure S3: Average time-matched controls for concentration response curves in R-PAT and ERC18 in Tyrode´s solution and high glucose DMEM respectively depicting changes in the contraction parameters; Force, time to peak force (TTP$_{-80\%}$), relaxation time (RT$_{80\%}$) and frequency (beats per minute) at submaximal calcium 0.5-1 mM Ca^{2+}. Depicted is scatter plot with mean values. One-way ANOVA with Dunnett's post-test vs. baseline conditions (BL), *p<0.05.
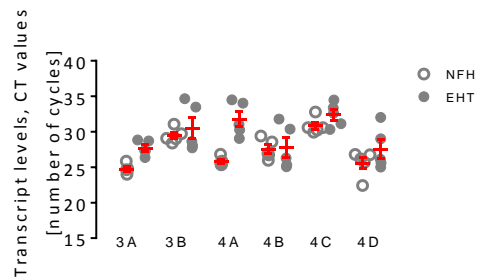
Figure S4: Raw CT values for PDE3 and 4 isoform transcript concentrations in hiPSC-CM EHT (closed grey circles) and non-failing human hearts (NFH; filled grey circles), related to Figure 28. mean±SEM.

10.2. Devices, materials and substances

10.2.1. Devices

AbiPrism 7900HT cycler	Applied Biosystems
Accu-jetR pro	Brand
Analytic scale Genius	Sartorius AG
Bio-Rad ChemiDocTM Touch Imaging System	Bio-Rad Laboratories
Combispin FVL-2400N with vortex function	PeqLab
FACSCanto II Flow Cytometer	BD Biosciences
Magnet plate Variomag/ Cimarec Biosystem 4 Direct	Thermo Scientific
Magnet plate Variomag/ Cimarec Biosystem Direct	Thermo Scientific
Magnet/heating plate IKA Combimag RET	Janke & Kunkel GmbH & Co KG
Force calcium analysis instrument	Custom-made
PCR cycler vapo.protect	Eppendorf
pH meter, digital	Mettler Toledo
Pipette 10/100/1000 µl	Eppendorf, Peqlab
Pipetus	Hirschmann
PowerPac Bacic Power Supply	Bio-Rad Laboratories
Security working hood HERAsafeR	Thermo Fisher Scientific
Spectrophotometer NanoDrop ND-1000	Thermo Fisher Scientific
Sub-cell® GT gel electrophorese tank	Bio-Rad Laboratories
Thermal Cycler vapo.protect	Eppendorf
Thermomixer 5436	Eppendorf
TissueLyser	Qiagen
Ventana, Benchmark XT staining device for IHC	Roche
Video-optical force analysis system	EHT technologies GmbH, Hamburg, A0001
Water bath	GFL
Water bath 2590	Medax

Centrifuges	
Centrifuge 5415 R	Eppendorf
Centrifuge 5810 R	Eppendorf
Centrifuge J-6B	Beckmann
Centrifuge Rotanta/RP	Hettich
Microscopes	
Axioskop 2 with AxioCam color camera	Zeiss
Axiovert 25 with Jenoptik ProgRes	Zeiss, Jenoptik (camera)
EVOS FL Cell Imaging System	Advanced Microscopy Group
LSM 800 Airyscan	Zeiss
T1-SM Nikon Eclipse TS100	Nikon
Softwares	
AxioVision Rel. 4.8.2,	Zeiss
CytoVision image analysis system,	Leica Biosystems
FACSDiva, BD	Biosciences
GraphPad Prism 5.0	
LSM 800 Airyscan,	Zeiss
MProRes Capture Pro V. 2.8.8. (Jenoptik)	MProRes Capture Pro V. 2.8.8. (Jenoptik)
SDS 2.4.1, Applied Biosystem	SDS 2.4.1, Applied Biosystem
Incubators for cell culture (hiPSC, EHT)	
CB 220	Binder
HERAcell 240	Thermo Fisher Scientific
HERAcell 150i	Thermo Fisher Scientific
MCO-19M	Sanyo
MCO-20AIC	Sanyo
S2020 1.8	Thermo Fisher Scientific
Sterile working benches	
HeraSafe	Heraeus
Safe 2020	Thermo Fisher Scientific
Mars 1200 GS	Scanlaf

10.2.2. Materials and equipment

Equipment	Company, Catalogue number
15 ml tubes	GreinerBio-one, 188271
24-well plates	Nunc, 144530
Cell imaging 24-well plate for CaT measurements	Eppendorf, 030741005
250 ml Vacuum Filtration "rapid"-Filtermax	TPP, 99250
500 ml Vacuum Filtration "rapid"-Filtermax	TPP, 99500
Aspiration pipette 2 ml	Sarstedt, 86.1252.011
Cell culture microplate, 96 well, PS, F-bottom, µCLEAR®, black, CELLSTAR®	Greiner Bio One, 655090
Cell culture tube, round bottom (for EHT generation)	GreinerBio One, 163160,
Cell scraper	Sarstedt, 83.1830
Cell strainer for FACS, 30 µm	Sysmex, 04-004-2326
Cell strainer mesh, 100 µm	Falcon, 352360
Centrifuge tubes 15 ml	Sarstedt, 62.554.502 and Greiner, 188280
Cryovial CryoPure tube 1.6 ml	Sarstedt, 72.380
EHT electrode	EHT Technologies GmbH, P0001
EHT pacing adapter/cable	EHT Technologies GmbH, P0002
EHT PDMS rack (24-well format)	EHT Technologies GmbH, C0001
EHT PTFE spacer	EHT Technologies GmbH, C0002
Falcon tube, graduated, 15 ml	Sarstedt, 62.554.502
Flow Cytometry tubes	Sarstedt, 55.1579
Isopropanol container (Mr. Frosty): Nalgene^{TM} Cryo 1 °C Freezing container	Thermo Fisher Scientific, 5100-0001
Neubauer counting chamber	Karl-Hecht KG
PDMS racks	EHT technologies GmbH, C0001
Pipette tips with filter Biosphere®	Sarstedt
Reaction tubes Safe Lock 0.2 – 2 ml	Eppendorf
Serological pipettes 1 ml, 2 ml, 5 ml, 10 ml, 25 ml, 50 ml; wide tip pipette 10 ml	Sarstedt
Spinner flask, 1000 ml	Integra, 182 101
Spinner flask, 500 ml	Integra, 182 051
Sterile filter Filtropur S 0.2 µm	Sarstedt, 83.1826.001
Stirrer Variomag/ Cimarec Biosystem 4 Direct	Thermo Fisher scientific, 50088060
Stirrer Variomag/ Cimarec Biosystem Direct	Thermo Fisher scientific, 70101
T175 cell culture flask	Sarstedt, 83.1812.002
T175 suspension cell culture flask	Sarstedt, 83.3912.502
T75 cell culture flask	Sarstedt, 83.1813.002
TC dish 100, cell+	Sarstedt, 83.3902.300
Teflon spacers (dimensions: length 12 mm, width 3 mm, height 13.5 mm)	EHT technologies GmbH, C0002
Tissue Lyser Steel Beads	Qiagen
V-shaped sedimentation rack (dimensions of the two side panels of the metal bracket: 30 cm x 10 cm, angle 90°)	Custom made at UKE Hamburg

10.2.3. Media and serum

DMEM	Biochrom, F0415
DMEM/F-12 without Glutamine	Gibco, 21331-046
Fetal Calf Serum superior (FCS)	Biochrom, S0615
Horse serum	Life technologies, 26050088
StemPro34-SFM	Gibco, 10640-019
DMEM high glucose	Gibco, 21068-028
Essential 8	Gibco, A15169-01
RPMI 1640	Gibco, 21875

10.2.4. Reagents, proteins and small molecules

10x DMEM	Gibco, 52100-021
1-Thioglycerol	Sigma-Aldrich, M6145
2-Mercaptoethanol	Sigma-Aldrich, M6250
2-Propanol	Merck Millipore, 107022
Accutase® Cell Dissociation Reagent	Sigma-Aldrich, A6964
Acetic acid (concentrated; glacial, 100%)	Merck, 100063
Activin A	R&D Systems, 338-AC
Agarose	Invitrogen, 15510-027
AmpliTaqGold (1kb/min)	Applied Biosystems
Aprotinin	Sigma-Aldrich, A1153
Aqua ad iniectabilia	Baxter S.A., 001428
B27 PLUS insulin	Gibco, 17504-044
B27 Minus insulin	Gibco
BMP4	R&D Systems, 314-BP
$CaCl_2$ x $2H_2O$	Merck, 2382
Collagenase II	Worthington, LS004176
D(+)-Glucose anhydrous	Roth, X997.2
Di-sodium hydrogen phosphate dihydrate (Na_2HPO_4-$2H_2O$)	Merck, 1065800
DMSO for cell culture	Sigma-Aldrich, D4540
DNA loading dye, 6x	Thermo Fisher Scientific, R0611
DNase II, type V (from bovine spleen)	Sigma-Aldrich, D8764
EDTA	Roth, 8043.2
Ethanol, absolute	Chemsolute, 2246.1000
Ethidium bromide	Sigma-Aldrich, E1510
Ethylenediamine-tetraacetic acid disodium salt dihydrate (Na_2EDTA x $2H_2O$)	Roth, 8043.2
FGF2 (human recombinant basic FGF)	Peprotech, #100-18B
Fibrinogen	Sigma-Aldrich, F8630
Formaldehyde	Merck Millipore, 107022
Gelatine	Sigma-Aldrich, G1890
Geltrex®	Gibco, A1413302
GeneRuler 100 bp DNA Ladder	Thermo Fisher Scientific, SM0243
HBSS minus Ca^{2+}/Mg^{2+}	Gibco, 14175-053
HEPES	Roth, 9105.4
Human serum albumin	Biological Industries, 05-720-1B
Hydrochloric acid 1 N	Roth, K025.1
Hydrochloric acid, 37% fuming	Merck 1.00317
Insulin, human	Sigma-Aldrich, I9278
L-Glutamine	Gibco, 25030-081
Lipidmix	Sigma-Aldrich, L5146
Magnesium chloride hexahydrate ($MgCl_2$ x $6H_2O$)	Sigma-Aldrich, M9272
Magnesium sulphate heptahydrate ($MgSO_4$ x $7H_2O$)	Merck,105886
Matrigel® Basement Membrane Matrix (for EHT generation and 2D differentiation)	Corning, 354234
Matrigel® Growth Factor Reduced (GFR) Basement Membrane Matrix (for hiPSC culture)	Corning, 354230
Methanol	J. Baker, 8045
$MgCl_2$	Fuka, 63063
Nitrogen, liquid (N_2)	TMG
Nuclease-free water	Thermo Fisher Scientific, R0581
Paraformaldehyde	Merck, 104005
PBS	Gibco, 10010-049
Phosphoascorbate (2-Phospho-L-ascorbic acid trisodium salt)	Sigma-Aldrich, 49752

Pluronic® F-127	Sigma-Aldrich, P2443
Polyvinyl alcohol	Sigma-Aldrich, P8136
Potassium chloride (KCl)	Merck, 1.04936
Potassium di-hydrogen phosphate (KH$_2$PO$_4$)	Merck, 104873
Roti®-Histofix 4%	Roth, P087.3
Saponin	Sigma-Aldrich, 47036 or Merck, 558255
Sodium azide	Sigma-Aldrich, 71290
Sodium chloride (NaCl)	JT Baker, 7647-14-5
Sodium chloride (NaCl) solution (0.9%)	B. Braun, 3570210
Sodium di-hydrogen phosphate mono-hydrate (NaH$_2$PO$_4$ x H$_2$O)	Merck, 6346
Sodium hydrogen carbonate (NaHCO$_3$)	Merck, 106329
Sodium hydroxide solution 0.1 N/1 N	Roth, K020.1/K021.1
Sodium selenite	Sigma-Aldrich, S5261
TBS	Sigma-Aldrich, T6664
TGF-ß1	Peprotech, 100-21
Thrombin	Sigma-Aldrich, T7513; Biopur, BP11-10-1104
Titriplex® III for analysis (ethylenedinitrilote-traacetic acid, disodium salt dihydrate)	Merck, 108418
Transferrin	Sigma-Aldrich, T8158
TRIS-hydrochloride	Roth, 9090.2
Trypan blue	Biochrom, L 6323
Y-27632 * 2 HCl	Biorbyt, orb154626
KY02111	Tocris, 4731

10.2.5. Small molecules and pharmacological agents

Bay K-8644	Tocris, 1544
BIOMYC-1	PromoCell, PK-CC03-036-1B
BIOMYC-2	PromoCell, PK-CC03-037-1B
BTS (N-Benzyl-p-Toluenesulfonamide)	TCI, B3082-25G
Digoxin	Tocris, 4583
Dorsomorphin	Abcam, ab120843 or Tocris, 3093
DS-I-7 (4-(cis-endo-1,3-dioxooctahydro-2H-4,7-methanoisoindol-2-yl)-N-(quinolin-8-yl)-transcyclohexylcarboxamide)	Dr. Dennis Schade, Technische Universität Dortmund, Germany
EMD-57033	--
Isoprenaline	Sigma-Aldrich, I6504
Ivabradine	Sigma-Aldrich, SML0281
Nifedipine	--
Omecamtiv mecarbil	
Penicillin/streptomycin	Gibco, 15140
XAV939	Tocris, 3748
Y-27632	Biaffin, PKI-Y27632-010

Drugs used in the blinded screening

Following drugs were packed and processed by GlaxoSmithKline® as part of blinded screening project: Epinephrine, forskolin, dobutamine, terbutaline, levosimendan, pimobendan, omecamtiv mecarbil, milrinone, verapamil, flecainide, sorafenib, sunitinib, citalopram, itraconazole, ivabradine, acetylsalicylic acid, paracetamol, captopril, enalapril, clonidine, atenolol, sildenafil, glibenclamide, tolbutamide, pravastatin, zimelidine.

10.2.6. Kits

DNeasy® Blood & Tissue Kit	Qiagen, 69504
dNTP mix, 10 mM	Thermo Fisher Scientific, R0192
High Capacity cDNA Reverse Transcription Kit	Applied Biosystems, 4368813
Maxima SYPBR Green/ROX qPCR Master Mix	Thermo Fisher Scientific, K0222
Phusion Hot Start II DNA Polymerase	Thermo Fisher Scientific, F549S
QIAquick® PCR purification Kit	Qiagen, 28106
RNeasy® Plus Mini Kit	Qiagen, 74134
Taq DNA Polymerase Kit (for mycoplasma test)	Qiagen, 201205
Ultra View Universal DAB Detections Kit	Ventana, 05269806001

10.2.7. Reagent setup, buffer and solutions

Table S1: Reagent setup, buffer and solutions.

Reagents, buffer and solutions	Ingredients
10x DMEM	134 mg/ml DMEM powder dissolved in 5 ml of sterile water for injection and filter sterilized (0.2 µm), stored at 4 °C for up to 2 months. Store DMEM powder at 4 °C. Make sure the box is properly closed as DMEM is hygroscopic.
Agarose for EHT casting molds	2% (w/v) Agarose was dissolved in 300 ml 1xPBS; after autoclaving storage at 60 °C.
Aprotinin	33 mg/ml Aprotinin was dissolved in sterile water for injection; 250 µl aliquots stored at -20 °C for 1 year.
BTS solution	BTS dissolved in DMSO; 250 µl aliquots stored at -20 °C for max. 1 year.
Dissociation buffer	HBSS minus calcium/magnesium Collagenase II, 200 units/ml 1 mM HEPES 10 µM Y-27632 30 µM BTS Sterile filtered (0.2 µm)
DNase solution	100 mg DNase II, type V, dissolved in 50 ml 1xPBS; 2 ml aliquots stored at -20 °C for max. 1 year.
DS-I-7	MW: 417.5 g/mol, dissolved in DMSO at a 10 mM stock solution.
EDTA	0.5 mM EDTA in 1x PBS, filter sterilized and stored at room temperature or 4 °C.
FACS buffer	PBS 5% (v/v) FCS 0,05% (v/v) Sodium azide 0,5% (w/v) Saponin (for intracellular staining)
Fibrinogen	200 g/l Fibrinogen was dissolved in pre-warmed (37 °C) 0.9%-NaCl solution. 33 g/l Aprotinin was added to a final concentration of 100 µg/ml. 200 µl Aliquots were stored at -20 °C for short term and at -80 °C for long term.
Gelatin (0.1%)	0.1% (w/v) gelatin dissolved in water and stored at 4 °C for max. 6 months
HEPES stock solution	1 M HEPES dissolved in 1xPBS and adjusted pH to 7.4 with potassium hydroxide. Filter sterilized (0.2 µm filter) and stored at 4 °C for max. 1 year.
Phosphoascorbate, 250 mM	1 g Phosphoascorbate 12.4 ml PBS
Pluronic F-127 solution	Pluronic F-127 dissolved in 1x PBS to a concentration of 1% (w/v), filter sterilized (0.2 µm filter) and stored at 4 °C for up to 1 year.
Polyvinyl alcohol (50x)	20 g of polyvinyl alcohol dissolved in 100 ml of aqua dest. by slow addition at ~20 °C. The temperature was increase to 80 °C under constant stirring until polyvinyl alcohol was fully dissolved. Aliquots (not sterile) can be stored at 4 °C for up to one year

TBS (10x)	1 M Trizma® base or Tris-HCl 1.5 M NaCl Aqua dest.; pH 7.5 (adjust with 37% HCl)
Thrombin	100 U/ml Thrombin dissolved in 60% (v/v) PBS and 40% (v/v) sterile water for injection; aliquots (450 µl storage, 3 µl for EHTs) stored at -20 °C for max. 1 year.
Transferrin–selenium	100 mg Transferrin dissolved in 2 ml sodium selenite (382 µM), stored at -80 °C for max. 1 year.

10.2.8. Antibodies

Table S2: Primary antibodies used for flow cytometry/FACS and immunohistochemistry (IHC) analysis.

Antibody	Details and dilution	Application	Company and order number
Anti-alpha actinin	Mouse monoclonal IgM, clone EA-53; FACS: 1:800;	FACS,	Sigma-Aldrich, A7811
Anti-cardiac troponin T-FITC	Recombinant human IgG1; clone REA400; 1:10	FACS	Miltenyi Biotec, 130-106-687
mIgG1 isotype control	Purified Mouse IgG1 κ; clone MOPC-21; 1:250	FACS	BD Biosciences, 554121
PE Rat IgM, κ Isotype Control	Rat IgM clone R4-22; 1:80	FACS	BD Biosciences, 553943
REA Control (I)-FITC	Isotype control IgG1, clone REA400; 1:10	FACS	Miltenyi Biotec 130-104-611
Anti-GFP	Rabbit polyclonal IgG; 1:1000	IHC	Abcam, ab290
Anti-sarcomeric Actin	Monoclonal mouse IgM, Clone Alpha-Sr-1; 1:200	IHC	Dako, M 0874

Table S3: Secondary antibodies used for flow cytometry/FACS, and immunohistochemistry (IHC) analysis.

Antibody	Dilution	Application	Company and order number
Alexa Fluor® 488 goat anti-mouse IgG	1:800	FACS,	Life technologies, A11001
Alexa Fluor® 488 goat anti-rabbit IgG	1:800	FACS	Life technologies, A11034
Alexa Fluor® 546 rabbit anti-mouse IgG	1:800	FACS	Life technologies, A11060
Alexa Fluor® 488 donkey anti-mouse IgG	1:500	IHC	A-21202
Alexa Fluor® 555 donkey anti-rabitt	1:500	IHC	A-31572

Supplement

10.2.9. PCR primers

Table S4: PCR primers

PDE isoform	Ref Seq	Primer forward	Primer reverse	PCR product size
PDE1A	NM_001258312.1	ATGGTGGCCCAGTCACAAAT	CACAATGGTGGTTGAGCTGC	159
PDE1B	NM_001288769.1	AGCCCAAGTTCCGAAGCATT	TCCAGGTTCTTGAGACAGTTGAG	130
PDE1C	NM_001191058.2	AGCCGTTTCAAGATCCCCATT	CATCGGCAGCGTGCATTAAG	109
PDE2A	NM_001243784.1	GGCTCTTCTCCAAGTGGCAA	TGCGGATCTCATAGCTCTCATC	194
PDE3A	NM_000921.4	CAGCTGATTGCTGGGACCAA	TGAATGCCCCATGAGCTGTT	156
PDE3B	NM_000922.3	GAGACCGTCGTTGCCTTGTA	CCATTTCCACCTCCAGAATTTTGAT	105
PDE4A	NM_001243121.1	GGCCTCGCACAAGTTCAAAA	CGTTCCTTCATCGTGGGTGA	153
PDE4B	NM_001037341.1	AGTGAGATGGCTTCTAACAAGTTCA	GGTCATGAGCTGCTGCTTTTT	192
PDE4C	NM_001098819.2	GCCTCCAACAAGTTCAAGCG	CCCATGTAGGCCACTGATCC	189
PDE4D	NM_001197220.1	CGAGCACCTAGCAAAAGATCAC	GCCTGGTCTGTAGGGTCTCT	148
PDE5A	NM_033437.3	CAGTACCAGAGAGCCTCCGA	CCATTTCTCTGGTGGCTTTTCTAA	197
PDE7A	NM_002603.3	TGCAGCTGCCACTCATGATCT	TGTCTCCATTTGTTGCCTGCT	196

10.2.10. Patient characteristics for non-failing human heart samples

Table S5: Patient characteristics. CAD: Coronary artery disease; VD: vascular disease; LVEF: Left ventricular ejection frcation; LA :Left atrial diameter; LVEDD: left ventricular end-diastolic diameter; AT: Angiotensin recpetor; ACE: Angiotensin converting enzyme.

Left ventricular CM from patients used for experiments	
N	15
Gender [m/f]	10 / 5
Age [years]	62.5 ± 2.8
BMI [kg/m^2]	27.4 ± 0.6
Hypertension, n	8
Diabetes mellitus, n	6
Hyperlipidaemia, n	6
CAD, n	5
VD	12
LVEF [%]	40.1 ± 4.4
LA [mm]	48.2 ± 2.2
LVEDD [mm]	56.7 ± 4.7
Cardiovascular medication (n)	
Digitalis	2
ACE-Inhibitors	8
LV-blockers	3
β-blockers	6
Ca^{2+}-channel blockers	0
Diuretics	8
Nitrates, n	0
Lipid-lowering drugs	5

10.3.   Security information

10.3.1. Security information for the used substances

Experiments were done in laboratories with the respective certified security standards S1 and S2 according to security data sheets. All chemicals and solutions were disposed off into appropriate containers by following the respective instructions. Contaminated materials and cell suspensions were disposed off after autoclaving.

Table S6: Security information (H- and P-statements) of all used substances.

Substance	CAS number	H-statement	P-statement
1-Thioglycerol	96-27-5	H: 302-311-315-319-335	P: 261-280-305+351+338-312
2-Mercaptoethanol	60-24-2	H: 301+331, 310, 315, 317, 318, 373, 410	P: 270, 280, 302+352, 330, 304+340, 305+351+338, 310
Acetic acid	64-19-7	H: 226-290-314	P: 210-280-301+330+331-305+351+338-308+310
Calcium chloride dihydrate ($CaCl_2$ x 2 H_2O)	10035-04-8	H: 319	P: 305+351+338
Dorsomorphin	866405-64-3	H: 302, 312, 332	P: 301+312, 304+340, 302+352, 261, 280, 264, 270, 271, 330, 501, 363
Ethanol, absolute	64-17-5	H: 225, 319	P: 210, 240, 305+351+338, 403+233
Ethidium bromide	1239-45-8	H: 331, 341	P: 261-281-311
Ethylenediamine tetraacetic acid (EDTA)	60-00-4	H: 319	P: 305+351+338
Formaldehyde	50-00-0	H: 351-331-311-301-314-317	P: 301+310-303+361+353-305+351+338, 320-361-405-501
Hydrochloric acid	7647-01-0	H: 314-335	P: 260-301+330+331-303+361+353-305+351+338-405-501
Hydrochloric acid, 37% fuming	---	H: 290, 314, 335	P: 280, 301+330+331, 305+351+338, 308+310
Isoprenaline hydrochloride	5984-95-2	H: 315, 319, 335	P: 261, 305+351+338
Lipidmix	64-17-5	H: 225, 319	P210, 280, 305+351+338, 337+313, 403+235
Methanol	67-56-1	H: 225-331-311-301-370	P: 210-233-280-302+352
Nitrogen, liquid (N_2)	7727-37-9	H: 281	P: 282, 336+315, 403
Paraformaldehyde	30525-89-4	H: 228-302-332-351-335-315-319-317	P: 281-302+352-305+351+338-308+313-304+340
Penicillin	61-33-6	H: 317	P: 280
Potassium di-hydrogen phosphate (KH_2PO4)	7778-77-0	--	P: 260
Roti®-Histofix 4%	50-00-0 67-56-1	H: 302, 317, 341, 350	P: 261, 280, 302+352, 308+313
Saponin	8047-15-2	H: 319, 335	P 261, 305+351+338
Sodium azide	26628-22-8	H: 300-400-410	P: 273–309-310

Sodium hydroxide (NaOH)	1310-73-2	H: 314	P: 280–301+330+331–309–310-305+351+338
Sodium selenite	10102-18-8	H: 300+330, 315, 317, 319, 411	P: 260, 280, 301+330+331+310, 304+340+310, 403+233
Streptomycin	57-92-1	H: 302	--
Thrombin	9002-04-4	H: 315, 319, 334, 335	P: 261, 305+351+338, 342+311
Titriplex® III	6381-92-6	H: 332-373	P: 314
TRIS-Hydrochlorid (Tris-HCl)	1185-53-1	H: 315, 319, 335	P: 280, 302+352, 305+351+338
Trypan blue	72-57-1	H: 350	P: 201-308+313
Y-27632	331752-47-7	H: 302-312-332	P: 280
Nifedipine	21829-25-4	H: 302	--
Bay K-8644	71145-03-4	--	--
Digoxin	20830-75-5	H: 300	P: 264, 301+310
EMD-57033	150151-10-3	--	--
KY02111	1118807-13-8	--	--
Omecamtiv mecarbil	--	--	--
Epinephrine		H: 301+311, 315, 319, 335	P: 261, 264, 280, 301+310+330, 302+P352+P312, 304+340+312
Forskolin		H: 312	P: 280, 302+352
Dobutamine		H: 361	P: 280, 308+313
Terbutaline		H: 361,	P: 281
Levosimendan		H: 302,312, 332	P: 280
Pimobendan		H: 301	P: 301+310+330
Omecamtiv mecarbil		--	--
Milrinone		H: 301	P: 264, 301+310
Verapamil		H: 301	P: 264, 301+310
Flecainide		--	--
Sorafenib		--	--
Sunitinib		H: 360, 372	P: 201, 308+P313
Citalopram		--	--
Itraconazole		H: 302	P: 264, 301+312
Ivabradine		--	--
Acetylsalicylic acid		--	--
Paracetamol		H: 302	P: 264, 301+312
Captopril		H: 361	P: 280, 308+313
Enalapril		H: 317, 361	P: 280
Clonidine		H: 301	P: 264, 301+310
Atenolol		--	--
Sildenafil		H: 302	P: 264, 301+312
Glibenclamide		--	--
Tolbutamide		--	--
Pravastatin		--	--
Zimelidine		H: 302	P: 264, 301+312

10.3.2. EU-GHS Hazard (H) and Precaution (P) statements

Table S7: Hazard (H) statements according to the 8th ATP of the CLP regulation of May 19, 2016.

H statement	H phrases
H225	Highly flammable liquid and vapour.
H226	Flammable liquid and vapour.
H228	Flammable solid.
H281	Contains refrigerated gas; may cause cryogenic burns or injury.
H290	May be corrosive to metals.
H300	Fatal if swallowed.
H301	Toxic if swallowed.
H301+311	Toxic if swallowed or in contact with skin.
H301+H331	Toxic if swallowed or if inhaled.
H302	Harmful if swallowed.
H308+310	IF exposed or concerned: immediately call a POISON CENTER or doctor/ physician.
H310	Fatal in contact with skin.
H311	Toxic in contact with skin.
H312	Harmful in contact with skin
H312	Harmful in contact with skin.
H314	Causes severe skin burns and eye damage.
H315	Causes skin irritation.
H317	May cause an allergic skin reaction.
H318	Causes serious eye damage.
H319	Causes serious eye irritation.
H330	Fatal if inhaled.
H331	Toxic if inhaled.
H332	Harmful if inhaled.
H334	May cause allergy or asthma symptoms or breathing difficulties if inhaled.
H335	May cause respiratory irritation.
H341	Suspected of causing genetic defects.
H350	May cause cancer.
H351	Suspected of causing cancer.
H360	May damage fertility or the unborn child.
H361	Suspected of damaging fertility or the unborn child
H370	Causes damage to organs.
H372	Causes damage to organs through prolonged or repeated exposure if swallowed.
H373	May cause damage to organs through prolonged or repeated exposure.
H400	Very toxic to aquatic life.
H410	Very toxic to aquatic life with long lasting effects.
H411	Toxic to aquatic life with long lasting effects.

Table S8: Precaution (P) statements according to the 8th ATP of the CLP regulation of May 19, 2016.

P statement	P phrase
P201	Obtain special instructions before use.
P210	Keep away from heat, hot surfaces, sparks, open flames and other ignition sources. No smoking.
P233	Keep container tightly closed.
P240	Ground and bond container and receiving equipment.

P260	Do not breathe dust/fume/gas/mist/vapors/spray.
P261	Avoid breathing dust/fume/gas/mist/vapors/spray.
P264	Wash ... thoroughly after handling.
P270	Do not eat, drink or smoke when using this product.
P271	Use only outdoors or in a well-ventilated area.
P273	Avoid release to the environment.
P280	Wear protective gloves/protective clothing/eye protection/face protection.
P281	P281 Use personal protective equipment as required.
P282	Wear cold insulating gloves and either face shield or eye protection.
P301	IF SWALLOWED:
P301+310+330	IF SWALLOWED: Immediately call a POISON CENTER or doctor/physician. Rinse mouth.
P301+P310	IF SWALLOWED: Immediately call a POISON CENTRE/doctor/....
P301+P312	IF SWALLOWED: Call a POISON CENTRE/doctor/... if you feel unwell.
P301+P330+ P331	IF SWALLOWED: Rinse mouth. Do NOT induce vomiting.
P301+P330+P331+ P310	IF SWALLOWED: Rinse mouth. Do NOT induce vomiting. Immediately call a POISON CENTER/doctor.
P302 +P352+P312	IF ON SKIN: Wash with plenty of water. Call a POISON CENTER/doctor if you feel unwell
P302+P352	IF ON SKIN: Wash with plenty of water/...
P303+P361+ P353	IF ON SKIN (or hair): Take off immediately all contaminated clothing. Rinse skin with water [or shower].
P304+340+312	IF INHALED: Remove person to fresh air and keep comfortable for breathing. Call a POISON CENTER/doctor if you feel unwell
P304+P340	IF INHALED: Remove person to fresh air and keep comfortable for breathing.
P304+P340+P310	IF INHALED: Remove person to fresh air and keep comfortable for breathing. Immediately call a POISON CENTER/doctor.
P305+P351+ P338	IF IN EYES: Rinse cautiously with water for several minutes. Remove contact lenses, if present and easy to do. Continue rinsing.
P308+ P313	IF exposed or concerned: Get medical advice/attention.
P309	IF exposed or if you feel unwell:
P310	Immediately call a POISON CENTRE/doctor/...
P311	Call a POISON CENTRE/doctor/....
P312	Call a POISON CENTRE/doctor/... if you feel unwell.
P313	Get medical advice/attention.
P314	Get medical advice/attention if you feel unwell.
P320	Specific treatment is urgent (see ... on this label).
P330	Rinse mouth.
P336+P315	Thaw frosted parts with lukewarm water. Do not rub affected area. Get immediate medical advice/attention.
P337+P313	If eye irritation persists: Get medical advice/attention.
P342+P311	If experiencing respiratory symptoms: Call a POISON CENTRE/doctor/...
P361	Take off immediately all contaminated clothing.
P363	Wash contaminated clothing before reuse.
P403	Store in a well-ventilated place.
P403+P233	Store in a well-ventilated place. Keep container tightly closed.
P403+P235	Store in a well-ventilated place. Keep cool.
P405	Store locked up.
P501	Dispose of contents/container to ...

10.4. Publications and congress participations

10.4.1. Publications

Saleem U, Ismaili D, Mannhardt I, Schulze T, Christ T, Eschenhagen T, Hansen A: Regulation of ICa,L and force by phosphodiesterases in human induced pluripotent stem cell-derived cardiomyocytes. Br J Pharmacol 2018 (Under review)

Sala L, Van Meer BJ, Tertoolen LGJ, Bakkers J, Bellin M, Davis RP, Denning C, Dieben MAE, Eschenhagen T, Giacomelli E, Grandela C, Hansen A, Holman ER, Jongbloed MRM, Kamel SM, Koopman CD, Lachaud Q, Mannhardt I, Mol MPH, Mosqueira D, Orlova VV, Passier R, Ribeiro MC, **Saleem U**, Smith GL, Burton FL, Mummery CL: Musclemotion: A versatile open software tool to quantify cardiomyocyte and cardiac muscle contraction in vitro and in vivo. Circ Res 2018, 122.

Breckwoldt K, Letuffe-Brenière D, Mannhardt I, Schulze T, Ulmer B, Werner T, Benzin A, Klampe B, Reinsch MC, Laufer S, Shibamiya A, Prondzynski M, Mearini G, Schade D, Fuchs S, Neuber C, Krämer E, **Saleem U**, Schulze ML, Rodriguez ML, Eschenhagen T, Hansen A: Differentiation of cardiomyocytes and generation of human engineered heart tissue. *Nat Protoc* 2017.

Mannhardt I, **Saleem U**, Benzin A, Schulze T, Klampe B, Eschenhagen T, Hansen A: Automated Contraction Analysis of Human Engineered Heart Tissue for Cardiac Drug Safety Screening. J Vis Exp 2017(April):e55461–e55461.

Saleem U, Ejaz S, Ashraf M, Omer MO, Iltaf I, Batool Z, Fatima R, Afzal M: Mutagenic and cytotoxic potential of Endosulfan and Lambda-cyhalothrin - In vitro study describing individual and combined effects of pesticides. J Environ Sci (China) 2014, 26:1471–1479.

Fatima R, Ashraf M, Ejaz S, Rasheed MA, Altaf I, Afzal M, Batool Z, **Saleem U**, Anwar K: In vitro toxic action potential of anti-tuberculosis drugs and their combinations. Environ Toxicol Pharmacol 2013, 36.

10.4.2. Conferences and workshops

2018 (July). International society of Heart research European section (ISHR-ES), Amsterdam, Netherlands. Poster presentation: **Saleem U**, Mannhardt I, Sadran H, Schulze T, Christ T, Eschenhagen T, Hansen A. Functional relevance of PDE3 and 4 isoforms in human induced pluripotent stem cell-derived cardiomyocytes in engineered heart tissue format.

2018 (June). International society of stem cell research, Melbourne, Australia. Poster presentation: **Saleem U,** Mannhardt I, Braren I, Eschenhagen T, Hansen A. Dual recordings of contractile force and calcium transients in human engineered heart tissues using genetically encoded calcium indicators.

2017 (Nov). American heart association, Anaheim, USA. Poster presentation: **Saleem U,** Mannhardt I, Braren I, Eschenhagen T, Hansen A. Optical analysis of contractile force and calcium transients in human engineered heart tissues with genetically encoded calcium indicators.

2017 (Sep). German stem cell network, Jena, Germany. Oral presentation: **Saleem U,** Mannhardt I, Braren I, Eschenhagen T, Hansen A. Genetically encoded calcium indicators for drug screening in human engineered heart tissues.

2017 (Aug). IBPS (Institut de Biologie Paris Seine) Summer School on optical biosensors, Paris, France.

2017 (July). <u>International society of Heart research European section (ISHR-ES), Hamburg, Germany</u>. Poster presentation: **Saleem U,** Mannhardt I, Braren I, Eschenhagen T, Hansen A. Genetically encoded calcium indicators for drug screening in human engineered heart tissues.

2017 (Feb). <u>International society of stem cell research, Basel, Switzerland</u>. Poster presentation: **Saleem U,** Mannhardt I, Sadran H, Schulze T, Christ T, Eschenhagen T, Hansen A. Phosphodiesterase inhibitors enhance positive inotropic effects of catecholamines in human iPSC-derived cardiomyocytes.

Quarterly oral presentations in Crack-IT (European consortium composed of academics and small to medium-sized enterprise) meetings held in Hamburg, London and Glasgow. Analysis of contraction force, calcium handling and action potential in hiPSC derived cardiomyocytes in engineered heart tissue model.

11 <u>ACKNOWLEDEMENTS</u>

First and foremost, I would like to express my sincere gratitude to Prof. Dr. Thomas Eschenhagen for giving me the opportunity to work in his lab under his supervision. I am grateful for his supportive attitude, motivating behaviour, kind guidance and constructive suggestions which made it possible for me to achieve my research goals. It has been a privilege for me to be his Ph.D. student and to share of his broad scientific knowledge.

I heartily thank Prof. Dr. Arne Hansen for his scientific guidance, great pieces of advice and immense support. He was always there to discuss any sort of theoretical and experimental issues. I want to acknowledge his incredible patience and extraordinary human qualities, which supported me throughout my Ph.D. studies. His friendly attitude always motivated me to perform my tasks efficiently, and his invaluable ideas and advice helped me in thesis writing. I also thank him for his practical help for data processing during blinded drug screening.

I thank Dr. rer. net. Ingra Mannhardt for her great support and kind suggestions and for always letting her door open for me. I am grateful for her confidence in me and for always encouraging me. She was the one who helped me to learn all the basic techniques and guided me throughout my Ph.D. at every basic step. She always took great interest in experiment planning and data interpretation. She was involved in all of my research activities. I also want to thank her for proof reading my thesis.

I want to thank Prof. Dr. Elke Oetjen for accepting supervision of my Ph.D. thesis in the Department of Chemistry, University of Hamburg and for her interest in my scientific work.

Cardiomyocyte differentiation was a group effort and I extend my warm gratitude to all the members involved. Without their support, it was not possible to differentiate enormous number of cardiomyocytes. I thank all the people in hiPSC differentiation and EHT group - Prof. Dr. Arne Hansen, Prof. Dr. Lucie Carrier, Dr. Ingra Mannhardt, Dr. Bärbel Ulmer, Dr. Kaja Breckwoldt, Dr. Pierre Bobin, Dr. Anika Eike Knaust, Dr. Tessa Werner, Dr. Alexandra Rhoden, Dr. Christiane Neuber, Dr. Marita Roudrigez, Dr. Marina Reinsch, Dr. Giulia Mearini, Dr. Sandra Laufer, Dr. Maksymilian Prondzynski, Mirja Schulze, Marta Lemme, Dr. Alexandra Löser, Antonia T. L. Zech, Thomas Schulze, Birgit Klampe and Elisabeth Krämer.

I am grateful to Dr. Ingke Braren from HEXT Core Vector Facility for preparing the viral vectors and Kristin Hartmann from the Facility of Mouse Pathology UKE for the immunohistological EHT staining.

I acknowledge the ideas and fruitful discussions with our partners in the "Crack-IT" project meetings for blinded drug screening.

I want to thank all my colleagues from the Department of Experimental Pharmacology and Toxicology, for providing me a very nice and warm environment and making me feel like home. A special mention to Thomas Schulze, Anika Eike Knaust and Mirja Schulze for their wonderful company and interesting conversations in the laboratory. I thank Frank Neumann who always helped me in all administration matters.

In the end, I would like to thank my family and friends who are always there for me. My heartily thank to my mother "Bushra Saleem" for her endless efforts and support. Whatever I am today is because of her. She always motivated me to do my best. I thank her for always lending an ear to me and for listening to my long telephonic conversations at midnight. I am thankful to my friends in Germany- Sana, Madiha and Hina, who always supported me and without whom I would not have

survived here far from my family. Finally, I thank my husband for his immense love and support. I am grateful for his encouraging attitude and patience.

12 DECLARATION OF ACADEMIC HONESTY -EIDESSTATTLICHE ERKLÄRUNG

Hereby, I declare that this thesis entitled

"Preclinical drug safety screening using induced pluripotent stem cell-derived cardiomyocytes in engineered heart tissue format "

carried out at the Department of Experimental Pharmacology and Toxicology, UKE Hamburg under the direction of Prof. Dr. med. Thomas Eschenhagen, the guidance of Prof. Dr. med. Arne Hansen and Dr. rer. nat. Ingra Mannhardt, and the supervision of Prof. Dr. med. Elke Oetjen from the Department of Chemistry, was completed independently by myself. Further, I did not use any other sources or aids other than those indicated. The submitted written form of the thesis complies with the electronic version. Moreover, this thesis was not handed over in any other form for another examination procedure.

Hamburg, 10 January 2019   Umber Saleem

Hiermit versichere ich an Eides statt, dass die vorliegende Dissertation mit dem Titel

"Preclinical drug safety screening using induced pluripotent stem cell-derived cardiomyocytes in engineered heart tissue format ",

durchgeführt am Institut für Experimentelle Pharmakologie und Toxikologie des Universitätsklinikums Hamburg-Eppendorf unter der Leitung von Herrn Prof. Dr. med. Thomas Eschenhagen, der Anleitung von Herrn Prof. Dr. med. Arne Hansen und Dr. rer. nat. Ingra Mannhardt, und der Betreuung durch Frau Prof. Dr. med. Elke Oetjen für den Fachbereich Chemie, selbst verfasst wurde und keine anderen als die angegebenen Hilfsmittel benutzt worden sind. Die eingereichte schriftliche Fassung entspricht der elektronischen Version. Ich versichere, dass diese Dissertation nicht in einem früheren Promotionsverfahren eingereicht wurde.

Hamburg, 10 January 2019   Umber Saleem